January 2011

Identification of the Molecular Basis of Morphological Variation in Avian Beaks

Kara Powder
Washington University in St. Louis

WASHINGTON UNIVERSITY IN ST. LOUIS

Division of Biology and Biomedical Sciences
Molecular Genetics and Genomics

Dissertation Examination Committee:
Michael Lovett (Advisor)
James Cheverud
Joseph Corbo
David Ornitz
James Skeath
Mark Warchol

Identification of the Molecular Basis of Morphological Variation in Avian Beaks

by

Kara Elizabeth Powder

A dissertation presented to the
Graduate School of Arts and Sciences
of Washington University in
partial fulfillment of the
requirements for the degree
of Doctor of Philosophy

August 2011

Saint Louis, Missouri

ABSTRACT OF THE DISSERTATION

Identification of the Molecular Basis of Morphological Variation in Avian Beaks
by

Kara Elizabeth Powder

Doctor of Philosophy in Biology and Biomedical Sciences

(Molecular Genetics and Genomics)

Washington University in St. Louis, 2009

Professor Michael Lovett, Thesis Advisor

Vertebrates, particularly birds, show extremely variable species-specific morphology in craniofacial structures. Cranial neural crest cells give rise to all the cartilage and bone of the face, and transplantation experiments have shown that these cells contain species-specific patterning information. First, I employed custom cross-species microarrays to analyze the spectrum of developmental signaling pathway and transcription factor gene expression changes in neural crest cells of the developing beaks for the chicken, duck, and quail, both before and after morphological variation is evident. I found that neural crest cells have established a species-specific gene expression profile that predates morphological variation. In addition to expression changes in the Bmp and Calmodulin pathways, previously associated with morphological variation in Darwin's finches, I observed dramatic changes in a number of Wnt signaling components in the broad-billed duck.

Second, given that deletion of the microRNA processing gene *DICER* in neural crest cells results in loss of nearly all facial structures, I utilized high-throughput sequencing to describe the microRNAs that are expressed and/or differentially expressed among the same neural crest samples used for the microarray analysis. In remarkable contrast to relatively unchanged pattern of transcription factor gene expression, microRNA expression is highly dynamic during stages when avians acquire species-specific morphology. The microRNA expression profiles also suggest that the transition from multipotent, proliferative neural crest cells into cells differentiating to form the tissues of the face may be delayed in the duck relative to the chicken and quail. This prolonged period of proliferation in duck neural crest may contribute to the increase in beak size and width of the adult duck bill versus the chicken beak.

Finally, I illustrate examples of how these genomic data sets can initiate new avenues of investigation and testable hypotheses. I found that the Wnt pathway acts upstream of the Bmp pathway and induces regional changes in growth of the developing beak. I also correlate changes in expression of miR-222 in the frontonasal prominence with alterations in protein (but not mRNA) levels of one of its target genes, the cell cycle regulator *p27(KIP1)*. I then identified seven mature microRNAs that appear to be specific to the avian lineage. Using PCR, I confirmed that two of these, miR-2954 and miR-2954*, are conserved across the avian lineage, from ratites to songbirds.

ACKNOWLEDGEMENTS

To my family for their endless support and patience.

TABLE OF CONTENTS

FIGURES AND TABLES

ABBREVIATIONS

All gene names not listed in text or Tables 2-1 and 2-2 can be found at NCBI GEO (http://www.ncbi.nlm.nih.gov/geo/) under accession number GSE11099

ºC	degrees Celsius
50mer	50 base pair oligonucleotide
BLAST	Basic Local Alignment Search Tool
bp	base pair
cDNA	complementary DNA
Cy(3,5)	cyanine (3,5)
DNA	deoxyribonucleic acid
dATP	deoxyadenosine triphosphate
dCTP	deoxycytidine triphosphate
dGTP	deoxyguanosine triphosphate
dNTPs	deoxynucleotide triphosphates (dATP+dCTP+dGTP+dTTP)
dTTP	deoxythymidine triphosphate
E	embryonic day number
EDTA	ethylenediaminetetraacetic acid
EST	expressed sequence tag
hr	hour
HH	Hamburger-Hamilton developmental stage number
kbp	kilobase pair
min	minute
miRNA	microRNA

mRNA	messenger RNA
NC	neural crest
NCBI	National Center for Biotechnology Information; www.ncbi.nlm.nih.gov
PCR	polymerase chain reaction
PBS	Phosphate-buffered saline (137mM NaCl, 2.7mM KCl, 8.1mM $Na_2HPO_4 \bullet 2\ H_2$), 1.76mM KH_2PO_4, pH 7.4)
pfu	plaque forming units
qRT-PCR	quantitative real-time PCR
RNA	ribonucleic acid
rpm	rounds per minute
RT-PCR	reverse transcription PCR
SDS	sodium dodecyl sulfate
sec	second
SNP	single nucleotide polymorphism
TBS	Tris-buffered saline (50mM Tris-HCl, 150mM NaCl, pH 7.6)
TF	transcription factor
Tm	oligonucleotide melting temperature
U	enzyme units
UTR	untranslated region
v/v	volume concentration (volume/volume)
w/v	mass concentration (weight/volume)
x g	times gravity

CHAPTER 1

Origins of Craniofacial Morphological Variation

In *On the Origins of Species* Charles Darwin observed how populations evolve through adaptations and natural selection to generate the "endless forms" found in nature (Darwin 1859). Since then, the fields of evolution and development have been trying to understand the genetic and molecular mechanisms that underlie these morphological variations. King and Wilson's seminal paper in 1975 observed that the proteins of chimpanzees and humans are too similar to explain their organismal differences, and thus many of the morphological differences are likely to be due to changes in gene regulation (King and Wilson 1975). This raises the question, what types of genes influence species-specific morphologies? The two largest classes of *trans*-acting regulatory molecules are transcription factors (TFs) and microRNAs (miRNAs), which control protein levels of hundreds of target genes through specific and combinatorial activation and repression (Hobert 2008). In addition, specific signaling pathways such as the fibroblast growth factor (Fgf), Hedgehog, Notch, transforming growth factor β/Bone morphogenetic protein (TGFβ/BMP), and Wnt signaling networks serve crucial roles in animal development--from body patterning to organogenesis and cell-fate specification (Gilbert Scott F. 2003a)--and modulations in these pathways may contribute to morphological variations (Pires-daSilva and Sommer 2003).

Regulatory sources of species-specific morphologies

It appears unlikely that morphological variation is due to the exploitation of entirely novel genes or genetic networks, but rather by ”tinkering” (Jacob 1977) with existing developmental programs (Carroll S.B. 2005, Gilbert S. F. 2003b). Indeed, the TF and signaling pathway spectrums are largely conserved from sponges to humans (Larroux et al. 2008, Nichols et al. 2006), though *cis* regulatory regions have gained remarkable complexity over this same time period (Levine M. and Tjian 2003). Intriguingly, microRNAs appear to have been continuously added during the metazoan lineage (Grimson et al. 2008, Heimberg et al. 2008, Hertel et al. 2006, Prochnik et al. 2007, Sempere et al. 2006, Wheeler et al. 2009), with increased rates of acquisition at the advent of bilaterians, vertebrates, and eutherian animals (Heimberg et al. 2008, Hertel et al. 2006, Wheeler et al. 2009). However, closely related organisms (e.g. Darwin’s finches or *Drosophila* species) that have undergone micro-evolutionary changes seem to have predominantly the same microRNAs (Tang et al. 2010 and unpublished data), though their targets may have evolved (Clop et al. 2006, Nozawa et al. 2010). So, if the arsenal of regulatory genes is largely the same, what is the regulatory source of species-specific morphologies?

Developmental regulatory genes such as TFs, miRNAs, and signaling pathways can be modified in multiple ways to alter the shape and organization of animal bodies (Gilbert S. F. 2003b). First, the regulatory gene itself may be mutated within its protein-coding regions. For instance, the homeobox (Hox)

transcription factor Ultrabithorax (Ubx) has undergone changes in at least two regions in the C-terminus of the protein in insects, but not in arthropods, that render it able to repress the *Distalless (Dll)* gene and thus repress abdominal limb formation (Galant and Carroll 2002, Ronshaugen et al. 2002). Also, the *Melanocortin-1-receptor (MC1R)* gene has been mutated at different locations in various lineages to control melanism in birds, cats, and mice (Eizirik et al. 2003, Nachman et al. 2003, Theron et al. 2001). Despite these clear examples of mutations within protein-coding domains, adaptive mutations affecting morphology are more likely to occur in *cis* regulatory elements of genes to prevent deleterious pleiotropic effects (Carroll S.B. 2005, Carroll S. B. 2008). Pleiotropy is largely avoided in the above cases as the changes between insects and arthropods in Ubx occur outside of its DNA-binding homeodomain and other motifs that are essential for its functions during body patterning in both species (Galant and Carroll 2002, Ronshaugen et al. 2002), and *MC1R* expression appears to be restricted to very specific cell types like melanocytes (Carroll S. B. 2008).

Current theories (Carroll S.B. 2005, Gilbert S. F. 2003b, Parsons and Albertson 2009) suggest that the predominant source of species-specific morphological forms is subtle quantitative, temporal, and/or spatial alterations in gene expression. These modulations occur through differences in *cis* regulation, via DNA changes (e.g. creation or ablation of TF binding sites) or epigenetic modification (e.g. DNA methylation or histone acetylation and methylation) of

promoter, enhancer, or insulator elements (Gibney and Nolan 2010, Levine M. and Tjian 2003). First, gene expression can be repressed or enhanced in one species or another. For instance, increased expression levels of the *ebony* gene underlies differential body color in *Drosophila* species (Wittkopp et al. 2003). Second, there may be differences in the timing of gene expression (heterochrony). This occurs between direct and indirect developing sea urchins, which skip or include a larval stage, respectively, based on the timing of *wnt-5* expression (Ferkowicz and Raff 2001). Third, species may have altered the location of gene expression (heterotopy) to affect species-specific morphologies. An example of this is how the duck has webbed feet: while the expression of the *GREMLIN* gene is localized to the digits of a chicken limb bud, its expression is expanded to include the interdigital mesoderm of ducks, which ultimately represses apoptosis of the interdigital web (Merino et al. 1999).

Craniofacial complex as a model system

I have focused on species-specific craniofacial morphologies for three reasons. First, vertebrates (and particularly birds) exhibit an extraordinary degree of natural facial variation, and these variations correlate with adaptive radiations to exploit new ecological niches. Second, despite the morphological differences in adult facial structures, vertebrates have conserved craniofacial morphologies during embryonic development (Figure 1-1). From this “phylotypic stage” (Slack et al. 1993) structures then diverge through changes in gene

expression and the delineation of discrete regions of responsiveness in the facial primordial (Abzhanov et al. 2004, Abzhanov et al. 2006, Brugmann et al. 2006b, Brugmann et al. 2010, Brugmann et al. 2007, Wu P. et al. 2004, Wu P. et al. 2006). The identification of this closely similar stage of craniofacial morphogenesis allows for the analysis of the molecular and genetic signals that drive subsequent morphological changes, as well as manipulation of facial primordia prior to the occurrence of differential structures. Third, given the conservation of the molecular genetic "toolkit" that is used to build the face across vertebrates, insights gained from work in evolutionary models can benefit human health. For instance, expression of the gene *BMP4* was first correlated with beak depth in Darwin's finches (see below) (Abzhanov et al. 2004), and was subsequently associated with cleft lip in both humans and mice (Liu et al. 2005, Suzuki et al. 2009). Thus, it is likely that genes which contribute to natural morphological variation will be a valuable source of candidate genes to study human craniofacial abnormalities, which account for approximately one third of congenital defects (Dixon et al. 2011).

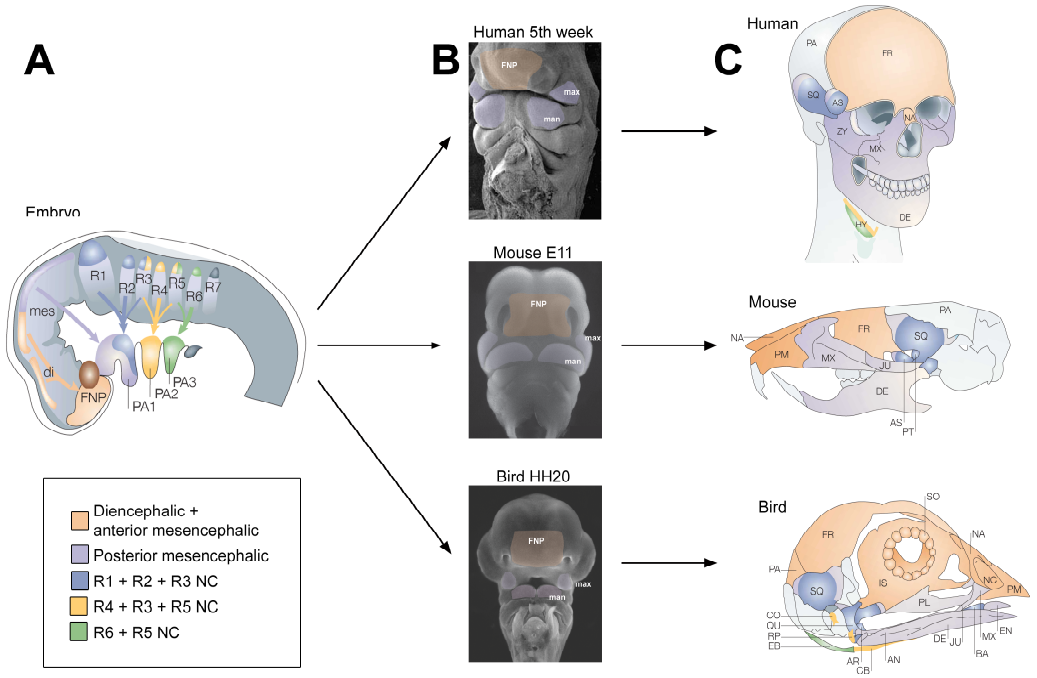

Figure 1-1: Embryonic and skeletal fate of cranial neural crest cells in vertebrates, modified from Santagati and Rijli (2003). **(A)** Schematic drawings depicting neural crest migration from the diencephalon, mesencephalon, and rhombomeres to embryonic pharyngeal arches. The diagram is representative of chick, mouse, and human embryos, although the neural crest migratory pathways differ slightly in different species (Kulesa et al. 2004). **(B)** The primordial embryonic facial structures populated by neural crest cells are highly conserved across vertebrates. **(C)** Contribution of neural crest cells to skull of humans, mice, and birds. AN, angular bone; AR, articular bone; BA, basihyal; CB, ceratobranchial; CO, columella; DE, dentary bone; di, diencephalon; EB, epibranchial; EN, entoglossum; FNP, frontonasal process; HY, hyoid bone; IS, interorbital septum; JU, jugal bone; man, mandibular prominence; max, maxillary prominence; mes, mesencephalon; MX, maxillary bone; NA, nasal bone; NC, nasal capsule; PA1–PA3, pharyngeal arches 1–3; PL, palatine bone; PM, premaxillary bone; QU, quadrate; RP, retroarticular process; R1–R7, rhombomeres 1–7; SO, scleral ossicles; ZY, zygomatic bone. Embryo images in **(B)** courtesy of Dr. S. Brugmann (chick and mouse) and Dr. K. Sulik (human).

Avians as a model organism

The wide range of different adult bill shapes in birds, coupled with the evolutionary conservation of vertebrate facial development, makes avians an ideal model system for exploring the genetic differences that specify facial

variation. In addition, eggs for a number of species are widely available, and the developing embryo is easily accessible for *in vivo* (*in ovo*) manipulations. For these reasons, many of the classic studies on neural crest initiation, migration, patterning, and contribution to the adult face were studied in avian systems (Kontges and Lumsden 1996, Lumsden et al. 1991, Noden 1978, 1983, Tosney 1982). Much of this was possible due to the ability to make quail-chicken chimeras and reliably mark donor and host cells (Kontges and Lumsden 1996, Le Douarin 2004, 2008, Noden 1978, 1983). The chicken, quail, and, more recently, the duck, are the most common experimental avian systems due to their availability. The chicken and quail are closely related, with the last common ancestor 38.8 ± 1.3 million years ago (MYA). The duck is more diverged, at 89.8 ± 7.0 MYA. By comparison, these three species are 104.2 ± 2.8 million years diverged from nearly all other birds, including Darwin's finches (van Tuinen and Hedges 2001). However, when comparing divergent species one must be cautious in assigning functional relevance. That is, what changes are causative in changing beak shape, and what changes are artifacts of comparing different genera? Yet, importantly, nearly all birds in the order *Galliformes*, including the chicken, quail, pheasant, grouse and turkey, have narrow, conical beaks while the duck, goose, swan, and other members of the order *Anseriformes* have a broad, flat bill.

Developmental origins of the beak

Craniofacial development begins with neural crest (NC) initiation in the neural folds of the forebrain and hindbrain, at the interface between the presumptive neural ectoderm and surface ectoderm. Soon before neural tube closure, NC is specified through the integration of Bmp, Fgf, and Wnt signaling (Knecht and Bronner-Fraser 2002, Sauka-Spengler and Bronner-Fraser 2008). At the 5-6 somite stage--approximately Hamburger-Hamilton stage 9 (HH9) (Hamburger and Hamilton 1951)—NC cells undergo an epithelial-to-mesenchymal transition and delaminate from the neural folds (Sauka-Spengler and Bronner-Fraser 2008, Tosney 1982). Via interactions between Eph receptor tyrosine kinases and their Ephrin ligands (Mellott and Burke 2008), NC cells from the diencephalon and mesencephalon migrate as a sheet to populate the frontonasal prominence (FNP) and NC cells from the mesencephalon and rhombomeres migrate in stereotypical streams to populate the pharyngeal, or branchial, arches (schematized in Figure 1-1A) (Lumsden et al. 1991). By HH14-HH15, the embryonic facial structures have been populated by NC (Figure 1-1B) (Lumsden et al. 1991), which ultimately form all of the cartilage and bones of the face (Figure 1-1C) (Kontges and Lumsden 1996).

One of these embryonic structures, the frontonasal prominence (FNP, Figure 1-1A-B), is of particular importance in vertebrate craniofacial variance. This structure forms the forehead and middle of the nose in humans and is the predominant source of the upper beak in avians (Figure 1-1C) (Kontges and

Lumsden 1996, Noden 1978). In addition, the skeletal elements most responsible for variation in length and width of the upper beak (prenasal cartilage and premaxilla, respectively) (Richman and Lee 2003) are derived from the FNP, implicating this prominence in determination of diversity in avian beaks. As analyzed visually and quantitatively by multivariate analysis, the frontonasal prominences of chickens, ducks, and quails exhibit a maximum degree of morphological similarity at HH20 (Figure 1-2, the phylotypic stage, as noted above), but have become morphologically distinct and developed different growth trajectories by HH25 (Brugmann et al. 2010). These differences in growth eventually give rise to species-specific morphologies (e.g., narrower beaks in chick and quail embryos vs. broader bills in duck embryos) (Brugmann et al. 2010).

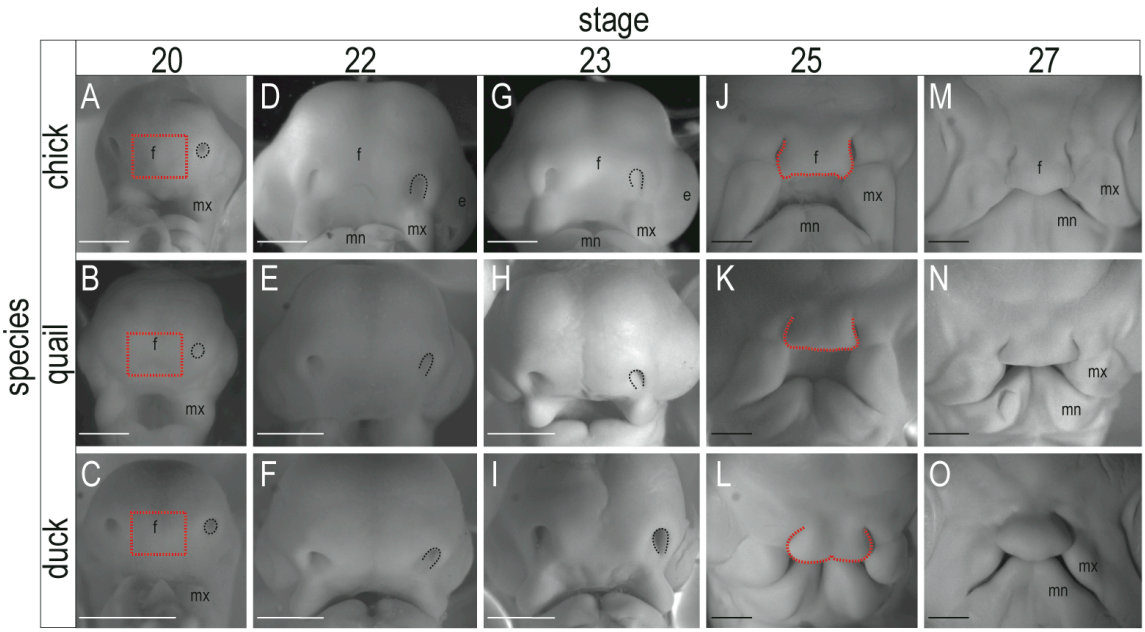

Figure 1-2: Morphological progression of the developing beak of the chick, quail, and duck (Brugmann et al. 2010). (A-C) The frontonasal prominence (f, red box) is highly similar in HH20

chick, quail and duck embryos. **(D-I)** At HH22 and HH23 the frontonasal (f) prominence remains indistinguishable between species. **(J-L)** At HH25 the frontonasal prominence (dotted red line) is morphologically distinct between species. While the frontonasal prominence of the chick and quail appears as rectangular projections, the frontonasal prominence of the duck has bilaterally symmetrical bulges. **(M-O)** At HH27 the morphological differences between the beaks and bill are exacerbated and can be used to identify species. White scale bar denotes 500 μm and black scale bar denotes 1 mm. e, eye; f, frontonasal prominence; mn, mandibular prominence; mx, maxillary prominence.

Hox patterning of the face

Frontonasal prominence (FNP) and first pharyngeal arch (PA1) derivatives are the principal components of the upper and lower face, respectively, while derivatives of the second and third pharyngeal arches (PA2 and PA3) have only minor contributions to the facial skeleton of vertebrates (Figure 1-1C). In addition, PA2 or PA3 neural crest transplanted to PA1 cannot form PA1 derivatives, but transplanted PA1 neural crest can form PA2 derivatives (Figure 1-3D-E) (Couly et al. 1998). This distinction between pharyngeal arches has been shown to be due to differences in *homeobox A2 (HOXA2)* gene expression (Figure 1-3). This gene is expressed in PA2 and PA3, but not in regions that contribute to the face (Figure 1-3A) (Hunt et al. 1991). Loss of *HOXA2* expression in the second arch results in a homeotic transformation, with the second arch taking on a first arch fate and developing into duplicate maxillary and mandibular structures (Figure 1-3B) (Gendron-Maguire et al. 1993, Rijli et al. 1993). Conversely, over-expression of *HOXA2* in PA1 causes this arch to take on a second arch fate and the loss of first arch derivatives (Figure 1-3C) (Creuzet et al. 2002, Grammatopoulos et al. 2000). Further work showed that PA1 crest is competent for *Hox* gene expression, but this expression is repressed by

fibroblast growth factor 8 (FGF8) expression from the isthmus region at the border between the midbrain and rhombomere 1 (Irving and Mason 2000). Furthermore, transplantation of the isthmus or over-expression of *FGF8* in the second arch phenocopies loss of *HOXA2* expression and results in duplications of PA1 derivatives (Figure 1-3B) (Irving and Mason 2000, Noden 1983, Trainor et al. 2002). Together, these experiments show that a lack of *HOXA2* expression is critical for jaw formation. Interestingly, the loss of *HOXA2* expression in the first arch may have been a critical step in evolution of the vertebrate face, as jawless lampreys retain *Hox* expression in PA1 (Figure 1-3F) (Cohn 2002).

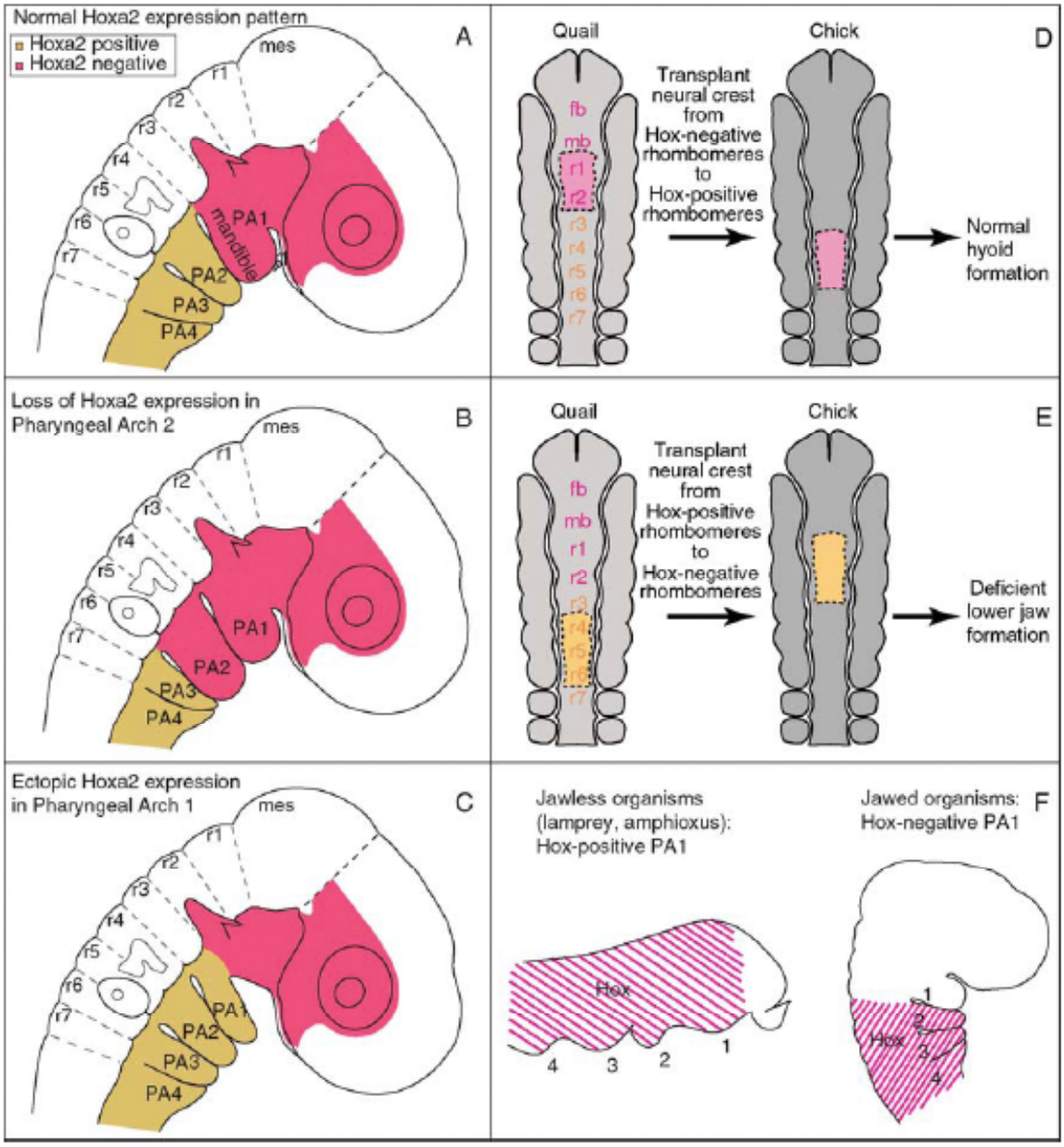

Figure 1-3: *Hox* patterning in the face (Brugmann et al. 2006a). **(A)** *HOXA2* expression distinguishes pharyngeal arches that form the face (PA1) from those that cannot (PA2-PA4). **(B)** Loss of *HOXA2* expression in the second arch (PA2) via gene knock-out or *FGF8* expression causes PA2 to adopt first arch fates. **(C)** Ectopic expression of *HOXA2* in PA1 results in these cells adopting second arch fates. **(D)** Transplanted *Hox*-negative cells can form *Hox*-positive derivates. **(E)** However, *Hox*-positive cells transplanted to PA1 cannot form the jaw. **(F)** Jawless organisms such as lampreys retain *Hox* expression in PA1. fb, forebrain; mb, midbrain; mes, mesencephalon; PA1–PA3, pharyngeal arches 1–3; r1–r7, rhombomeres 1–7.

Tissue control of facial patterning

The frontonasal prominence and the pharyngeal arches consist of a mesenchymal core--neural crest cells only in the FNP (Tapadia et al. 2005), and predominantly neural crest cells in other structures--surrounded by epithelia, and reciprocal interactions between these tissues provide patterning beyond anterior-posterior patterning by *HOXA2* (Brugmann et al. 2006a). Both the endoderm and facial ectoderm provide patterning and positioning information to neural crest cells to induce them to form the cartilage and bones of the face (Couly et al. 2002, Hu et al. 2003). For instance, a small region of facial ectoderm, termed the FEZ (frontonasal ectodermal zone), consists of juxtaposed expression domains of *fibroblast growth factor 8 (FGF8)* and *sonic hedgehog (SHH)* and demarcates the dorsoventral axis of the upper beak. Ectopic transplantation of the FEZ initiates reprogramming of the underlying neural crest, resulting in duplications of the upper and lower beak, whose polarity is entirely dependent on the orientation of the FEZ (Hu et al. 2003). However, the experiments detailed below demonstrate that while neural crest cells receive positional information from the endoderm and facial ectoderm, they integrate this with the species-specific patterning information they contain.

Neural crest cells and species-specific patterning

Reciprocal transplantations of neural crest cells of the presumptive beak (midbrain and rhombomeres 1 and 2) between ducks and quails have shown that

neural crest cells inherently possess directions for species-specific facial development (Schneider and Helms 2003, Tucker and Lumsden 2004). Transplantation of quail neural crest cells onto a duck host (quck) resulted in a quail beak on a duck body (Figure 1-4C), while duck neural crest cells transplanted onto a quail host (duail) develop into a duck-like bill (Figure 1-4D). This indicates that populations of cranial neural crest cells are able to maintain their own molecular programs. In addition, neural crest cells are able to alter gene expression patterns in non-neural crest host tissues, for instance the egg tooth ("et" in Figure 1-4). This structure is epidermal in origin and used by the bird to crack the egg during hatching; it is thick and rounded in the quail and the quck (Figure 1-4F,G), while it is flat and leathery in the duck and duail (Figure 1-4E,H) (Schneider and Helms 2003). Overall, these experiments suggest that transplanted neural crest cells receive positional clues from the ectoderm and epithelia instructing them to make a beak, and they reply by producing their own type of beak. While they have revealed a cellular origin for species-specific facial morphology, they left unanswered how that patterning information was encoded.

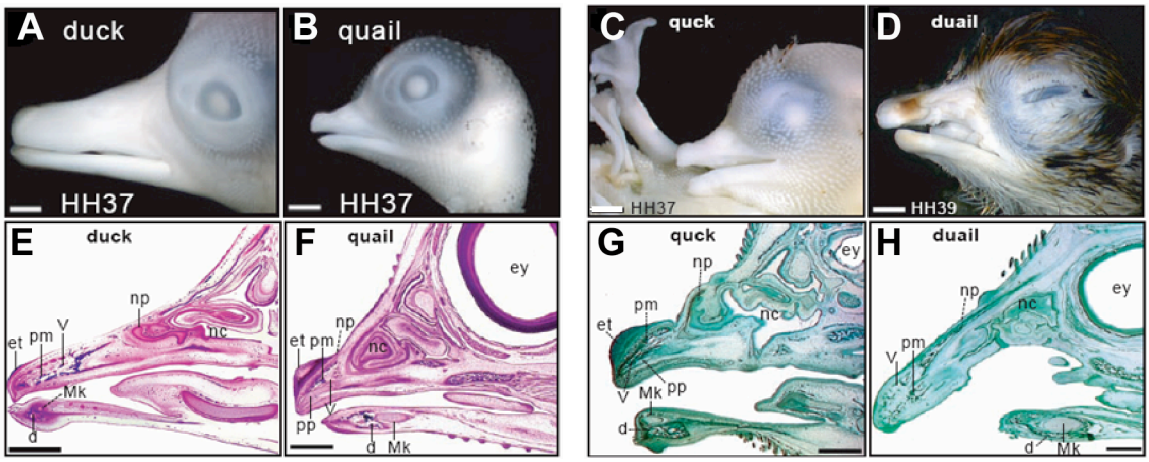

Figure 1-4: Cranial neural crest cells contain species-specific patterning information, adapted from Schneider and Helms (2003). (A) The duck has a broad, flat bill. **(B)** The quail has a narrower, conical bill. **(C)** Quail neural crest cells generate quail-like beaks in duck hosts. **(D)** Duck neural crest cells generate duck-like beaks in quail hosts. **(E-H)** Sagittal sections of embryos from A-D. White scale bar denotes 2 mm (A-D) and black scale bar denotes 1 mm (E-H). ey, orbital region; d, dentary; et, egg tooth; Mk, Meckel's cartilage; nc, nasal capsule; np, nasal passage; pm, premaxilla; pp, prenasal process; v, trigeminal sensory neurons.

Species-specific differences in craniofacial form

Recently, a number of studies have addressed the molecular basis of species-specificity in craniofacial structures. Quantitative trait loci (QTLs) that underlie craniofacial variation have been identified in mice (Cheverud et al. 2004, Ehrich et al. 2003) and baboons (Sherwood et al. 2008). In addition, many studies have centered on a small, East African fish known as the cichlid. In Lake Malawi alone, over 500 unique species of this fish have evolved in the past 1-2 million years (Kocher 2004); diversification of jaw structures contributed significantly to this adaptive radiation (Danley and Kocher 2001). Between 1 and 11 QTLs account for variability in different parts of the cichlid head, including the dentary, premaxilla, and mandible (Albertson et al. 2003, Albertson et al. 2005). *Bone morphogenetic protein 4 (bmp4)* has emerged as one likely candidate

gene. This gene underlies one of the QTL peaks (Albertson et al. 2005), exhibits increased amino acid substitutions in its pro-domain (Terai et al. 2002), and increases cartilage formation in the jaw when over-expressed in zebrafish (Albertson et al. 2005). Further, cDNA microarray approaches identified two additional genes, *cichlid metalloproteinase 1 (cimp1)* and a homolog of *microfibril-associated glycoprotein 4 (magp4)*, that are differentially expressed between cichlid jaws and may contribute to diversity via alterations in the extracellular matrix (Kijimoto et al. 2005, Kobayashi et al. 2006).

BMP4 has also received considerable attention based on studies in Darwin's finches, a set of 14 closely related birds that have become a classic example of adaptive evolution. *BMP4* is expressed at earlier stages and over a larger domain in the mesenchyme of finches with broad beaks (e.g. ground finches such as *Geospiza magnirostris*) than those with narrower beaks (e.g. cactus finches such as *Geospiza scandens*) (Figure 1-5) (Abzhanov et al. 2004). Using a cDNA microarray, it was found that broader beaks also express increased levels of *transforming growth factor beta receptor II (TGFBR2),* the Wnt inhibitor *dickkopf homolog 3 (DKK3),* and *β-catenin (CTNNB1)* (Mallarino et al. 2011), while *calmodulin 1 (CALM1)* expression associates with a narrower beak shape (Figure 1-5) (Abzhanov et al. 2006). Further, *BMP4* has increased expression in the wide-billed duck compared to the conical beak of the chicken, and correlates with differential regions of proliferation to influence depth, width, and curvature of the beak (Wu P. et al. 2004, Wu P. et al. 2006). While these

studies implicate Calmodulin, TGFβ, and Wnt signaling in differential facial shapes and provide valuable insight into the molecular basis of morphological variation, we are only just beginning to identify the gene expression changes that control species-specificity of cranial neural crest cells. Additionally, these studies were conducted after morphological variation is evident (Abzhanov et al. 2004, Abzhanov et al. 2006, Brugmann et al. 2010, Wu P. et al. 2004, Wu P. et al. 2006) and did not resolve what upstream regulators might be responsible for regulating differential *β-catenin, BMP4, Calmodulin, DKK3,* and *TGFBR2* expression.

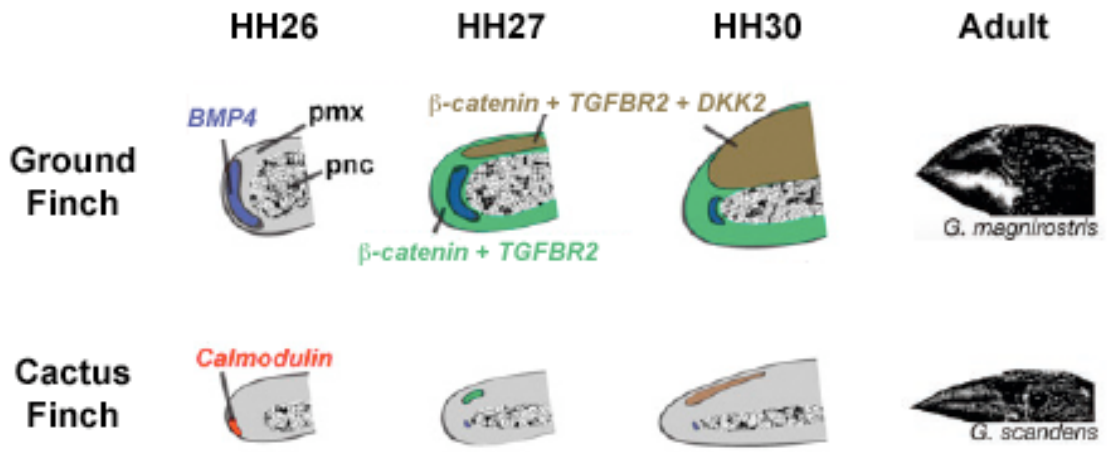

Figure 1-5: Species-specific gene expression patterns in Darwin's finches, modified from Abzhanov et al. (2004) and Mallarino et al. (2011). The ground finch (e.g. *Geospiza magnirostris*) shows earlier and broader expression of *BMP4, TGFBR2, β-catenin*, and *DKK3* and develops a broad beak, whereas the cactus finch (e.g. *Geospiza scandens*) shows increased expression of *Calmodulin* and develops an elongated beak. pmx, premaxilla; pnc, prenasal cartilage.

microRNAs in facial development

An additional level of gene regulation is controlled by microRNAs (miRNAs), 19-25 nucleotide-long RNAs that affect gene expression via mRNA

degradation or translational inhibition. These short RNAs have been implicated in a wide range of regulatory roles in development and differentiation, including cellular proliferation, migration, differentiation, apoptosis, and epithelial-mesenchymal transitions (all of which also occur in the developing face) (Stefani and Slack 2008). Like transcription factors, miRNAs regulate hundreds of target genes, and they do so by specifically (but imperfectly) binding the 3' UTR of gene transcripts (Hobert 2008). miRNAs are thought to function during development to confer robustness by repressing leaky transcription (Hornstein and Shomron 2006), fine tuning gene expression levels to optimal ranges (Cohen et al. 2006, Hornstein and Shomron 2006, Wu C. I. et al. 2009), sharpening spatial and temporal expression patterns (Levine E. et al. 2007), and acting as a "clean-up" mechanism to avoid formation of a mixed developmental fate (Giraldez et al. 2006). Intriguingly, miRNAs may have a role in species-specific diversification as well. While humans (Chen and Rajewsky 2006) and mice (Hiard et al. 2010) show negative selection against mutations that destroy conserved miRNA binding sites, the morphologically divergent cichlids of Lake Malawi have increased levels of polymorphism in predicted miRNA binding sites within 3' UTRs (Loh et al. 2011). However, the divergence times within these lineages vary drastically-- approximately 370,000 years for humans (Noonan et al. 2006), 23 million years for mice (Adkins et al. 2001), and 1-2 million years for cichlids (Kocher 2004).

MicroRNAs also appear to be essential for normal facial development. Conditional knockout of the miRNA processing gene *Dicer1* in *Wnt1*-expressing tissues (which include the neural crest [NC]) results in severe craniofacial malformations in mice due to nearly complete ablation of all crest-derived facial bones (Figure 1-6) (Huang et al. 2010, Zehir et al. 2010). Importantly, NC cells migrate normally in these *Dicer* mutant animals, demonstrating that miRNAs are likely necessary for neural crest survival and differentiation (Zehir et al. 2010). To date, only one miRNA has been correlated with a known function in facial development. miR-140 negatively regulates *platelet derived growth factor receptor alpha (pdgfra)* during palatogenesis in zebrafish, and loss of this miRNA causes cleft palate due a defect in NC migration (Eberhart et al. 2008). Recently, a single nucleotide polymorphism (SNP) that affects the processing of miR-140 has been identified in human cases of nonsyndromic cleft palate (Li et al. 2010), reinforcing how insights gained from model systems can be readily translated to human biology. While some of the microRNAs expressed during facial development are known (Eberhart et al. 2008, Mukhopadhyay et al. 2010), the potential roles of microRNAs in facial development and species-specific facial variation are largely unknown.

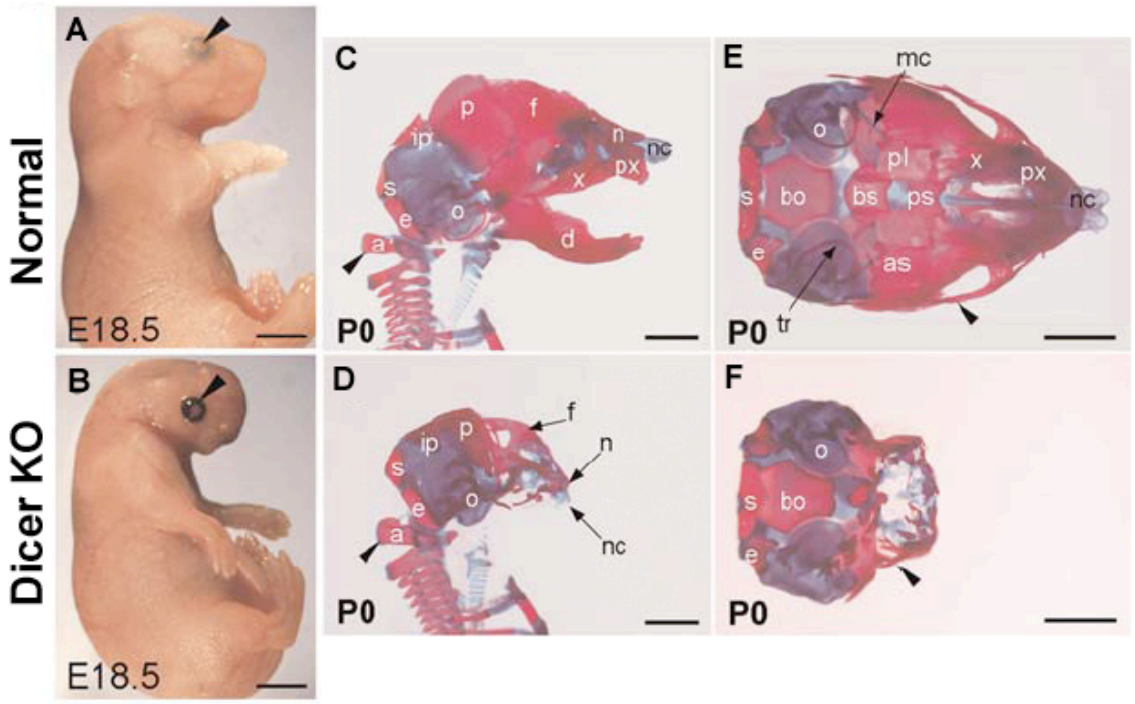

Figure 1-6. Loss of microRNAs result in dramatic craniofacial malformations, adapted from Huang et al. (2010). **(A-B)** Compared to control mice **(A)**, mice with conditional knock-out (CKO) of *DICER* in neural crest cells **(B)** have severe facial abnormalities. **(C-F)** Embryos from **(A-B)** stained with Alizarin Red and Alcian Blue. Scale bar denotes 2 mm. a, atlas; as, alisphenoid; bo, basioccipital; bs, basisphenoid; d, mandible; e, exoccipital; f, frontal; ip, interparietal; n, nasal; nc, nasal capsule; o, otic capsule; p, parietal; pl, palatine; ps, presphenoid; px, premaxilla; s, supraoccipital; x, maxilla.

Future directions

Craniofacial abnormalities are among the most common birth defects, accounting for approximately one third of congenital abnormalities (Dixon et al. 2011). Targeted mutagenesis in animal models such as the mouse have provided important information on the effects of single genes in defects such as cleft lip and/or palate and craniofacial development in general. However, we still lack a comprehensive description of the spectrum of molecular genetic players,

including microRNAs, in vertebrate facial development. We also have only a very rudimentary description of the genes and pathways that underlie species-specific variation in facial structures. Using custom, cross-species microarrays, I first identified the set of transcription factors and developmental signaling pathways that differ in neural crest cells of the embryonic upper beak in chickens, quails, and ducks. I then conducted unbiased deep sequencing to comprehensively analyze the microRNA transcriptome of the samples, in the first large-scale evaluation of miRNA expression in the duck and quail, and the first investigation of the role of miRNAs in species-specific facial development. Finally, I functionally analyzed differentially expressed mRNA and miRNA genes through viral over-expression and Western blots. I further evaluated the application of these data sets as candidate genes to investigate human craniofacial abnormalities. Understanding the molecular mechanisms that control natural craniofacial variation in the avian beak enhances our insights into variations that underlie adaptive evolution, and may serve as a novel source of candidate genes for studies of mammalian craniofacial development.

References

Abzhanov A, Protas M, Grant BR, Grant PR, Tabin CJ. 2004. Bmp4 and morphological variation of beaks in Darwin's finches. Science 305: 1462-1465.

Abzhanov A, Kuo WP, Hartmann C, Grant BR, Grant PR, Tabin CJ. 2006. The calmodulin pathway and evolution of elongated beak morphology in Darwin's finches. Nature 442: 563-567.

Adkins RM, Gelke EL, Rowe D, Honeycutt RL. 2001. Molecular phylogeny and divergence time estimates for major rodent groups: evidence from multiple genes. Mol Biol Evol 18: 777-791.

Albertson RC, Streelman JT, Kocher TD. 2003. Genetic basis of adaptive shape differences in the cichlid head. J Hered 94: 291-301.

Albertson RC, Streelman JT, Kocher TD, Yelick PC. 2005. Integration and evolution of the cichlid mandible: the molecular basis of alternate feeding strategies. Proc Natl Acad Sci U S A 102: 16287-16292.

Brugmann SA, Tapadia MD, Helms JA. 2006a. The molecular origins of species-specific facial pattern. Curr Top Dev Biol 73: 1-42.

Brugmann SA, Kim J, Helms JA. 2006b. Looking different: understanding diversity in facial form. Am J Med Genet A 140: 2521-2529.

Brugmann SA, Powder KE, Young NM, Goodnough LH, Hahn SM, James AW, Helms JA, Lovett M. 2010. Comparative gene expression analysis of avian embryonic facial structures reveals new candidates for human craniofacial disorders. Hum Mol Genet 19: 920-930.

Brugmann SA, Goodnough LH, Gregorieff A, Leucht P, ten Berge D, Fuerer C, Clevers H, Nusse R, Helms JA. 2007. Wnt signaling mediates regional specification in the vertebrate face. Development 134: 3283-3295.

Carroll SB. 2005. Endless Forms Most Beautiful: The New Science of Evo Devo and the Making of the Animal Kingdom. New York: W.W. Norton.

—. 2008. Evo-devo and an expanding evolutionary synthesis: a genetic theory of morphological evolution. Cell 134: 25-36.

Chen K, Rajewsky N. 2006. Natural selection on human microRNA binding sites inferred from SNP data. Nat Genet 38: 1452-1456.

Cheverud JM, Ehrich TH, Vaughn TT, Koreishi SF, Linsey RB, Pletscher LS. 2004. Pleiotropic effects on mandibular morphology II: differential epistasis and genetic variation in morphological integration. J Exp Zool B Mol Dev Evol 302: 424-435.

Clop A, et al. 2006. A mutation creating a potential illegitimate microRNA target site in the myostatin gene affects muscularity in sheep. Nat Genet 38: 813-818.

Cohen SM, Brennecke J, Stark A. 2006. Denoising feedback loops by thresholding--a new role for microRNAs. Genes Dev 20: 2769-2772.

Cohn MJ. 2002. Evolutionary biology: lamprey Hox genes and the origin of jaws. Nature 416: 386-387.

Couly G, Grapin-Botton A, Coltey P, Ruhin B, Le Douarin NM. 1998. Determination of the identity of the derivatives of the cephalic neural crest: incompatibility between Hox gene expression and lower jaw development. Development 125: 3445-3459.

Couly G, Creuzet S, Bennaceur S, Vincent C, Le Douarin NM. 2002. Interactions between Hox-negative cephalic neural crest cells and the foregut endoderm in patterning the facial skeleton in the vertebrate head. Development 129: 1061-1073.

Creuzet S, Couly G, Vincent C, Le Douarin NM. 2002. Negative effect of Hox gene expression on the development of the neural crest-derived facial skeleton. Development 129: 4301-4313.

Danley PD, Kocher TD. 2001. Speciation in rapidly diverging systems: lessons from Lake Malawi. Mol Ecol 10: 1075-1086.

Darwin C. 1859. On the Origins of Species. London: John Murray.

Dixon MJ, Marazita ML, Beaty TH, Murray JC. 2011. Cleft lip and palate: understanding genetic and environmental influences. Nat Rev Genet 12: 167-178.

Eberhart JK, He X, Swartz ME, Yan YL, Song H, Boling TC, Kunerth AK, Walker MB, Kimmel CB, Postlethwait JH. 2008. MicroRNA Mirn140 modulates Pdgf signaling during palatogenesis. Nat Genet 40: 290-298.

Ehrich TH, Vaughn TT, Koreishi SF, Linsey RB, Pletscher LS, Cheverud JM. 2003. Pleiotropic effects on mandibular morphology I. Developmental morphological integration and differential dominance. J Exp Zool B Mol Dev Evol 296: 58-79.

Eizirik E, Yuhki N, Johnson WE, Menotti-Raymond M, Hannah SS, O'Brien SJ. 2003. Molecular genetics and evolution of melanism in the cat family. Curr Biol 13: 448-453.

Ferkowicz MJ, Raff RA. 2001. Wnt gene expression in sea urchin development: heterochronies associated with the evolution of developmental mode. Evol Dev 3: 24-33.

Galant R, Carroll SB. 2002. Evolution of a transcriptional repression domain in an insect Hox protein. Nature 415: 910-913.

Gendron-Maguire M, Mallo M, Zhang M, Gridley T. 1993. Hoxa-2 mutant mice exhibit homeotic transformation of skeletal elements derived from cranial neural crest. Cell 75: 1317-1331.

Gibney ER, Nolan CM. 2010. Epigenetics and gene expression. Heredity 105: 4-13.

Gilbert SF. 2003a. Developmental Biology. Sunderland, MA: Sinauer Associates.

—. 2003b. Opening Darwin's black box: teaching evolution through developmental genetics. Nat Rev Genet 4: 735-741.

Giraldez AJ, Mishima Y, Rihel J, Grocock RJ, Van Dongen S, Inoue K, Enright AJ, Schier AF. 2006. Zebrafish MiR-430 promotes deadenylation and clearance of maternal mRNAs. Science 312: 75-79.

Grammatopoulos GA, Bell E, Toole L, Lumsden A, Tucker AS. 2000. Homeotic transformation of branchial arch identity after Hoxa2 overexpression. Development 127: 5355-5365.

Grimson A, Srivastava M, Fahey B, Woodcroft BJ, Chiang HR, King N, Degnan BM, Rokhsar DS, Bartel DP. 2008. Early origins and evolution of microRNAs and Piwi-interacting RNAs in animals. Nature 455: 1193-1197.

Hamburger V, Hamilton HL. 1951. A Series of Normal Stages in the Development of the Chick Embryo. J Morphology 88: 49-92.

Heimberg AM, Sempere LF, Moy VN, Donoghue PC, Peterson KJ. 2008. MicroRNAs and the advent of vertebrate morphological complexity. Proc Natl Acad Sci U S A 105: 2946-2950.

Hertel J, Lindemeyer M, Missal K, Fried C, Tanzer A, Flamm C, Hofacker IL, Stadler PF. 2006. The expansion of the metazoan microRNA repertoire. BMC Genomics 7: 25.

Hiard S, Charlier C, Coppieters W, Georges M, Baurain D. 2010. Patrocles: a database of polymorphic miRNA-mediated gene regulation in vertebrates. Nucleic Acids Res 38: D640-651.

Hobert O. 2008. Gene regulation by transcription factors and microRNAs. Science 319: 1785-1786.

Hornstein E, Shomron N. 2006. Canalization of development by microRNAs. Nat Genet 38 Suppl: S20-24.

Hu D, Marcucio RS, Helms JA. 2003. A zone of frontonasal ectoderm regulates patterning and growth in the face. Development 130: 1749-1758.

Huang T, Liu Y, Huang M, Zhao X, Cheng L. 2010. Wnt1-cre-mediated conditional loss of Dicer results in malformation of the midbrain and cerebellum and failure of neural crest and dopaminergic differentiation in mice. J Mol Cell Biol 2: 152-163.

Hunt P, Gulisano M, Cook M, Sham MH, Faiella A, Wilkinson D, Boncinelli E, Krumlauf R. 1991. A distinct Hox code for the branchial region of the vertebrate head. Nature 353: 861-864.

Irving C, Mason I. 2000. Signalling by FGF8 from the isthmus patterns anterior hindbrain and establishes the anterior limit of Hox gene expression. Development 127: 177-186.

Jacob F. 1977. Evolution and tinkering. Science 196: 1161-1166.

Kijimoto T, Watanabe M, Fujimura K, Nakazawa M, Murakami Y, Kuratani S, Kohara Y, Gojobori T, Okada N. 2005. cimp1, a novel astacin family metalloproteinase gene from East African cichlids, is differentially expressed between species during growth. Mol Biol Evol 22: 1649-1660.

King MC, Wilson AC. 1975. Evolution at two levels in humans and chimpanzees. Science 188: 107-116.

Knecht AK, Bronner-Fraser M. 2002. Induction of the neural crest: a multigene process. Nat Rev Genet 3: 453-461.

Kobayashi N, Watanabe M, Kijimoto T, Fujimura K, Nakazawa M, Ikeo K, Kohara Y, Gojobori T, Okada N. 2006. magp4 gene may contribute to the diversification of cichlid morphs and their speciation. Gene 373: 126-133.

Kocher TD. 2004. Adaptive evolution and explosive speciation: the cichlid fish model. Nat Rev Genet 5: 288-298.

Kontges G, Lumsden A. 1996. Rhombencephalic neural crest segmentation is preserved throughout craniofacial ontogeny. Development 122: 3229-3242.

Kulesa P, Ellies DL, Trainor PA. 2004. Comparative analysis of neural crest cell death, migration, and function during vertebrate embryogenesis. Dev Dyn 229: 14-29.

Larroux C, Luke GN, Koopman P, Rokhsar DS, Shimeld SM, Degnan BM. 2008. Genesis and expansion of metazoan transcription factor gene classes. Mol Biol Evol 25: 980-996.

Le Douarin NM. 2004. The avian embryo as a model to study the development of the neural crest: a long and still ongoing story. Mech Dev 121: 1089-1102.

—. 2008. Developmental patterning deciphered in avian chimeras. Dev Growth Differ 50 Suppl 1: S11-28.

Levine E, McHale P, Levine H. 2007. Small regulatory RNAs may sharpen spatial expression patterns. PLoS Comput Biol 3: e233.

Levine M, Tjian R. 2003. Transcription regulation and animal diversity. Nature 424: 147-151.

Li L, Meng T, Jia Z, Zhu G, Shi B. 2010. Single nucleotide polymorphism associated with nonsyndromic cleft palate influences the processing of miR-140. Am J Med Genet A 152A: 856-862.

Liu W, Sun X, Braut A, Mishina Y, Behringer RR, Mina M, Martin JF. 2005. Distinct functions for Bmp signaling in lip and palate fusion in mice. Development 132: 1453-1461.

Loh YH, Yi SV, Streelman JT. 2011. Evolution of microRNAs and the diversification of species. Genome Biol Evol 3: 55-65.

Lumsden A, Sprawson N, Graham A. 1991. Segmental origin and migration of neural crest cells in the hindbrain region of the chick embryo. Development 113: 1281-1291.

Mallarino R, Grant PR, Grant BR, Herrel A, Kuo WP, Abzhanov A. 2011. Two developmental modules establish 3D beak-shape variation in Darwin's finches. Proc Natl Acad Sci U S A 108: 4057-4062.

Mellott DO, Burke RD. 2008. Divergent roles for Eph and ephrin in avian cranial neural crest. BMC Dev Biol 8: 56.

Merino R, Rodriguez-Leon J, Macias D, Ganan Y, Economides AN, Hurle JM. 1999. The BMP antagonist Gremlin regulates outgrowth, chondrogenesis and programmed cell death in the developing limb. Development 126: 5515-5522.

Mukhopadhyay P, Brock G, Pihur V, Webb C, Pisano MM, Greene RM. 2010. Developmental microRNA expression profiling of murine embryonic orofacial tissue. Birth Defects Res A Clin Mol Teratol 88: 511-534.

Nachman MW, Hoekstra HE, D'Agostino SL. 2003. The genetic basis of adaptive melanism in pocket mice. Proc Natl Acad Sci U S A 100: 5268-5273.

Nichols SA, Dirks W, Pearse JS, King N. 2006. Early evolution of animal cell signaling and adhesion genes. Proc Natl Acad Sci U S A 103: 12451-12456.

Noden DM. 1978. The control of avian cephalic neural crest cytodifferentiation. I. Skeletal and connective tissues. Dev Biol 67: 296-312.

—. 1983. The role of the neural crest in patterning of avian cranial skeletal, connective, and muscle tissues. Dev Biol 96: 144-165.

Noonan JP, et al. 2006. Sequencing and analysis of Neanderthal genomic DNA. Science 314: 1113-1118.

Nozawa M, Miura S, Nei M. 2010. Origins and evolution of microRNA genes in Drosophila species. Genome Biol Evol 2: 180-189.

Parsons KJ, Albertson RC. 2009. Roles for Bmp4 and CaM1 in shaping the jaw: evo-devo and beyond. Annu Rev Genet 43: 369-388.

Pires-daSilva A, Sommer RJ. 2003. The evolution of signalling pathways in animal development. Nat Rev Genet 4: 39-49.

Prochnik SE, Rokhsar DS, Aboobaker AA. 2007. Evidence for a microRNA expansion in the bilaterian ancestor. Dev Genes Evol 217: 73-77.

Richman JM, Lee SH. 2003. About face: signals and genes controlling jaw patterning and identity in vertebrates. Bioessays 25: 554-568.

Rijli FM, Mark M, Lakkaraju S, Dierich A, Dolle P, Chambon P. 1993. A homeotic transformation is generated in the rostral branchial region of the head by disruption of Hoxa-2, which acts as a selector gene. Cell 75: 1333-1349.

Ronshaugen M, McGinnis N, McGinnis W. 2002. Hox protein mutation and macroevolution of the insect body plan. Nature 415: 914-917.

Sauka-Spengler T, Bronner-Fraser M. 2008. A gene regulatory network orchestrates neural crest formation. Nat Rev Mol Cell Biol 9: 557-568.

Schneider RA, Helms JA. 2003. The cellular and molecular origins of beak morphology. Science 299: 565-568.

Sempere LF, Cole CN, McPeek MA, Peterson KJ. 2006. The phylogenetic distribution of metazoan microRNAs: insights into evolutionary complexity and constraint. J Exp Zool B Mol Dev Evol 306: 575-588.

Sherwood RJ, Duren DL, Havill LM, Rogers J, Cox LA, Towne B, Mahaney MC. 2008. A genomewide linkage scan for quantitative trait loci influencing the craniofacial complex in baboons (Papio hamadryas spp.). Genetics 180: 619-628.

Slack JM, Holland PW, Graham CF. 1993. The zootype and the phylotypic stage. Nature 361: 490-492.

Stefani G, Slack FJ. 2008. Small non-coding RNAs in animal development. Nat Rev Mol Cell Biol 9: 219-230.

Suzuki S, et al. 2009. Mutations in BMP4 are associated with subepithelial, microform, and overt cleft lip. Am J Hum Genet 84: 406-411.

Tang T, Kumar S, Shen Y, Lu J, Wu ML, Shi S, Li WH, Wu CI. 2010. Adverse interactions between micro-RNAs and target genes from different species. Proc Natl Acad Sci U S A 107: 12935-12940.

Tapadia MD, Cordero DR, Helms JA. 2005. It's all in your head: new insights into craniofacial development and deformation. J Anat 207: 461-477.

Terai Y, Morikawa N, Okada N. 2002. The evolution of the pro-domain of bone morphogenetic protein 4 (Bmp4) in an explosively speciated lineage of East African cichlid fishes. Mol Biol Evol 19: 1628-1632.

Theron E, Hawkins K, Bermingham E, Ricklefs RE, Mundy NI. 2001. The molecular basis of an avian plumage polymorphism in the wild: a melanocortin-1-receptor point mutation is perfectly associated with the melanic plumage morph of the bananaquit, Coereba flaveola. Curr Biol 11: 550-557.

Tosney KW. 1982. The segregation and early migration of cranial neural crest cells in the avian embryo. Dev Biol 89: 13-24.

Trainor PA, Ariza-McNaughton L, Krumlauf R. 2002. Role of the isthmus and FGFs in resolving the paradox of neural crest plasticity and prepatterning. Science 295: 1288-1291.

Tucker AS, Lumsden A. 2004. Neural crest cells provide species-specific patterning information in the developing branchial skeleton. Evol Dev 6: 32-40.

van Tuinen M, Hedges SB. 2001. Calibration of avian molecular clocks. Mol Biol Evol 18: 206-213.

Wheeler BM, Heimberg AM, Moy VN, Sperling EA, Holstein TW, Heber S, Peterson KJ. 2009. The deep evolution of metazoan microRNAs. Evol Dev 11: 50-68.

Wittkopp PJ, Williams BL, Selegue JE, Carroll SB. 2003. Drosophila pigmentation evolution: divergent genotypes underlying convergent phenotypes. Proc Natl Acad Sci U S A 100: 1808-1813.

Wu CI, Shen Y, Tang T. 2009. Evolution under canalization and the dual roles of microRNAs: a hypothesis. Genome Res 19: 734-743.

Wu P, Jiang TX, Suksaweang S, Widelitz RB, Chuong CM. 2004. Molecular shaping of the beak. Science 305: 1465-1466.

Wu P, Jiang TX, Shen JY, Widelitz RB, Chuong CM. 2006. Morphoregulation of avian beaks: comparative mapping of growth zone activities and morphological evolution. Dev Dyn 235: 1400-1412.

Zehir A, Hua LL, Maska EL, Morikawa Y, Cserjesi P. 2010. Dicer is required for survival of differentiating neural crest cells. Dev Biol 340: 459-467.

CHAPTER 2

Microarray Gene Expression Profiles of Chicken, Quail, and Duck Frontonasal Neural Crest Cells

Introduction

Both mammals and birds exhibit remarkable morphological variation in craniofacial structures, particularly in those derived from the frontonasal prominence (FNP), the structure that forms the upper beak of the bird (Figure 1-1) (Kontges and Lumsden 1996, Noden 1978). Cranial neural crest (NC) cells of the FNP give rise to the facial bones and cartilage in both species (Kontges and Lumsden 1996, Noden 1978), and have been shown in avians to contain molecular information that regulates species-specific facial variation (Schneider and Helms 2003, Tucker and Lumsden 2004). However, these studies did not resolve how that patterning information was actually encoded. Subsequent studies in birds (Abzhanov et al. 2004, Abzhanov et al. 2006, Mallarino et al. 2011, Wu et al. 2004, Wu et al. 2006) and fish (Albertson et al. 2005, Terai et al. 2002) identified two genes involved in regulating species-specific growth of facial prominences. *BMP4* has increased expression levels in Darwin's finches with broad beaks (Abzhanov et al. 2004), while *CALM1* is up-regulated in finches that exhibit an elongated beak morphology (Abzhanov et al. 2006). While these studies demonstrated that modulations in these genes can alter beak morphology, they were conducted after morphological variation is evident and did not clarify whether these genes are initiating morphological changes or whether their expression is simply changing in response to an upstream mediator.

Therefore, I sought to identify the set of transcription factors and signaling molecules that differ during embryonic development of the avian face in three

bird species (chicken, quail, and duck) that exhibit very different facial adaptations than Darwin's finches. My objective was to identify early mediators of species-specific craniofacial morphology, at stages prior to morphological variation and differential *BMP4* and *CALM1* expression, and to identify a set of genes that may play major roles in driving vertebrate facial development and evolution.

For this study, our collaborators first determined when the chicken, quail, and duck begin to demonstrate species-specific morphological differences (Brugmann et al. 2010). Based on these results, I was able to restrict my studies to the embryonic period preceding (HH20) and following (HH25) morphological variation (Figure 1-2), and to the relevant cellular population (the FNP neural crest). I used custom, cross-species microarrays (Hawkins et al. 2003, Hawkins et al. 2007, Messina et al. 2004) to identify the developmental signaling pathway and transcription factor gene expression changes that differ between cranial neural crest cells in the developing beaks of chickens, quails, and ducks. Through a combination of DNA sequencing and BLAST comparisons of known chicken, quail, and duck gene sequences, I determined that sequence divergence is likely not a major source of error in my microarray data. I verified a number of changes in gene expression using RNA *in situ* hybridization and reverse transcription PCR (RT-PCR). Finally, I analyzed gene expression changes in duck and chicken wing buds and hearts to analyze the specificity of the gene expression changes I identified in the developing face.

RESULTS

Cross-species microarray analysis

To identify the differences in expression that may be responsible for the morphological variation between the species, I measured changes in gene expression among frontonasal neural crest samples from three birds (chickens, quails, and ducks) at two different developmental stages. Our collaborators micro-dissected frontonasal neural crest samples both before (HH20) and after (HH25) morphological distinctions between the species are evident (Brugmann et al. 2010). Commercially available chicken microarray gene chips (e.g. Affymetrix) are not suitable for cross-species comparisons, given that they require 100% conservation across probes or are designed to the 3' UTR of genes, which have high divergence rates. Therefore, I utilized a custom, cross-species microarray platform (Hawkins et al. 2007, Messina et al. 2004). In all, expression changes were measured for approximately 2,400 genes, encompassing nearly all known or predicted transcription factors (TFs) (Messina et al. 2004) and developmental signaling pathways (see **Materials and Methods**).

For each species, the early (HH20) was compared to the later (HH25) developmental stage. Stage-matched comparisons were also performed for each pair of bird species at both HH20 and HH25. A minimum of four separate microarray hybridizations (two comparisons and two dye switches) were

conducted for each comparison; for interspecies comparisons, six to nine microarrays were analyzed. A total of 55 array comparisons were conducted for this study. All microarray analysis is described in **Materials and Methods**. To assess the similarity and quality of replicate microarray experiments, I performed unsupervised hierarchical clustering using the dChip software package (Figure 2-1). This analysis showed that replicate microarray chips show a high degree of data reproducibility. For instance, all microarray comparisons of chicken versus quail samples were most similar to each other than they were to any other microarray comparisons.

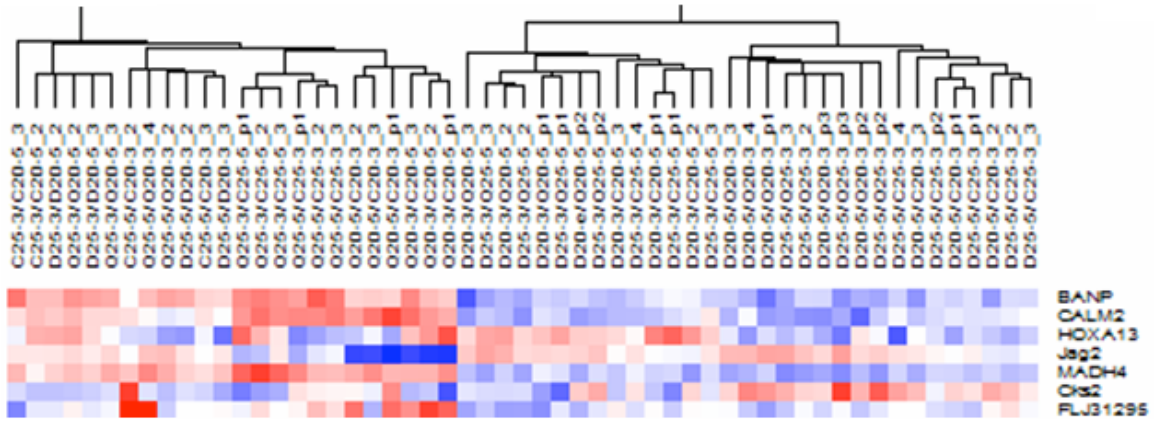

Figure 2-1: Unsupervised hierarchical clustering of microarray comparisons. All 55 microarray comparisons are across the top, connected by a tree representing the similarity of their gene expression patterns. A small sample of genes interrogated is shown on the right.

Differential gene expression among frontonasal neural crest of three avian species

I detected 232 differentially expressed genes in any two-species comparison at either developmental stage (>2-fold change and p-values<0.05; see Figure 2-2 for examples and Table 2-1 for a complete listing). This number is almost certainly an underestimate since it includes only those genes that have clearly identifiable orthologs in the *Gallus gallus* genome (International Chicken Genome Sequencing Consortium 2004). Unfortunately, it appears that approximately 10% of chicken orthologs are still missing from the published genomic DNA sequence (Hawkins et al. 2003, International Chicken Genome Sequencing Consortium 2004). For example, the *Wnt10b* microarray probe, designed from the mouse *Wnt10b* gene, reported a >20-fold increase in transcript levels in duck versus chicken, or duck versus quail, NC cells. However, we could not computationally identify a clear *Wnt10b* ortholog in the chicken genome and thus filtered out data of that type. The 102 genes with unclear orthologs in the *Gallus gallus* genome are listed in Table 2-2, but not discussed in the sections below. Note that full gene names not listed in text or Tables 2-1 and 2-2 can be found at NCBI GEO (http://www.ncbi.nlm.nih.gov/geo/) under accession number GSE11099.

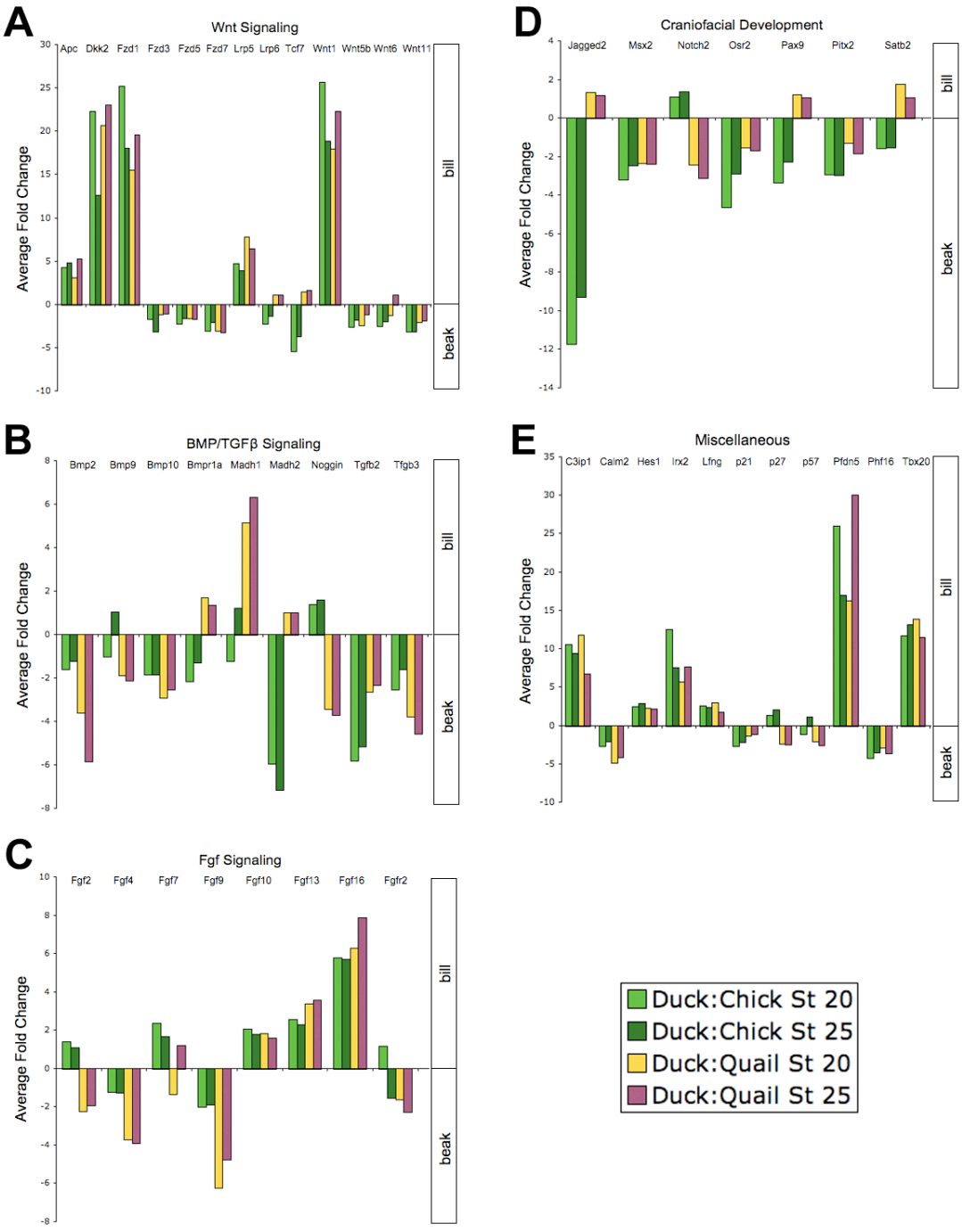

Figure 2-2: Examples of differentially expressed genes. Average relative fold change at HH20 and HH25 between frontonasal neural crest cells of chickens, quails, and ducks for components of **(A)** Wnt signaling, **(B)** the TGF-beta/BMP family, **(C)** FGF pathway, **(D)** genes previously implicated in craniofacial development, and **(E)** miscellaneous genes of interest. Fold changes are expressed as duck relative to chicken or quail, where genes with a negative fold change are expressed at lower levels in the duck versus either chicken or quail. For a complete listing of genes, see Table 2-1.

ProbeID	Description	NCBI Accession Chick	DC HH20 Ave Fold	DC HH20 P-Value	DC HH25 Ave Fold	DC HH25 P-value	DQ HH20 Ave Fold	DQ HH20 P-value	DQ HH25 Ave Fold	DQ H25 P-value	QC HH20 Ave Fold	QC HH20 P-value	QC HH25 Ave Fold	QC HH25 P-value
AEBP2	AE(adipocyte enhancer) - binding protein 2	XM_416415	-2.39	1.7E-03	-2.14	3.3E-04	0.00	0.00	0.00	0.00	-1.55	2.6E-04	-1.60	1.5E-04
ALDH3A2	aldehyde dehydrogenase 3 family, member A2	NM_001006223	0.00	0.00	0.00	0.00	-1.71	5.2E-04	-1.38	2.0E-04	1.97	1.0E-04	1.95	1.8E-03
AMOT	angiomotin	XM_420309	0.59	0.012	0.67	0.012	-0.44	2.1E-03	-0.79	2.5E-03	1.07	5.0E-04	1.12	5.1E-04
ANAPC2	anaphase-promoting complex subunit 2	XM_415533	0.24	0.079	0.39	1.7E-03	-0.45	0.021	-0.08	0.52	0.74	1.3E-03	1.15	7.6E-05
ARC	activity-regulated cytoskeleton-associated protein	NM_204432	-0.82	0.24	-1.14	6.9E-03	-1.14	6.8E-03	-0.25	0.59	-0.05	0.89	-0.91	9.5E-04
ARNT2	aryl-hydrocarbon receptor nuclear translocator 2	XM_413854	-2.13	5.8E-03	-1.60	1.4E-04	-1.83	1.3E-03	-1.71	1.1E-03	-0.45	0.025	-0.35	0.031
ASCL1	achaete-scute complex (Drosophila) homolog-like 1	U01339	-1.01	5.7E-04	-0.94	1.0E-03	0.05	0.74	0.37	0.017	-1.09	4.0E-03	-1.20	0.015
ATF7	activating transcription factor 7	XR_026691	-1.61	3.3E-04	-1.34	8.2E-04	-0.36	0.28	-0.65	7.6E-03	-0.81	8.9E-03	-0.77	0.010
BANP	BTG3 associated nuclear protein	XM_414196	-2.34	5.6E-04	-1.89	1.5E-07	-2.68	1.4E-05	-2.68	7.7E-07	-0.25	0.057	1.05	1.8E-03
BATF	basic leucine zipper transcription factor, ATF-like	XM_421279	1.49	0.016	1.15	3.7E-03	0.91	0.015	1.25	0.011	0.26	0.41	-0.61	8.8E-03
BC052269	zinc finger and BTB domain containing 46 (ZBTB46)	XM_417431	-1.59	6.3E-04	-1.36	2.5E-05	-0.87	0.054	-0.86	4.6E-04	-1.03	1.8E-04	-0.75	1.7E-03
BC052625	zinc finger protein ZNF467	XM_001235894	0.79	9.2E-04	0.68	1.5E-04	1.23	2.2E-06	1.04	3.0E-04	0.00	0.00	0.00	0.00
BCL6B	B-cell CLL/lymphoma 6, member B (zinc finger protein)	NM_001012930	-1.70	8.4E-06	-1.05	6.5E-07	-0.31	0.12	0.28	0.29	-1.36	3.7E-03	-1.00	1.7E-03
Bmp10	bone morphogenetic protein 10	XM_417667	-0.88	0.24	-0.87	0.47	-1.53	0.033	-1.33	0.067	0.43	0.51	-0.18	0.73
Bmp2	bone morphogenetic protein 2	NM_204358	-0.67	0.12	-0.26	0.37	-1.85	2.6E-05	-2.54	1.1E-08	1.44	7.9E-03	1.41	7.6E-05
Bmp9	bone morphogenetic protein 9	NM_205432	-0.01	0.93	0.06	0.51	-0.88	2.8E-03	-1.08	5.4E-04	0.81	4.8E-04	0.80	1.8E-04
Bmpr1a	bone morphogenetic protein receptor, type 1A	NM_205357	-1.10	6.5E-04	-0.33	0.042	0.77	0.15	0.42	0.17	-1.30	2.4E-05	-0.73	0.010
BRD3	bromodomain-containing 3	XM_425330	0.00	0.00	0.00	0.00	-2.71	1.7E-05	-3.07	4.8E-05	2.33	1.5E-03	2.48	3.9E-04

ProbeID	Description	NCBI Accession Chick	DC HH20 Ave Fold	DC HH20 P-Value	DC HH25 Ave Fold	DC HH25 P-value	DQ HH20 Ave Fold	DQ HH20 P-value	DQ HH25 Ave Fold	DQ H25 P-value	QC HH20 Ave Fold	QC HH20 P-value	QC HH25 Ave Fold	QC HH25 P-value
BRD9	bromodomain containing 9	XM_418893	2.38	6.1E-05	2.26	2.1E-05	3.21	4.5E-07	2.94	7.1E-05	-1.15	4.2E-03	-1.13	8.8E-04
BS69	adenovirus 5 E1A binding protein (ZMYND11)	XM_418557	1.40	6.1E-04	0.51	0.053	0.45	0.16	0.37	6.9E-03	-0.52	0.20	0.05	0.83
BTF3L2	basic transcription factor 3	XM_423823	1.49	4.9E-04	1.46	3.6E-04	1.07	7.9E-03	1.02	1.3E-04	0.46	0.066	0.75	8.6E-03
BTK	Bruton agammaglobulinemia tyrosine kinase	NM_204233	2.70	6.6E-04	1.96	2.9E-06	2.05	1.7E-06	1.82	1.2E-04	0.11	0.73	0.04	0.81
C3IP1	kelch-like 12 (Drosophila) (KLJL12)	XM_419251	3.40	2.2E-06	3.23	2.8E-07	3.55	1.6E-05	2.75	4.8E-04	0.00	0.00	0.00	0.00
CALM2	calmodulin 2 (phosphorylase kinase, delta)	NM_205005	-1.39	3.7E-04	-1.00	7.0E-04	-2.26	4.6E-05	-2.02	5.5E-06	1.58	2.6E-03	1.54	2.0E-05
CBFA2T3	core-binding factor, runt domain, alpha subunit 2; translocated to, 3	NM_001030580	0.00	0.00	0.00	0.00	-1.85	0.038	-1.98	1.4E-05	2.91	8.7E-03	1.25	0.033
CCNB2	G2/mitotic-specific cyclin B2	NM_001004369	-0.67	4.6E-03	-0.81	6.4E-04	0.46	2.7E-03	0.52	0.017	-1.07	5.3E-04	-1.33	2.7E-03
CCND2_Human	G1/S-specific cyclin D2	NM_204213	-1.26	2.0E-03	-1.35	7.7E-04	0.01	0.97	-0.34	0.022	-1.10	6.6E-03	-0.96	2.3E-03
CDC2	cell division control protein 2	NM_205314	-0.81	0.17	-1.39	3.1E-05	0.05	0.90	0.01	0.91	-0.47	0.037	-1.00	8.4E-04
CDK5	cyclin-dependent kinase 5	CR353821	0.56	0.019	0.63	4.8E-04	-0.04	0.79	-0.45	5.7E-03	0.57	7.5E-03	1.00	1.9E-04
CDKN2C_Chick	cyclin-dependent kinase 6 inhibitor (P18-INK6), cyclin-dependent kinase 4 inhibitor C (P18-INK4C)	XM_426660	-0.83	1.7E-04	-0.69	1.8E-03	1.01	3.0E-03	0.72	3.6E-04	-1.62	3.8E-06	-1.51	2.2E-04
CDKN3	cyclin-dependent kinase inhibitor 3	BX933305	0.68	8.9E-03	0.41	0.014	-0.72	0.16	-0.82	4.7E-03	1.12	7.3E-03	1.30	1.5E-03
CITED2	Cbp/p300-interacting transactivator, with Glu/Asp-rich carboxy-terminal domain, 2	NM_206844	0.31	0.25	0.63	2.4E-03	1.16	0.039	1.04	6.2E-03	-0.12	0.76	0.10	0.63
CKS1B	cyclin-dependent kinases regulatory subunit 1 (CKS-1) (SID1334) (PNAS-16 / PNAS-143)	NM_001112806	0.52	6.2E-03	1.15	8.4E-07	0.56	2.7E-03	0.50	1.5E-05	-0.07	0.47	0.29	2.4E-03

ProbeID	Description	NCBI Accession Chick	DC HH20 Ave Fold	DC HH20 P-Value	DC HH25 Ave Fold	DC HH25 P-value	DQ HH20 Ave Fold	DQ HH20 P-value	DQ HH25 Ave Fold	DQ H25 P-value	QC HH20 Ave Fold	QC HH20 P-value	QC HH25 Ave Fold	QC HH25 P-value
Cks2	cyclin-dependent kinases regulatory subunit 2 (CKS-2)	XM_001231966	-1.26	2.0E-03	2.41	3.4E-05	2.45	2.8E-08	2.51	9.2E-07	0.04	0.91	0.07	0.78
COL5A1	collagen, type V, alpha 1	U39621	-0.78	0.14	0.11	0.43	-1.34	8.9E-06	-0.59	0.12	1.01	0.11	1.10	0.012
CREB3L2	cAMP responsive element binding protein 3-like 2	XM_416356	0.84	6.8E-03	0.86	1.1E-04	1.31	1.2E-05	1.09	1.3E-04	-0.44	0.081	-0.24	0.10
CREBL2	cAMP responsive element binding protein-like 2	XM_001231305	-3.04	1.7E-04	-2.44	8.4E-07	-1.63	4.4E-03	-1.69	2.1E-04	-1.98	1.1E-03	-1.24	1.9E-03
CRIP1	cysteine-rich protein 1 (intestinal)	BX934543	-1.11	0.040	-1.19	9.7E-04	-0.25	0.052	-0.66	0.074	-1.10	2.3E-03	-0.48	3.1E-03
DKK2	dickkopf homolog 2	XM_420494	4.48	1.8E-03	3.65	0.023	4.37	0.045	4.53	6.4E-04	0.00	0.00	0.00	0.00
E2F4	E2F transcription factor 4, p107/p130-binding	XM_001231947	-1.87	1.4E-05	-1.43	8.6E-07	-0.03	0.89	-0.55	4.2E-03	-0.98	0.041	-0.86	1.7E-04
EED	embryonic ectoderm development	NM_001031376	0.30	0.40	-0.10	0.58	-0.72	4.6E-03	-0.72	0.015	1.24	2.9E-03	0.39	0.17
EGR2	early growth response 2	AF291747	0.24	0.39	0.43	0.010	-1.94	4.0E-05	-2.50	3.4E-07	1.61	6.7E-04	1.93	2.7E-04
ELL	elongation factor RNA polymerase II	NM_001012847	1.85	0.054	1.67	0.082	3.17	9.7E-05	3.53	5.9E-03	-1.32	0.017	-1.90	5.2E-04
EOMES	eomesodermin (Xenopus laevis) homolog	XM_426003	0.32	0.40	0.66	0.022	-0.30	0.58	-1.02	0.017	1.56	0.064	1.74	2.0E-04
ETS2	v-ets avian erythroblastosis virus E26 oncogene homolog 2	NM_205312	0.04	0.82	-0.39	4.6E-03	-1.53	2.6E-04	-1.01	9.4E-03	0.77	0.037	0.84	2.0E-04
ETV4	ets variant gene 4 (E1A enhancer-binding protein, E1AF)	XM_418106	-1.09	3.4E-03	-0.17	0.21	0.31	0.045	-0.50	7.8E-05	-1.20	2.1E-05	0.11	0.43
EVI1	ecotropic viral integration site 1	XM_422804	1.13	8.9E-03	0.65	7.6E-04	1.73	3.4E-04	1.93	1.3E-04	-0.68	0.011	-1.03	9.3E-04
FBI1	HIV-1 inducer of short transcripts binding protein; lymphoma related factor	NM_204680	2.13	8.7E-05	2.24	6.2E-07	2.07	3.6E-07	1.69	1.9E-04	0.30	0.40	0.36	0.080
Fgf10	fibroblast growth factor 10	NM_204696	1.04	2.3E-04	0.83	6.5E-05	0.86	3.3E-03	0.65	0.019	0.29	2.7E-03	-0.05	0.49
Fgf13	fibroblast growth factor 13	NM_001001743 XM_420238	1.35	0.020	1.18	6.3E-03	1.75	3.3E-03	1.83	1.4E-06	-0.14	0.46	-0.19	0.29

ProbeID	Description	NCBI Accession Chick	DC HH20 Ave Fold	DC HH20 P-Value	DC HH25 Ave Fold	DC HH25 P-value	DQ HH20 Ave Fold	DQ HH20 P-value	DQ HH25 Ave Fold	DQ H25 P-value	QC HH20 Ave Fold	QC HH20 P-value	QC HH25 Ave Fold	QC HH25 P-value
Fgf16	fibroblast growth factor 16	NM_001044650	2.53	2.4E-05	2.51	1.3E-06	2.65	1.8E-08	2.97	2.5E-09	0.00	0.00	0.00	0.00
Fgf2	fibroblast growth factor 2	NM_205433	0.46	0.022	0.09	0.53	-1.16	8.4E-03	-0.94	0.014	1.85	2.2E-03	1.71	4.6E-04
Fgf4	fibroblast growth factor 4	NM_001031546	-0.27	0.078	-0.31	6.1E-05	-1.89	8.9E-04	-1.96	1.1E-03	1.28	3.8E-03	1.21	7.6E-03
Fgf7	fibroblast growth factor 7	NM_001012525	1.23	1.0E-03	0.73	8.1E-05	-0.39	0.21	0.25	0.16	1.70	8.3E-05	0.67	5.2E-04
Fgf9	fibroblast growth factor 9	NM_204399	-0.98	1.1E-04	-0.89	1.3E-05	-2.64	2.0E-07	-2.24	3.2E-05	1.02	7.9E-05	1.41	7.4E-05
Fgfr2	fibroblast growth factor receptor 2	NM_205319	0.19	0.26	-0.61	2.9E-05	-0.68	5.5E-03	-1.18	1.6E-04	1.09	3.4E-04	0.63	0.025
FLJ10895	cyclin J (CCNJ)	XM_421691	1.00	1.1E-03	0.75	7.3E-05	0.98	7.1E-05	1.04	0.021	-0.25	0.15	-0.40	0.10
FLJ11040	mitochondrial Rho 1 (MIRO-1)	NM_001006208	-0.18	0.24	0.04	0.66	-1.40	5.0E-06	-1.50	2.5E-04	1.33	0.052	1.72	1.1E-03
FLJ11078	kelch-like 26 (Drosophila) (KLJL26)	XM_418239	3.15	1.9E-05	3.25	6.6E-08	2.14	8.8E-09	2.37	1.5E-05	1.08	0.018	1.39	2.7E-03
FLJ12517	jumonji domain containing 4 (JMJD4)	NM_001030959	2.30	2.5E-04	2.02	9.3E-06	2.91	1.0E-05	3.12	5.5E-06	-1.01	0.026	-0.94	0.010
FLJ36155	GLIS family zinc finger 1 (GLIS1)	XM_422485	0.50	3.4E-03	0.33	0.021	-0.78	2.1E-04	-1.24	2.5E-05	1.27	8.8E-05	1.62	6.6E-04
FMR2	fragile X mental retardation 2	XR_027199	0.14	0.48	0.00	1.00	-1.51	3.0E-04	-1.92	3.1E-03	0.97	0.038	2.04	0.023
FOXC2	forkhead box C2 (MFH-1, mesenchyme forkhead 1)	NM_205138	1.01	0.014	0.95	5.8E-07	1.74	1.0E-05	1.54	6.6E-07	-0.68	0.18	-0.25	0.087
FOXO3A	forkhead box O3A	XM_001234495	-1.05	0.016	-1.24	1.6E-04	-0.23	0.31	-0.16	0.65	-0.47	0.19	-1.27	1.7E-03
FREQ	frequenin homolog (Drosophila)	NM_205377	-0.86	7.9E-03	-0.37	2.7E-03	0.65	2.5E-03	0.78	7.6E-04	-1.32	9.7E-05	-1.19	7.1E-05
Fzd1	frizzled homolog 1	NM_001030337	4.65	2.6E-06	4.18	1.1E-08	3.96	2.7E-07	4.29	7.2E-07	0.00	0.00	0.00	0.00
Fzd3	frizzled homolog 3	XM_420029	-0.74	2.0E-03	-1.64	5.7E-06	-0.20	0.39	-0.04	0.85	-0.11	0.79	-1.34	3.1E-03
Fzd5	frizzled homolog 5	AF463494	-1.13	3.8E-04	-0.66	4.2E-04	-0.67	1.7E-03	-0.71	1.3E-04	-0.07	0.67	0.06	0.28
Fzd7	frizzled homolog 7	NM_204221	-1.59	1.3E-03	-1.04	7.1E-05	-1.58	1.0E-05	-1.69	8.9E-04	0.29	0.057	0.68	2.0E-03

ProbeID	Description	NCBI Accession Chick	DC HH20 Ave Fold	DC HH20 P-Value	DC HH25 Ave Fold	DC HH25 P-value	DQ HH20 Ave Fold	DQ HH20 P-value	DQ HH25 Ave Fold	DQ H25 P-value	QC HH20 Ave Fold	QC HH20 P-value	QC HH25 Ave Fold	QC HH25 P-value
GATA6	GATA-binding protein 6	NM_205420	-0.90	0.072	-1.07	5.5E-04	-0.16	0.59	-0.55	0.092	-0.18	0.58	-1.12	9.3E-04
gCDH23	cadherin-related 23 protein (otocadherin)	XM_421595	0.02	0.96	0.08	0.19	-0.77	0.010	-0.88	2.5E-03	0.78	0.038	1.01	4.3E-03
gCLDN14	claudin 14	XM_425552	-1.30	0.020	-0.48	0.011	-0.90	0.012	-1.15	1.6E-03	0.11	0.53	0.68	0.028
GCN5L2	GCN5 (general control of amino-acid synthesis, yeast, homolog)-like 2	NM_204329	0.23	0.051	0.02	0.95	1.97	1.2E-04	1.97	0.020	-1.31	8.1E-04	-1.21	0.037
gCREB3	cAMP responsive element binding protein 3	XM_425893	-1.11	0.022	-0.55	0.12	-0.50	0.095	-0.56	0.065	-0.25	0.45	-0.03	0.91
gGJB5	gap junction protein, beta 5 (connexin 31.1)	XM_425784	1.02	5.8E-03	1.47	1.0E-04	1.18	0.045	1.21	8.4E-03	0.00	0.00	0.00	0.00
gHES1	hairy and enhancer of split 1	NM_204472	1.28	2.8E-03	1.50	7.5E-05	1.17	9.7E-04	1.06	2.4E-03	0.40	0.047	0.57	2.7E-03
gHES5	hairy and enhancer of split 5	NM_001012695	-1.21	0.027	-0.79	8.6E-03	-0.67	0.091	-0.65	0.088	-0.59	0.086	-0.36	0.25
gID3	inhibitor of DNA binding 3	NM_204589	-0.35	0.14	0.16	0.015	-0.89	0.025	-1.04	0.010	0.88	7.0E-03	0.92	4.7E-03
gID4	inhibitor of DNA binding 4	NM_204282	-1.06	0.029	-0.39	0.32	-0.47	0.25	-0.23	0.27	-0.49	0.22	-0.18	0.34
gMADH1	mothers against decapentaplegic homolog 1 (SMAD1)	XM_420428	-0.26	0.55	0.29	0.37	2.36	8.0E-03	2.66	3.9E-04	-2.17	1.6E-03	-2.26	1.0E-03
gNog	noggin	NM_204123	0.46	3.2E-03	0.66	2.6E-05	-1.78	1.7E-04	-1.89	2.7E-05	2.41	1.8E-04	2.42	5.9E-06
gNUP153	nucleoporin 153kDa	XM_418937	-5.11	7.7E-04	-5.17	2.0E-03	0.00	0.00	0.00	0.00	-4.66	1.8E-03	-5.19	3.0E-05
gOSR2	odd-skipped related 2	XM_001234796	-2.20	1.6E-03	-1.52	9.4E-04	-0.61	6.2E-03	-0.72	2.4E-03	-1.58	1.4E-03	-1.41	8.3E-03
GPA33	glycoprotein A33 (transmembrane)	XM_416656	-0.88	5.1E-04	-1.14	3.6E-06	-0.68	0.26	-0.78	4.9E-03	-0.89	0.15	-0.08	0.65
gPAX1	paired box gene 1	U22046	-1.49	0.028	-1.26	1.8E-05	0.41	0.11	0.29	0.12	-1.57	7.8E-03	-1.72	1.2E-03
gPAX9	paired box gene 9	NM_204912	-1.74	0.011	-1.16	5.1E-04	0.25	0.23	0.09	0.66	-1.65	2.3E-03	-1.35	1.3E-03
gPOU4F3	POU domain, class 4, transcription factor 3	NM_204759	-1.25	0.019	-1.31	7.3E-04	-0.49	0.064	-0.70	0.010	-0.55	0.023	-0.63	0.059
GPRC5C	G protein-coupled receptor, family C, group 5 member C	XM_425386	-0.91	5.1E-03	-0.55	0.010	-1.11	5.1E-04	-1.21	3.2E-05	0.37	0.40	0.38	0.10

ProbeID	Description	NCBI Accession Chick	DC HH20 Ave Fold	DC HH20 P-Value	DC HH25 Ave Fold	DC HH25 P-value	DQ HH20 Ave Fold	DQ HH20 P-value	DQ HH25 Ave Fold	DQ H25 P-value	QC HH20 Ave Fold	QC HH20 P-value	QC HH25 Ave Fold	QC HH25 P-value
GTF3C1	general transcription factor IIIC, polypeptide 1 (alpha subunit, 220kD)	XR_027220	2.80	2.4E-04	2.15	3.0E-05	2.31	6.5E-05	2.21	1.1E-04	0.00	0.00	0.00	0.00
gTGFB3	transforming growth factor, beta 3	NM_205454	-1.32	0.14	-0.68	0.11	-1.91	0.030	-2.19	0.017	0.77	0.21	1.18	0.065
HAND1	heart and neural crest derivatives expressed 1	NM_204965	-1.18	5.9E-04	-1.14	2.6E-03	0.35	0.18	0.19	0.27	-1.05	1.1E-04	-1.46	7.7E-05
HEY1	hairy/enhancer-of-split related with YRPW motif 1	XM_425926	-1.34	0.036	-1.06	8.4E-04	-2.08	5.2E-05	-2.84	1.3E-03	0.13	0.52	0.55	2.4E-03
HIC1	hypermethylated in cancer 1	NM_205236	-1.21	2.9E-05	-1.11	7.0E-07	-0.51	0.15	-0.33	0.28	-0.61	0.041	-0.79	7.1E-05
HMG1	high-mobility group box 1 (HMGB1)	NM_204902	0.24	0.13	0.47	1.9E-03	-0.39	9.3E-03	-0.31	0.14	1.27	0.029	0.92	3.0E-03
HMG20A	high-mobility group 20A	NM_001030394	-0.25	0.048	-0.34	0.017	0.58	2.6E-03	0.70	2.5E-04	-0.60	2.0E-04	-1.26	2.4E-03
HMGIC	high mobility group AT-hook 2 (HMGA2)	NM_205001	-1.42	2.2E-03	-0.84	1.4E-03	0.77	3.9E-04	0.71	0.072	-1.10	0.026	-1.50	1.1E-04
HNF1A	transcription factor 1, hepatic	NM_001030668	-0.41	0.18	0.00	0.99	0.47	0.067	0.32	0.059	-1.06	7.3E-03	-0.34	0.048
HNF4A	hepatocyte nuclear factor 4, alpha	NM_001030855	0.00	0.00	0.00	0.00	-2.19	2.5E-07	-2.32	2.3E-06	1.32	0.021	2.27	1.7E-03
HOX11	T-cell leukemia, homeobox 1 (TLX1)	NM_205015	1.47	0.020	1.00	0.032	1.20	6.7E-03	1.33	1.5E-03	0.44	0.23	-0.38	0.38
HOXA3	homeobox A3	NM_204548	0.45	0.42	0.28	0.51	0.58	0.21	1.03	0.021	-0.56	0.37	-0.46	0.24
HOXB6	homeobox B6	BX931212	-1.74	6.0E-04	-1.18	2.5E-06	0.12	0.52	-0.17	0.51	-1.25	6.3E-03	-1.06	4.3E-03
HRIHFB2122	TRIO and F-actin binding protein (TRIOBP or TARA)	XM_416272	-1.55	0.022	-1.16	3.4E-03	-0.10	0.68	-0.03	0.88	-1.55	0.080	-1.94	4.0E-03
HSHPX5	msh homeobox 2	NM_204559	-1.67	5.2E-04	-1.29	2.9E-04	-1.23	1.4E-03	-1.25	0.030	-0.74	6.7E-03	-0.03	0.88
HSPC063	zinc finger and BTB domain containing 44 (ZBTB44)	XM_417873	1.63	3.0E-03	1.61	1.2E-03	2.07	0.013	2.58	6.1E-04	-0.22	0.34	-0.68	7.3E-03
HSPX153	NK1 transcription factor related, locus 1 (Drosophila) (NKX1-1)	XM_001234891	-1.50	0.022	-2.16	9.0E-03	-0.94	0.027	-0.90	0.046	-0.71	0.25	-0.82	0.13
IGFBP3	insulin-like growth factor binding protein 3	EF624351	-0.34	0.57	-0.77	4.9E-03	-0.35	0.020	-0.08	0.59	-1.65	0.037	-0.42	0.16
IRLB	DENN/MADD domain containing 4A (DENND4A)	XM_413911	-1.28	1.4E-03	-0.81	4.1E-04	-1.45	4.2E-04	-1.93	6.1E-05	0.44	0.029	0.85	0.014

ProbeID	Description	NCBI Accession Chick	DC HH20 Ave Fold	DC HH20 P-Value	DC HH25 Ave Fold	DC HH25 P-value	DQ HH20 Ave Fold	DQ HH20 P-value	DQ HH25 Ave Fold	DQ H25 P-value	QC HH20 Ave Fold	QC HH20 P-value	QC HH25 Ave Fold	QC HH25 P-value
IRX2	iroquois homeobox protein 2	NM_001030336	3.64	8.8E-05	2.91	2.3E-05	2.51	1.2E-05	2.93	2.1E-05	0.83	1.5E-03	0.96	4.7E-04
Jag2	jagged 2	XM_001235688	-3.55	2.9E-06	-3.21	1.0E-06	0.40	3.0E-03	0.23	0.14	-3.19	1.1E-06	-3.42	9.5E-06
JUN	v-jun avian sarcoma virus 17 oncogene homolog	NM_001031289	-0.26	0.38	-0.12	0.47	1.02	0.024	1.20	8.9E-04	-0.73	0.071	-0.60	0.079
KCNN2	potassium intermediate/small conductance calcium-activated channel, subfamily N, member 2	NM_204798	0.94	8.8E-04	0.47	9.0E-03	0.69	0.026	1.14	7.6E-04	0.40	0.23	-0.15	0.40
KIAA0130	thyroid hormone receptor-associated protein, 100 kDa (TRAP100)	NM_001031363	-1.34	0.039	-1.09	1.3E-03	-1.52	7.7E-05	-1.36	2.0E-04	0.43	0.021	0.53	0.060
KIAA0161	ubiquitin conjugating enzyme 7 interacting protein 4 (UBCE7IP4)	XM_419938	-0.36	0.37	0.06	0.74	1.75	0.073	1.01	0.018	-1.28	0.019	-1.94	8.7E-03
KIAA0669	TSC22 domain family, member 2 (TSC22D2 or TILZ4)	CR522985	2.15	1.5E-04	2.41	3.5E-07	1.69	2.8E-03	2.63	6.4E-05	1.29	0.055	0.61	0.14
KIAA0952	BTB (POZ) domain containing 3 (BTBD3)	XM_425262	1.77	1.2E-04	1.61	4.7E-05	1.82	1.2E-03	1.44	2.8E-05	0.89	3.9E-04	0.76	3.2E-03
KIAA1076	SET domain containing 1B (SETD1B)	NM_001030661	-1.00	3.4E-04	-0.67	3.6E-05	-1.12	6.3E-05	-1.54	1.4E-04	0.33	1.9E-03	1.38	1.8E-05
KIAA1172	splicing factor, arginine/serine-rich 15 (SFRS15) (pre-mRNA splicing SR protein rA4)	NM_001012822	0.58	0.22	0.43	0.075	1.20	1.8E-04	0.71	0.058	-0.15	0.63	-0.59	0.054
KIAA1190	zinc finger and BTB domain containing 47 (ZBTB47)	XM_425959	-0.28	0.27	0.65	2.1E-04	1.01	1.6E-03	1.04	6.2E-06	-0.17	0.82	-0.24	0.089
KIAA1388	zinc finger protein ZNF319	XM_425100	-1.13	2.0E-04	-1.10	1.5E-05	-1.33	9.9E-09	-1.43	3.4E-05	0.31	0.17	0.45	0.026
KLF13	Kruppel-like factor 13	XM_425065	1.79	9.3E-03	2.98	2.9E-03	2.62	2.9E-08	2.73	1.1E-04	0.00	0.00	0.00	0.00
KRT12	keratin 12 (Meesmann corneal dystrophy)	XM_425874	-1.58	0.012	-1.84	2.2E-07	-0.02	0.89	0.02	0.84	-1.67	8.5E-05	-1.80	3.1E-04
Lfng	lunatic fringe gene homolog	NM_204948	1.37	4.7E-03	1.23	5.8E-04	1.55	8.6E-04	0.82	0.074	-0.21	0.23	0.47	0.10
LMO1	LIM domain only 1 (rhombotin 1)	XM_420991	-0.95	1.0E-03	-0.69	7.9E-04	-0.22	0.26	-0.06	0.75	-1.25	2.3E-05	-0.53	6.9E-03

ProbeID	Description	NCBI Accession Chick	DC HH20 Ave Fold	DC HH20 P-Value	DC HH25 Ave Fold	DC HH25 P-value	DQ HH20 Ave Fold	DQ HH20 P-value	DQ HH25 Ave Fold	DQ H25 P-value	QC HH20 Ave Fold	QC HH20 P-value	QC HH25 Ave Fold	QC HH25 P-value
LOC152485	zinc finger protein ZNF827	XM_420430	-1.61	3.9E-03	-2.48	1.1E-05	0.11	0.79	-0.53	0.079	-1.99	4.9E-05	-2.26	3.1E-05
LOC168850	zinc finger protein ZNF800	XM_415991	-0.70	5.2E-04	-0.72	3.7E-03	0.14	0.45	0.46	0.10	-1.11	7.9E-03	-1.08	4.8E-03
LOC51580	recombining binding protein suppressor of hairless (Drosophila) (RBPSUH)	XM_420752	1.78	5.4E-04	2.75	5.7E-08	2.59	2.1E-05	2.08	8.8E-06	-0.03	0.94	0.43	0.039
LOC51652	vacuolar protein sorting 24 homolog (S. cerevisiae) (VPS24)	XM_420858	-0.44	0.23	-0.62	0.012	-2.66	1.2E-03	-1.59	1.6E-03	1.12	0.023	1.63	3.8E-03
LOC90322	chromobox homolog 7 (CBX7)	XR_027064	-0.73	8.4E-03	-1.15	8.1E-04	0.15	0.17	0.10	0.54	-1.14	2.8E-04	-1.21	2.1E-04
LRP5	low density lipoprotein receptor-related protein 5	NM_001012897	2.24	1.6E-04	1.95	8.4E-07	2.97	1.2E-05	2.68	2.9E-08	-0.83	0.010	-0.44	0.019
LRP6	Low-density lipoprotein receptor-related protein 6	XM_417286	-1.14	0.027	-0.39	0.12	0.09	0.65	0.15	0.47	-0.50	0.17	-0.77	0.017
LZTR1	leucine-zipper-like transcriptional regulator, 1	XM_419246	1.13	3.4E-04	0.67	0.018	1.07	0.025	0.80	0.039	0.65	0.021	0.19	0.45
LZTS1	leucine zipper, putative tumor suppressor 1	XM_428882	1.25	0.024	0.84	0.028	1.46	7.6E-03	1.39	1.3E-04	-0.63	0.12	-0.01	0.95
MADH2	mothers against decapentaplegic homolog 2 (SMAD2)	NM_204561	-2.57	2.7E-05	-2.83	9.2E-07	0.00	0.00	0.00	0.00	-3.57	8.8E-04	-3.89	4.5E-04
MAFK	v-maf musculoaponeurotic fibrosarcoma oncogene family, protein K (avian)	NM_204756	0.91	6.3E-03	0.57	2.7E-03	1.00	5.3E-03	1.20	0.044	-0.42	0.12	-0.47	0.17
mAPC	adenomatosis polyposis coli	XM_001233410	2.08	0.046	2.26	1.6E-03	1.60	0.057	2.40	0.040	0.25	0.32	0.38	0.12
MEF2A	MADS box transcription enhancer factor 2, polypeptide A (myocyte enhancer factor 2A)	AJ010072	2.41	0.020	3.06	5.2E-04	1.92	0.030	2.14	0.010	0.43	0.042	0.69	0.025
Mfng	manic fringe homolog	XM_416278	-0.53	1.5E-03	-0.39	4.3E-03	0.25	0.017	0.34	0.018	-1.21	1.6E-05	-1.02	5.9E-03
MGC15631	retina and anterior neural fold homeobox like 1 (RAXL1)	NM_204104	2.47	5.6E-03	2.13	5.5E-06	0.89	0.052	0.79	7.7E-03	1.22	2.6E-06	1.15	8.1E-06
MGC16733	integrator complex subunit 4 (INST4)	XM_417220	3.84	2.7E-04	3.45	2.0E-06	3.53	1.2E-06	3.11	1.5E-03	0.00	0.00	0.00	0.00

ProbeID	Description	NCBI Accession Chick	DC HH20 Ave Fold	DC HH20 P-Value	DC HH25 Ave Fold	DC HH25 P-value	DQ HH20 Ave Fold	DQ HH20 P-value	DQ HH25 Ave Fold	DQ H25 P-value	QC HH20 Ave Fold	QC HH20 P-value	QC HH25 Ave Fold	QC HH25 P-value
MID2	midline 2	XM_420134	-2.65	2.5E-05	-2.99	2.1E-07	0.48	0.088	1.06	6.6E-03	-4.44	9.0E-07	-5.28	0.023
MLLT1	myeloid/lymphoid or mixed-lineage leukemia (trithorax (Drosophila) homolog); translocated to, 1	XM_418209	0.30	0.049	0.50	9.9E-04	-1.03	2.0E-04	-1.63	6.4E-05	1.41	7.7E-04	2.11	6.3E-04
MLLT6	myeloid/lymphoid or mixed-lineage leukemia (trithorax (Drosophila) homolog); translocated to 6	XM_418117	-1.83	4.8E-04	-1.50	4.4E-07	-0.44	0.19	-0.97	1.0E-04	-1.04	0.011	-0.53	0.019
MLLT7	forkhead box O4 (FOXO4)	XM_426261	3.39	0.023	2.70	2.9E-05	2.02	2.3E-04	2.82	5.0E-07	0.00	0.00	0.00	0.00
MORF	MYST histone acetyltransferase (monocytic leukemia) 4 (MYST4)	XM_421609	1.17	3.8E-03	0.45	0.19	-0.03	0.92	0.04	0.91	0.88	0.060	0.79	3.7E-03
MORF4	mortality factor 4 like 1 (MORF4L1)	NM_001037173	0.39	3.1E-03	0.26	0.017	-0.34	0.16	-0.49	0.025	1.05	6.9E-04	0.69	2.4E-03
mOSR1	odd-skipped related 1	XM_419967	-0.30	0.38	0.50	0.11	2.64	1.4E-03	2.59	4.7E-04	-2.43	2.4E-03	-2.49	4.9E-04
mPAXIP1L	transcription activation domain interacting protein 1 like	XM_418546	-0.03	0.82	0.38	0.20	1.45	0.023	1.98	7.6E-04	-1.37	0.019	-1.61	3.3E-03
MYCBP	c-myc binding protein	BX933751	0.68	9.0E-03	0.82	0.026	-1.08	0.013	-0.35	0.23	0.96	0.023	0.83	2.0E-04
MYH11	myosin, heavy polypeptide 11, smooth muscle	NM_205274	-1.34	8.1E-04	-1.08	9.9E-04	-1.61	3.1E-05	-1.97	1.1E-04	-0.16	0.63	0.48	0.33
MYNN	myoneurin	XM_001233289	4.30	1.0E-04	3.36	1.9E-05	3.83	5.8E-07	4.76	2.3E-06	0.14	0.27	-0.59	2.9E-03
NAB1	NGFI-A binding protein 1 (EGR1 binding protein 1)	NM_204268	1.83	4.8E-04	1.36	1.9E-05	0.46	0.13	0.57	0.039	1.13	1.8E-03	1.87	5.0E-04
NCOR2	nuclear receptor co-repressor 2	XM_415107	1.33	1.6E-03	1.64	4.4E-06	0.98	1.5E-04	0.44	0.012	0.71	0.41	0.97	1.4E-03
NFE2L2	nuclear factor (erythroid-derived 2)-like 2	NM_205117	2.71	2.5E-06	2.53	2.7E-04	1.98	6.8E-05	1.78	1.3E-04	0.52	0.29	0.73	2.6E-03
NKX6-2	NK6 transcription factor related, locus 2 (Drosophila)	XM_421832	-0.99	0.037	-0.30	0.19	-1.38	9.4E-03	-1.64	3.8E-03	0.38	0.015	0.88	3.7E-03
NKX6A	NK6 transcription factor related, locus 1 (Drosophila)	AF102991	1.31	0.18	1.02	2.5E-04	1.40	9.6E-04	1.16	1.8E-03	-0.01	0.97	-0.35	0.047

ProbeID	Description	NCBI Accession Chick	DC HH20 Ave Fold	DC HH20 P-Value	DC HH25 Ave Fold	DC HH25 P-value	DQ HH20 Ave Fold	DQ HH20 P-value	DQ HH25 Ave Fold	DQ H25 P-value	QC HH20 Ave Fold	QC HH20 P-value	QC HH25 Ave Fold	QC HH25 P-value
Notch2	Notch gene homolog 2	XM_001233595	0.11	0.60	0.46	0.13	-1.26	5.6E-05	-1.62	1.9E-05	1.02	1.3E-03	1.17	4.9E-05
NR1I3	nuclear receptor subfamily 1, group I, member 3	NM_204702	-0.83	0.011	-0.61	6.1E-03	-1.58	4.9E-04	-1.65	7.6E-05	0.82	0.026	1.56	0.020
NR3C2	nuclear receptor subfamily 3, group C, member 2	XM_420437	0.00	0.00	0.00	0.00	-2.68	1.3E-08	-3.36	3.6E-07	2.69	1.4E-04	3.16	7.0E-06
OCT11	POU domain, class 2, transcription factor 3 (POU2F3)	XM_425799	0.05	0.90	0.03	0.86	-2.31	2.5E-05	-2.09	3.3E-04	2.19	1.4E-04	2.79	0.018
p21_Chick	cyclin-dependent kinase inhibitor 1	NM_204396	-1.42	2.1E-04	-1.08	8.7E-07	-0.31	0.011	-0.09	0.32	-1.04	1.3E-05	-0.81	2.1E-04
p27KIP1_Chick	cyclin-dependent kinase inhibitor 1B	NM_204256	0.38	0.044	1.04	5.9E-06	-1.20	9.5E-07	-1.28	3.5E-06	1.63	2.1E-04	2.26	5.5E-06
p57KIP2_Chick	cyclin-dependent kinase inhibitor 1C	BM489375	-0.18	0.27	0.10	0.16	-0.98	4.9E-06	-1.34	3.9E-05	0.78	2.3E-03	1.46	6.8E-05
PCMT1	protein-L-isoaspartate (D-aspartate) O-methyltransferase	NM_001031525	0.73	0.16	-0.57	0.079	-3.67	7.2E-06	-2.91	1.0E-04	3.49	6.0E-08	2.47	1.6E-03
PCQAP	PC2 (positive cofactor 2, multiprotein complex) glutamine/Q-rich-associated protein	XM_415235	0.28	0.39	0.22	0.33	-0.34	0.21	-0.40	0.36	1.28	0.017	1.23	5.2E-03
PDEF	SAM pointed domain containing ets transcription factor (SPDEF)	XM_425831	-0.43	6.7E-03	-0.20	0.079	0.13	0.22	0.52	0.055	-1.14	0.023	-1.37	0.067
PFDN5	prefoldin 5	BX931362	4.70	1.4E-04	4.08	7.4E-08	4.02	9.0E-07	4.91	7.7E-06	0.00	0.00	0.00	0.00
PFKL	phosphofructokinase, liver	XM_001232620	2.90	7.8E-05	2.25	3.4E-05	2.45	2.0E-06	2.37	9.1E-05	-0.11	0.34	0.58	0.10
PHF16	PHD finger protein 16	XM_416870	-2.07	5.7E-05	-1.78	3.4E-07	-1.51	3.6E-07	-1.82	6.2E-06	-0.45	5.9E-03	-0.33	5.2E-03
PITX2	paired-like homeodomain transcription factor 2	AF077092	-1.55	1.6E-03	-1.56	1.8E-04	-0.33	0.33	-0.86	5.0E-03	-0.54	0.043	-1.42	2.1E-03
PLTP	phospholipid transfer protein	XM_425722	-1.67	5.4E-03	-1.40	4.9E-03	0.00	0.65	0.90	0.014	-1.62	0.026	-2.30	8.1E-03
POU1F1	POU domain, class 1, transcription factor 1	NM_204319	1.35	0.020	1.33	2.2E-05	-2.18	2.4E-06	-2.37	1.6E-05	3.89	8.3E-04	3.60	3.2E-05
PPARA	peroxisome proliferative activated receptor, alpha	XM_001236111	-1.23	8.5E-03	-0.83	2.3E-04	-1.02	1.9E-03	-1.24	4.4E-05	0.10	0.77	0.55	0.17

ProbeID	Description	NCBI Accession Chick	DC HH20 Ave Fold	DC HH20 P-Value	DC HH25 Ave Fold	DC HH25 P-value	DQ HH20 Ave Fold	DQ HH20 P-value	DQ HH25 Ave Fold	DQ H25 P-value	QC HH20 Ave Fold	QC HH20 P-value	QC HH25 Ave Fold	QC HH25 P-value
PPARBP	peroxisome proliferator activated receptor binding protein	XM_418125	1.25	7.3E-04	1.54	7.0E-05	1.18	5.3E-04	0.65	1.4E-03	-0.13	0.63	0.31	0.22
PRDM12	PR domain containing 12	XM_415465	-1.64	0.12	-0.71	0.086	-0.63	0.27	-1.32	8.2E-03	0.42	0.52	0.10	0.72
PRDM5	PR domain containing 5	XM_420628	-0.20	0.50	0.05	0.68	-1.49	4.6E-05	-2.44	1.8E-05	1.42	0.023	1.15	2.6E-03
PSIP1	PC4 and SFRS1 interacting protein 1	NM_001031610	1.17	7.2E-03	-0.27	0.075	0.94	3.0E-03	1.67	1.2E-04	-0.11	0.72	-2.12	1.7E-04
PSMB4	proteasome (prosome, macropain) subunit, beta type, 4	XM_427542	0.00	0.00	0.00	0.00	-2.73	3.9E-05	-3.30	4.4E-08	2.37	5.1E-04	2.01	3.3E-05
Ptch2	patched homolog 2	AF409095	-0.11	0.12	-0.31	6.9E-03	-1.30	5.1E-04	-1.27	9.2E-04	1.30	1.2E-03	0.93	1.4E-03
PTTG1IP	pituitary tumor-transforming 1 interacting protein	XM_422649	-0.80	2.6E-03	-0.63	6.2E-05	-1.40	2.3E-03	-1.05	3.5E-05	0.50	0.12	0.45	0.031
R32184_3	chromosome 19 open reading frame 6 (C19orf6) (aka aspecific BCL2 ARE-binding protein 1)	XM_418222	-0.07	0.75	-0.21	0.031	1.24	2.4E-03	1.58	1.0E-03	-1.24	4.9E-03	-1.17	0.022
RAI15	retinoic acid induced 15 (aka SMYD family member 5)	NM_001012894	-0.42	0.094	-0.18	0.29	-1.09	4.0E-04	-1.07	1.5E-04	0.83	4.8E-03	1.01	3.6E-03
RALGDS	ral guanine nucleotide dissociation stimulator	XM_425331	-0.84	0.039	-1.20	2.2E-05	-0.23	0.73	1.08	3.2E-03	-1.37	1.2E-03	-1.95	1.7E-04
RAX	retina and anterior neural fold homeobox	XM_001232118	-0.08	0.54	0.34	0.065	1.69	1.5E-06	1.58	4.9E-05	-1.49	8.8E-05	-1.60	2.9E-04
RBBP5	retinoblastoma binding protein 5	NM_001030914	-0.52	0.45	-1.14	0.010	-0.11	0.70	0.17	0.57	-0.55	0.31	-1.46	7.5E-04
RELB	v-rel reticuloendotheliosis viral oncogene homolog B, nuclear factor of kappa light polypeptide gene enhancer in B-cells 3 (avian)	AF029260	-1.28	5.0E-04	-0.55	9.2E-03	-0.51	0.078	-0.85	8.4E-05	0.14	0.59	0.17	0.25
RGC32	response gene to complement 32	XM_417029	0.26	0.24	0.12	0.48	1.50	2.0E-04	0.90	8.5E-05	-1.31	7.1E-04	-1.02	1.2E-04
RIPX	rap2 interacting protein x	XM_001233433	-1.87	3.2E-05	-1.50	1.1E-06	-1.21	1.7E-05	-1.22	4.1E-04	-0.59	0.034	-0.54	0.015
RNF24	ring finger protein 24	CR385827	0.23	0.31	0.10	0.69	-0.72	0.011	-1.26	6.4E-04	0.80	0.056	1.30	0.023

ProbeID	Description	NCBI Accession Chick	DC HH20 Ave Fold	DC HH20 P-Value	DC HH25 Ave Fold	DC HH25 P-value	DQ HH20 Ave Fold	DQ HH20 P-value	DQ HH25 Ave Fold	DQ H25 P-value	QC HH20 Ave Fold	QC HH20 P-value	QC HH25 Ave Fold	QC HH25 P-value
RREB1	ras responsive element binding protein 1	NM_205049	-1.97	0.13	-0.30	3.5E-03	0.99	3.5E-03	0.77	3.7E-03	-1.23	1.5E-04	-1.04	0.013
Rxrg	retinoid X receptor gamma	NM_205294	-0.85	6.1E-04	-0.46	0.066	0.07	0.79	-0.10	0.70	-1.42	2.3E-05	-0.86	4.6E-03
SAFB	scaffold attachment factor B	XM_423726	-0.02	0.96	0.23	0.31	-1.11	1.3E-05	-0.79	0.31	0.19	0.73	0.40	0.53
SATB2	SATB family member 2	XM_421919	-0.64	0.011	-0.58	2.4E-04	0.82	2.6E-04	0.10	0.61	-1.28	8.2E-06	-0.77	2.1E-04
SCA2	spinocerebellar ataxia 2 (olivopontocerebellar ataxia 2, autosomal dominant, ataxin 2)	XM_415169	-1.15	5.0E-06	-0.34	5.0E-03	0.05	0.77	-0.46	0.017	-1.50	1.2E-04	-0.25	3.8E-03
SCML4	sex comb on midleg-like 4	XM_426184	0.59	9.3E-04	0.74	1.9E-04	0.83	0.012	1.14	4.2E-05	-0.24	0.045	-0.17	0.19
SFRS8	splicing factor, arginine/serine-rich 8 (suppressor-of-white-apricot, Drosophila)	XM_415093	-0.83	0.087	-0.94	0.042	-1.28	3.5E-04	-2.18	1.1E-06	0.14	0.56	0.68	0.051
SIAH2	seven in absentia homolog 2 (Drosophila)	XM_426719	-0.38	0.28	-0.78	9.9E-05	-1.15	0.011	-1.24	6.2E-03	1.20	0.024	1.14	1.5E-03
SMARCA2	SWI/SNF related, matrix associated, actin dependent regulator of chromatin, subfamily a, member 2	NM_205139	0.11	0.26	-0.31	0.053	-1.44	7.3E-04	-1.66	1.8E-03	2.08	1.5E-03	1.53	5.6E-03
SMARCA4	SWI/SNF related, matrix associated, actin dependent regulator of chromatin, subfamily a, member 4	NM_205059	1.10	7.1E-04	0.80	1.8E-03	0.53	0.081	0.92	8.4E-03	0.39	0.25	0.08	0.44
SMARCC1	SWI/SNF related, matrix associated, actin dependent regulator of chromatin, subfamily c, member 1	XR_026888	-0.19	0.35	0.14	0.17	-1.40	1.3E-03	-1.30	4.2E-03	0.59	7.1E-03	1.08	8.3E-05
SNAPC4	small nuclear RNA activating complex, polypeptide 4, 190kDa	XM_415416	1.86	2.3E-03	1.38	3.5E-03	1.76	3.0E-03	3.06	1.9E-04	-0.51	0.21	-1.38	1.0E-03
SNAPC5	small nuclear RNA activating complex, polypeptide 5, 19kDa	NM_001007829	2.24	1.2E-03	1.94	4.0E-06	0.83	0.011	1.01	3.1E-03	0.95	9.4E-03	1.15	4.4E-04

ProbeID	Description	NCBI Accession Chick	DC HH20 Ave Fold	DC HH20 P-Value	DC HH25 Ave Fold	DC HH25 P-value	DQ HH20 Ave Fold	DQ HH20 P-value	DQ HH25 Ave Fold	DQ H25 P-value	QC HH20 Ave Fold	QC HH20 P-value	QC HH25 Ave Fold	QC HH25 P-value
SOX10	SRY (sex determining region Y)-box 10	AJ245601	2.56	9.1E-03	1.36	3.0E-04	2.48	0.012	2.35	0.063	0.04	0.94	-0.63	0.013
SOX7	SRY (sex determining region Y)-box 7	XM_001234627	2.20	1.0E-03	1.92	4.6E-04	-0.56	1.3E-03	-0.55	9.9E-05	2.76	8.9E-07	3.02	4.2E-06
SREBF1	sterol regulatory element binding transcription factor 1	AY029224	-0.74	0.27	0.04	0.76	0.04	0.87	-1.04	6.2E-04	0.84	0.093	1.03	6.3E-03
SRF	serum response factor (c-fos serum response element-binding transcription factor)	U50596	-0.11	0.27	0.06	0.43	-1.28	7.2E-04	-1.79	4.4E-03	1.24	5.1E-05	1.38	1.4E-05
STOML1	stomatin (EBP72)-like 1	XR_026998	0.63	0.023	0.67	3.2E-03	2.22	1.0E-05	2.31	4.1E-06	-1.46	2.4E-03	-1.94	4.0E-04
SUPT4H1	suppressor of Ty 4 homolog (S.cerevisiae)	unknown	0.37	0.040	1.08	1.5E-03	1.80	1.8E-04	2.07	2.6E-04	-0.75	0.18	-0.93	6.7E-03
TAF2C2	TAF4b RNA polymerase II, TATA box binding protein (TBP)-associated factor, 105kDa	XM_419170	-0.19	0.77	-0.38	2.1E-03	-2.02	6.3E-06	-1.88	1.3E-04	1.94	4.8E-04	1.52	7.5E-04
TAF3	TAF3 RNA polymerase II, TATA box binding protein (TBP)-associated factor, 140kDa	NM_001030841	3.02	5.8E-04	3.29	1.7E-08	2.40	1.9E-04	2.89	2.5E-04	0.00	0.00	0.00	0.00
TBX2	T-box 2	XM_001235320	1.52	6.7E-03	1.52	1.0E-05	0.16	0.63	0.52	0.018	0.90	0.13	1.18	0.020
TBX20	T-box 20	NM_204144	3.55	1.7E-03	3.72	5.3E-03	3.79	9.8E-04	3.52	1.1E-04	-0.22	0.31	-0.12	0.70
TCEB1	transcription elongation factor B (SIII), polypeptide 1 (15kDa, elongin C)	CR390316	-0.01	0.93	-0.41	2.9E-03	-0.37	0.079	-0.66	0.020	0.04	0.76	1.04	1.9E-03
TCF20	transcription factor 20 (AR1)	XM_416218	-3.36	3.5E-05	-2.64	4.4E-04	0.00	0.00	0.00	0.00	-2.79	3.4E-04	-3.29	6.8E-06
TCF7	transcription factor 7 (T-cell specific, HMG-box)	NM_204547	-2.44	2.6E-03	-1.86	2.1E-05	0.55	0.15	0.70	0.023	-1.91	0.039	-2.24	2.2E-03
TGFB2	transforming growth factor, beta 2	NM_001031045	-2.53	7.5E-03	-2.36	3.3E-07	-1.39	1.7E-03	-1.21	1.6E-05	-0.43	0.086	-0.95	2.5E-04
THBS3	thrombospondin 3	L81165	1.15	4.7E-03	0.35	0.12	1.39	0.010	1.06	6.9E-04	-0.46	0.076	-0.25	0.27
TIEG2	TGFB inducible early growth response 2	XM_419947	-0.50	0.23	-0.69	3.0E-04	-0.77	0.027	-1.04	1.4E-03	0.11	0.73	0.73	1.9E-03

ProbeID	Description	NCBI Accession Chick	DC HH20 Ave Fold	DC HH20 P-Value	DC HH25 Ave Fold	DC HH25 P-value	DQ HH20 Ave Fold	DQ HH20 P-value	DQ HH25 Ave Fold	DQ H25 P-value	QC HH20 Ave Fold	QC HH20 P-value	QC HH25 Ave Fold	QC HH25 P-value
TNRC12	E1A binding protein p400 (EP400)	XM_001234819	-1.45	7.3E-04	-1.21	4.8E-04	0.45	0.14	0.27	0.19	-1.75	2.5E-03	-1.77	3.0E-05
TNRC15	trinucleotide repeat containing 15	XM_422565	1.27	2.2E-03	1.42	7.4E-04	1.36	2.9E-04	1.24	1.9E-05	-0.37	0.030	-0.22	0.13
TRAF4	TNF receptor-associated factor 4	XR_027121	-0.13	0.27	-0.21	0.19	-0.95	6.7E-04	-0.92	6.9E-03	0.97	2.2E-03	1.10	1.8E-03
TRAF5	TNF receptor-associated factor 5	NM_204219	-1.25	2.5E-04	-1.13	4.5E-04	0.00	0.97	0.48	0.085	-1.23	1.3E-03	-1.36	1.5E-03
TRIM9	tripartite motif-containing 9	XM_421468	2.13	1.2E-05	1.65	9.0E-04	1.42	1.8E-03	1.56	3.1E-04	0.72	1.8E-03	0.26	0.12
TRIP11	thyroid hormone receptor interactor 11	XM_421324	2.27	2.1E-04	2.41	1.3E-05	1.86	6.1E-03	1.52	6.4E-04	2.00	0.016	1.35	0.16
WHSC1	Wolf-Hirschhorn syndrome candidate 1	XM_420839	1.50	9.2E-04	1.64	2.5E-05	1.63	1.0E-03	1.84	5.3E-03	0.66	0.052	0.35	0.30
Wnt1	wingless-related MMTV integration site 1	AY753286	4.68	8.5E-07	4.24	7.2E-06	4.17	1.8E-08	4.48	2.4E-07	-0.73	0.031	-0.30	0.18
Wnt11	wingless-related MMTV integration site 11	NM_204784	-1.63	1.8E-04	-1.64	6.2E-05	-1.00	2.6E-03	-0.84	3.7E-03	-0.93	7.9E-04	-0.81	7.5E-03
Wnt5b	wingless-related MMTV integration site 5B	NM_001037269	-1.34	3.8E-03	-0.83	0.28	-1.24	0.24	-0.19	0.43	-0.65	0.22	-0.11	0.69
Wnt6	wingless-related MMTV integration site 6	NM_001007594	-1.32	2.3E-05	-0.97	3.1E-05	-0.29	2.8E-03	0.04	0.46	-1.09	5.7E-05	-1.18	2.0E-04
ZBTB2	zinc finger and BTB domain containing 2	NM_001031070	0.55	0.028	0.25	0.084	1.02	1.3E-03	1.53	4.9E-04	-0.27	0.10	-0.93	1.3E-04
ZFP276	zinc finger protein 276 homolog	XM_414213	0.45	7.5E-04	-0.32	7.0E-05	-1.93	2.0E-06	-2.01	6.6E-05	2.21	4.8E-05	1.15	3.1E-04
ZFPM1	zinc finger protein, multitype 1 (FOG1)	XM_414197	-0.04	0.84	-0.05	0.75	-0.61	0.12	-1.52	6.4E-04	1.04	6.0E-04	1.70	5.0E-05
ZNF384	zinc finger protein 384	NM_001079496	0.20	0.28	0.21	0.093	1.48	4.1E-03	0.96	4.4E-03	-1.03	9.3E-04	-0.56	0.054

Table 2-1: Genes differentially expressed among stage-matched chicken, quail, and duck samples. Average fold changes and p-vales for genes differentially expressed between staged-matched chicken, quail, and duck at HH20 and HH25. Fold changes are log2 scale, with expression in duck relative to chicken or quail (or in quail relative to chicken). For example, a negative number is expressed at a lower level in the duck versus chicken. Highlighted comparisons pass >2-fold change and p-values<0.05 criteria. Comparisons which were below threshold expression levels in both samples are listed with a fold change and p-value of "0.00." ave, average; DC, duck/chicken comparison; DQ, duck/quail comparison; QC, quail/chicken comparison

Probe ID	Description	DC HH20 Ave Fold	DC HH20 P-value	DC HH25 Ave Fold	DC HH25 P-value	DQ HH20 Ave Fold	DQ HH20 P-value	DQ HH25 Ave Fold	DQ HH25 P-value	QC HH20 Ave Fold	QC HH20 P-value	QC HH25 Ave Fold	QC HH25 P-value
AB075831	zinc finger protein ZNF526	0.98	2.3E-04	1.15	1.0E-06	1.12	5.4E-05	0.87	5.2E-05	-0.34	0.044	0.29	5.0E-03
ABT1	activator of basal transcription 1	-1.43	1.3E-03	-1.21	0.015	-0.41	0.30	-0.69	2.9E-04	-1.27	2.3E-03	-1.11	0.031
AI022870	catalytic subunit of DNA polymerase zeta	3.02	8.2E-05	2.63	1.0E-06	2.45	1.8E-07	2.48	4.1E-07	0.34	0.044	0.44	2.7E-03
AK128361	zinc finger protein ZNF615	-1.16	3.9E-04	-1.30	2.5E-06	-1.35	7.9E-06	-1.33	2.3E-05	0.83	7.7E-04	0.06	0.65
ATF5	activating transcription factor 5	-0.47	0.014	-0.59	9.0E-03	-1.17	2.1E-03	-0.89	7.2E-03	1.01	9.1E-03	0.56	0.020
BRD4	bromodomain-containing 4	-1.20	3.4E-03	-0.38	0.020	0.22	0.47	-0.15	0.38	-1.28	3.4E-04	-0.60	4.1E-03
C5orf7	jumonji domain containing 1B (JMJD1B)	-1.45	0.011	-1.16	1.3E-03	-0.41	0.064	-0.33	0.40	-1.25	6.4E-03	-1.45	9.8E-04
CCNB1	G2/mitotic-specific cyclin B1	-0.69	2.0E-03	-1.17	1.3E-03	-0.26	0.45	0.02	0.95	-0.44	7.8E-03	-1.00	0.015
CDKN2D	cyclin-dependent kinase 4 inhibitor D (P19-INK4D)	0.53	0.013	0.60	2.9E-04	-0.24	0.13	-0.68	1.4E-03	0.68	6.7E-03	1.27	8.4E-06
CG9879	CG9879 (fly) homolog	-0.83	0.021	-1.13	7.9E-04	-0.49	0.032	-0.45	4.8E-03	-0.52	0.036	-0.78	8.6E-03
CITED1	Cbp/p300-interacting transactivator, with Glu/Asp-rich carboxy-terminal domain, 1	1.26	0.050	0.92	0.16	1.58	0.036	2.04	5.8E-03	0.46	0.12	0.03	0.93
CL469780	zinc finger protein ZNF364	2.36	0.013	2.34	8.5E-05	1.44	4.1E-03	2.43	3.0E-05	0.34	0.27	0.33	0.17
CNNM1	cyclin M1	0.20	0.40	0.07	0.48	-1.11	3.7E-05	-0.63	3.8E-03	1.24	2.0E-04	1.02	4.6E-04
CREBL1	cAMP responsive element binding protein-like 1	0.00	0.00	0.00	0.00	-1.67	9.6E-05	-1.66	0.021	1.70	2.1E-03	1.36	5.6E-04
DKFZp564D0472	hypothetical protein	-0.85	0.12	-0.17	0.58	-0.36	0.52	-0.80	0.19	0.77	5.9E-03	1.41	6.4E-04
DKFZp686B0797	zinc finger protein ZNF568	0.51	2.9E-03	0.52	2.2E-04	0.85	1.3E-07	1.04	1.0E-05	-0.27	0.022	-0.63	6.8E-04
DUX1-DUX3-DUX5	double homeobox genes 1, 3, and 5 (probe common to all)	0.37	0.14	0.48	5.3E-04	-1.61	2.2E-05	-1.99	2.6E-03	2.21	1.4E-05	1.72	8.1E-04
DUX4	double homeobox, 4	1.11	6.2E-03	0.73	9.0E-03	1.58	5.0E-04	1.59	0.020	-0.39	0.24	-0.37	8.1E-04

Probe ID	Description	DC HH20 Ave Fold	DC HH20 P-value	DC HH25 Ave Fold	DC HH25 P-value	DQ HH20 Ave Fold	DQ HH20 P-value	DQ HH25 Ave Fold	DQ HH25 P-value	QC HH20 Ave Fold	QC HH20 P-value	QC HH25 Ave Fold	QC HH25 P-value
EVX2	even-skipped homeo box homolog 2	4.29	4.5E-05	4.01	3.3E-06	4.61	1.1E-07	4.37	2.8E-08	0.00	0.00	0.00	0.00
Fgf11	fibroblast growth factor 11	-1.30	1.0E-04	-0.52	3.3E-03	-0.56	0.013	-0.43	0.14	-0.48	0.011	0.35	9.2E-03
Fgf17	fibroblast growth factor 17	-1.29	0.015	-0.36	0.031	-1.36	3.1E-06	-1.62	2.1E-06	0.67	2.9E-03	1.21	6.2E-05
Fgf5	fibroblast growth factor 5	-0.46	0.10	-1.00	0.011	-1.10	0.10	-0.89	0.077	0.43	0.41	-1.27	0.012
Fgfr4	fibroblast growth factor receptor 4	-1.32	4.5E-04	-1.45	3.9E-05	-0.38	0.053	-0.07	0.82	-1.14	0.010	-1.11	2.5E-03
FLJ10469	zinc finger protein ZNF334	4.92	4.6E-05	4.73	2.7E-06	3.24	1.7E-03	4.43	1.2E-04	0.17	0.55	-0.56	0.024
FLJ12586	zinc finger protein ZNF329	-0.13	0.39	-0.14	0.22	-1.58	3.3E-04	-1.36	9.2E-04	1.90	7.2E-04	1.27	2.8E-03
FLJ13265	cyclin N-terminal domain containing 2 (CNTD2)	1.28	3.5E-04	0.99	2.3E-04	-0.15	0.077	-0.17	0.021	1.33	1.0E-05	1.29	1.2E-06
FLJ14297	ATP-binding cassette, sub-family A (ABC1), member 10 (ABCA10)	-1.96	3.8E-03	-1.16	4.5E-04	0.55	0.033	0.35	0.013	-1.72	6.1E-04	-2.04	5.3E-05
FLJ14779	zinc finger protein ZNF566	0.08	0.88	-0.19	0.14	-1.67	2.3E-03	-1.47	5.9E-03	1.39	1.4E-03	0.78	0.022
FLJ22059	zinc finger protein ZNF574	-0.13	0.73	-0.62	0.012	-0.72	6.1E-03	-1.23	1.0E-03	0.51	0.064	0.42	0.11
FLJ22301	zinc finger protein ZNF672	0.00	0.00	0.00	0.00	-2.07	1.2E-05	-2.14	2.1E-03	1.26	7.8E-03	2.09	8.5E-05
FLJ23233	zinc finger protein ZNF419	-0.89	0.012	-0.66	1.3E-03	-1.33	2.5E-04	-1.21	3.0E-03	0.49	0.012	0.44	0.12
FLJ30726	zinc finger protein 3 homolog (mouse) (ZFP3)	-0.58	6.2E-03	-0.69	7.2E-04	0.42	9.1E-03	0.60	3.3E-03	-0.97	2.6E-04	-1.57	6.8E-04
FLJ31295	zinc finger protein ZNF641	-2.41	4.3E-04	-2.02	5.0E-05	-3.41	2.1E-06	-3.49	1.7E-07	1.50	0.047	1.77	1.4E-03
FLJ32191	zinc finger protein ZNF420	-0.57	0.026	0.16	0.37	-0.81	3.0E-05	-0.84	1.2E-04	0.54	0.019	1.09	2.0E-05
FLJ34231	zinc finger protein 62 homolog (mouse) (ZFP62)	0.24	0.19	0.68	3.3E-05	-0.38	0.14	-0.90	8.0E-03	0.98	3.7E-04	1.30	5.0E-06
FLJ35863	zinc finger protein ZNF383	-1.28	1.4E-05	-0.73	0.011	0.09	0.82	0.07	0.62	-0.57	0.070	-0.61	0.092
FLJ36666	chromosome 19 open reading frame 25 (C19orf25)	-1.83	2.2E-04	-1.94	3.3E-06	-1.31	3.0E-04	-1.54	1.3E-04	-0.83	4.0E-05	-0.96	2.2E-04
FLJ39963	zinc finger protein ZNF713	0.90	1.5E-03	1.01	6.7E-07	0.26	0.29	0.47	0.13	0.53	1.7E-03	0.73	6.0E-04

Probe ID	Description	DC HH20 Ave Fold	DC HH20 P-value	DC HH25 Ave Fold	DC HH25 P-value	DQ HH20 Ave Fold	DQ HH20 P-value	DQ HH25 Ave Fold	DQ HH25 P-value	QC HH20 Ave Fold	QC HH20 P-value	QC HH25 Ave Fold	QC HH25 P-value
FLJ90396	zinc finger protein ZNF791	1.55	2.5E-04	1.83	4.7E-05	1.69	3.5E-03	2.19	7.3E-05	-0.32	0.15	-0.04	0.77
FOXE3	forkhead box E3	-0.16	0.75	-0.26	0.52	0.59	0.025	1.02	7.0E-03	-0.94	8.9E-04	-0.35	0.094
FOXF2	forkhead box F2	-1.27	0.013	-1.63	1.1E-05	-1.77	2.9E-04	-1.54	4.4E-04	0.33	0.68	0.15	0.57
FOXQ1	forkhead box Q1	-1.70	5.1E-05	-1.52	4.5E-06	0.04	0.77	-0.21	0.044	-1.84	3.5E-05	-1.56	5.1E-04
GSH1	genomic screened homeo box 1 (mouse) homolog	0.58	0.15	0.68	0.027	-0.36	0.27	-1.10	1.8E-03	1.54	5.4E-04	2.13	4.1E-05
GTF2F1	general transcription factor IIF, polypeptide 1 (74kD subunit)	1.76	4.4E-03	0.92	0.016	-1.32	0.010	-2.06	3.6E-03	0.92	0.018	1.00	0.060
GTF2I	general transcription factor II, i	0.47	0.036	0.43	0.12	1.50	3.6E-03	1.65	4.3E-06	-1.40	2.9E-04	-1.14	1.1E-03
HIF3A	hypoxia inducible factor 3, alpha subunit	-1.52	1.1E-04	-1.35	8.6E-05	-0.97	2.0E-03	-0.50	0.037	-0.77	8.2E-04	-0.94	1.9E-03
HOXC9	homeobox C9	-0.74	0.085	-0.77	5.3E-04	-1.29	3.9E-04	-1.12	1.3E-03	1.15	0.014	0.31	0.39
HOXD1	homeobox D1	-1.05	0.042	0.37	0.14	1.54	1.9E-03	1.65	8.8E-05	-1.37	0.051	-0.82	9.4E-03
INSM1	insulinoma-associated 1	-0.51	0.046	-0.33	0.089	-0.59	2.6E-03	-1.12	1.1E-03	0.53	0.026	0.92	2.8E-04
KBTBD7	kelch repeat and BTB (POZ) domain containing 7	2.79	3.1E-03	2.64	3.0E-05	1.76	0.014	3.08	3.4E-07	1.38	1.3E-03	1.21	1.3E-03
KIAA0339	SET domain containing 1A (SETD1A)	-0.54	0.012	-0.77	9.4E-06	-0.81	0.019	-1.09	1.1E-03	0.78	5.2E-04	0.55	3.1E-03
KIAA0543	KIAA0543 gene product	-0.88	0.20	-1.63	5.4E-05	-3.13	1.4E-05	-3.00	3.7E-05	1.07	3.5E-04	1.65	2.2E-05
KIAA0798	zinc finger protein ZNF432	0.56	0.60	0.59	0.42	-0.99	0.10	-1.27	2.2E-03	0.94	0.21	0.86	0.063
KIAA1441	zinc finger protein ZNF687	0.00	0.00	0.00	0.00	-2.16	1.6E-04	-2.32	2.1E-06	2.28	7.7E-05	3.27	3.1E-05
KLF14	Kruppel-like factor 14	2.38	0.016	1.89	7.2E-04	-1.44	0.055	-0.93	0.18	3.07	1.1E-05	3.19	1.0E-06
LISCH7	liver-specific bHLH-Zip transcription factor	0.55	0.021	0.43	8.7E-05	3.17	1.9E-06	3.46	5.7E-07	-2.95	3.0E-06	-3.10	1.2E-06
LOC115468	zinc finger protein ZNF493	0.07	0.56	0.17	0.14	-1.36	1.2E-04	-1.58	3.4E-04	2.19	1.9E-03	1.70	8.4E-05

Probe ID	Description	DC HH20 Ave Fold	DC HH20 P-value	DC HH25 Ave Fold	DC HH25 P-value	DQ HH20 Ave Fold	DQ HH20 P-value	DQ HH25 Ave Fold	DQ HH25 P-value	QC HH20 Ave Fold	QC HH20 P-value	QC HH25 Ave Fold	QC HH25 P-value
LOC51058	zinc finger protein ZNF691	-0.84	1.0E-03	-0.39	0.065	-1.13	0.021	-0.23	0.54	-0.52	0.35	-0.24	0.33
LOC90589	zinc finger protein ZNF625	1.36	1.2E-03	1.12	2.3E-03	1.19	1.5E-05	1.50	1.6E-04	0.33	2.2E-04	0.47	9.1E-04
MADH4	mothers against decapentaplegic homolog 4 (SMAD4)	-2.80	9.1E-05	-2.47	3.6E-07	-2.84	4.1E-07	-3.35	6.3E-06	0.67	0.012	1.55	0.024
MCM7	minichromosome maintenance deficient (S. cerevisiae) 7	-0.85	6.3E-03	-0.71	0.055	0.31	0.34	0.06	0.69	-0.55	0.26	-1.19	0.019
MEF2B	MADS box transcription enhancer factor 2, polypeptide B (myocyte enhancer factor 2B)	1.15	4.8E-03	0.90	6.2E-04	0.61	0.062	1.03	3.6E-05	0.51	0.074	0.34	0.23
MGC4400	zinc finger protein ZNF577	4.38	2.2E-04	4.33	3.3E-08	3.33	3.9E-05	4.47	2.9E-06	0.65	4.5E-03	0.42	0.10
MGC45380	zinc finger protein ZNF545	-1.53	0.045	-2.66	2.7E-05	-1.09	0.018	-0.58	0.24	0.25	0.39	-1.95	6.1E-04
MHC2TA	MHC class II transactivator	0.62	0.016	0.92	4.7E-03	-0.76	0.064	-0.55	0.020	0.42	0.11	1.34	1.1E-04
MTX1	metaxin 1	-0.72	0.018	-0.48	5.6E-04	-2.36	4.9E-05	-1.73	4.3E-04	1.31	7.6E-03	2.19	1.9E-03
NFKBIL1	nuclear factor of kappa light polypeptide gene enhancer in B-cells inhibitor-like 1	-1.37	1.1E-03	-0.99	0.010	0.71	0.066	0.39	0.10	-1.32	0.017	-1.23	0.064
Notch3	Notch gene homolog 3	0.27	0.11	0.36	0.026	-1.04	5.8E-04	-0.94	1.6E-04	1.09	1.0E-03	1.56	5.3E-05
OG2x	NOBOX oogenesis homeobox	3.14	1.5E-04	2.83	2.0E-05	2.77	1.5E-06	3.09	1.4E-05	0.00	0.00	0.00	0.00
OLIG1	oligodendrocyte transcription factor 1	-1.19	0.030	-0.89	4.8E-04	-1.51	9.5E-04	-1.01	2.6E-04	0.58	0.10	0.10	0.69
OLIG2	oligodendrocyte transcription factor 2	-1.65	2.0E-06	-1.23	2.0E-04	-0.43	4.5E-03	-0.57	2.1E-03	-1.23	2.2E-05	-0.45	4.1E-03
PAX8	paired box gene 8	2.13	1.0E-04	2.39	4.6E-03	3.44	4.9E-04	3.99	0.031	-0.48	0.25	-0.89	0.29
PRDM7	PR domain containing 7	0.57	0.019	0.87	1.6E-03	1.55	0.015	1.07	4.2E-03	-0.08	0.80	-0.87	3.0E-03
RELA	v-rel reticuloendotheliosis viral oncogene homolog A, nuclear factor of kappa light polypeptide gene enhancer in B-cells 3, p65 (avian)	1.33	0.038	0.87	3.4E-03	1.50	0.010	1.57	2.3E-03	0.01	0.97	-0.28	0.25

Probe ID	Description	DC HH20 Ave Fold	DC HH20 P-value	DC HH25 Ave Fold	DC HH25 P-value	DQ HH20 Ave Fold	DQ HH20 P-value	DQ HH25 Ave Fold	DQ HH25 P-value	QC HH20 Ave Fold	QC HH20 P-value	QC HH25 Ave Fold	QC HH25 P-value
RORC	RAR-related orphan receptor C	0.25	0.57	-0.05	0.89	-1.97	1.5E-05	-2.66	1.4E-04	2.38	2.6E-03	2.25	7.2E-03
Rxrb	retinoid X receptor beta	-0.11	0.28	0.51	8.8E-04	-1.51	4.5E-06	-1.62	1.8E-06	1.49	5.2E-06	0.54	0.030
SALL3	sal-like 3 (Drosophila)	0.74	0.014	0.81	2.9E-03	0.67	0.014	1.17	0.014	-0.65	0.067	-0.75	0.031
SBB103	ring finger protein RNF41	2.62	4.9E-04	2.11	1.6E-03	2.46	3.4E-06	2.94	1.2E-05	-1.38	0.041	-0.74	0.16
SP100	nuclear antigen Sp100	0.89	0.035	1.13	1.3E-03	0.96	0.010	1.22	6.5E-04	-0.21	0.11	0.00	0.98
SZF1	KRAB-zinc finger protein SZF1-1	0.64	4.1E-03	0.23	0.038	-0.74	0.028	-1.26	4.7E-04	1.26	1.6E-04	1.28	6.3E-03
TAF2H	TAF10 RNA polymerase II, TATA box binding protein (TBP)-associated factor, 30kDa	0.04	0.94	-0.31	0.033	-0.54	0.019	-1.07	4.6E-06	0.59	0.080	0.55	2.8E-03
TRIM	T cell receptor associated transmembrane adaptor 1	-1.03	0.38	-1.33	0.068	-2.78	6.4E-04	-2.05	0.014	1.16	0.074	0.89	0.17
TRIM4	tripartite motif-containing 4	-1.42	4.8E-03	-0.99	3.5E-03	-0.50	0.043	-0.61	0.010	-0.45	0.065	0.02	0.88
VAV1	vav 1 oncogene	3.81	3.1E-04	3.90	2.7E-04	2.68	8.5E-03	3.59	5.5E-04	0.07	0.85	0.28	0.30
Wnt10b	wingless related MMTV integration site 10b	3.72	3.0E-03	3.75	1.3E-05	5.01	1.7E-03	4.98	1.7E-04	0.00	0.00	0.00	0.00
ZBTB4	zinc finger and BTB domain containing 4	0.00	0.00	0.00	0.00	-2.63	7.6E-04	-2.33	3.0E-05	1.68	1.4E-03	2.36	2.4E-05
ZFD25	zinc finger protein (ZFD25)	-0.52	0.075	-1.00	1.4E-04	-1.11	6.3E-05	-0.81	1.0E-03	0.59	0.010	-0.29	2.6E-03
ZFP1	zinc finger protein 1 homolog	1.33	0.016	2.15	1.4E-05	1.84	8.5E-03	1.92	2.1E-03	-0.33	0.037	0.67	0.032
ZIC5	zinc finger protein of the cerebellum 5	-1.89	8.9E-05	-1.33	2.5E-05	0.34	0.19	0.49	7.4E-03	-2.45	5.9E-06	-2.05	1.5E-04
ZNF12	zinc finger protein 12 (KOX 3)	-0.49	0.30	-0.02	0.93	-1.01	3.0E-03	-1.19	2.2E-03	0.77	0.052	0.89	4.9E-03
ZNF2	zinc finger protein 2 (A1-5)	-3.69	6.3E-06	-4.05	3.7E-09	0.00	0.00	0.00	0.00	-3.36	4.6E-07	-4.21	2.7E-07
ZNF21	zinc finger protein ZNF182	-1.12	0.040	-0.93	0.021	-1.46	1.8E-04	-1.71	1.3E-03	0.54	0.017	1.01	0.022
ZNF211	zinc finger protein 211	0.88	5.5E-03	1.31	2.1E-05	1.37	7.0E-03	2.23	1.7E-04	-0.59	0.27	-0.83	0.023

Probe ID	Description	DC HH20 Ave Fold	DC HH20 P-value	DC HH25 Ave Fold	DC HH25 P-value	DQ HH20 Ave Fold	DQ HH20 P-value	DQ HH25 Ave Fold	DQ HH25 P-value	QC HH20 Ave Fold	QC HH20 P-value	QC HH25 Ave Fold	QC HH25 P-value
ZNF223	zinc finger protein 223	-0.95	1.1E-03	-0.74	3.0E-05	-0.21	0.15	-0.10	0.55	-1.09	1.2E-04	-0.72	2.5E-03
ZNF31	zinc finger protein 31 (KOX 29)	3.37	3.3E-03	2.80	3.5E-04	3.67	6.4E-05	4.27	1.2E-03	-0.83	0.049	-0.10	0.77
ZNF323	zinc finger protein 323	-0.42	0.015	-0.19	0.10	-1.39	7.5E-06	-1.35	5.6E-05	0.88	2.3E-04	1.30	1.4E-04
ZNF42	zinc finger protein 42 (myeloid-specific retinoic acid-responsive)	-0.08	0.80	-0.53	7.6E-03	-1.16	5.7E-04	-1.72	6.6E-05	1.64	5.2E-04	1.39	2.5E-04
ZNF426	zinc finger protein 426	-1.79	4.2E-04	-2.07	1.2E-06	-1.67	1.8E-04	-1.31	1.6E-04	-0.57	6.2E-03	-1.38	1.0E-04
ZNF433	zinc finger protein 433	-0.75	4.5E-03	-1.40	2.2E-06	-1.07	1.9E-05	-1.16	0.010	-0.05	0.51	-0.47	0.012
ZNF495	zinc finger protein 495	-0.41	4.9E-03	-0.12	0.59	-1.69	2.9E-05	-1.55	2.5E-05	1.22	7.3E-04	1.28	3.1E-04
ZNF496	zinc finger protein 496	-0.39	0.041	-0.59	4.1E-03	-1.57	3.8E-05	-1.32	8.9E-03	0.55	6.4E-03	0.44	0.046
ZNF514	zinc finger protein 514	0.77	3.8E-04	0.92	2.7E-04	-0.77	3.1E-04	-0.89	3.9E-03	1.64	1.9E-05	1.76	2.0E-05

Table 2-2: Genes differentially expressed with unclear orthologs in the chicken genome. Data are presented as in Table 2-1.

Species-specific patterns can be defined for these differentially expressed genes (Table 2-3). For instance, 65 of the 232 genes with known orthologs are expressed at higher levels in NC cells of the duck than in NC cells from either the chicken or the quail in at least one (though generally at both) of the developmental stages. The largest group of genes, and those with the largest fold changes, are differentially expressed in the morphologically distinct duck compared to either the chicken or the quail. One notable exception to this is the gene with the largest fold change. The nucleoporin gene *NUP153* encodes a nuclear pore complex subunit and is expressed 36-fold higher in chicken NC compared to quail NC. This gene product is involved with mitosis and shuttles a transducer for TGFβ signaling (Mackay et al. 2009, Xu et al. 2002), which has a number of changes in expression in birds (Figure 2-2, Table 2-1 and Table 2-2, and see below).

Overall trend	Number of genes with known orthologs	Number of genes with unknown orthologs
Up-regulated Chicken	53	18
Down-regulated Chicken	8	6
Up-regulated Duck	65	25
Down-regulated Duck	32	19
Up-regulated Quail	55	30
Down-regulated Quail	19	4

Table 2-3: Trends of differentially expressed genes.

The differentially expressed genes can also be classified into functional categories based on their described functions in NCBI (Table 2-4). Of the 232 genes with know orthologs, 37 genes (16%) are members of the Fgf, Notch,

Tgfβ, and Wnt signaling pathways and an additional 20 genes (9%) have been previously implicated in craniofacial development. I also identified 140 genes that were not previously known to be expressed in the developing face; 115 of these have a described function in another developmental system, but 25 transcription factors have, as yet, unknown functions (Table 2-4).

Functional Group	Number of genes with known orthologs	Number of genes with unknown orthologs
Cell cycle	15	3
Chromatin modification or polycomb	9	2
Craniofacial development	20	5
Fgf signaling	8	4
General transcription factor	11	4
Notch signaling	7	1
TGFβ/BMP signaling	9	1
Wnt signaling	13	1
Not previously implicated in craniofacial development	115	42
Unknown function	25	39

Table 2-4: Functional categories of differentially expressed genes.

Assessing divergence as a source of false positives

In this study I used three species of birds that diverged approximately 90 million years ago (MYA) (van Tuinen and Hedges 2001). While the oligonucleotides on the cross-species microarray have been shown to accurately report in the chicken (Hawkins et al. 2003, Hawkins et al. 2007), it is possible that evolutionary divergence between the chicken, quail, and duck could contribute to false positives in the data set due to varying degrees of sequence homology with the probes on the microarray. This might be expected to manifest itself as higher

chicken signals relative to duck, due to more extensive base pairing. In other words, microarrays cannot distinguish between a transcript that is not expressed and one in which the sequence has diverged enough in duck or quail so it no longer hybridizes to the microarray probe. To address this issue, I first analyzed quail and duck sequences that have been deposited in the NCBI GenBank database (http://www.ncbi.nlm.nih.gov/genbank/) using BLAST. I found that duck and quail sequences are well conserved to chicken transcripts--92.6% and 95.8% average identity, respectively (Table 2-5). It is not surprising that the quail has a slightly higher sequence conservation to chicken given that these two species diverged from each other 38.8 MYA, while both diverged from the duck 89.8 MYA (van Tuinen and Hedges 2001). Further, I found that the duck and chicken have an equal degree of sequence divergence from human--73.0% and 72.7%, respectively (Table 2-5)—and these values agree with homology estimates across the entire chicken genome (70-75%) (International Chicken Genome Sequencing Consortium 2004).

Species comparison	Total sequence analyzed (kbp)	Average sequence identity	Range of sequence identity
Duck vs Chicken	25.9	92.6%	82.2% to 100%
Quail vs Chicken	37.4	95.8%	92.1% to 98.5%
Duck vs Human	5.6	73.0%	67.8% to 89.3%
Quail vs Human	12.0	72.7%	64.1% to 85.4%

Table 2-5: Sequence identity of NCBI GenBank entries. Summary of BLAST analysis of chicken, duck, quail, and human GenBank sequences.

To directly address whether sequence identity between the species may be causing false positives in the microarray data set, I DNA sequenced selected cDNA segments from regions that include microarray probe targets for duck and quail. These sequences were then aligned to the reference chicken genome using BLAST. This analysis was conducted for five genes—*CALM2* (quail only), *OSR1, SATB2, TCEA2,* and *TGFB2*—all of which showed higher gene expression in NC cells of the chicken than those of the duck by cross-species microarray analysis, and were thus potential false positives. In total, 953bp of duck and 778bp of quail were sequenced and had overall sequence identity to the chicken genome of 96.7% and 98.7%, respectively. In regions where the 50-70mer microarray probes align, there were at most one or two base pair changes. As this is not enough to appreciably affect target hybridization under the conditions I employed (see **Materials and Methods**), I conclude that sequence divergence is most probably not a major source of error in our microarray data.

Minimal changes in gene expression between HH20 and HH25

I first compared HH20 to HH25 neural crest samples within each species to measure temporal differences in TF expression between stages that exhibit substantial morphological changes (Figure 1-2). In general, I found only minimal changes in gene expression between HH20 and HH25 for all three species. Ten genes were differentially expressed by >1.5-fold, but only one of these genes

(the transcriptional coactivator *PSIP1*) had more than a 1.7-fold change between the two developmental stages (Table 2-6). These data indicate that, at least for the ~2,400 genes measured on our array, the species-specific genetic program for frontonasal mesenchyme was established by HH20, prior to visible morphological variations. This genetic program is then largely maintained through HH25, when morphological variations are evident. Thus, frontonasal mesenchymal cells show dramatic, species-specific changes in gene expression and importantly, these changes predate any species-specific variation in facial morphology.

ProbeID	Description	NCBI Accession Chick	Chick HH25/HH20 Ave Fold	Chick HH25/HH20 Pvalue	Duck HH25/HH20 Ave Fold	Duck HH25/HH20 Pvalue	Quail HH25/HH20 Ave Fold	Quail HH25/HH20 Pvalue
CDK5RAP1	CDK5 regulatory subunit associated protein 1	XM_417464	-0.61	4.4E-03	0.00	0.98	-0.21	0.29
ETV4	ets variant gene 4 (E1A enhancer-binding protein, E1AF)	XM_418106	-0.88	0.023	0.00	0.99	0.62	0.048
FMR2	fragile X mental retardation 2	XR_027199	-0.06	0.20	-0.18	0.23	0.73	9.8E-04
HOXB6	homeobox B6	BX931212	-0.27	0.43	-0.66	7.1E-03	-0.17	0.34
JUN	v-jun avian sarcoma virus 17 oncogene homolog	NM_001031289	0.41	0.065	0.66	0.048	-0.50	0.058
LMO1	LIM domain only 1 (rhombotin 1)	XM_420991	-0.68	0.024	-0.18	0.055	0.16	0.37
MYNN	myoneurin	XM_001233289	0.69	8.2E-03	0.20	0.30	0.21	0.052
PSIP1	PC4 and SFRS1 interacting protein 1	NM_001031610	1.98	4.2E-03	0.53	5.3E-03	-0.09	0.42
RBBP5	retinoblastoma binding protein 5	NM_001030914	0.63	0.020	0.22	0.39	-0.50	0.35
SMARCC1	SWI/SNF related, matrix associated, actin dependent regulator of chromatin, subfamily c, member 1	XR_026888	-0.05	0.75	0.06	0.52	0.71	3.8E-03

Table 2-6: Genes differentially expressed between HH20 and HH25 in chick, quail, and duck embryos. Average fold changes and p-values for comparisons between HH20 and HH25 for chicken, duck and quail. Fold changes are log2 scale, with HH25 relative to HH20. Highlighted comparisons pass >1.5-fold change and p-values<0.05 criteria. Highlighted gene names are also differentially expressed between the three species (see Table 2-1).

Dramatic changes in Wnt signaling in duck neural crest

Although there were only subtle changes between the developmental stages within each species, the interspecies comparisons at both HH20 and HH25 revealed numerous gene expression differences. In particular, thirteen members of the canonical Wnt signaling included some dramatic variations between the three species. For instance, *DKK2*, *FZD1,* and *WNT1* were all expressed 20-fold higher in duck NCs compared to either chicken or quail, at either HH20 or HH25 (Figure 2-2, Table 2-1). Additionally, the Wnt antagonist *APC* and receptor *LRP5* were elevated 4- to 5-fold, and the expression levels of genes with known Wnt interactions including *C3IP1* (Angers et al. 2006), *PFDN5* (Yoshida et al. 2008), and *TBX20* (Buescher et al. 2004, Song et al. 2006) were elevated by at least 9-fold in duck NCs compared to the other species.

Although Wnt signaling has been extensively studies in other aspects of facial development—e.g. neural crest induction (Sauka-Spengler and Bronner-Fraser 2008)—it is just beginning to be evaluated as controlling the facial development of different species. Our collaborators found that the regions of Wnt responsiveness differ in mice and birds (Brugmann et al. 2007), as well as between different bird species (see **Chapter 4**). However, my work was the first description of changes in specific Wnt signaling molecules in the species-specific facial morphologies. After this study was published, it was demonstrated that the Wnt signaling components *DKK3* and *CTNNB1* are more highly expressed in

Darwin's finches with a broader beak (Mallarino et al. 2011). This finding agrees very well with my finding that Wnt signaling is differential in the broad-billed duck.

Many additional gene expression changes are observed in the duck

In contrast to changes in Wnt signaling, nine members of the TGFβ signaling pathway are differentially expressed between the species and many of these are up-regulated in chick and quail compared to duck. For example, *BMP10, TGFB2,* and *TGFB3* were up-regulated in both quail and chick by 2- to 4-fold relative to the duck (Figure 2-2 and Table 2-1). Furthermore, eight components of Fgf signaling and seven components of Notch signaling varied across the comparisons, including a 2- to 6-fold up-regulation of *FGF10, FGF13, FGF16, HES1,* and *LFNG* in duck.

Finally, I observed remarkably large gene expression changes in specific transcription factor genes (TFs). Given the fact that the microarray platform interrogates mostly transcription factor gene expression changes, it is not surprising that the majority of differences (180 out of 232 genes with known orthologs) are in this class of genes. Many of the observed TF differences, however, were remarkably large, particularly between duck and the other two species. For example, the homeobox gene *IRX2* was up-regulated by ~8-fold in duck NC cells relative to the chicken or quail (Figure 2-2, Table 2-1). Numerous studies have indicated that TF gene expression changes as low as 1.5-fold can have biological relevance, since small changes in these regulators can have

large effects on downstream targets (Hawkins et al. 2003, Hawkins et al. 2007, Wagner et al. 2005).

Changes between morphologically similar chicken and quail

Despite their similar beak morphologies, comparisons between chicken and quail embryo FNP NCs revealed a few large differences in gene expression. Among these were the Calmodulin pathway members *CALM1* and *CALM2* genes, which were expressed 2-fold less in duck than in chicken (see also Figure 2-3), and 2-fold less in chicken than in quail. Comparisons between duck and quail showed similar results, with expression of *CALM1* and *CALM2* being 4-fold less in duck than in quail. Up-regulation of calmodulin gene expression in quail was coupled with changes in the Bmp signaling network, in agreement with previous observations in the beaks of Darwin's finches (Abzhanov et al. 2004, Abzhanov et al. 2006). In quail NCs there is a 2- to 4-fold up-regulation of Bmp pathway members *BMP2*, *BMP9,* and the Bmp antagonist *NOGGIN*, along with a 5-fold down-regulation of *MADH1*. By contrast, chicken NCs exhibited up-regulated *BMPR1A, JAGGED2, MADH2, OSR2, PAX9, PITX2,* and *SATB2* (Figure 2-2, Table 2-1). It is interesting to note that knock-out of any of these genes in mice results in a variety of craniofacial defects (Stanier and Moore 2004).

RNA *in situ* hybridization confirms the microarray data

In order to qualitatively validate the microarray data, I conducted whole mount RNA *in situ* hybridizations on HH25 chicken and duck embryos (Figure 2-3). All *in situs* confirmed the trends observed in the microarray data and revealed spatial variations in gene expression. Sense strand controls for all probes showed no signal (data not shown).

I started by confirming expression of three genes that have been previously implicated in facial development: *CALM2, SATB2,* and *WNT1* (Figure 2-3). First, as previously mentioned, the Calmodulin pathway has been previously associated with species-specific beak morphology (Abzhanov et al. 2006). By *in situ*, *CALM2* (and *CALM1*, see below) is expressed in higher levels and across the entire width of the frontonasal prominence (FNP) of the chicken, while its expression is absent from the midline in the duck (Figure 2-3B-C). The probe used was designed to the coding region of *CALM2*, and could potentially cross-hybridize with *CALM1*. Therefore, I also designed probes to *CALM1* and *CALM2* 3'UTRs, which are conserved between species, but not between the genes within a species. *In situ* hybridization using *CALM1* UTR and *CALM2* UTR probes demonstrated no appreciable differences in gene expression between the two genes, and showed similar expression patterns to the *CALM2* coding probe (data not shown, Figure 2-3B-C). Second, mutation of the transcription factor *SATB2* in mice results in isolated cleft palate (FitzPatrick et al. 2003). *In situs* show that this gene has a similar expression pattern in chicken and duck as it

does in mouse (FitzPatrick et al. 2003): it is expressed across the FNP, with the strongest expression in regions that will fuse with the maxillary prominence (Figure 2-3F-G). By both microarray and *in situ, SATB2* is expressed at higher levels in the FNP of the chicken than the duck. In contrast, this gene is expressed at higher levels in the mandibular prominences of the duck compared to the chicken (Figure 2-3F-G). Finally, *WNT1* is a marker of neural crest cells when they are migrating to the face (Echelard et al. 1994). I found that this gene is extensively expressed throughout the facial prominences in both species (Figure 2-3J-K), but at higher levels in both the epithelia and mesenchyme of the duck FNP compared to the chicken (Figure 2-3L-M).

Additionally, I confirmed differential expression patterns for two genes that were previously not known to be expressed in the developing face, *PHF16* and *TBX20* (Figure 2-3). *PHF16,* a transcription factor of as yet unknown function, is expressed throughout the FNP, maxillary, and mandibular prominences. It has higher transcript levels in chicken relative to duck, but a similar spatial distribution in both species (Figure 2-3D-E). *TBX20* is particularly interesting since it has been shown to negatively regulate the Wnt signaling pathway during *Drosophila* segmentation (Buescher et al. 2004) and positively regulate non-canonical Wnt signaling during facial neuron development (Song et al. 2006). It is strongly expressed in the developing heart of both species, as previously described (Figure 2-4 and data not shown) (Iio et al. 2001), but has never before been implicated in facial development. *TBX20* is highly expressed in the FNP of the

duck, but it is only detectable after extensive RT-PCR in the developing face of the chicken (Figure 2-3H-I and Figure 2-4).

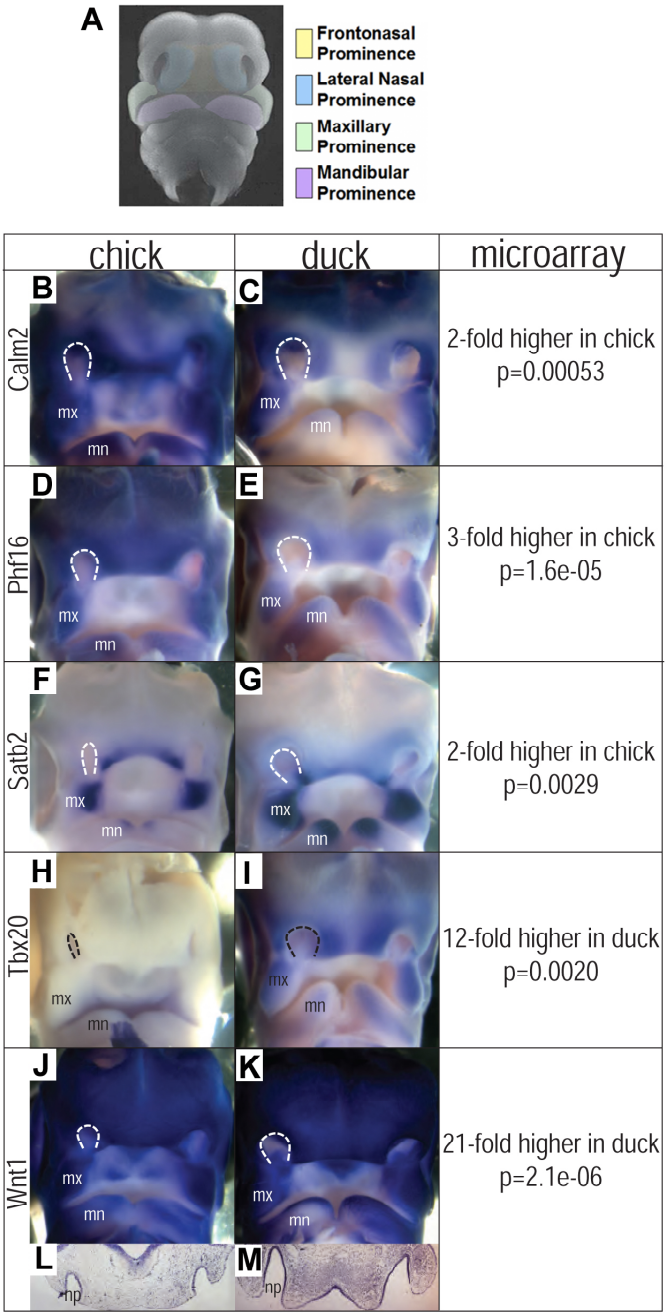

Figure 2-3: RNA *in situ* hybridization confirmation on HH25 chickens and ducks. (A) Schematic of vertebrate embryonic facial structures. **(B,D,F,H,J,L)** HH25 chicken embryos and **(C,E,G,I,K,M)** HH25 duck embryos probed for **(B-C)** *CALM2,* **(D-E)** *PHF16,* **(F-G)** *SATB2,* **(H-I)** *TBX20,* or **(J-M)** *WNT1*. See text for description of expression patterns. mn, mandibular prominence; mx, maxillary prominence; np, nasal pits (indicated by dotted lines).

RT-PCR confirmation

PCR-based approaches are not ideal for verification of cross-species comparisons. As discussed above, the chicken, quail, and duck diverged approximately 90 MYA (van Tuinen and Hedges 2001), and thus may have minor differences in DNA sequences. While these sequence differences are not a large source of error in the microarray data, the duck and quail genomes are not sequenced, and primers designed against the chicken genome may or may not work as efficiently in other birds. For example, if there is sequence divergence in the duck it would be predicted that primers designed to the chicken reference sequence would have less sequence matches, and thus may produce less or no PCR products.

With these caveats in mind, I verified differential expression of two genes, *FZD1* and *TBX20,* both of which are more highly expressed in the duck. This RT-PCR analysis confirmed that *FZD1 and TBX20* are more highly expressed in the FNP of the duck than in chicken FNP from HH17 to HH27 (Figure 2-4A). In contrast to this differential FNP expression, *TBX20* gene expression in the hearts of chicken and duck appeared quite uniform (Figure 2-4B). It should be noted that of those genes verified by RT-PCR and *in situ* hybridization, none were found to be uniquely expressed in one species, but not in the others. This is consistent with the idea that evolutionary pressures primarily result in modifications to current genetic programs, rather than utilizing novel genes and

pathways, to develop species-specific expression (Carroll S.B. 2005, Carroll S. B. 2008, Jacob 1977).

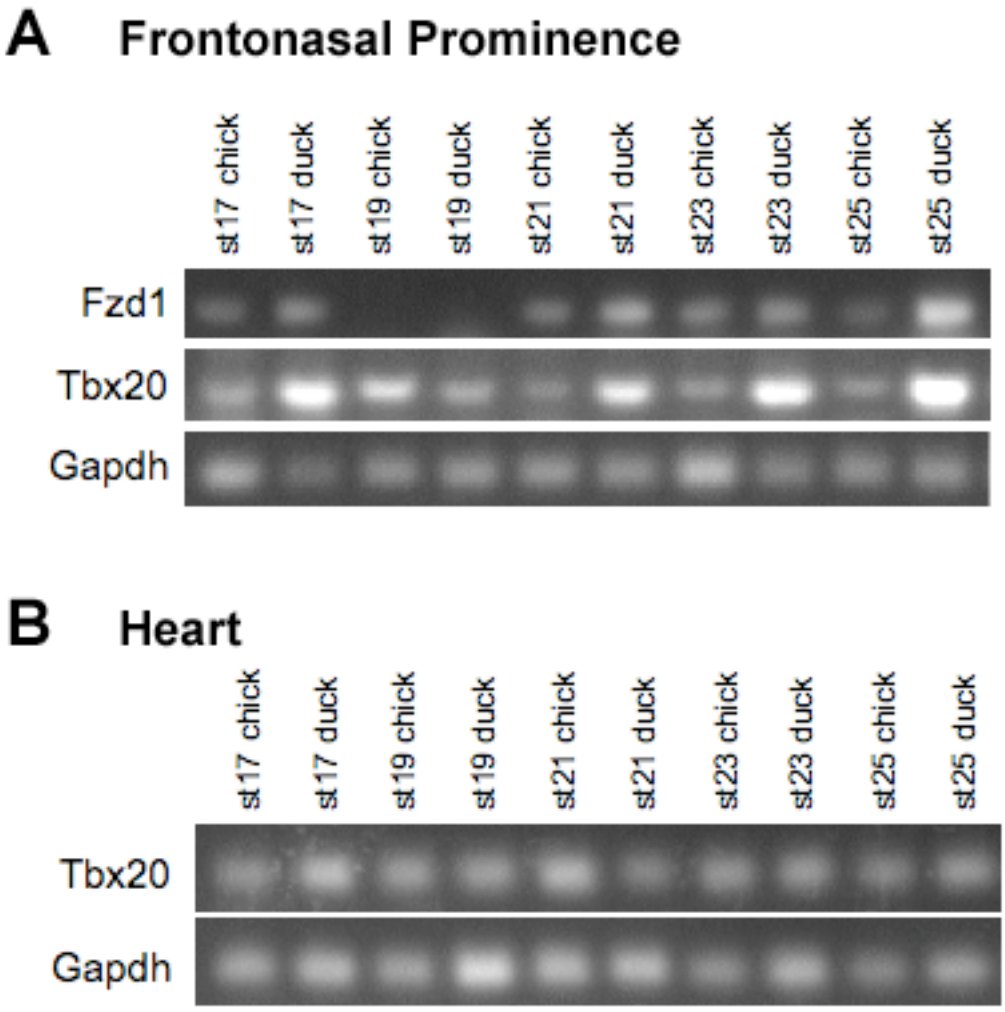

Figure 2-4: RT-PCR confirmation on HH17 to HH25 FNPs and hearts from the chicken and duck. **(A)** *FZD1* and *TBX20* are expressed at higher levels in duck versus chicken FNPs. Amplicons for *FZD1* in HH19 embryos were detected in replicate PCR reactions. **(B)** In contrast the frontonasal prominence, the developing heart of chickens and ducks has similar *TBX20* levels during the same developmental timecourse.

Gene expression changes in the FNP are largely specific to facial structures, rather than reflecting species-specific changes in all tissues

RT-PCR results suggest that the up-regulation of *TBX20* may be specific to the FNP, as these same changes are not seen in stage-matched hearts (Figure 2-4). I wanted to further evaluate whether the genes changing in the FNP have a general upregulation in duck or chicken embryos, rather than differential expression specifically in the FNP. Therefore, I used our cross-species microarrays to compare gene expression in HH23 chickens and ducks for both the developing heart and limb bud. At later stages the limb buds have species-specific morphologies between the speciess—i.e. webbed feet in the duck (Merino et al. 1999). However, at HH23 the leg and wing buds are visually indistinguishable (data not shown).

Though the hearts and wing buds of chickens and ducks have numerous changes in gene expression (79 and 155 genes, respectively, with >2-fold change and p-value<0.05), only 4 of these genes—the transcription factors *FBI1, GPA33, IRX2*, and *JMJD1B*--are also differentially expressed with the same trend in both these tissues and the FNP (Table 2-7). Importantly, neither wing buds nor hearts show most of the gene expression changes I identified in the FNP--for instance the dramatic differences in Wnt signaling. This suggests that the genes listed in Tables 2-1 and 2-2 are likely contributors to differential beak morphology between the chicken, quail, and duck.

ProbeID	Description	NCBI Accession Chick	Fold change FNP	Fold change limb bud	Fold change heart
C5orf7	jumonji domain containing 1B (JMJD1B)	Unclear	-1.31	-2.93	-3.47
FBI1	HIV-1 inducer of short transcripts binding protein; lymphoma related factor	NM_204680	2.19	1.50	1.71
GPA33	glycoprotein A33 (transmembrane)	XM_416656	-1.01	-2.45	-2.55
IRX2	iroquois homeobox protein 2	NM_001030336	3.28	2.04	3.53

Table 2-7: Genes differentially expressed in the same trends among FNP, heart, and limb of chicken and duck. Average fold changes for genes differentially expressed (>2-fold, p-value<0.05) between staged-matched chicken and duck, and common to the FNP, wing bud, and heart. Fold changes are log2 scale, with expression in duck relative to chicken. For example, a negative number is expressed at a lower level in the duck versus chicken.

Conclusions

In this study, I employed custom cross-species microarrays to describe the molecular genetic signatures, developmental signaling pathways, and the spectrum of transcription factor gene expression changes that differ between cranial neural crest cells in the developing beaks of ducks, quails and chickens. Surprisingly, I observed that the neural crest cells established a species-specific transcription factor gene expression profile that predates morphological differences between the species and this profile remains relatively constant even after morphological changes are visually evident.

I identified 232 genes that were differentially expressed between the three species (>2-fold and p-value <0.05) and have identifiable chicken orthologs. Twenty-two of these genes, including *FGFR2, JAGGED2, MSX2, SATB2,* and

TGFB3, have already been implicated in a variety of mammalian craniofacial defects (Stanier and Moore 2004). However, the vast majority of genes were not previously known to be expressed in the developing face (e.g. *TBX20*, Figure 2-3 and Figure 2-4). Furthermore, 25 of these genes have as yet unknown functions (e.g. *PHF16*, Figure 2-3). Confirmatory whole-mount RNA *in situ* hybridizations revealed spatial differences in expression; for example, *CALM1* and *CALM2* are expressed across the width of the chicken FNP, but are not expressed at the midline of the duck.

The most dramatic observed changes were in the Wnt signaling pathway. Duck neural crest cells show a 20-fold up-regulation of *DKK2, FZD1,* and *WNT1*, as well as a 10-fold elevation of transcripts for the Wnt interacting genes *C3IP1* (Angers et al. 2006), *PFDN5* (Yoshida et al. 2008), and *TBX20* (Buescher et al. 2004, Song et al. 2006). Additionally, I identified changes in both Bmp and Calmodulin signaling between the three bird species. My work is thus, complimentary to, and extends upon previous studies of morphological variation in avian beaks (Abzhanov et al. 2004, Abzhanov et al. 2006, Merino et al. 1999, Wu et al. 2004, Wu et al. 2006).

Previous studies (Abzhanov et al. 2004, Abzhanov et al. 2006, Wu et al. 2004, Wu et al. 2006) that implicated modulations in *BMP4* and *CALM1* activity in altered beak morphology were conducted after morphological variation is evident. They did not clarify whether these genes are initiating morphological changes or whether their expression is simply changing in response to an upstream

mediator. Consistent with this latter role for Bmp activity in patterning the face, our microarray analyses did not detect significant variations in *BMP4* expression levels between billed and beaked embryos, though they do demonstrate differences in gene expression as morphological variation arises (Brugmann et al. 2006). One explanation for this finding is that *BMP4* expression begins to gradually switch to mesenchyme (which we analyzed in this study) from epithelia at HH24 (Francis-West et al. 1994) and it may be at this later stage of embryonic development when Bmp signaling becomes most critical for the growth of the facial prominences.

In contrast to the previous studies, my study evaluated the developing beak of chickens, quails, and ducks prior to morphological variation and thus may identify the early modulators of differential form. The >300 genes I identified using an unbiased microarray approach of transcription factors and members of developmental signaling pathways can therefore be used to further study evolution of the face. This study is the first of its kind, extending on previous work in Darwin's finches, and provides the first large-scale insights into cross-species facial morphogenesis. Additionally, given the conserved molecular "toolbox" of facial development (Abzhanov et al. 2004, Albertson et al. 2005, Liu et al. 2005, Suzuki et al. 2009, Terai et al. 2002) exploiting natural variation in bird beak shapes may be a useful tool to discover new candidate genes that regulate mammalian craniofacial development. I explore this concept further in **Chapter 4**.

References

Abzhanov A, Protas M, Grant BR, Grant PR, Tabin CJ. 2004. Bmp4 and Morphological Variation of Beaks in Darwin's Finches. Science 305: 1462-1465.

Abzhanov A, Kuo WP, Hartmann C, Grant BR, Grant PR, Tabin CJ. 2006. The calmodulin pathway and evolution of elongated beak morphology in Darwin's finches. Nature 442: 563-567.

Albertson RC, Streelman JT, Kocher TD, Yelick PC. 2005. Integration and evolution of the cichlid mandible: The molecular basis of alternate feeding strategies. Proceedings of the National Academy of Sciences of the United States of America 102: 16287-16292.

Angers S, Thorpe CJ, Biechele TL, Goldenberg SJ, Zheng N, MacCoss MJ, Moon RT. 2006. The KLHL12-Cullin-3 ubiquitin ligase negatively regulates the Wnt-beta-catenin pathway by targeting Dishevelled for degradation. Nat. Cell Biol. 8: 348-357.

Brugmann SA, Kim J, Helms JA. 2006. Looking different: understanding diversity in facial form. Am J Med Genet A 140: 2521-2529.

Brugmann SA, Powder KE, Young NM, Goodnough LH, Hahn SM, James AW, Helms JA, Lovett M. 2010. Comparative gene expression analysis of avian embryonic facial structures reveals new candidates for human craniofacial disorders. Hum Mol Genet 19: 920-930.

Brugmann SA, Goodnough LH, Gregorieff A, Leucht P, ten Berge D, Fuerer C, Clevers H, Nusse R, Helms JA. 2007. Wnt signaling mediates regional specification in the vertebrate face. Development 134: 3283-3295.

Buescher M, Svendsen PC, Tio M, Miskolczi-McCallum C, Tear G, Brook WJ, Chia W. 2004. Drosophila T box proteins break the symmetry of hedgehog-dependent activation of wingless. Curr. Biol. 14: 1694-1702.

Carroll SB. 2005. Endless Forms Most Beautiful: The New Science of Evo Devo and the Making of the Animal Kingdom. New York: W.W. Norton.

—. 2008. Evo-devo and an expanding evolutionary synthesis: a genetic theory of morphological evolution. Cell 134: 25-36.

Echelard Y, Vassileva G, McMahon AP. 1994. Cis-acting regulatory sequences governing Wnt-1 expression in the developing mouse CNS. Development 120: 2213-2224.

FitzPatrick DR, et al. 2003. Identification of SATB2 as the cleft palate gene on 2q32-q33. Hum Mol Genet 12: 2491-2501.

Francis-West PH, Tatla T, Brickell PM. 1994. Expression patterns of the bone morphogenetic protein genes Bmp-4 and Bmp-2 in the developing chick face suggest a role in outgrowth of the primordia. Dev. Dyn. 201: 168-178.

Hawkins RD, Bashiardes S, Helms CA, Hu L, Saccone NL, Warchol ME, Lovett M. 2003. Gene expression differences in quiescent versus regenerating hair cells of avian sensory epithelia: implications for human hearing and balance disorders. Hum. Mol. Genet. 12: 1261-1272.

Hawkins RD, Bashiardes S, Powder KE, Sajan SA, Bhonagiri V, Alvarado DM, Speck J, Warchol ME, Lovett M. 2007. Large Scale Gene Expression Profiles of Regenerating Inner Ear Sensory Epithelia. PLoS ONE 2: e525.

Iio A, Koide M, Hidaka K, Morisaki T. 2001. Expression pattern of novel chick T-box gene, *Tbx20*. Dev. Genes Evol. 211: 559-562.

International Chicken Genome Sequencing Consortium. 2004. Sequence and comparative analysis of the chicken genome provide unique perspectives on vertebrate evolution. Nature 432: 695-716.

Jacob F. 1977. Evolution and tinkering. Science 196: 1161-1166.

Kontges G, Lumsden A. 1996. Rhombencephalic neural crest segmentation is preserved throughout craniofacial ontogeny. Development 122: 3229-3242.

Liu W, Sun X, Braut A, Mishina Y, Behringer RR, Mina M, Martin JF. 2005. Distinct functions for Bmp signaling in lip and palate fusion in mice. Development 132: 1453-1461.

Mackay DR, Elgort SW, Ullman KS. 2009. The nucleoporin Nup153 has separable roles in both early mitotic progression and the resolution of mitosis. Mol Biol Cell 20: 1652-1660.

Mallarino R, Grant PR, Grant BR, Herrel A, Kuo WP, Abzhanov A. 2011. Two developmental modules establish 3D beak-shape variation in Darwin's finches. Proc Natl Acad Sci U S A 108: 4057-4062.

Merino R, Rodriguez-Leon J, Macias D, Ganan Y, Economides AN, Hurle JM. 1999. The BMP antagonist Gremlin regulates outgrowth, chondrogenesis and programmed cell death in the developing limb. Development 126: 5515-5522.

Messina DN, Glasscock J, Gish W, Lovett M. 2004. An ORFeome-based analysis of human transcription factor genes and the construction of a microarray to interrogate their expression. Genome Res. 14: 2041-2047.

Noden DM. 1978. The control of avian cephalic neural crest cytodifferentiation. I. Skeletal and connective tissues. Dev Biol 67: 296-312.

Sauka-Spengler T, Bronner-Fraser M. 2008. A gene regulatory network orchestrates neural crest formation. Nat Rev Mol Cell Biol 9: 557-568.

Schneider RA, Helms JA. 2003. The cellular and molecular origins of beak morphology. Science 299: 565-568.

Song M-R, Shirasaki R, Cai C-L, Ruiz EC, Evans SM, Lee S-K, Pfaff SL. 2006. T-Box transcription factor Tbx20 regulates a genetic program for cranial motor neuron cell body migration. Development 133: 4945-4955.

Stanier P, Moore GE. 2004. Genetics of cleft lip and palate: syndromic genes contribute to the incidence of non-syndromic clefts. Hum. Mol. Genet. 13 Spec No 1: R73-R81.

Suzuki S, et al. 2009. Mutations in BMP4 are associated with subepithelial, microform, and overt cleft lip. Am J Hum Genet 84: 406-411.

Terai Y, Morikawa N, Okada N. 2002. The evolution of the pro-domain of bone morphogenetic protein 4 (Bmp4) in an explosively speciated lineage of East African cichlid fishes. Molecular Biology & Evolution 19: 1628-1632.

Tucker AS, Lumsden A. 2004. Neural crest cells provide species-specific patterning information in the developing branchial skeleton. Evol Dev 6: 32-40.

van Tuinen M, Hedges SB. 2001. Calibration of Avian Molecular Clocks. Mol. Biol. Evol. 18: 206-213.

Wagner RA, Tabibiazar R, Liao A, Quertermous T. 2005. Genome-wide expression dynamics during mouse embryonic development reveal similarities to Drosophila development. Dev. Biol. 288: 595-611.

Wu P, Jiang T-X, Suksaweang S, Widelitz RB, Chuong C-M. 2004. Molecular Shaping of the Beak. Science 305: 1465-1466.

Wu P, Jiang T-X, Shen J-Y, Widelitz RB, Chuong C-M. 2006. Morphoregulation of avian beaks: Comparative mapping of growth zone activities and morphological evolution. Developmental Dynamics 235: 1400-1412.

Xu L, Kang Y, Col S, Massague J. 2002. Smad2 nucleocytoplasmic shuttling by nucleoporins CAN/Nup214 and Nup153 feeds TGFbeta signaling complexes in the cytoplasm and nucleus. Mol Cell 10: 271-282.

Yoshida T, Kitaura H, Hagio Y, Sato T, Iguchi-Ariga SMM, Ariga H. 2008. Negative regulation of the Wnt signal by MM-1 through inhibiting expression of the wnt4 gene. Exp. Cell Res. 314: 1217-1228.

CHAPTER 3

Next-Generation Sequencing to Detect miRNAs in Frontonasal Neural Crest Cells of Chickens, Ducks, and Quails

Introduction

Through my studies in **Chapter 2** and previous work (Abzhanov et al. 2004, Abzhanov et al. 2006, Mallarino et al. 2011, Wu et al. 2004, Wu et al. 2006), we are beginning to understand some of the changes in transcription factor and developmental signaling pathway gene expression that influence species-specific beak morphology. However, the potential roles of microRNAs (miRNAs) in craniofacial development and species-specific facial form are largely unexplored. It is clear that miRNAs play major roles in overall facial specification, since disruption of their processing pathway results in widespread failures in facial development (Huang T. et al. 2010, Zehir et al. 2010). One previous study (Mukhopadhyay et al. 2010) described an analysis of some of the miRNAs expressed in one area of the developing vertebrate face. Using microarrays, 70 miRNAs were detected in the developing mouse palate from embryonic stages E12-E14. Many of these miRNAs were developmentally regulated and potentially regulate mRNAs involved in cell proliferation, differentiation, apoptosis, and other processes necessary for normal facial development (Mukhopadhyay et al. 2010).

In this chapter, I used comprehensive deep miRNA sequencing to assess all the miRNAs that are expressed in frontonasal neural crest cells, which give rise to the bones and cartilage of the upper bill in birds (Kontges and Lumsden 1996, Noden 1978, Schneider and Helms 2003, Tucker and Lumsden 2004). I employed genome-wide bioinformatic approaches to identify miRNAs expressed

in the developing beak of chickens, ducks, and quails both before (HH20) and after (HH25) morphological variations are evident (Figure 1-2). I then examined patterns of differential miRNA expression between the developmental stages within the three bird species. Finally, I verified a number of changes in miRNA gene expression using quantitative reverse transcription PCR (qRT-PCR) and RNA *in situ* hybridization. My follow-up studies on potential mRNA targets of these various miRNAs are presented in **Chapter 4**.

Results

Identification of expressed microRNAs and novel avian microRNA orthologs

Short RNAs were purified from the upper beak primordia of the chicken, duck, and quail (see **Materials and Methods**) and were analyzed by Next-Generation miRNA sequencing (miRNA-seq) on the Illumina GAIIX platform. Figure 3-1 illustrates the analysis pathway used to annotate the resulting sequence reads and Figure 3-2 displays the classification of reads for each sample.

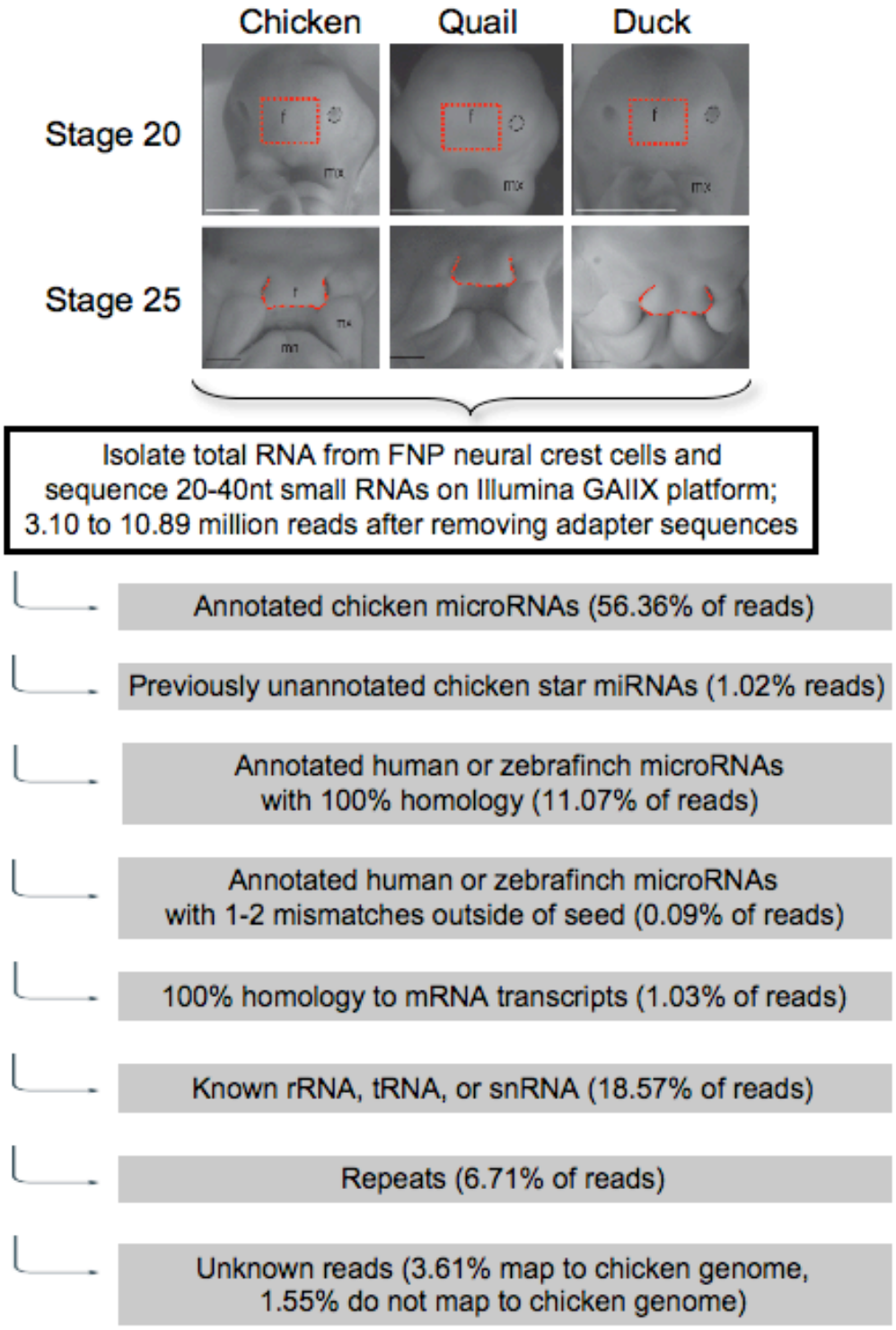

Figure 3-1: Schematic of analysis pipeline to annotate small RNA reads from frontonasal neural crest cells. See text for further details. Embryo images adapted from (Brugmann et al. 2010).

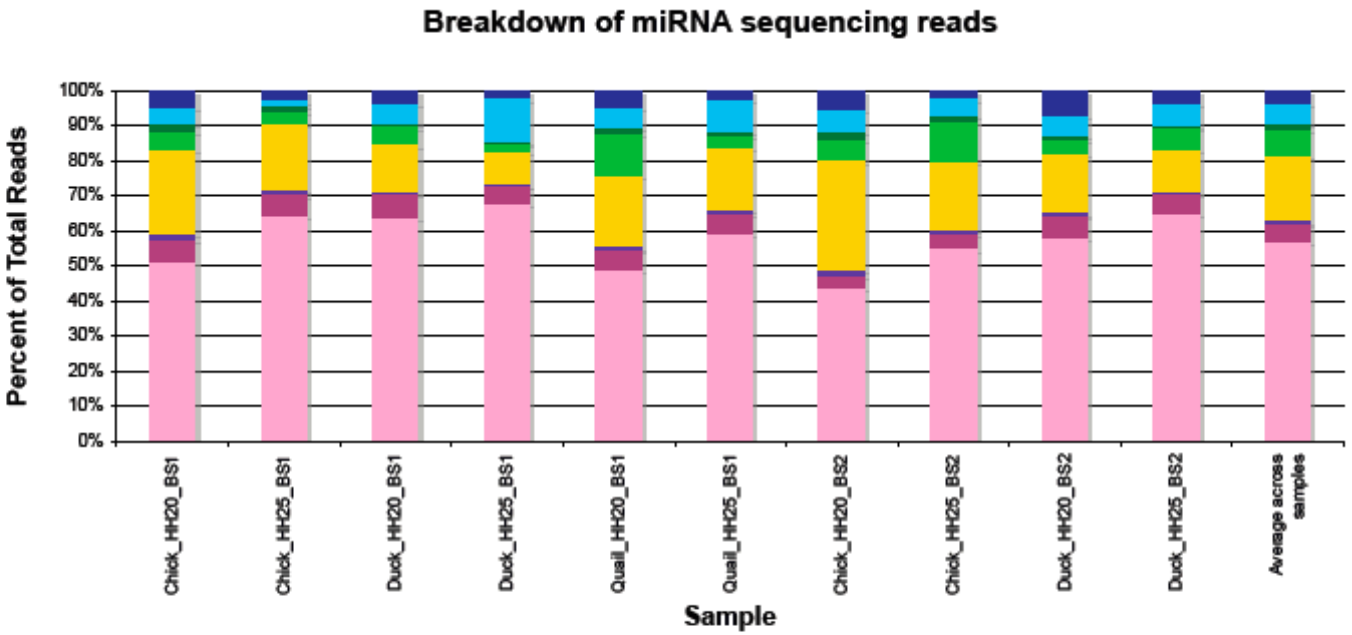

	Chicken HH20 BS1	Chicken HH25 BS1	Duck HH20 BS1	Duck HH25 BS1	Quail HH20 BS1	Quail HH25 BS1	Chicken HH20 BS2	Chicken HH25 BS2	Duck HH20 BS2	Duck HH25 BS2	Average across samples
map/chicken miRNA	2243592 (51.20%)	2350161 (64.24%)	2158767 (64.01%)	2156941 (67.87%)	2164810 (49.29%)	1834940 (59.24%)	2708463 (43.71%)	7344003 (55.05%)	5402280 (58.33%)	7101898 (65.19%)	3567488 (57.38%)
map/human+zebrafinch miRNA	275994 (6.30%)	226621 (6.19%)	231240 (6.86%)	158801 (5.00%)	230965 (5.26%)	183089 (5.91%)	223562 (3.61%)	554520 (4.16%)	568546 (6.14%)	601535 (5.52%)	317449 (5.27%)
map/transcript	69157 (1.58%)	43274 (1.18%)	22337 (0.66%)	13562 (0.43%)	46716 (1.06%)	24788 (0.80%)	112428 (1.81%)	151623 (1.14%)	79679 (0.86%)	58694 (0.54%)	64490 (1.03%)
map/rRNA+tRNA+snRNA	1069496 (24.41%)	699636 (19.12%)	443011 (13.13%)	303960 (9.56%)	899566 (20.48%)	552586 (17.84%)	1923517 (31.05%)	2597589 (19.47%)	1535985 (16.59%)	1332925 (12.24%)	1162988 (18.57%)
map/repeats	224098 (5.11%)	128370 (3.51%)	174620 (5.18%)	62635 (1.97%)	525466 (11.96%)	103809 (3.35%)	355075 (5.73%)	1520382 (11.40%)	366025 (3.95%)	638879 (5.86%)	468312 (6.71%)
map/other	89395 (2.04%)	58654 (1.60%)	36968 (1.10%)	25482 (0.80%)	75132 (1.71%)	46302 (1.49%)	161125 (2.60%)	217381 (1.63%)	128741 (1.39%)	111465 (1.02%)	97336 (1.55%)
unmap/human+zebrafinch miRNA	197970 (4.52%)	50646 (1.38%)	178880 (5.30%)	391586 (12.32%)	234912 (5.35%)	271852 (8.78%)	385430 (6.22%)	666943 (5.00%)	524000 (5.66%)	670475 (6.15%)	353303 (5.89%)
unmap/other	212159 (4.84%)	100910 (2.76%)	126939 (3.76%)	65193 (2.05%)	214837 (4.89%)	80345 (2.59%)	326252 (5.27%)	288061 (2.16%)	655903 (7.08%)	378373 (3.47%)	228086 (3.61%)
total reads (after filtering adapters)	4381861	3658272	3372762	3178161	4392404	3097711	6195852	13340502	9261159	10894243	6259452

Figure 3-2: Classification of Next-Generation short RNA sequencing (miRNA-seq) reads. Reads are annotated as "mapped" if they can be located within the current version of the chicken genome (*Gallus gallus*, gga3 genome build).

microRNA	Sequence	Chicken genomic location	Chick HH20 BS1 (PMMR)	Chick HH25 BS1 (PMMR)	Duck HH20 BS1 (PMMR)	Duck HH25 BS1 (PMMR)	Quail HH20 BS1 (PMMR)	Quail HH25 BS1 (PMMR)	Chick HH20 BS2 (PMMR)	Chick HH25 BS2 (PMMR)	Duck HH20 BS2 (PMMR)	Duck HH25 BS2 (PMMR)
gga-let-7a	UGAGGUAGUAGGUUGUAUAGUU	chr12: 6302911-6303000 (7a-1), chr24: 3380993-3381064 (7a-2), chr1: 73421272-73421347 (7a-3)	9139.27	52203.34	15524.66	30817.19	7790.49	19168.02	3356.76	22898.99	4151.64	18529.14
gga-let-7a_ukstar	CUAUACAAUCUACUGUCUUUC	chr12: 6302911-6303000 (7a-1), chr24: 3380993-3381064 (7a-2), chr1: 73421272-73421347 (7a-3)	3.88	107.97	1.48	8.81	4.10	5.81	56.33	28.78	7.99	11.66
gga-let-7b	UGAGGUAGUAGGUUGUGUGGUU	chr1: 73422101-73422185	11.64	519.10	25.79	29.89	24.59	30.02	4.20	44.90	3.46	19.00
gga-let-7c	UGAGGUAGUAGGUUGUAUGGUU	chr1: 102425086-102425169	12995.39	36930.00	23616.55	25975.08	8306.84	18837.46	3579.49	30090.55	4702.11	21031.66
gga-let-7c_ukstar	CUGUACAACCUUCUAGCUUUCC	chr1: 102425086-102425169	9.58	44.56	5.93	17.62	10.70	17.43	46.00	47.52	18.68	15.79
gga-let-7d	AGAGGUAGUGGGUUGCAUAGU	chr12: 6301452-6301554	7.53	47.02	12.75	25.80	19.12	38.42	3.07	15.82	2.05	15.60
gga-let-7f	UGAGGUAGUAGAUUGUAUAGUU	chr12: 6302497-6302583	4781.53	20195.87	13096.68	45740.92	6532.64	13093.86	3843.05	11984.18	6518.30	19168.47
gga-let-7g	UGAGGUAGUAGUUUGUACAGU	chr12: 2809078-2809160	478.11	4179.30	930.10	3278.63	670.02	1363.26	334.42	1668.08	354.49	1948.37
gga-let-7i	UGAGGUAGUAGUUUGUGCUGU	chr1: 34895687-34895770	9.58	259.96	22.53	116.10	14.80	23.89	7.91	67.76	9.50	79.58
gga-let-7k	UGAGGUAGUAGAUUGAAUAGUU	chr26: 1442897-1442979	192.16	839.47	460.75	801.41	133.64	192.40	211.43	662.57	712.76	713.59
gga-miR-100	AACCCGUAGAUCCGAACUUGUG	chr24: 3372894-3372973	4589.60	18485.50	4184.40	2852.59	4243.01	5955.04	3406.47	7458.49	2209.23	5100.49
gga-miR-100_ukstar	CAAGCUUGUAUCUAUAGGUAUG	chr24: 3372894-3372973	20.54	89.66	44.47	37.44	30.73	53.59	17.59	26.84	27.10	36.90
gga-miR-101	GUACAGUACUGUGAUAACUGAA	chrZ: 28037874-28037952 (101), chr8: 29051918-29051993 (101-2)	3513.12	12511.64	7237.39	10232.96	6213.68	6156.80	2646.13	3894.38	6980.77	8868.35
gga-miR-103	AGCAGCAUUGUACAGGGCUAUGA	chr13: 4449242-4449319 (103-1), chr4: 91906889-91906971 (103-2)	25409.30	39170.41	29183.20	43640.02	18788.34	30038.95	31857.93	23456.31	39423.90	29628.86
gga-miR-106	AAAAGUGCUUACAGUGCAGGUA	chr4: 3970359-3970439	14118.66	14005.25	10901.75	13715.48	12962.38	15972.76	9061.38	9670.48	12530.94	11001.87
gga-mir-106_ukstar	CUGCAGUAUAAGCACUUCUGGC	chr4: 3970359-3970439	12.10	7.38	28.17	20.45	4.33	5.17	19.85	9.52	25.37	17.26

microRNA	Sequence	Chicken genomic location	Chick HH20 BS1 (PMMR)	Chick HH25 BS1 (PMMR)	Duck HH20 BS1 (PMMR)	Duck HH25 BS1 (PMMR)	Quail HH20 BS1 (PMMR)	Quail HH25 BS1 (PMMR)	Chick HH20 BS2 (PMMR)	Chick HH25 BS2 (PMMR)	Duck HH20 BS2 (PMMR)	Duck HH25 BS2 (PMMR)
gga-miR-107	AGCAGCAUUGUACAGGGCUAUCA	chr6: 20487964-20488044	135.33	303.15	94.58	205.15	90.16	132.03	152.20	131.85	87.79	96.56
gga-miR-10a	UACCCUGUAGAUCCGAAUUUGU	chrUn_random: 379304-379377	18.03	3.28	22.83	7.55	22.54	24.86	11.94	72.49	29.37	41.12
gga-miR-10b	UACCCUGUAGAACCGAAUUUGU	chr7: 17389048-17389157	2.51	0.82	3.85	13.22	19.81	15.50	4.03	26.16	2.48	16.06
gga-miR-122	UGGAGUGUGACAAUGGUGUUUGU	chrZ: 649337-649413 (122-1), chrUn_random: 12066796-12066872 (122-2)	19.40	2.19	20.46	3.78	142.75	18.72	50.52	525.99	49.45	140.17
gga-miR-125b	UCCCUGAGACCCUAACUUGUGA	chr1: 102457647-102457736	5816.25	13707.29	3012.96	2806.97	3014.29	4129.18	4673.77	7733.29	2382.64	4737.18
gga-miR-125b_ukstar	UCACAAGUCAGGCUCUUGGGAC	chr1: 102457647-102457736	1056.86	2341.27	1062.93	909.33	782.49	1733.22	1037.63	1369.14	956.79	1244.24
gga-miR-126	UCGUACCGUGAGUAAUAAUGCGC	chr17: 8431742-8431825	29194.22	4782.04	39285.01	23690.12	20419.57	22925.64	15666.45	16078.93	34285.67	36728.21
gga-miR-126*	CAUUAUUACUUUUGGUACGCG	chr17: 8431742-8431825	1080.59	209.94	1393.22	1090.57	1354.61	1573.74	740.82	517.30	1140.14	991.81
gga-miR-128	UCACAGUGAACCGGUCUCUUU	chr7: 32228150-32228231 (128-1), chr2: 45549176-45549259 (128-2)	420.37	638.01	489.21	665.48	737.64	499.40	866.06	390.61	1059.91	524.86
gga-miR-130a	CAGUGCAAUAUUAAAAGGGCAU	chr15: 408399-408481	1352.62	1307.72	1376.02	1868.06	1252.84	1647.67	1527.47	1375.29	1561.79	2197.95
gga-mir-130a_ukstar	GCCCUUUUUCUGUUGUACUAC	chr15: 408399-408481	36.97	39.36	21.64	21.40	49.63	34.86	130.41	60.34	41.03	16.61
gga-miR-130b	CAGUGCAAUAAUGAAAGGGCGU	chr15: 398720-398796	12435.58	9991.33	20911.35	36747.67	15780.65	20471.89	21554.74	12525.17	23722.30	23780.17
gga-miR-130b_ukstar	CCUCUUUCCCUGUUGCACUAC	chr15: 398720-398796	326.80	227.43	578.75	384.18	605.59	425.48	688.36	391.29	597.87	461.90
gga-miR-130c	CAGUGCAAUGUUAAAAGGGCAU	chr19: 7145027-7145120	242.36	361.37	206.06	430.44	254.76	333.15	206.43	198.57	304.07	360.10
gga-miR-1329	UACAGUGAUCACGUUACGAUGG	chr3: 99798387-99798481	243.73	194.08	104.66	131.84	12.29	15.50	122.18	340.99	63.06	192.67

microRNA	Sequence	Chicken genomic location	Chick HH20 BS1 (PMMR)	Chick HH25 BS1 (PMMR)	Duck HH20 BS1 (PMMR)	Duck HH25 BS1 (PMMR)	Quail HH20 BS1 (PMMR)	Quail HH25 BS1 (PMMR)	Chick HH20 BS2 (PMMR)	Chick HH25 BS2 (PMMR)	Duck HH20 BS2 (PMMR)	Duck HH25 BS2 (PMMR)
gga-miR-135a	UAUGGCUUUUUAUUCCUAUGUGA	chr12: 2830742-2830829 (135a-1), chr1: 48192659-48192758 (135a-2), chr26: 1925942-1926037 (135a-3)	47.01	2706.74	110.59	186.59	222.88	215.00	223.86	121.06	167.15	216.90
gga-mir-135a-3_ukstar	AUGUAGGGCGAAAAGCCAUGG	chr26: 1925942-1926037	32.18	907.26	61.67	75.20	111.56	129.45	35.83	55.32	38.44	87.39
gga-miR-135b_ukstar	AUGUAGGGCUAAAAGCCAUGGG	chr3: 38893084-38893150	10.73	160.73	13.94	15.10	20.03	11.94	5.33	15.97	12.20	25.61
gga-miR-137	UAUUGCUUAAGAAUACGCGUAG	chr8: 13210193-13210288	51.80	1119.38	97.55	65.76	37.11	64.24	25.66	47.07	60.79	54.16
gga-miR-138	AGCUGGUGUUGUGAAUC	chr2: 40745148-40745243 (138-1), chr11: 2023954-2024036 (138-2)	382.03	707.71	295.60	364.68	454.19	385.45	239.03	170.08	298.02	264.73
gga-miR-140-3p	CCACAGGGUAGAACCACGGAC	chr11: 21030641-21030735	12042.14	10822.60	15195.26	24397.44	14850.41	25781.62	14906.10	33941.15	16723.39	39693.35
gga-miR-140-5p	AGUGGUUUUACCCUAUGGUAG	chr11: 21030641-21030735	923.81	697.87	1256.83	2036.08	1361.67	1704.48	859.61	2149.54	1461.16	3658.17
gga-miR-142-3p	UGUAGUGUUUCCUACUUUAUGG	chr19: 496983-497070	201.06	54.40	386.63	127.12	259.31	160.12	132.19	109.14	501.88	312.92
gga-miR-142-5p	CCCAUAAAGUAGAAAGCACUAC	chr19: 496983-497070	6.16	1.37	11.56	9.44	13.66	5.49	12.43	6.07	18.68	15.70
gga-miR-144	CUACAGUAUAGAUGAUGUACUC	chr19: 5824123-5824207	4.79	6.83	21.94	5.03	16.16	3.55	9.36	5.40	32.83	26.16
gga-miR-144_ukstar	GGAUAUCAUCAUAUACUGUAAG	chr19: 5824123-5824207	786.88	269.80	2274.10	2272.38	1305.44	1107.91	1784.74	660.99	1953.00	1733.39
gga-miR-1451	UCGCACAGGAGCAAGUUACCGC	chr3: 78710207-78710316	121.64	188.89	104.96	158.27	116.79	118.47	165.27	81.41	92.54	85.46
gga-miR-146a	UGAGAACUGAAUUCCAUGGGUU	chr13: 7555593-7555691	44126.00	39674.20	57559.65	30769.05	49111.38	48752.13	45759.32	68575.23	60226.16	59003.92
gga-miR-146b	UGAGAACUGAAUUCCAUAGGCG	chr6: 24570060-24570164	262.90	43.46	3041.42	1394.20	235.63	254.38	145.74	275.40	3533.79	2752.19
gga-miR-146c	UGAGAACUGAAUUCCAUGGACUG	chr4: 92169271-92169399 (146c-1), chrUn_random: 14731534-14731662 (146c-2)	35344.57	33936.24	45844.03	26167.02	39107.06	39397.80	40658.01	55716.57	51278.36	46702.65
gga-miR-148a	UCAGUGCACUACAGAACUUUGU	chr2: 32053543-32053610	20508.64	14914.42	38440.31	28040.43	21598.65	31209.50	18211.05	14185.15	20588.78	21031.66

microRNA	Sequence	Chicken genomic location	Chick HH20 BS1 (PMMR)	Chick HH25 BS1 (PMMR)	Duck HH20 BS1 (PMMR)	Duck HH25 BS1 (PMMR)	Quail HH20 BS1 (PMMR)	Quail HH25 BS1 (PMMR)	Chick HH20 BS2 (PMMR)	Chick HH25 BS2 (PMMR)	Duck HH20 BS2 (PMMR)	Duck HH25 BS2 (PMMR)
gga-miR-148a_ukstar	AAAGUUCUGUGACACUCAGACU	chr2: 32053543-32053610	104.07	147.88	165.74	64.19	131.59	190.79	147.03	168.81	180.00	149.62
gga-miR-1552-5p	UUAGUGCGCGGUAAGCUAGGGUG	chrUn_random: 9521375-9521457	136.93	113.17	689.05	499.03	269.33	202.73	71.02	87.93	366.37	731.03
gga-miR-1552-5p	UUAGUGCGCGGUAAGCUAGGGU	chrUn_random: 9521375-9521457	94.94	79.27	671.56	484.87	230.85	166.25	53.91	62.82	360.32	717.72
gga-miR-1559	UUCGAUGCUUGUAUGCUACUCC	chr7: 1330064-1330139	344.37	322.56	767.62	530.81	512.02	591.08	216.92	343.24	567.21	714.32
gga-miR-15a	UAGCAGCACAUAAUGGUUUGU	chr1: 173700493-173700575	43.82	181.51	107.33	155.12	133.18	121.70	62.62	55.17	157.00	116.12
gga-miR-15b	UAGCAGCACAUCAUGGUUUGCA	chr9: 23742966-23743056	263.13	844.93	476.76	1023.23	369.73	484.23	256.14	292.64	431.16	561.76
gga-miR-15b_ukstar	CGAAUCAUUAUUUGCUGCUUUA	chr9: 23742966-23743056	27.16	54.67	19.57	19.51	62.61	58.75	138.16	50.52	46.43	24.42
gga-miR-15c	UAGCAGCACAUCAUGGUUUGUA	chr4: 4049055-4049130	178.23	576.23	366.47	686.88	169.16	292.15	148.81	233.42	292.51	455.47
gga-miR-16	UAGCAGCACGUAAAUAUUGGUG	chr1: 173700351-173700434 (16-1), chr9: 23742791-23742884 (16-2)	16928.20	29409.24	31949.48	44855.19	11699.74	20355.35	8993.60	15636.74	26935.07	30370.26
gga-miR-1662	UUGACAUCAUCAUACUUGGGAU	chr2: 1721334-1721406	9.13	24.33	43.58	30.21	4.55	3.55	2.74	7.50	43.95	57.19
gga-miR-16c	UAGCAGCACGUAAAUACUGGAG	chr4: 4048689-4048759	16410.15	28254.60	30839.12	42737.29	10673.65	19017.91	8427.90	15028.30	25473.16	29228.28
gga-miR-17-3p	ACUGCAGUGAAGGCACUUGU	chr1: 152248781-152248865	101.78	281.83	135.20	97.23	167.33	186.27	124.28	87.33	207.64	149.71
gga-miR-17-5p	CAAAGUGCUUACAGUGCAGGUAGU	chr1: 152248781-152248865	11764.64	12780.08	11717.40	10119.37	11092.10	13575.83	7089.42	7634.80	9103.83	9958.56
gga-miR-181a	AACAUUCAACGCUGUCGGUGAGU	chr8: 2001561-2001664 (181a-1), chr17: 10218497-10218587 (181a-2)	1451.67	4046.99	1448.07	1033.30	1641.93	1353.26	1231.31	2299.61	1524.65	2821.40
gga-miR-181a*	ACCAUCGACCGUUGAUUGUACC	chr8: 2001561-2001664 (181a-1), chr17: 10218497-10218587 (181a-2)	237.34	1162.30	565.71	580.52	479.24	614.32	276.96	615.27	309.90	600.41
gga-miR-181b	AACAUUCAUUGCUGUCGGUGGG	chr8: 2001750-2001838 (181b-1), chr17: 10220137-10220221 (181b-2)	2704.10	2432.84	3412.04	1328.13	2094.53	1443.65	1972.93	4275.70	3248.19	4556.35
gga-miR-183	UAUGGCACUGGUAGAAUUCACUG	chrUn_random: 22621072-22621094	1270.24	183.69	2622.78	2653.74	712.82	1142.13	1288.60	2724.64	2079.76	795.74

microRNA	Sequence	Chicken genomic location	Chick HH20 BS1 (PMMR)	Chick HH25 BS1 (PMMR)	Duck HH20 BS1 (PMMR)	Duck HH25 BS1 (PMMR)	Quail HH20 BS1 (PMMR)	Quail HH25 BS1 (PMMR)	Chick HH20 BS2 (PMMR)	Chick HH25 BS2 (PMMR)	Duck HH20 BS2 (PMMR)	Duck HH25 BS2 (PMMR)
gga-miR-184	UGGACGGAGAACUGAUAAGGGU	chr10: 22146245-22146318	1430.44	271.17	245.79	801.72	67.16	135.26	1897.24	1883.59	189.93	597.93
gga-miR-187	UCGUGUCUUGUGUUGCAGCC	chr2: 85892470-85892555	11.41	10.66	11.86	7.87	11.61	10.98	12.75	18.66	5.83	14.23
gga-miR-18a	UAAGGUGCAUCUAGUGCAGAUA	chr1: 152248626-152248718	6312.39	6845.86	7633.80	4018.68	6270.60	6026.39	2851.75	3031.67	6071.38	4489.89
gga-miR-18a_ukstar	ACUGCCCUAAAUGCUCCUUCUGG	chr1: 152248626-152248718	149.71	239.73	90.13	92.51	204.67	143.65	288.74	76.98	211.64	49.57
gga-miR-18b	UAAGGUGCAUCUAGUGCAGUUA	chr4: 3970228-3970311	10043.22	12087.13	12142.87	6179.99	9121.88	9911.51	5545.00	5292.68	10383.47	7043.35
gga-mir-18b_ukstar	CUGCCCUAAAUGCUCCUUCU	chr4: 3970228-3970311	82.61	154.72	54.26	52.86	175.99	95.23	255.17	51.65	161.43	30.11
gga-miR-190	UGAUAUGUUUGAUAUAUUAGGU	chr10: 5209724-5209808	83.75	132.85	81.54	52.55	150.94	138.81	32.60	68.59	54.31	89.13
gga-miR-193a_ukstar	UGGGUCUUUGCGGGCGAGAUGA	chr18: 6423770-6423846	31.49	3.01	13.64	3.78	23.68	18.08	11.46	14.24	9.39	11.93
gga-miR-193b	AACUGGCCCACAAAGUCCCGCUUU	chr14: 759453-759535	6.16	5.19	4.15	5.66	10.24	4.20	13.88	2.62	3.56	3.03
gga-miR-193b_ukstar	UGGGUCUUUGCGGGCGAGAUGA	chr14: 759453-759535	31.49	3.01	13.64	3.78	23.68	18.08	11.46	14.24	9.39	11.93
gga-miR-199	CCCAGUGUUCAGACUACCUGUUC	chr17: 5667150-5667243 (199-1), chr8: 4732773-4732880 (199-2)	1521.04	57.40	2897.92	3282.09	2252.75	2856.63	2217.29	3865.90	2553.24	5004.85
gga-miR-199*	UACAGUAGUCUGCACAUUGG	chr17: 5667150-5667243 (199-1), chr8: 4732773-4732880 (199-2)	6804.19	258.05	5740.10	9006.78	21859.10	18221.84	6160.57	12982.12	3724.05	7882.70
gga-miR-19a	UGUGCAAAUCUAUGCAAAACUGA	chr1: 152248492-152248572	301.93	955.64	511.15	429.18	653.40	385.77	244.52	247.44	748.83	825.57
gga-mir-19a_ukstar	GUUAGUUUUGCAUAGUUGCAC	chr1: 152248492-152248572	119.36	307.52	354.90	516.65	295.97	316.04	134.77	71.66	577.68	337.61
gga-miR-19b	UGUGCAAAUCCAUGCAAAACUGA	chr1: 152248183-152248269	1461.94	2687.61	1779.25	2471.56	3101.26	2085.41	1594.13	826.51	2965.50	2288.73
gga-miR-19b_ukstar	AGUUUUGCAGGUUUGCAUCCAGC	chr1: 152248183-152248269	33.32	64.24	45.07	60.10	120.66	78.12	65.53	17.47	67.27	24.60
gga-miR-1a	UGGAAUGUAAAGAAGUAUGUA	chr20: 8107831-8107901 (1a-1), chr2: 105673483-105673567 (1a-2)	168.42	89.93	374.17	284.76	259.77	497.46	43.09	339.87	138.64	179.54
gga-miR-1b	UGGAAUGUUAAGAAGUAUGUA	chr23: 4663912-4663975	3.88	3.28	18.68	11.96	5.69	13.24	0.48	3.90	8.64	21.11

microRNA	Sequence	Chicken genomic location	Chick HH20 BS1 (PMMR)	Chick HH25 BS1 (PMMR)	Duck HH20 BS1 (PMMR)	Duck HH25 BS1 (PMMR)	Quail HH20 BS1 (PMMR)	Quail HH25 BS1 (PMMR)	Chick HH20 BS2 (PMMR)	Chick HH25 BS2 (PMMR)	Duck HH20 BS2 (PMMR)	Duck HH25 BS2 (PMMR)
gga-miR-200a	UAACACUGUCUGGUAACGAUGU	chr21: 2583317-2583403	193.75	11.75	869.02	642.51	473.54	308.94	75.21	201.27	284.31	127.59
gga-miR-200b	UAAUACUGCCUGGUAAUGAUGAU	chr21: 2585642-258572	57.97	2.19	211.70	128.38	144.34	75.22	34.54	80.88	79.47	33.04
gga-miR-203	GUGAAAUGUUUAGGACCACUUG	chr5: 53206814-53206911	28.98	11.75	88.06	143.48	42.12	33.90	12.91	23.16	22.68	91.24
gga-miR-204	UUCCCUUUGUCAUCCUAUGCCU	chr28: 1784403-1784424 (204-1), chr10: 6651274-6651374 (204-2)	26.47	79.55	18.68	23.60	38.70	20.01	52.29	67.91	53.34	68.84
gga-miR-205a	UCCUUCAUUCCACCGGAGUCUG	chr26: 2896047-2896142	35.60	14.49	95.17	138.76	287.77	81.03	47.45	18.14	23.00	67.01
gga-miR-20a	UAAAGUGCUUAUAGUGCAGGUAG	chr1: 152248306-152248403	15628.98	18886.79	16715.38	19226.21	16075.25	19027.92	8407.72	10160.94	17014.29	16477.33
gga-miR-20b	CAAAGUGCUCAUAGUGCAGGUAG	chr4: 3970047-3970131	51596.57	36893.10	43401.82	21338.44	30810.92	36328.44	25007.21	29799.48	30020.22	29747.73
gga-mir-20b_ukstar	ACUGUAAUGUGGGCACUUACAGU	chr4: 3970047-3970131	19.40	15.85	24.91	7.87	18.90	12.59	15.82	8.02	8.42	7.80
gga-miR-21	UAGCUUAUCAGACUGAUGUUGA	chr19: 7322072-7322168	62784.97	18764.32	38879.41	31810.22	29582.43	32997.91	37014.76	43764.32	33669.00	29563.14
gga-miR-211	UUCCCUUUGUCAUCCUAUGCCU	chr28: 1784394-1784467	26.02	75.99	18.09	22.34	37.11	19.37	51.49	66.41	51.83	64.80
gga-miR-2131	AUGCAGAAGUGCACGGAAACAGC	chrZ: 68816728-68816816	13.92	29.80	16.60	33.35	23.68	29.70	46.32	14.62	18.03	17.35
gga-mir-2131_ukstar	CUGUUACUGUUCUUCUGAUG	chrZ: 68816728-68816816	115.93	213.49	67.90	122.40	42.57	45.52	182.38	153.29	99.56	84.17
gga-miR-215	AUGACCUAUGAAUUGACAGAC	chr3: 19924793-19924897	249.44	889.49	26.09	47.51	275.70	524.58	168.82	289.42	31.42	61.50
gga-miR-218	UUGUGCUUGAUCUAACCAUGU	chr4: 77774698-77774806 (218-1), chr13: 4322860-4322954 (218-2)	377.47	1379.89	428.43	850.18	480.83	737.96	214.50	429.59	298.34	651.81
gga-miR-2188	AAGGUCCAACCUCACAUGUCCU	chr22: 2684926-2685094	19.40	8.75	23.72	21.71	41.66	33.25	70.05	23.16	41.14	14.50
gga-miR-22	AAGCUGCCAGUUGAAGAACUGU	chr19: 5352096-5352195	65.50	53.85	172.56	113.59	104.50	204.67	40.51	53.45	163.59	145.40
gga-miR-22*	AGUUCUUCAGUGGCAAGCUUUA	chr19: 5352096-5352195	3.88	2.73	8.60	18.88	15.94	7.75	6.62	3.97	28.72	15.60
gga-miR-221	AGCUACAUUGUCUGCUGGGUUUC	chr1: 114218926-114219024	433.83	384.06	588.54	616.39	1302.70	613.03	646.40	368.65	619.25	360.10
gga-miR-221_ukstar	ACCUGGCAUACAAUGUAGAUUU	chr1: 114218926-114219024	852.15	533.04	1514.19	1046.20	1154.49	1087.90	1436.93	449.38	660.39	427.66

microRNA	Sequence	Chicken genomic location	Chick HH20 BS1 (PMMR)	Chick HH25 BS1 (PMMR)	Duck HH20 BS1 (PMMR)	Duck HH25 BS1 (PMMR)	Quail HH20 BS1 (PMMR)	Quail HH25 BS1 (PMMR)	Chick HH20 BS2 (PMMR)	Chick HH25 BS2 (PMMR)	Duck HH20 BS2 (PMMR)	Duck HH25 BS2 (PMMR)
gga-miR-222	AGCUACAUCUGGCUACUGGGUCUC	chr1: 114216027-114216124 (222-1), chr1: 114218422-114218519 (222-2)	849.41	470.17	1321.77	1586.14	988.75	555.57	952.25	437.69	1204.28	630.24
gga-miR-223	UGUCAGUUUGUCAAAUACCCC	chr4: 232949-233048	65.50	16.67	58.11	70.80	70.35	66.50	171.73	57.49	154.52	51.04
gga-miR-23b	AUCACAUUGCCAGGGAUUACC	chrZ: 41157406-41157491	160.66	202.01	347.49	533.01	272.97	286.66	268.08	243.24	483.63	705.33
gga-miR-24	UGGCUCAGUUCAGCAGGAACAG	chrZ: 41158175-41158242	2993.71	2171.52	5471.18	5497.52	1837.72	3069.36	1993.27	2060.72	3837.75	5740.83
gga-miR-26a	UUCAAGUAAUCCAGGAUAGGC	chr2: 4467516-4467592	1662.31	2299.72	3483.79	5407.84	2847.42	2994.79	1984.23	2207.41	4573.08	4836.96
gga-miR-27b	UUCACAGUGGCUAAGUUCUGC	chrZ: 41157642-41157738	1497.77	1554.56	2873.31	3137.98	1166.79	1735.48	1083.47	1219.97	2422.05	3828.35
gga-miR-27b_ukstar	AGAGCUUAGCUGAUUGGUGAAC	chrZ: 41157642-41157738	54.77	30.89	91.32	39.96	33.24	36.80	19.69	46.03	40.17	98.31
gga-miR-2954	CAUCCCCAUUCCACUCCUAGCA	chrZ	7016.43	11991.73	4868.71	2553.99	12564.87	6274.96	11848.73	1668.38	4839.57	2301.49
gga-miR-2954_ukstar	GCUGAGAGGGCUUGGGGAGAGGA	chrZ	674.60	367.93	1362.09	174.94	909.52	588.50	2070.58	76.76	522.72	72.88
gga-miR-2964	CACAAGAAUUGCGUUUGGACAA	chr17: 5577814-5577902	372.44	532.49	99.33	188.79	407.29	635.63	252.27	333.50	148.15	182.39
gga-miR-301	CAGUGCAAUAAUAUUGUCAAAGCAU	chr15: 406313-406405	257.20	636.09	528.94	557.24	403.65	197.24	390.26	277.65	564.62	833.74
gga-mir-301_ukstar	UCUGACAAUGUUGCACUAC	chr15: 406313-406405	109.09	110.71	108.52	78.66	351.29	181.42	151.88	84.25	107.65	81.05
gga-miR-301b-3p	CAGUGCAAUAGUAUUGUCAAAGCAU	chr19: 7144739-7144828	214.52	516.36	447.70	453.09	319.42	161.41	316.82	231.85	451.89	686.97
gga-miR-302b	UAAGUGCUUCCAUGUUUUAGUAG	chr4: 58651314-58651385	444.79	84.74	271.88	66.39	613.33	197.57	306.33	58.02	585.89	68.29
gga-miR-302b*	ACUUUAACAUGGAGGUGCUUUCU	chr4: 58651314-58651385	130.99	16.67	85.69	16.68	89.47	22.27	121.69	17.62	245.65	18.17
gga-miR-302c	UAAGUGCUUCCAUGUUUCAGUGG	chr4: 58651576-58651640	170.25	73.81	177.30	59.47	476.28	171.09	238.06	28.78	447.46	47.00
gga-miR-30a-3p	CUUUCAGUCGGAUGUUUGCAGC	chr3: 85102239-85102310	2230.79	6708.63	4468.74	9692.71	3766.73	5483.08	7062.79	3622.35	8660.26	7415.11
gga-miR-30a-5p	UGUAAACAUCCUCGACUGGAAG	chr3: 85102239-85102310	3014.70	23342.44	11160.29	22406.35	7587.64	13890.26	3701.35	5572.95	12593.78	20119.25
gga-miR-30b	UGUAAACAUCCUACACUCAGCU	chr2: 148331598-148331684	69.83	238.64	42.99	87.47	295.74	190.79	239.19	97.60	90.59	55.72

microRNA	Sequence	Chicken genomic location	Chick HH20 BS1 (PMMR)	Chick HH25 BS1 (PMMR)	Duck HH20 BS1 (PMMR)	Duck HH25 BS1 (PMMR)	Quail HH20 BS1 (PMMR)	Quail HH25 BS1 (PMMR)	Chick HH20 BS2 (PMMR)	Chick HH25 BS2 (PMMR)	Duck HH20 BS2 (PMMR)	Duck HH25 BS2 (PMMR)
gga-miR-30c	UGUAAACAUCCUACACUCUCAGCU	chr23: 5249637-5249725 (30c-1), chr3: 85126853-85126924 (30c-2)	1217.29	3467.21	2112.51	3377.11	3642.65	2435.99	3511.06	2046.85	4232.19	2262.39
gga-miR-30c-1_ukstar	CUGGGAGAGGAUUGUUUACGCC	chr23: 5249637-5249725	80.10	91.85	109.70	167.71	94.03	96.52	143.00	91.23	121.15	93.72
gga-miR-30c-2_ukstar	CUGGGAGAAGGCUGUUUACUCU	chr3: 85126853-85126924	71.89	290.57	194.50	238.50	125.67	219.19	149.62	119.04	233.88	203.13
gga-miR-30d	UGUAAACAUCCCCGACUGGAAG	chr2: 148337263-148337326	7494.76	15599.44	7904.20	12015.75	5863.53	8637.67	9888.87	10383.79	10866.78	13060.02
gga-miR-30d_ukstar	CUUUCAGUCAGAUGUUUGCUGC	chr2: 148337263-148337326	15.29	50.57	14.23	24.86	19.12	31.96	23.89	12.74	52.80	22.31
gga-miR-30e	UGUAAACAUCCUUGACUGG	chr23: 5248414-5248509	6082.12	17439.11	8356.95	11012.66	9500.26	11260.57	4613.57	7937.03	10644.56	16134.12
gga-miR-30e_ukstar	CUUUCAGUCGGAUGUUUACAGC	chr23: 5248414-5248509	1881.85	4385.40	2803.64	6567.32	2771.60	3937.75	6007.24	2835.50	5456.66	4424.36
gga-miR-31	AGGCAAGAUGUUGGCAUAGCUG	chrZ: 71882171-71882264	130.31	24.60	378.32	93.76	8.42	13.88	155.59	161.01	74.50	48.47
gga-miR-32	UAUUGCACAUUACUAAGUUGC	chr2: 86506451-86506520	5.48	154.99	19.87	19.19	17.76	8.39	6.94	7.20	47.51	41.58
gga-miR-33	GUGCAUUGUAGUUGCAUUGC	chr1: 51372282-51372350	37.66	334.31	192.72	92.19	128.40	51.97	8.55	35.98	139.51	227.00
gga-miR-34a	UGGCAGUGUCUUAGCUGGUUGUU	chr21: 3251514-3251622	11.41	10.93	9.49	1.89	18.44	11.94	4.20	4.95	4.00	2.48
gga-miR-34c	AGGCAGUGUAGUUAGCUGAUUGC	chr24: 5685637-5685710	13.24	466.61	529.54	771.52	135.69	54.23	6.46	4.12	166.61	422.06
gga-miR-3529	AGGCAGACUGUGACUUGUUGU	chr10: 14823529-14823619	120.27	90.21	13.64	8.50	489.25	622.72	105.07	75.93	9.83	9.73
gga-miR-3535	GGAUAUGAUGACUGAUUAUCUGAAA	chr9: 16372628-16372709	523.98	900.15	198.35	482.98	252.48	465.51	636.23	1175.22	241.11	376.90
gga-miR-365	UAAUGCCCCUAAAAAUCCUUAU	chr14: 764271-764355 (365-1), chr18: 6437296-6437391 (365-2)	6.39	1.91	7.12	17.31	11.38	21.63	28.73	16.49	36.71	19.74
gga-miR-367	AAUUGCACUUUAGCAAUGGUG	chr4: 58652350-58652422	2.28	3.01	4.45	0.63	15.25	3.87	1.78	0.75	6.48	1.19
gga-miR-429	UAAUACUGUCUGGUAAUGCCGU	chr21: 2580812-2580895	217.94	22.41	651.10	408.10	339.22	254.06	81.83	235.15	233.66	98.58
gga-miR-451	AAACCGUUACCAUUACUGAGUUU	chr19: 5823968-5824036	184.85	92.67	163.96	250.77	310.99	509.73	455.30	259.06	206.02	182.67
gga-miR-454	UAGUGCAAUAUUGCUUAUAGGGU	chr15: 399833-399953	1841.46	2298.63	3462.44	5903.73	3428.87	3652.70	2834.15	3052.81	6890.82	4315.58

microRNA	Sequence	Chicken genomic location	Chick HH20 BS1 (PMMR)	Chick HH25 BS1 (PMMR)	Duck HH20 BS1 (PMMR)	Duck HH25 BS1 (PMMR)	Quail HH20 BS1 (PMMR)	Quail HH25 BS1 (PMMR)	Chick HH20 BS2 (PMMR)	Chick HH25 BS2 (PMMR)	Duck HH20 BS2 (PMMR)	Duck HH25 BS2 (PMMR)
gga-miR-455-3p	UGCAGUCCAUGGGCAUAUACAC	chr17: 5339701-5339786	58.65	27.06	55.15	92.51	125.44	88.13	51.16	69.41	47.08	68.29
gga-miR-455-5p	UAUGUGCCCUUGGACUACAUCG	chr17: 5339701-5339786	126.43	53.30	83.31	117.68	183.27	132.36	167.53	106.59	71.48	109.60
gga-miR-456	CAGGCUGGUUAGAUGGUUGUCA	chr3: 32679710-32679821	1983.18	1114.73	1750.49	775.29	1599.12	1196.37	1184.18	640.31	600.90	454.83
gga-miR-460	CCUGCAUUGUACACACUGUGUG	chr2: 3583690-3583779	252.63	9.57	118.60	47.51	311.45	267.94	75.21	178.55	66.84	49.57
gga-mir-460a_ukstar	CACAGCGCAUACAAUGUGGAUU	chr2: 3583690-3583779	227.76	9.02	357.57	52.23	277.07	327.02	111.53	44.23	135.51	39.56
gga-miR-460b-5p	UCCUCAUUGUACAUGCUGUGUG	chr4: 2687396-2687485	12.10	98.95	7.71	6.92	5.69	2.26	11.78	24.74	2.81	18.73
gga-miR-489	AGUGACAUCAUAUGUACGGCUGC	chr2: 23068877-23068960	5.71	21.32	16.60	5.03	16.85	16.46	10.17	8.02	7.34	5.32
gga-miR-551	GCGACCCAUACUUGGUUUCAG	chr9: 21966405-21966517	22.59	25.15	44.18	76.77	62.84	66.82	27.44	22.19	56.26	51.31
gga-miR-7	UGGAAGACUAGUGAUUUUGUUG	chrZ: 39554766-39554874 (7-1), chr10: 14823525-14823623 (7-2), chr28: 4436025-4436119 (7-3)	349.85	1164.76	781.26	259.27	476.05	386.41	459.34	80.28	375.87	134.29
gga-miR-7-1_ukstar	CAACAAAUCACAGUCUGCCAUA	chrZ: 39554766-39554874	12.78	34.99	12.16	18.25	44.62	37.45	37.12	20.16	29.80	18.27
gga-miR-92	UAUUGCACUUGUCCCGGCCUG	chr1: 152248070-152248147	9590.45	14333.82	11031.31	8608.44	20642.00	11947.85	17238.47	5177.99	15575.26	6672.61
gga-miR-99a	AACCCGUAGAUCCGAUCUUGUG	chr1: 102424333-102424413	1351.02	2452.52	1427.32	1179.30	1200.48	1316.46	1044.09	1566.36	1049.33	1484.55
gga-miR-99a*	CAAGCUCGCUUCUAUGGGUCUG	chr1: 102424333-102424413	82.39	133.94	88.35	64.19	39.16	85.55	53.58	77.06	71.37	100.51
hsa-miR-1246	AAUGGAUUUUUGGAGCAGG	unclear	4.34	1.64	2.96	1.26	38.25	10.65	3.71	24.89	3.24	12.67
hsa-miR-125b-1*	ACGGGUUAGGCUCUUGGGAGCU	unclear	88.78	226.06	91.91	185.96	93.57	120.41	126.05	115.36	77.10	110.24
hsa-miR-1261	AUGGAUAAGGCUUUGGCUU	unclear	52.26	118.36	90.73	126.80	7.74	22.60	19.53	158.69	89.08	251.23
hsa-miR-129-3p	AAGCCCUUACCCCAAAAAGCAU	unclear	10.50	33.08	9.49	13.53	22.54	15.17	24.53	7.87	29.26	9.36
hsa-miR-129-5p	CUUUUUGCGGUCUGGGCUUGC	unclear	189.42	469.89	328.81	269.97	109.51	202.73	138.80	104.57	294.56	229.94
hsa-miR-132	UAACAGUCUACAGCCAUGGUCG	unclear	19.17	8.75	35.88	21.08	38.93	44.87	13.40	27.81	14.47	14.59
hsa-miR-132*	ACCGUGGCUUUCGAUUGUUACU	unclear	5.71	6.29	12.45	11.64	16.16	13.56	8.72	12.97	6.91	8.63

microRNA	Sequence	Chicken genomic location	Chick HH20 BS1 (PMMR)	Chick HH25 BS1 (PMMR)	Duck HH20 BS1 (PMMR)	Duck HH25 BS1 (PMMR)	Quail HH20 BS1 (PMMR)	Quail HH25 BS1 (PMMR)	Chick HH20 BS2 (PMMR)	Chick HH25 BS2 (PMMR)	Duck HH20 BS2 (PMMR)	Duck HH25 BS2 (PMMR)
hsa-miR-139-5p	UCUACAGUGCACGUGUCUCCAG	unclear	23.05	30.62	30.24	25.49	78.54	55.20	51.81	45.35	37.90	20.93
hsa-miR-143	UGAGAUGAAGCACUGUAGCUC	unclear	37422.46	5166.92	40077.54	112893.90	45352.39	80640.83	54488.39	39637.86	45335.04	53520.65
hsa-miR-143*	GGUGCAGUGCUGCAUCUCUGGU	unclear	76.68	11.21	71.75	63.24	98.58	91.68	37.44	43.25	46.86	70.77
hsa-miR-145	GUCCAGUUUUCCCAGGAAUCCCU	unclear	173.67	15.85	107.92	246.05	474.91	521.03	546.82	314.46	379.54	197.08
hsa-miR-145*	GGAUUCCUGGAAAUACUGUUCU	unclear	269.29	14.21	158.62	46.57	114.29	147.85	135.57	296.99	88.00	182.76
hsa-miR-148b	UCAGUGCAUCACAGAACUUUGU	unclear	2239.23	1254.69	3283.66	918.77	2930.74	1863.96	943.05	946.59	1160.11	985.02
hsa-miR-150	UCUCCCAACCCUUGUACCAGUG	unclear	4.79	3.83	21.05	9.44	15.48	4.52	16.95	5.55	15.87	9.18
hsa-miR-181c*	AACCAUCGACCGUUGAGUGGAC	unclear	9.81	25.70	12.45	6.61	16.62	16.14	13.72	18.29	8.75	11.57
hsa-miR-182	UUUGGCAAUGGUAGAACUCACACU	unclear	2683.79	322.01	4595.05	4681.32	1623.71	1997.28	4023.66	6222.48	5335.73	1946.99
hsa-miR-190b	UGAUAUGUUUGAUAUUGGGUU	unclear	7.99	27.34	4.74	4.72	17.53	15.17	1.78	4.72	3.13	5.69
hsa-miR-191	CAACGGAAUCCCAAAAGCAGCUG	unclear	181.66	168.11	189.16	131.52	122.48	122.67	181.25	140.62	205.91	169.81
hsa-miR-192	CUGACCUAUGAAUUGACAGCC	unclear	6.62	8.75	11.56	14.79	55.10	24.21	68.43	223.75	47.08	107.58
hsa-miR-210	CUGUGCGUGUGACAGCGGCUGA	unclear	72.80	364.65	123.93	240.71	187.82	187.88	65.20	74.58	184.97	161.74
hsa-miR-23a	AUCACAUUGCCAGGGAUUUCC	unclear	71.43	49.48	237.49	397.71	172.57	191.43	148.49	142.80	370.04	488.42
hsa-miR-27a	UUCACAGUGGCUAAGUUCCGC	unclear	473.31	252.03	1529.90	1694.06	433.93	521.35	375.74	469.02	1416.67	1915.42
hsa-miR-338-3p	UCCAGCAUCAGUGAUUUUGUUG	unclear	37.66	128.20	35.28	40.59	32.56	45.52	42.45	39.65	66.62	62.51
hsa-miR-338-5p	AACAAUAUCCUGGUGCUGAGUG	unclear	28.07	54.94	24.31	16.36	21.63	29.05	17.92	22.49	17.06	17.26
hsa-miR-363	AAUUGCACGGUAUCCAUCUGUA	chr4: 3968811-3968832	53650.26	53033.51	53740.52	26901.72	43613.93	47618.06	24529.15	32400.95	38399.19	34717.05
hsa-miR-363*	CGGGUGGAUCACGAUGCAAUUU	chr4: 3968811-3968832	8822.74	8746.75	14453.73	22670.03	8254.48	10740.19	10767.85	8414.38	22453.24	19997.26
hsa-miR-369-3p	AAUAAUACAUGGUUGAUCUUU	unclear	5.02	0.82	3.26	0.63	16.85	4.52	4.03	48.50	5.72	20.29
hsa-miR-378	ACUGGACUUGGAGUCAGAAGG	unclear	18.71	16.95	22.83	49.40	143.66	77.48	14.04	57.64	4.64	18.27
hsa-miR-423-5p	UGAGGGGCAGAGAGCGAGACUUU	unclear	5.48	1.37	9.19	1.57	28.46	9.36	9.68	13.34	1.51	1.74

microRNA	Sequence	Chicken genomic location	Chick HH20 BS1 (PMMR)	Chick HH25 BS1 (PMMR)	Duck HH20 BS1 (PMMR)	Duck HH25 BS1 (PMMR)	Quail HH20 BS1 (PMMR)	Quail HH25 BS1 (PMMR)	Chick HH20 BS2 (PMMR)	Chick HH25 BS2 (PMMR)	Duck HH20 BS2 (PMMR)	Duck HH25 BS2 (PMMR)
hsa-miR-425	AAUGACACGAUCACUCCCGUUGA	unclear	141.26	161.28	207.25	102.89	139.79	68.11	122.18	118.14	225.89	141.73
hsa-miR-92a-2*	GGGUGGGGAUUUGUUGCAUUAC	unclear	461.22	217.32	1160.47	636.22	512.93	382.54	342.81	295.72	954.31	558.00
hsa-miR-92b	UAUUGCACUCGUCCCGGCCUCC	unclear	107.26	3359.51	256.47	187.22	256.81	106.85	288.10	104.79	250.72	166.51
hsa-miR-96	UUUGGCACUAGCACAUUUUUGCU	unclear	40.17	5.47	113.26	62.61	45.76	24.86	21.63	41.68	83.90	30.38
tgu-miR-1388	AUCUCAGGUUCGUCAGCCCAUG	unclear	64.81	56.31	12.16	4.09	33.01	43.58	31.31	59.67	17.71	10.01
tgu-miR-2970	GACAGUCAGCAGUUGGUCUG	unclear	372.90	745.71	63.15	50.34	400.69	522.32	258.56	298.41	45.03	57.83

Table 3-1: microRNAs detectably expressed in frontonasal neural crest of chicken, quail, and duck at HH20 and HH25. 186 mature miRNAs that are expressed at a normalized read count of >15 sequences per million mapped reads (PMMR) in at least one sample. Genomic locations are mapped to the gga3 build of the *Gallus gallus* genome.

Sequencing yielded between 3.10 and 10.89 million reads per sample (after removing adapter reads) with 98.45% of reads mapping to either the chicken genome or to known microRNA orthologs (see below, Figure 3-1 and Figure 3-2). Technical replicate sequence runs had correlation coefficients of >95% (data not shown). Sequence runs on second biological samples had correlation coefficients of >80%. Much of the variation in the latter comparison consisted of changes in very high abundance (>10,000 sequences per million mapped reads [PMMR]) miRNAs, whereas the more moderately-expressed miRNAs remained comparable between biological replicates (data not shown).

While the majority of reads (56.36%) can be clearly identified as 122 previously annotated chicken miRNAs (Table 3-1; www.mirbase.org, version 16) (Griffiths-Jones et al. 2008), the computational annotation of chicken miRNAs is clearly incomplete. An additional 1.02% of reads map to 31 star (*) strands of known chicken microRNAs for which there is no annotated star activity in current databases (Figure 3-1 and Table 3-1). Star strands are usually found at lower steady state levels than their partner strands, but many have been shown to be biologically active and relevant (Okamura et al. 2008, Yang et al. 2010). These miRNAs are listed with the suffix “ukstar” in Table 3-1 and Table 3-2 to indicate that the star strand was previously not annotated in the chicken, although in all 31 cases star activity is annotated in other vertebrates. For simplicity, in the text below I refer to all star strands with an asterisk (*) irrespective of whether they are newly or previously described.

The *Gallus gallus* genomic sequence (gga3 genome build) is not yet gap-free and may be missing as much as 10% in gapped areas (Brugmann et al. 2010, Hawkins et al. 2006, International Chicken Genome Sequencing Consortium 2004). This raises the possibility that additional miRNAs may not be annotated in microRNA databases (Griffiths-Jones et al. 2008) or are contained within the sequences that do not map back to the currently available chicken genome. Therefore, I analyzed reads that did not map to known chicken miRNAs to assess whether additional orthologs to known human or zebrafinch miRNAs are present within this set. Another 11.07% of the total reads had 100% sequence identity to 29 human mature miRNAs and 2 zebrafinch miRNAs (Figure 3-1 and Table 3-1). While 4 of these map to the chicken genome and are likely missing due to poor annotation, the other 27 miRNAs did not map to the current chicken genome assembly and likely fall into gapped regions of the genome. For example, miR-143 and miR-143* have not previously been annotated in the chicken, but we identified multiple reads that matched the human versions of these miRNAs and confirmed expression of miR-143 in avians using qRT-PCR (see below). These miRNAs are listed in Table 3-1 and Table 3-2 with the prefix “hsa” or “tgu” to indicate they are newly described avian orthologs of known human or zebrafinch miRNAs, respectively. I also searched the miRNA sequences for candidate miRNAs that had slight sequence divergence from the known human miRNAs by setting our search algorithms to allow one or two base mismatches outside of the miRNA seed sequence. This

identified 4 additional miRNAs that are novel orthologs of human miRNAs (Figure 3-1). Together these only account for 0.09% of total reads. Of the 35 total predicted novel orthologs, only 4 clearly align to the available chicken genomic DNA sequence, suggesting that the majority of these miRNAs are not annotated because they fall into gaps in the current chicken genomic assembly.

After these various computational steps, 68.54% of total sequence reads mapped to chicken, human, or zebrafinch miRNAs (Figure 3-1 and Figure 3-2). Within the remaining reads, 1.03% derive from degraded mRNA transcript, 6.71% map to repetitive sequence families, and 18.57% are tRNA, rRNA, or snRNA sequences (Figure 3-1 and Figure 3-2). The possibility cannot be discounted that additional data mining of the remaining reads (5.16% of total reads, Figure 3-1 and Figure 3-2) may yield novel miRNA families (Li T. et al. 2011).

Overall, by the various analysis and filtering steps described above, I identified 186 mature miRNAs that are detectably expressed in the frontonasal NC cells of the chicken, duck, and quail at a normalized read count of >15 sequences per million mapped reads (PMMR) in at least one sample (Table 3-1). The 15 PMMR threshold of detection was selected based on the lowest read counts of miRNAs for which I could reproducibly verify trends by qRT-PCR (see below).

Dramatic changes in miRNAs occur between developmental stages

As detailed in **Chapter 2**, I previously measured changes in steady state mRNA levels in these same neural crest samples for ~2,400 genes involved in developmental signaling pathways and nearly all known and predicted transcription factor. Although I found many interesting gene expression differences between species, gene expression was essentially unchanged between HH20 and HH25 within species, suggesting that the gene expression profile is established prior to morphological variation. In remarkable contrast to the relatively unchanged pattern of mRNA expression, in the current study I found that miRNA expression is dramatically different between the two developmental stages. Of the 186 miRNAs that were detectably expressed, 170 (91%) were differentially expressed by at least 2-fold either between the three species or between the two developmental stages, with fold changes as large as 74-fold (Figure 3-2). Of the 170 miRNAs that were differentially expressed, the vast majority (132 or 78%) showed at least 2-fold changes between the developmental stages in one or more of the species. The specific miRNAs, patterns and trends of miRNA expression are shown in detail in Table 3-2. Table 3-3 and the sections below summarize these trends and relate specific miRNAs to their potential cellular functions.

microRNA	DC HH20 Fold	DC HH25 Fold	DQ HH20 Fold	DQ HH25 Fold	QC HH20 Fold	QC HH25 Fold	Chick HH25/HH20 Fold	Duck HH25/HH20 Fold	Quail HH25/HH20 Fold
gga-let-7a	0.76	-0.76	0.99	0.69	-0.23	-1.45	2.51	0.99	1.30
gga-let-7a_ukstar	-1.39	-3.62	-1.47	0.60	0.08	-4.22	4.80	2.57	0.50
gga-let-7b	1.15	-4.12	0.07	-0.01	1.08	-4.11	5.48	0.21	0.29
gga-let-7c	0.86	-0.51	1.51	0.46	-0.65	-0.97	1.51	0.14	1.18
gga-let-7c_ukstar	-0.69	-1.34	-0.85	0.02	0.16	-1.35	2.22	1.57	0.70
gga-let-7d	0.76	-0.87	-0.58	-0.57	1.34	-0.29	2.64	1.02	1.01
gga-let-7f	1.45	1.18	1.00	1.80	0.45	-0.63	2.08	1.80	1.00
gga-let-7g	0.96	-0.35	0.47	1.27	0.49	-1.62	3.13	1.82	1.02
gga-let-7i	1.23	-1.16	0.61	2.28	0.63	-3.44	4.76	2.37	0.69
gga-let-7k	1.26	-0.07	1.79	2.06	-0.52	-2.13	2.13	0.80	0.53
gga-miR-100	-0.13	-2.70	-0.02	-1.06	-0.11	-1.63	2.01	-0.55	0.49
gga-miR-100_ukstar	1.11	-1.26	0.53	-0.52	0.58	-0.74	2.13	-0.25	0.80
gga-miR-101	1.04	-0.29	0.22	0.73	0.82	-1.02	1.83	0.50	-0.01
gga-mir-106_ukstar	1.22	1.47	2.70	1.99	-1.48	-0.51	-0.71	-0.46	0.26
gga-miR-107	-0.52	-0.56	0.07	0.64	-0.59	-1.20	1.16	1.12	0.55
gga-miR-10a	0.34	1.20	0.02	-1.72	0.32	2.92	-2.46	-1.60	0.14
gga-miR-10b	0.62	4.01	-2.36	-0.23	2.98	4.24	-1.61	1.78	-0.35
gga-miR-122	0.08	0.79	-2.80	-2.31	2.88	3.10	-3.15	-2.44	-2.93
gga-miR-125b	-0.95	-2.29	0.00	-0.56	-0.95	-1.73	1.24	-0.10	0.45
gga-miR-125b_ukstar	0.01	-1.36	0.44	-0.93	-0.43	-0.43	1.15	-0.23	1.15
gga-miR-126	0.43	2.31	0.94	0.05	-0.52	2.26	-2.61	-0.73	0.17
gga-miR-126*	0.37	2.38	0.04	-0.53	0.33	2.91	-2.36	-0.35	0.22

microRNA	DC HH20 Fold	DC HH25 Fold	DQ HH20 Fold	DQ HH25 Fold	QC HH20 Fold	QC HH25 Fold	Chick HH25/HH20 Fold	Duck HH25/HH20 Fold	Quail HH25/HH20 Fold
gga-mir-130a_ukstar	-0.77	-0.88	-1.20	-0.70	0.42	-0.18	0.09	-0.02	-0.51
gga-miR-130b	0.75	1.88	0.41	0.84	0.34	1.03	-0.32	0.81	0.38
gga-miR-130c	-0.23	0.25	-0.31	0.37	0.07	-0.12	0.58	1.06	0.39
gga-miR-1329	-1.22	-0.56	3.09	3.09	-4.31	-3.65	-0.33	0.33	0.33
gga-miR-135a	1.23	-3.86	-1.01	-0.20	2.25	-3.65	5.85	0.75	-0.05
gga-mir-135a-3_ukstar	0.94	-3.59	-0.86	-0.78	1.79	-2.81	4.82	0.29	0.21
gga-miR-135b_ukstar	0.38	-3.41	-0.52	0.34	0.90	-3.75	3.91	0.12	-0.75
gga-miR-137	0.91	-4.09	1.39	0.03	-0.48	-4.12	4.43	-0.57	0.79
gga-miR-140-3p	0.34	1.17	0.03	-0.08	0.30	1.25	-0.15	0.68	0.80
gga-miR-140-5p	0.44	1.54	-0.12	0.26	0.56	1.29	-0.40	0.70	0.32
gga-miR-142-3p	0.94	1.22	0.58	-0.33	0.37	1.56	-1.89	-1.60	-0.70
gga-miR-142-5p	0.91	2.79	-0.24	0.78	1.15	2.01	-2.17	-0.29	-1.32
gga-miR-144	2.19	-0.44	0.44	0.50	1.75	-0.94	0.51	-2.12	-2.19
gga-miR-144_ukstar	1.53	3.07	0.80	1.04	0.73	2.04	-1.54	0.00	-0.24
gga-miR-146b	3.53	5.00	3.69	2.45	-0.16	2.55	-2.60	-1.13	0.11
gga-miR-148a	0.91	0.91	0.83	-0.15	0.07	1.07	-0.46	-0.46	0.53
gga-miR-148a_ukstar	0.67	-1.20	0.33	-1.57	0.34	0.37	0.51	-1.37	0.54
gga-miR-1552-5p	2.33	2.14	1.36	1.30	0.98	0.84	-0.27	-0.47	-0.41
gga-miR-1559	1.16	0.72	0.58	-0.16	0.57	0.87	-0.09	-0.53	0.21
gga-miR-15a	1.29	-0.23	-0.31	0.35	1.60	-0.58	2.05	0.53	-0.13

microRNA	DC HH20 Fold	DC HH25 Fold	DQ HH20 Fold	DQ HH25 Fold	QC HH20 Fold	QC HH25 Fold	Chick HH25/HH20 Fold	Duck HH25/HH20 Fold	Quail HH25/HH20 Fold
gga-miR-15b	0.86	0.28	0.37	1.08	0.49	-0.80	1.68	1.10	0.39
gga-miR-15b_ukstar	-0.47	-1.49	-1.68	-1.59	1.21	0.10	1.01	0.00	-0.09
gga-miR-15c	1.04	0.25	1.12	1.23	-0.08	-0.98	1.69	0.91	0.79
gga-miR-16	0.92	0.61	1.45	1.14	-0.53	-0.53	0.80	0.49	0.80
gga-miR-1662	2.26	0.31	3.26	3.09	-1.00	-2.78	1.41	-0.53	-0.36
gga-miR-16c	0.91	0.60	1.53	1.17	-0.62	-0.57	0.78	0.47	0.83
gga-miR-17-3p	0.41	-1.54	-0.31	-0.94	0.72	-0.60	1.47	-0.48	0.15
gga-miR-181a	0.00	-1.97	-0.18	-0.39	0.18	-1.58	1.48	-0.49	-0.28
gga-miR-181a*	1.25	-1.00	0.24	-0.08	1.01	-0.92	2.29	0.04	0.36
gga-miR-181b	0.34	-0.87	0.70	-0.12	-0.37	-0.75	-0.15	-1.36	-0.54
gga-miR-183	1.05	3.85	1.88	1.22	-0.83	2.64	-2.79	0.02	0.68
gga-miR-184	-2.54	1.56	1.87	2.57	-4.41	-1.00	-2.40	1.71	1.01
gga-miR-18a_ukstar	-0.73	-1.37	-1.18	-0.63	0.45	-0.74	0.68	0.04	-0.51
gga-mir-18b_ukstar	-0.61	-1.55	-1.70	-0.85	1.09	-0.70	0.91	-0.04	-0.89
gga-miR-190	-0.04	-1.34	-0.89	-1.40	0.85	0.06	0.67	-0.63	-0.12
gga-miR-193a_ukstar	-1.21	0.33	-0.80	-2.26	-0.41	2.59	-3.39	-1.85	-0.39
gga-miR-193b	-0.57	0.12	-1.30	0.43	0.73	-0.31	-0.25	0.45	-1.29
gga-miR-193b_ukstar	-1.21	0.33	-0.80	-2.26	-0.41	2.59	-3.39	-1.85	-0.39
gga-miR-199	0.93	5.84	0.36	0.20	0.57	5.64	-4.73	0.18	0.34
gga-miR-199*	-0.25	5.13	-1.93	-1.02	1.68	6.14	-4.72	0.65	-0.26
gga-miR-19a	0.76	-1.15	-0.35	0.15	1.11	-1.31	1.66	-0.25	-0.76

microRNA	DC HH20 Fold	DC HH25 Fold	DQ HH20 Fold	DQ HH25 Fold	QC HH20 Fold	QC HH25 Fold	Chick HH25/HH20 Fold	Duck HH25/HH20 Fold	Quail HH25/HH20 Fold
gga-mir-19a_ukstar	1.57	0.75	0.26	0.71	1.31	0.04	1.37	0.54	0.09
gga-miR-19b	0.28	-0.12	-0.80	0.25	1.08	-0.37	0.88	0.47	-0.57
gga-miR-19b_ukstar	0.44	-0.10	-1.42	-0.38	1.86	0.28	0.95	0.42	-0.63
gga-miR-1a	1.15	1.66	0.53	-0.80	0.63	2.47	-0.91	-0.39	0.94
gga-miR-1b	2.27	1.87	1.71	-0.15	0.55	2.01	-0.24	-0.64	1.22
gga-miR-200a	2.17	5.77	0.88	1.06	1.29	4.72	-4.04	-0.44	-0.62
gga-miR-200b	1.87	5.88	0.55	0.77	1.32	5.10	-4.73	-0.72	-0.94
gga-miR-203	1.60	3.61	1.06	2.08	0.54	1.53	-1.30	0.70	-0.31
gga-miR-204	-0.50	-1.75	-1.05	0.24	0.55	-1.99	1.59	0.34	-0.95
gga-miR-205a	1.42	3.26	-1.60	0.78	3.01	2.48	-1.30	0.54	-1.83
gga-miR-20b	-0.25	-0.79	0.49	-0.77	-0.74	-0.02	-0.48	-1.02	0.24
gga-mir-20b_ukstar	0.36	-1.01	0.40	-0.68	-0.04	-0.33	-0.29	-1.66	-0.59
gga-miR-21	-0.69	0.76	0.39	-0.05	-1.09	0.81	-1.74	-0.29	0.16
gga-miR-211	-0.52	-1.77	-1.04	0.21	0.51	-1.97	1.55	0.30	-0.94
gga-miR-2131	0.25	0.16	-0.51	0.17	0.77	0.00	1.10	1.01	0.33
gga-mir-2131_ukstar	-0.77	-0.80	0.67	1.43	-1.45	-2.23	0.88	0.85	0.10
gga-miR-215	-3.26	-4.23	-3.40	-3.46	0.14	-0.76	1.83	0.86	0.93
gga-miR-218	0.18	-0.70	-0.17	0.20	0.35	-0.90	1.87	0.99	0.62
gga-miR-2188	0.29	1.31	-0.81	-0.61	1.10	1.93	-1.15	-0.13	-0.33
gga-miR-22	1.40	1.08	0.72	-0.85	0.67	1.93	-0.28	-0.60	0.97
gga-miR-22*	1.15	2.79	-0.89	1.28	2.04	1.50	-0.51	1.13	-1.04
gga-miR-221	0.44	0.68	-1.15	0.01	1.59	0.67	-0.18	0.07	-1.09

microRNA	DC HH20 Fold	DC HH25 Fold	DQ HH20 Fold	DQ HH25 Fold	QC HH20 Fold	QC HH25 Fold	Chick HH25/HH20 Fold	Duck HH25/HH20 Fold	Quail HH25/HH20 Fold
gga-miR-221_ukstar	0.83	0.97	0.39	-0.06	0.44	1.03	-0.68	-0.53	-0.09
gga-miR-222	0.64	1.75	0.42	1.51	0.22	0.24	-0.85	0.26	-0.83
gga-miR-223	-0.17	2.09	-0.28	0.09	0.10	2.00	-1.97	0.28	-0.08
gga-miR-23b	1.11	1.40	0.35	0.89	0.76	0.50	0.33	0.62	0.07
gga-miR-24	0.87	1.34	1.57	0.84	-0.70	0.50	-0.46	0.01	0.74
gga-miR-26a	1.07	1.23	0.29	0.85	0.78	0.38	0.47	0.63	0.07
gga-miR-27b	0.94	1.01	1.30	0.85	-0.36	0.16	0.05	0.13	0.57
gga-miR-27b_ukstar	0.74	0.37	1.46	0.12	-0.72	0.25	-0.83	-1.19	0.15
gga-miR-2954	-0.53	-2.23	-1.37	-1.30	0.84	-0.93	0.77	-0.93	-1.00
gga-miR-2954_ukstar	1.01	-1.07	0.58	-1.75	0.43	0.68	-0.87	-2.96	-0.63
gga-miR-2964	-1.91	-1.50	-2.04	-1.75	0.13	0.26	0.52	0.93	0.64
gga-miR-301	1.04	-0.19	0.39	1.50	0.65	-1.69	1.31	0.08	-1.03
gga-mir-301_ukstar	-0.01	-0.49	-1.69	-1.21	1.69	0.71	0.02	-0.46	-0.95
gga-miR-301b-3p	1.06	-0.19	0.49	1.49	0.57	-1.68	1.27	0.02	-0.98
gga-miR-302b	-0.71	-0.35	-1.17	-1.57	0.46	1.22	-2.39	-2.03	-1.63
gga-miR-302b*	-0.61	0.00	-0.06	-0.42	-0.55	0.42	-2.97	-2.36	-2.01
gga-miR-302c	0.06	-0.31	-1.43	-1.52	1.48	1.21	-1.21	-1.58	-1.48
gga-miR-30a-3p	1.00	0.53	0.25	0.82	0.76	-0.29	1.59	1.12	0.54
gga-miR-30a-5p	1.89	-0.06	0.56	0.69	1.33	-0.75	2.95	1.01	0.87
gga-miR-30b	-0.70	-1.45	-2.78	-1.13	2.08	-0.32	1.77	1.02	-0.63
gga-miR-30c	0.80	-0.04	-0.79	0.47	1.58	-0.51	1.51	0.68	-0.58

microRNA	DC HH20 Fold	DC HH25 Fold	DQ HH20 Fold	DQ HH25 Fold	QC HH20 Fold	QC HH25 Fold	Chick HH25/HH20 Fold	Duck HH25/HH20 Fold	Quail HH25/HH20 Fold
gga-miR-30c-2_ukstar	1.44	-0.28	0.63	0.12	0.81	-0.41	2.02	0.29	0.80
gga-miR-30d	0.08	-0.38	0.43	0.48	-0.35	-0.85	1.06	0.60	0.56
gga-miR-30d_ukstar	-0.10	-1.02	-0.43	-0.36	0.32	-0.66	1.73	0.80	0.74
gga-miR-30e	0.46	-0.66	-0.18	-0.03	0.64	-0.63	1.52	0.40	0.25
gga-miR-30e_ukstar	0.58	0.58	0.02	0.74	0.56	-0.16	1.22	1.23	0.51
gga-miR-31	1.54	1.93	5.49	2.76	-3.95	-0.83	-2.41	-2.01	0.72
gga-miR-32	1.86	-3.01	0.16	1.19	1.70	-4.21	4.82	-0.05	-1.08
gga-miR-33	2.36	-1.86	0.59	0.83	1.77	-2.69	3.15	-1.06	-1.30
gga-miR-34a	-0.27	-2.53	-0.96	-2.66	0.69	0.13	-0.06	-2.33	-0.63
gga-miR-34c	5.32	0.73	1.96	3.83	3.36	-3.10	5.14	0.54	-1.32
gga-miR-3529	-3.14	-3.41	-5.16	-6.20	2.02	2.79	-0.41	-0.68	0.35
gga-miR-3535	-1.40	-0.90	-0.35	0.05	-1.05	-0.95	0.78	1.28	0.88
gga-miR-365	0.16	3.18	-0.68	-0.32	0.83	3.50	-1.74	1.28	0.93
gga-miR-367	0.96	-2.26	-1.78	-2.62	2.74	0.37	0.40	-2.82	-1.98
gga-miR-429	1.58	4.19	0.94	0.68	0.64	3.50	-3.28	-0.67	-0.42
gga-miR-451	-0.17	1.44	-0.92	-1.02	0.75	2.46	-1.00	0.61	0.71
gga-miR-454	0.91	1.36	0.01	0.69	0.90	0.67	0.32	0.77	0.09
gga-miR-455-3p	-0.09	1.77	-1.19	0.07	1.10	1.70	-1.12	0.75	-0.51
gga-miR-455-5p	-0.60	1.14	-1.14	-0.17	0.54	1.31	-1.25	0.50	-0.47
gga-miR-456	-0.18	-0.52	0.13	-0.63	-0.31	0.10	-0.83	-1.17	-0.42
gga-miR-460	-1.09	2.31	-1.39	-2.50	0.30	4.81	-4.72	-1.32	-0.22
gga-mir-460a_ukstar	0.65	2.53	0.37	-2.65	0.28	5.18	-4.66	-2.78	0.24

microRNA	DC HH20 Fold	DC HH25 Fold	DQ HH20 Fold	DQ HH25 Fold	QC HH20 Fold	QC HH25 Fold	Chick HH25/HH20 Fold	Duck HH25/HH20 Fold	Quail HH25/HH20 Fold
gga-miR-460b-5p	-0.65	-3.84	0.44	1.62	-1.09	-5.45	3.03	-0.16	-1.33
gga-miR-489	1.54	-2.08	-0.02	-1.71	1.56	-0.37	1.90	-1.72	-0.03
gga-miR-551	0.97	1.61	-0.51	0.20	1.48	1.41	0.15	0.80	0.09
gga-miR-7	1.16	-2.17	0.71	-0.58	0.44	-1.59	1.74	-1.59	-0.30
gga-miR-7-1_ukstar	-0.07	-0.94	-1.88	-1.04	1.80	0.10	1.45	0.59	-0.25
gga-miR-92	0.20	-0.74	-0.90	-0.47	1.11	-0.26	0.58	-0.36	-0.79
gga-miR-99a	0.08	-1.06	0.25	-0.16	-0.17	-0.90	0.86	-0.28	0.13
gga-miR-99a*	0.10	-1.06	1.17	-0.41	-1.07	-0.65	0.70	-0.46	1.13
hsa-miR-1246	-0.55	-0.38	-3.69	-3.08	3.14	2.70	-1.40	-1.24	-1.84
hsa-miR-125b-1*	0.05	-0.28	-0.03	0.63	0.08	-0.91	1.35	1.02	0.36
hsa-miR-1261	0.80	0.10	3.55	2.49	-2.76	-2.39	1.18	0.48	1.55
hsa-miR-129-3p	-0.15	-1.29	-1.25	-0.17	1.10	-1.12	1.66	0.51	-0.57
hsa-miR-129-5p	0.80	-0.80	1.59	0.41	-0.79	-1.21	1.31	-0.28	0.89
hsa-miR-132	0.90	1.27	-0.12	-1.09	1.02	2.36	-1.13	-0.77	0.20
hsa-miR-132*	1.13	0.89	-0.38	-0.22	1.50	1.11	0.14	-0.10	-0.25
hsa-miR-139-5p	0.39	-0.26	-1.38	-1.11	1.77	0.85	0.41	-0.25	-0.51
hsa-miR-143	0.10	4.45	-0.18	0.49	0.28	3.96	-2.86	1.49	0.83
hsa-miR-143*	-0.10	2.50	-0.46	-0.54	0.36	3.03	-2.77	-0.18	-0.10
hsa-miR-145	-0.69	3.96	-2.14	-1.08	1.45	5.04	-3.45	1.19	0.13
hsa-miR-145*	-0.76	1.71	0.47	-1.67	-1.24	3.38	-4.24	-1.77	0.37
hsa-miR-148b	0.55	-0.45	0.16	-1.02	0.39	0.57	-0.84	-1.84	-0.65
hsa-miR-150	2.14	1.30	0.44	1.06	1.69	0.24	-0.32	-1.16	-1.78
hsa-miR-181c*	0.34	-1.96	-0.42	-1.29	0.76	-0.67	1.39	-0.91	-0.04

microRNA	DC HH20 Fold	DC HH25 Fold	DQ HH20 Fold	DQ HH25 Fold	QC HH20 Fold	QC HH25 Fold	Chick HH25/HH20 Fold	Duck HH25/HH20 Fold	Quail HH25/HH20 Fold
hsa-miR-182	0.78	3.86	1.50	1.23	-0.72	2.63	-3.06	0.03	0.30
hsa-miR-190b	-0.75	-2.53	-1.89	-1.68	1.13	-0.85	1.77	-0.01	-0.21
hsa-miR-192	0.81	0.76	-2.25	-0.71	3.06	1.47	0.40	0.35	-1.19
hsa-miR-210	0.77	-0.60	-0.60	0.36	1.37	-0.96	2.32	0.96	0.00
hsa-miR-23a	1.73	3.01	0.46	1.05	1.27	1.95	-0.53	0.74	0.15
hsa-miR-27a	1.69	2.75	1.82	1.70	-0.13	1.05	-0.91	0.15	0.26
hsa-miR-338-3p	-0.09	-1.66	0.12	-0.17	-0.21	-1.49	1.77	0.20	0.48
hsa-miR-338-5p	-0.21	-1.75	0.17	-0.83	-0.38	-0.92	0.97	-0.57	0.43
hsa-miR-363	0.00	-0.98	0.30	-0.82	-0.30	-0.16	-0.02	-1.00	0.13
hsa-miR-363*	0.71	1.37	0.81	1.08	-0.10	0.30	-0.01	0.65	0.38
hsa-miR-369-3p	-0.62	-0.38	-2.37	-2.84	1.75	2.46	-2.61	-2.37	-1.90
hsa-miR-378	0.29	1.54	-2.65	-0.65	2.94	2.19	-0.14	1.11	-0.89
hsa-miR-423-5p	0.75	0.20	-1.63	-2.57	2.38	2.78	-2.00	-2.55	-1.60
hsa-miR-425	0.55	-0.65	0.57	0.60	-0.02	-1.24	0.19	-1.01	-1.04
hsa-miR-92a-2*	1.33	1.55	1.18	0.73	0.15	0.82	-1.09	-0.87	-0.42
hsa-miR-92b	1.26	-4.17	0.00	0.81	1.26	-4.97	4.97	-0.45	-1.27
hsa-miR-96	1.50	3.52	1.31	1.33	0.19	2.18	-2.88	-0.86	-0.88
tgu-miR-1388	-2.41	-3.78	-1.44	-3.41	-0.97	-0.37	-0.20	-1.57	0.40
tgu-miR-2970	-2.56	-3.89	-2.67	-3.38	0.10	-0.51	1.00	-0.33	0.38

Table 3-2: microRNAs differentially expressed among chicken, quail, and duck frontonasal neural crest cells. Fold changes for the first biological sample only (BS1 in Table 3-1) are log2 scale, with expression in duck relative to chicken or quail, in quail relative to chicken, or HH25 relative to HH20. For example, a negative number is expressed at a lower level in the duck versus chicken. Highlighted comparisons pass >2-fold change and normalized read count of >15 sequences per million mapped reads (PMMR) criteria. DC, duck/chicken comparison; DQ, duck/quail comparison; QC, quail/chicken comparison.

Expressed at higher levels at HH20 than HH25 in all three species			
microRNA	**Average Fold Change**	**Known Functions and/or Targets**	**Reference**
gga-miR-122	7.30	Targets *CyclinG1* to induce *p53* and inhibit cell cycle progression at G1	(Fornari et al. 2009)
gga-miR-142-3p	2.79	Down-regulates cAMP production	(Huang B. et al. 2009a)
gga-miR-2954_ukstar	3.72	Unknown	
gga-miR-302b	4.15	Expression of miRNA cluster promotes somatic cell reprogramming	(Lin et al. 2010, Lin et al. 2008)
gga-miR-302b*	5.67		
gga-miR-302c	2.69		
hsa-miR-1246	2.86	Unknown	
hsa-miR-148b	2.31	Targets DNA methyltransferase *DNMT3B*	(Duursma et al. 2008)
hsa-miR-369-3p	5.01	Unknown	
hsa-miR-423-5p	4.30	Unknown	
hsa-miR-92a-2*	1.76	Unknown	
hsa-miR-96	3.67	Morpholino results in abnormal cranial cartilage; overexpression leads to cell cycle arrest in G1	(Gessert et al. 2010, Yu S. et al. 2010)
Expressed at higher levels at HH25 than HH20 in all three species			
microRNA	**Average Fold Change**	**Known Functions and/or Targets**	**Reference**
gga-let-7a	3.39	miRNA family associated with cellular differentiation	(Roush and Slack 2008)
gga-let-7a_ukstar	11.73		
gga-let-7c_ukstar	3.08		
gga-let-7d	3.43		
gga-let-7f	3.24		
gga-let-7g	4.77		
gga-let-7i	11.30		
gga-let-7k	2.52		
gga-miR-107	1.96	Induced by p53 to inhibit cell cycle progression at G1	(Takahashi et al. 2009, Yamakuchi et al. 2010)
gga-miR-15b	2.22	Targets *BCL2* to induce apoptosis; Targets *CCNE1* to inhibit cell cycle progression at G1	(Xia H. et al. 2009b, Xia L. et al. 2008)
gga-miR-15c	2.28	Unknown	
gga-miR-218	2.39	Targets *ROBO1* and *IKK-beta* to	(Song et al.

		inhibit cell migration and invasion	2010, Tie et al. 2010)
gga-miR-30a-3p	2.21	miRNA family targets EMT regulators *SNAIL1* and *VIMENTIN*	(Braun J. et al. 2010, Joglekar et al. 2009)
gga-miR-30a-5p	3.86		
gga-miR-30d_ukstar	2.24		
gga-miR-30e_ukstar	2.03		
hsa-miR-1261	2.19	Unknown	
Expressed at higher levels in duck versus quail and chick at both HH20 and HH25			
microRNA	**Average Fold Change**	**Known Functions and/or Targets**	**Reference**
gga-miR-106_ukstar	3.89	Unknown	
gga-miR-144_ukstar	3.78	Unknown	
gga-miR-146b	15.51	Targets metalloprotease *MMP16* to inhibit cell migration	(Xia H. et al. 2009a)
gga-miR-1552-5p	3.62	Unknown	
gga-miR-16c	2.13	Unknown	
gga-miR-183	5.63	Targets stemness regulator *BMI1* and pro-apoptotic *PDCD4*; Repressed by EMT regulator ZEB1	(Li J. et al. 2010, Wellner et al. 2009)
gga-miR-200a	2.10	miRNA family targets positive Wnt signaling regulators; Negative feedback loop with EMT regulators *ZEB1* and *ZEB2*	(Bracken et al. 2008, Gregory et al. 2008, Kennell et al. 2008)
gga-miR-200b	1.71	Morpholino results in abnormal cranial cartilage; miRNA family targets positive Wnt signaling regulators; Negative feedback loop with EMT regulators *ZEB1* and *ZEB2*	(Bracken et al. 2008, Gessert et al. 2010, Gregory et al. 2008, Kennell et al. 2008)
gga-miR-203	5.39	Targets Wnt signaling activator *LEF1/TCF1*; Repressed by EMT regulator ZEB1; Targets *BMI1* and *p63* to inhibit stemness	(Thatcher et al. 2008, Wellner et al. 2009, Yi et al. 2008)
gga-miR-24	2.28	Inhibited by RUNX2; Targets *SATB2*	(Hassan et al. 2010)
gga-miR-27b	2.05	Activates Wnt signaling; Targets *RUNX1*	(Feng et al. 2009, Wang and Xu 2010)
hsa-miR-182	5.36	Targets *FOXO1* transcription factor	(Guttilla and

			White 2009)
hsa-miR-23a	3.70	Inhibited by RUNX2; Targets *SATB2*	(Hassan et al. 2010)
hsa-miR-27a	4.18	Activates Wnt signaling; Targets *RUNX1* and *SATB2*; Inhibited by RUNX2	(Feng et al. 2009, Hassan et al. 2010, Wang and Xu 2010)
hsa-miR-363*	2.02	Unknown	
Expressed at higher levels quail and chick versus duck at both HH20 and HH25			
microRNA	**Average Fold Change**	**Known Functions and/or Targets**	**Reference**
gga-miR-18a_ukstar	2.02	Targets *K-RAS* oncogene	(Tsang and Kwok 2009)
gga-miR-215	12.47	Induced by p53 to inhibit cell cycle progression at G2	(Braun C. J. et al. 2008)
gga-miR-2964	3.51	Unknown	
gga-miR-3529	32.15	Unknown	
tgu-miR-1388	8.12	Unknown	
tgu-miR-2970	9.36	Unknown	
Expressed at higher levels in quail and chick versus duck only at HH25			
microRNA	**Average Fold Change**	**Known Functions and/or Targets**	**Reference**
gga-let-7c	2.55	miRNA family associated with cellular differentiation	(Roush and Slack 2008)
gga-miR-100_ukstar	3.05	related to let-7 family	(Christodoulou et al. 2010)
gga-miR-125b_ukstar	2.22	related to let-7 family	(Christodoulou et al. 2010)
gga-miR-137	11.67	Targets *CDK6* and *CDC42* to inhibit cell cycle progression at G1 and promote differentiation	(Liu M. et al. 2010b, Silber et al. 2008)
gga-miR-148a_ukstar	2.58	Unknown	
gga-miR-30c-2_ukstar	2.89	miRNA family targets EMT regulators *SNAIL1* and *VIMENTIN*	(Braun J. et al. 2010, Joglekar et al. 2009)
hsa-miR-129-5p	2.17	Target stem cell regulator *SOX4*	(Huang Y. W. et al. 2009b, Shen et al. 2010)

Expressed at higher levels in duck versus quail and chicken only at HH25			
microRNA	**Average Fold Change**	**Known Functions and/or Targets**	**Reference**
gga-miR-10b	3.43	Induced by EMT regulator TWIST1	(Ma et al. 2007)
gga-miR-142-5p	3.40	Induced by miR-223 via CEBPB and LMO2	(Sun W. et al. 2010)
gga-miR-205a	3.00	Coordinately expressed with miR-200 family; Targets *SHIP2* to induce the AKT pathway	(Gregory et al. 2008, Yu J. et al. 2008)
gga-miR-22*	2.20	Unknown	
gga-miR-222	1.79	Targets *p27(KIP1)* to induce cell cycle progression	(Galardi et al. 2007, Lambeth et al. 2009)
gga-miR-454	1.71	Unknown	
gga-miR-551	1.74	Unknown	

Table 3-3: Differentially expressed microRNAs with discernable trends among chicken, duck, and quail. For a complete list of differentially expressed microRNAs, see Table 3-2.

MiRNAs that regulate stemness, cellular differentiation and epithelia-mesenchyme transitions are differentially regulated between the two developmental stages in all three species

Twelve miRNAs are down-regulated and seventeen are up-regulated from HH20 to HH25 in all three bird species (Table 3-3). The extent of these changes varies depending upon the particular species. For example, miR-96 is down-regulated at HH25 by 1.81-fold in duck, by 1.84-fold in quail and by 7.35-fold in chicken NC cells. Knockdown of this particular microRNA in zebrafish has previously been shown to result in abnormal cranial cartilage (Gessert et al. 2010). MiR-302b, miR-302b*, and miR-302c, which are the only members of the 9-member miR-302 family that are detectable at either stage, are down-regulated

between 2.3- and 7.8-fold at HH25 in all three species (Table 3-2). This miRNA family has been previously associated with “stemness.” They are highly expressed in embryonic stem cells and when induced can reprogram somatic cells into a pleuripotent state (Lin et al. 2010, Lin et al. 2008).

Of the seventeen miRNAs that are expressed at higher levels at the later stage of development (HH25) in the chicken, duck, and quail (Table 3-3) four belong to the miR-30 family (miR-30a-3p, miR-30a-5p, miR-30d*, and miR-30e*). These are up-regulated by between 1.4- to 7.7-fold (Table 3-2). This family of miRNAs has been previously implicated in regulating mesenchymal-to-epithelial transitions (MET) (Braun J. et al. 2010, Joglekar et al. 2009). While epithelial-to-mesenchymal transitions (EMT) are crucial for neural crest migration (Sauka-Spengler and Bronner-Fraser 2008) and later events of facial development such as lip fusion (Sun D. et al. 2000), it is unclear if MET or EMT is occurring in the HH20-HH25 developmental window. Interestingly, EMT has also been associated with stemness, while MET is associated with cellular differentiation (Brabletz and Brabletz 2010, Mani et al. 2008, Wellner et al. 2009). Thus, up-regulation of the miR-30 family might reflect an increase in cellular differentiation at HH25. In agreement with this, let-7a, let-7a*, let-7c*, let-7d, let-7f, let-7g, let-7i, and let-7k are all up-regulated by 1.4- to 27.9-fold at HH25 in all three species (Table 3-2). These 8 miRNAs belong to the 19 member let-7 family of miRNAs, the expression of which has been associated with cellular differentiation (Roush and Slack 2008). An additional seven miRNAs are up-regulated at HH25 only in

chicken and quail, but not in duck neural crest (Table 3-3). These include miR-30c-2*, miR-129-5p which targets the stem cell regulator *SOX4* (Huang Y. W. et al. 2009b, Shen et al. 2010), let-7c, the differentiation-promoting miR-137 (Silber et al. 2008), and the let-7-related miR-100* and miR-125b-2* (Christodoulou et al. 2010) (Table 3-2). In all, 9 of 10 detectable members of the let-7 family are up-regulated in chicken and quail NC by HH25 (Table 3-2).

A final set of seven miRNAs are only up-regulated in the duck NC compared to chicken and quail after morphological variations are evident at HH25 (Table 3-3). For example, miR-222 is expressed at similar levels in the duck, chicken, and quail at HH20. However, by HH25, it is down-regulated 1.8-fold in the beaked birds, but remains more highly expressed in duck (Table 3-2). This miRNA has been shown to down-regulate the cell cycle regulator *p27(KIP1)* in a number of systems, including chicken cell lines (Galardi et al. 2007, Lambeth et al. 2009) (see **Chapter 4** for more on this).

MiRNAs that regulate bone formation and Wnt signaling are differentially regulated in the duck compared to the chicken and quail

Twenty-one miRNAs are differentially regulated in the duck compared to chicken and quail (which are, at least superficially, quite similar in bill morphology) at both developmental stages. Six miRNAs with unrelated or unknown functions are expressed at lower levels in the flat-billed duck compared to the conical-billed chicken and quail (Table 3-3). Fifteen miRNAs are more

highly expressed in duck NC cells at both stages (Table 3-3), including the miR-23a-27a-24-2 cluster, which is negatively regulated by the osteoblast transcription factor RUNX2 (Hassan et al. 2010). Expression of each of these miRNAs suppresses bone formation and directly down-regulates *SATB2* (Hassan et al. 2010), which has been previously implicated in facial development and associated with morphological variation in the avian beak (Brugmann et al. 2010, FitzPatrick et al. 2003).

Additionally, miR-200a, miR-200b, miR-203, miR-27a, and miR-27b, all of which interact with Wnt signaling (Kennell et al. 2008, Thatcher et al. 2008, Wang and Xu 2010), are all expressed at 1.5- to 58.9-fold higher levels in duck neural crest cells versus the other species (Table 3-2). As shown in **Chapter 4**, the Wnt pathway regulates regional growth in facial structures and its activation correlates with differences in beak morphology. MiR-200a and 200b have also been shown to regulate mesenchymal-to-epithelia transitions (MET) via direct repression of *ZEB1* and *ZEB2* (Bracken et al. 2008, Gregory et al. 2008), though, as stated above, it is unclear if MET is occurring in the HH20 to HH25 developmental window.

qRT-PCR and *in situ* hybridization validate the sequencing data

I confirmed miRNA trends from the sequencing data both *in vitro* and *in vivo*. First, I conducted quantitative real-time polymerase chain reaction (qRT-PCR) on mature miRNAs using a second biological sample of NC cells from HH20 and HH25 ducks and chickens. For nine of ten miRNAs examined, qRT-PCR confirmed expression trends identified by Next-Generation sequencing (Table 3-2 and Table 3-4). One miRNA, gga-miR-215, showed a slight discrepancy between qRT-PCR and miRNA-seq data. By sequencing, this microRNA is expressed at higher levels in chicken than duck neural crest at both developmental stages. However, by qRT-PCR I only confirmed differential expression at HH20. This microRNA has lower read numbers (approximately 50 PMMR, rather than hundreds or thousands of reads) than most of the other miRNAs confirmed by qRT-PCR, which may account for this discrepancy. Further, absolute changes in miRNA expression did not always agree between sequence data and qRT-PCR as the only commercially available primers for miRNA qRT-PCR are designed from human, not chicken, orthologs. Some sequence differences exist between the miRNAs across that evolutionary period --approximately 310 million years (Kumar and Hedges 1998)-- and this may account for the differences observed between the sequencing and RT-PCR data.

	Chick HH20	Chick HH25	Duck HH20	Duck HH25	Overall trend from qRT-PCR	Overall trend from sequencing
gga-let-7a	2.13	3.90	3.54	6.05	Higher at HH25 than HH20 in both species	Higher at HH25 than HH20 in both species
gga-miR-146b	1.00	0.50	3.29	3.84	Higher in duck than chick at both stages	Higher in duck than chick at both stages
gga-miR-16	4.00	3.79	5.15	5.84	Higher in duck than chick at both stages	Higher in duck than chick at both stages
gga-miR-183	-2.65	-2.29	-0.68	-0.96	Higher in duck than chick at both stages	Higher in duck than chick at both stages
gga-miR-200a	-0.29	-0.44	1.74	1.14	Higher in duck than chick at both stages	Higher in duck than chick at both stages
gga-miR-200b	-1.20	-1.16	0.98	0.11	Higher in duck than chick at both stages	Higher in duck than chick at both stages
gga-miR-203	-4.52	-4.58	-2.50	-0.04	Higher in duck than chick at both stages	Higher in duck than chick at both stages
gga-miR-215	-6.67	-6.30	-8.02	-6.35	Higher in chicken than duck only at HH20	Higher in chicken than duck at both stages
gga-miR-222	5.23	4.19	6.61	7.01	Higher in duck than chick only at HH25	Higher in duck than chick only at HH25
hsa-miR-143	3.16	3.06	4.05	5.66	Higher in duck than chick at both stages	Higher in duck than chick at both stages

Table 3-4: qRT-PCR validation of miRNA sequencing data. Delta Ct (cycle threshold) values for all microRNAs relative to *RNU6B* input control. Note that values are in log2 scale, with more positive values being more highly expressed.

For one of the differentially expressed miRNAs, miR-222, I performed RNA *in situ* to assess the relative levels and pattern of the mature miRNA in FNPs from duck and chicken (Figure 3-3). In both duck and chicken, this miRNA is expressed throughout the facial prominences, and at higher levels in the maxillary prominences and around the nasal pits. Though they have similar spatial patterns, miR-222 is expressed at higher levels in the duck, in agreement with my sequencing data (Figure 3-3).

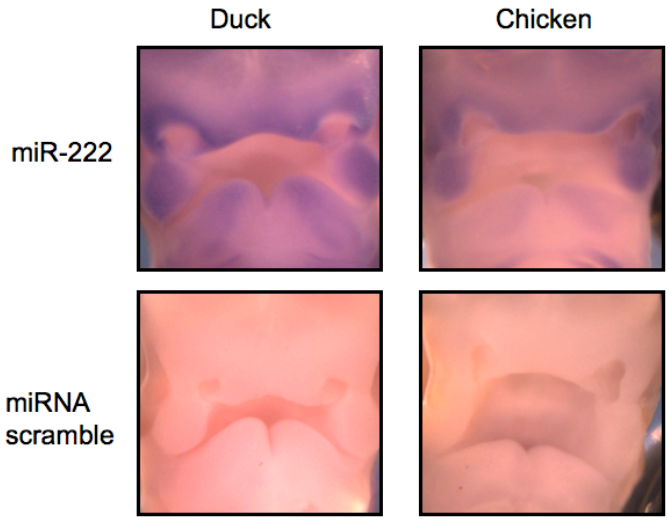

Figure 3-3: *in situ* validation of expression changes for gga-miR-222 in HH25 chickens and ducks.

Conclusions

The unbiased genomic approaches presented in this chapter are the first large-scale investigations of the roles of microRNAs in species-specific facial development and the first comprehensive analysis of miRNAs in the developing facial primordial. Using Next-Generation miRNA sequencing and various

bioinformatic approaches, I identified 186 microRNAs that are expressed in the frontonasal neural crest cells of the chicken, duck, and quail. The vast majority of these are differentially expressed. In remarkable contrast to the relatively unchanged pattern of mRNA expression presented in **Chapter 2**, I found that miRNA expression is dramatically different between developmental stages before (HH20) and after (HH25) morphological variation in the beak is evident.

The patterns of differentially expressed microRNAs (Table 3-3) are consistent with the following model (summarized in Figure 3-4). At HH20, both the chicken and the duck have a multipotent, proliferative neural crest population that expresses high levels of the miR-302 family as well as high levels of miR-222 (Table 3-3), which promote an undifferentiated fate (Lin et al. 2010, Lin et al. 2008) and proliferation via repression of *p27(KIP1)* (Galardi et al. 2007, Lambeth et al. 2009), respectively. By HH25, chicken NC cells have adopted molecular signatures of differentiation. At the same time as the miR-302 family and miR-222 have been down-regulated, eleven miRNAs related to the let-7 family are up-regulated, as well as 2 additional miRNAs associated with cellular differentiation (Table 3-3) (Roush and Slack 2008). By HH26, chicken facial primordia express molecular markers of the bones and skeleton that will eventually form the adult face (Eames and Helms 2004).

Duck NC cells at HH25 have down-regulated the miR-302 family and up-regulated some of the miRNAs associated with cellular differentiation (i.e. the let-7 family), though not as many as chicken NC (Table 3-3). However, in contrast

to the chicken, duck NC still express high levels of miR-222, and this may act to maintain a higher proliferation rate via continued repression of *p27(KIP1)* (Galardi et al. 2007, Lambeth et al. 2009). The duck also has higher levels of the miR-23a-27a-24-2 cluster (Table 3-3). Each of these miRNAs can independently repress the bone-promoting transcription factor *SATB2* (Dobreva et al. 2006, Hassan et al. 2010), and thus the duck may also have a delay in bone formation, as NC cells continue to proliferate.

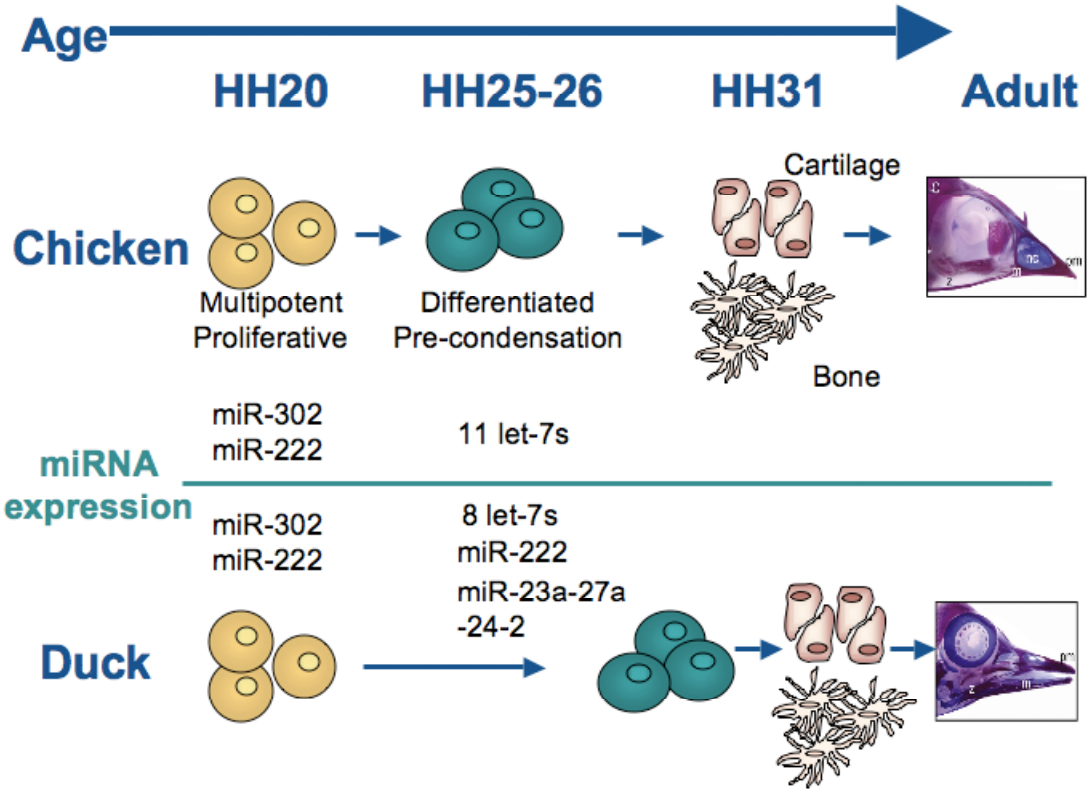

Figure 3-4: Model of differences in timing of neural crest differentiation and bone formation in duck and chicken based on miRNA expression changes. HH20 to HH25 may be the developmental window when multipotent, proliferative neural crest cells (yellow) gain the molecular signatures of differentiation (green) before becoming the cartilage and bones of the face. See text for further descriptions. Adult skeletal pictures adapted from (Liu B. et al. 2010a)

Taken together, these miRNA changes (Table 3-3 and Figure 3-4), including differential expression of let-7, miR-302, and miR-30 families (Table 3-3), indicate that the HH20-HH25 developmental window may be a critical transition phase in which multipotent NC cells begin to differentiate to form the various tissues of the face. In addition, given that a number of miRNAs related to let-7 and cellular differentiation are only up-regulated in the chicken and quail at HH25 (Table 3-3), the timing of this transition may be slightly delayed in the morphologically different duck, perhaps allowing a more prolonged period of proliferation. This fits well with current theories that differential regions and levels of proliferation can influence the depth, width, and curvature of the beak (Wu et al. 2004, Wu et al. 2006) and that microRNAs function during the transitions between different cellular states (Giraldez et al. 2006).

References

Abzhanov A, Protas M, Grant BR, Grant PR, Tabin CJ. 2004. Bmp4 and morphological variation of beaks in Darwin's finches. Science 305: 1462-1465.

Abzhanov A, Kuo WP, Hartmann C, Grant BR, Grant PR, Tabin CJ. 2006. The calmodulin pathway and evolution of elongated beak morphology in Darwin's finches. Nature 442: 563-567.

Brabletz S, Brabletz T. 2010. The ZEB/miR-200 feedback loop--a motor of cellular plasticity in development and cancer? EMBO Rep 11: 670-677.

Bracken CP, Gregory PA, Kolesnikoff N, Bert AG, Wang J, Shannon MF, Goodall GJ. 2008. A double-negative feedback loop between ZEB1-SIP1 and the microRNA-200 family regulates epithelial-mesenchymal transition. Cancer Res 68: 7846-7854.

Braun CJ, Zhang X, Savelyeva I, Wolff S, Moll UM, Schepeler T, Orntoft TF, Andersen CL, Dobbelstein M. 2008. p53-Responsive micrornas 192 and 215 are capable of inducing cell cycle arrest. Cancer Res 68: 10094-10104.

Braun J, Hoang-Vu C, Dralle H, Huttelmaier S. 2010. Downregulation of microRNAs directs the EMT and invasive potential of anaplastic thyroid carcinomas. Oncogene 29: 4237-4244.

Brugmann SA, Powder KE, Young NM, Goodnough LH, Hahn SM, James AW, Helms JA, Lovett M. 2010. Comparative gene expression analysis of avian embryonic facial structures reveals new candidates for human craniofacial disorders. Hum Mol Genet 19: 920-930.

Christodoulou F, Raible F, Tomer R, Simakov O, Trachana K, Klaus S, Snyman H, Hannon GJ, Bork P, Arendt D. 2010. Ancient animal microRNAs and the evolution of tissue identity. Nature 463: 1084-1088.

Dobreva G, Chahrour M, Dautzenberg M, Chirivella L, Kanzler B, Farinas I, Karsenty G, Grosschedl R. 2006. SATB2 is a multifunctional determinant of craniofacial patterning and osteoblast differentiation. Cell 125: 971-986.

Duursma AM, Kedde M, Schrier M, le Sage C, Agami R. 2008. miR-148 targets human DNMT3b protein coding region. RNA 14: 872-877.

Eames BF, Helms JA. 2004. Conserved molecular program regulating cranial and appendicular skeletogenesis. Dev Dyn 231: 4-13.

Feng J, Iwama A, Satake M, Kohu K. 2009. MicroRNA-27 enhances differentiation of myeloblasts into granulocytes by post-transcriptionally downregulating Runx1. Br J Haematol 145: 412-423.

FitzPatrick DR, et al. 2003. Identification of SATB2 as the cleft palate gene on 2q32-q33. Hum Mol Genet 12: 2491-2501.

Fornari F, et al. 2009. MiR-122/cyclin G1 interaction modulates p53 activity and affects doxorubicin sensitivity of human hepatocarcinoma cells. Cancer Res 69: 5761-5767.

Galardi S, Mercatelli N, Giorda E, Massalini S, Frajese GV, Ciafre SA, Farace MG. 2007. miR-221 and miR-222 expression affects the proliferation potential of human prostate carcinoma cell lines by targeting p27Kip1. J Biol Chem 282: 23716-23724.

Gessert S, Bugner V, Tecza A, Pinker M, Kuhl M. 2010. FMR1/FXR1 and the miRNA pathway are required for eye and neural crest development. Dev Biol 341: 222-235.

Giraldez AJ, Mishima Y, Rihel J, Grocock RJ, Van Dongen S, Inoue K, Enright AJ, Schier AF. 2006. Zebrafish MiR-430 promotes deadenylation and clearance of maternal mRNAs. Science 312: 75-79.

Gregory PA, Bert AG, Paterson EL, Barry SC, Tsykin A, Farshid G, Vadas MA, Khew-Goodall Y, Goodall GJ. 2008. The miR-200 family and miR-205 regulate epithelial to mesenchymal transition by targeting ZEB1 and SIP1. Nat Cell Biol 10: 593-601.

Griffiths-Jones S, Saini HK, van Dongen S, Enright AJ. 2008. miRBase: tools for microRNA genomics. Nucleic Acids Res 36: D154-158.

Guttilla IK, White BA. 2009. Coordinate regulation of FOXO1 by miR-27a, miR-96, and miR-182 in breast cancer cells. J Biol Chem 284: 23204-23216.

Hassan MQ, Gordon JA, Beloti MM, Croce CM, van Wijnen AJ, Stein JL, Stein GS, Lian JB. 2010. A network connecting Runx2, SATB2, and the miR-23a~27a~24-2 cluster regulates the osteoblast differentiation program. Proc Natl Acad Sci U S A 107: 19879-19884.

Hawkins RD, Helms CA, Winston JB, Warchol ME, Lovett M. 2006. Applying genomics to the avian inner ear: development of subtractive cDNA resources for exploring sensory function and hair cell regeneration. Genomics 87: 801-808.

Huang B, Zhao J, Lei Z, Shen S, Li D, Shen GX, Zhang GM, Feng ZH. 2009a. miR-142-3p restricts cAMP production in CD4+CD25- T cells and CD4+CD25+ TREG cells by targeting AC9 mRNA. EMBO Rep 10: 180-185.

Huang T, Liu Y, Huang M, Zhao X, Cheng L. 2010. Wnt1-cre-mediated conditional loss of Dicer results in malformation of the midbrain and cerebellum and failure of neural crest and dopaminergic differentiation in mice. J Mol Cell Biol 2: 152-163.

Huang YW, Liu JC, Deatherage DE, Luo J, Mutch DG, Goodfellow PJ, Miller DS, Huang TH. 2009b. Epigenetic repression of microRNA-129-2 leads to overexpression of SOX4 oncogene in endometrial cancer. Cancer Res 69: 9038-9046.

International Chicken Genome Sequencing Consortium. 2004. Sequence and comparative analysis of the chicken genome provide unique perspectives on vertebrate evolution. Nature 432: 695-716.

Joglekar MV, Patil D, Joglekar VM, Rao GV, Reddy DN, Mitnala S, Shouche Y, Hardikar AA. 2009. The miR-30 family microRNAs confer epithelial phenotype to human pancreatic cells. Islets 1: 137-147.

Kennell JA, Gerin I, MacDougald OA, Cadigan KM. 2008. The microRNA miR-8 is a conserved negative regulator of Wnt signaling. Proc Natl Acad Sci U S A 105: 15417-15422.

Kontges G, Lumsden A. 1996. Rhombencephalic neural crest segmentation is preserved throughout craniofacial ontogeny. Development 122: 3229-3242.

Kumar S, Hedges SB. 1998. A molecular timescale for vertebrate evolution. Nature 392: 917-920.

Lambeth LS, Yao Y, Smith LP, Zhao Y, Nair V. 2009. MicroRNAs 221 and 222 target p27Kip1 in Marek's disease virus-transformed tumour cell line MSB-1. J Gen Virol 90: 1164-1171.

Li J, Fu H, Xu C, Tie Y, Xing R, Zhu J, Qin Y, Sun Z, Zheng X. 2010. miR-183 inhibits TGF-beta1-induced apoptosis by downregulation of PDCD4 expression in human hepatocellular carcinoma cells. BMC Cancer 10: 354.

Li T, Wu R, Zhang Y, Zhu D. 2011. A systematic analysis of the skeletal muscle miRNA transcriptome of chicken varieties with divergent skeletal muscle growth identifies novel miRNAs and differentially expressed miRNAs. BMC Genomics 12: 186.

Lin SL, Chang DC, Lin CH, Ying SY, Leu D, Wu DT. 2010. Regulation of somatic cell reprogramming through inducible mir-302 expression. Nucleic Acids Res.

Lin SL, Chang DC, Chang-Lin S, Lin CH, Wu DT, Chen DT, Ying SY. 2008. Mir-302 reprograms human skin cancer cells into a pluripotent ES-cell-like state. RNA 14: 2115-2124.

Liu B, Rooker SM, Helms JA. 2010a. Molecular control of facial morphology. Semin Cell Dev Biol 21: 309-313.

Liu M, et al. 2010b. miR-137 targets Cdc42 expression, induces cell cycle G1 arrest and inhibits invasion in colorectal cancer cells. Int J Cancer.

Ma L, Teruya-Feldstein J, Weinberg RA. 2007. Tumour invasion and metastasis initiated by microRNA-10b in breast cancer. Nature 449: 682-688.

Mallarino R, Grant PR, Grant BR, Herrel A, Kuo WP, Abzhanov A. 2011. Two developmental modules establish 3D beak-shape variation in Darwin's finches. Proc Natl Acad Sci U S A 108: 4057-4062.

Mani SA, et al. 2008. The epithelial-mesenchymal transition generates cells with properties of stem cells. Cell 133: 704-715.

Mukhopadhyay P, Brock G, Pihur V, Webb C, Pisano MM, Greene RM. 2010. Developmental microRNA expression profiling of murine embryonic orofacial tissue. Birth Defects Res A Clin Mol Teratol 88: 511-534.

Noden DM. 1978. The control of avian cephalic neural crest cytodifferentiation. I. Skeletal and connective tissues. Dev Biol 67: 296-312.

Okamura K, Phillips MD, Tyler DM, Duan H, Chou YT, Lai EC. 2008. The regulatory activity of microRNA* species has substantial influence on microRNA and 3' UTR evolution. Nat Struct Mol Biol 15: 354-363.

Roush S, Slack FJ. 2008. The let-7 family of microRNAs. Trends Cell Biol 18: 505-516.

Sauka-Spengler T, Bronner-Fraser M. 2008. A gene regulatory network orchestrates neural crest formation. Nat Rev Mol Cell Biol 9: 557-568.

Schneider RA, Helms JA. 2003. The cellular and molecular origins of beak morphology. Science 299: 565-568.

Shen R, Pan S, Qi S, Lin X, Cheng S. 2010. Epigenetic repression of microRNA-129-2 leads to overexpression of SOX4 in gastric cancer. Biochem Biophys Res Commun 394: 1047-1052.

Silber J, et al. 2008. miR-124 and miR-137 inhibit proliferation of glioblastoma multiforme cells and induce differentiation of brain tumor stem cells. BMC Med 6: 14.

Song L, Huang Q, Chen K, Liu L, Lin C, Dai T, Yu C, Wu Z, Li J. 2010. miR-218 inhibits the invasive ability of glioma cells by direct downregulation of IKK-beta. Biochem Biophys Res Commun 402: 135-140.

Sun D, Baur S, Hay ED. 2000. Epithelial-mesenchymal transformation is the mechanism for fusion of the craniofacial primordia involved in morphogenesis of the chicken lip. Dev Biol 228: 337-349.

Sun W, Shen W, Yang S, Hu F, Li H, Zhu TH. 2010. miR-223 and miR-142 attenuate hematopoietic cell proliferation, and miR-223 positively regulates miR-142 through LMO2 isoforms and CEBP-beta. Cell Res 20: 1158-1169.

Takahashi Y, Forrest AR, Maeno E, Hashimoto T, Daub CO, Yasuda J. 2009. MiR-107 and MiR-185 can induce cell cycle arrest in human non small cell lung cancer cell lines. PLoS One 4: e6677.

Thatcher EJ, Paydar I, Anderson KK, Patton JG. 2008. Regulation of zebrafish fin regeneration by microRNAs. Proc Natl Acad Sci U S A 105: 18384-18389.

Tie J, et al. 2010. MiR-218 inhibits invasion and metastasis of gastric cancer by targeting the Robo1 receptor. PLoS Genet 6: e1000879.

Tsang WP, Kwok TT. 2009. The miR-18a* microRNA functions as a potential tumor suppressor by targeting on K-Ras. Carcinogenesis 30: 953-959.

Tucker AS, Lumsden A. 2004. Neural crest cells provide species-specific patterning information in the developing branchial skeleton. Evol Dev 6: 32-40.

Wang T, Xu Z. 2010. miR-27 promotes osteoblast differentiation by modulating Wnt signaling. Biochem Biophys Res Commun 402: 186-189.

Wellner U, et al. 2009. The EMT-activator ZEB1 promotes tumorigenicity by repressing stemness-inhibiting microRNAs. Nat Cell Biol 11: 1487-1495.

Wu P, Jiang TX, Suksaweang S, Widelitz RB, Chuong CM. 2004. Molecular shaping of the beak. Science 305: 1465-1466.

Wu P, Jiang TX, Shen JY, Widelitz RB, Chuong CM. 2006. Morphoregulation of avian beaks: comparative mapping of growth zone activities and morphological evolution. Dev Dyn 235: 1400-1412.

Xia H, et al. 2009a. microRNA-146b inhibits glioma cell migration and invasion by targeting MMPs. Brain Res 1269: 158-165.

—. 2009b. MicroRNA-15b regulates cell cycle progression by targeting cyclins in glioma cells. Biochem Biophys Res Commun 380: 205-210.

Xia L, Zhang D, Du R, Pan Y, Zhao L, Sun S, Hong L, Liu J, Fan D. 2008. miR-15b and miR-16 modulate multidrug resistance by targeting BCL2 in human gastric cancer cells. Int J Cancer 123: 372-379.

Yamakuchi M, Lotterman CD, Bao C, Hruban RH, Karim B, Mendell JT, Huso D, Lowenstein CJ. 2010. P53-induced microRNA-107 inhibits HIF-1 and tumor angiogenesis. Proc Natl Acad Sci U S A 107: 6334-6339.

Yang JS, Phillips MD, Betel D, Mu P, Ventura A, Siepel AC, Chen KC, Lai EC. 2010. Widespread regulatory activity of vertebrate microRNA* species. RNA.

Yi R, Poy MN, Stoffel M, Fuchs E. 2008. A skin microRNA promotes differentiation by repressing 'stemness'. Nature 452: 225-229.

Yu J, Ryan DG, Getsios S, Oliveira-Fernandes M, Fatima A, Lavker RM. 2008. MicroRNA-184 antagonizes microRNA-205 to maintain SHIP2 levels in epithelia. Proc Natl Acad Sci U S A 105: 19300-19305.

Yu S, Lu Z, Liu C, Meng Y, Ma Y, Zhao W, Liu J, Yu J, Chen J. 2010. miRNA-96 suppresses KRAS and functions as a tumor suppressor gene in pancreatic cancer. Cancer Res 70: 6015-6025.

Zehir A, Hua LL, Maska EL, Morikawa Y, Cserjesi P. 2010. Dicer is required for survival of differentiating neural crest cells. Dev Biol 340: 459-467.

CHAPTER 4

Follow-up Studies

Introduction

My studies detailed in **Chapter 2** and **Chapter 3** describe new approaches and new candidate pathways in craniofacial morphogenesis. In this chapter I illustrate specific examples of how these genomic approaches can initiate new avenues of investigation and testable hypotheses. The experiments described below have either already been incorporated into my published work or are parts of my miRNA studies. I have grouped them together here as they all stem from the genomic data sets presented in the previous two chapters.

First, I present follow-up studies of the differences in Wnt signaling that I observed in my cross-species analysis. Viral mis-expression of the Wnt signaling pathway completed by our collaborators functionally validates some of the gene expression changes identified in **Chapter 2**. Next, I show how differentially expressed miRNAs described in **Chapter 3** can be correlated with the protein levels of specific mRNA targets in frontonasal neural crest cells. I then present an assessment of the application of my work to human health by evaluating whether the differentially expressed genes I identified in **Chapter 3** may serve as candidates for genes involved in human craniofacial disorders. Finally, I use DNA sequence analysis and PCR to show that my approaches in **Chapter 3** can identify and validate interesting species-specific miRNAs.

Results

Changes in Wnt activity promote proliferation, regional growth, and Bmp expression in the frontonasal prominence

Following upon my gene expression studies our collaborators evaluated one of our microarray observations, the dramatic up-regulation of multiple components of Wnt signaling in the duck neural crest relative to chicken and quail, by examining the functional consequences of Wnt mis-expression in the developing face. First, they found that an ectopic Wnt signal is sufficient to increase cell proliferation in frontonasal neural crest cells. Using a retrovirus expressing a Wnt ligand, they found that injection of RCAS-*WNT2B* into an HH20 chicken face (Figure 4-1A) resulted in wide-spread infection of frontonasal mesenchyme after 24hrs, as measured by *in situ* hybridization using probes against the virus and *WNT2B* (Figure 4-1D-G). Additionally, this increased activation of the Wnt pathway was sufficient to increase the size of the facial prominences after 24 hrs (Figure 4-1, B-C). On the control (uninjected) side, the FNP is close to the lateral nasal and maxillary prominences but has yet to fuse with them to create the nasal pit (Figure 4-1B-C). In contrast, the Wnt infected side demonstrated dramatic enlargement of the FNP (Figure 4-1B-C). Further, FNPs infected with RCAS-*WNT2B* showed increased expression of *BMP4* by *in situ* (Figure 4-1H-I) and quantitative real-time PCR (qRT-PCR, data not shown), placing these findings in context with previously published reports regarding

molecular mechanisms involved in beak morphology (Abzhanov et al. 2004, Abzhanov et al. 2006, Wu et al. 2004, Wu et al. 2006).

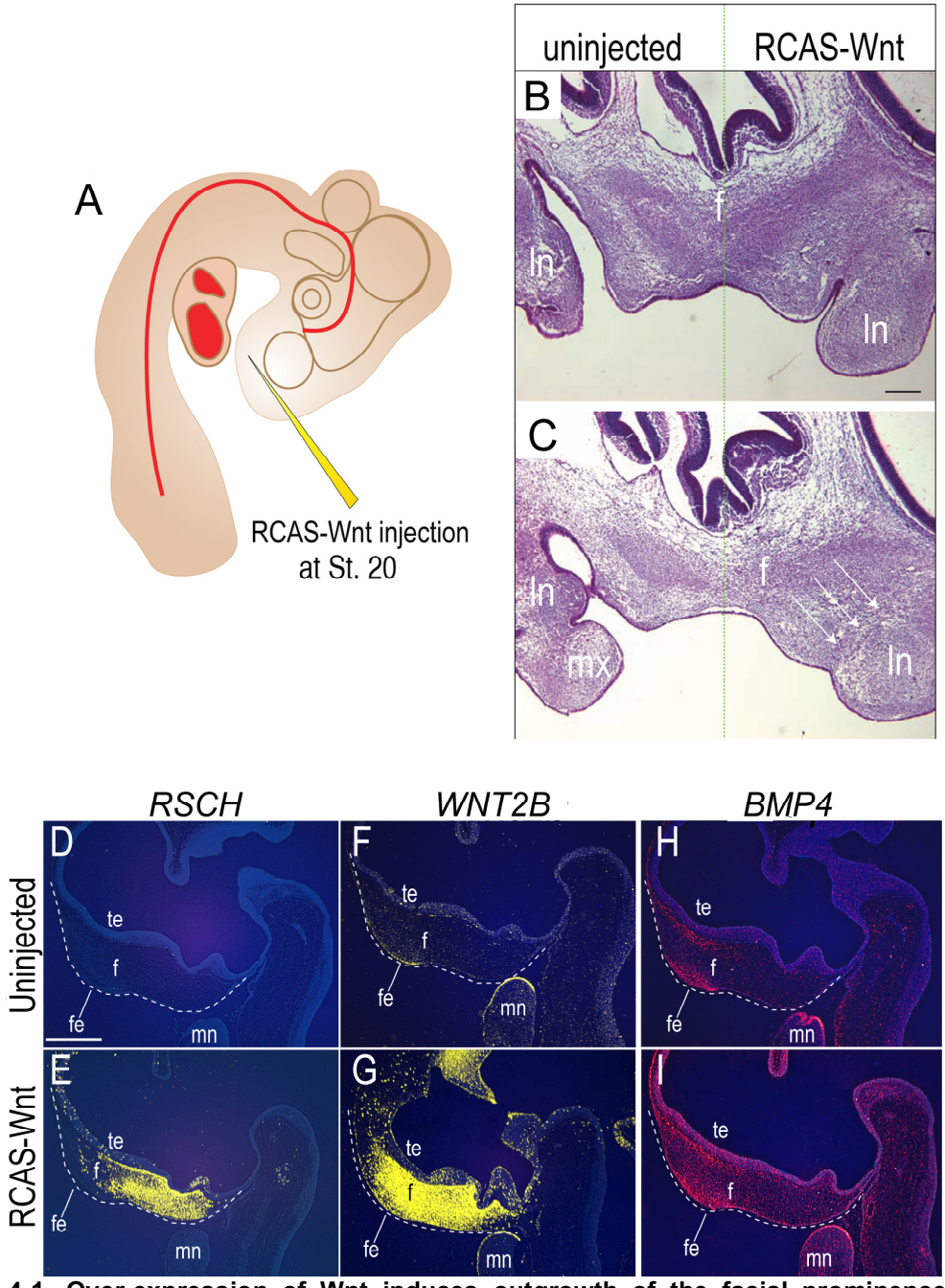

Figure 4-1. Over-expression of Wnt induces outgrowth of the facial prominences and expression of *BMP4*. **(A)** Schematic diagram of unilateral injection of RCAS-*WNT2B* in HH20 chicks. **(B-C)** Transverse sections of uninjected side shows normal facial morphology, with the frontonasal prominence (f) not fused to the lateral nasal (ln) prominence. On the RCAS-Wnt

injected side, the frontonasal prominence has fused to the lateral nasal and maxillary prominences (mx) and the nasal pit has been drastically reduced in size. White arrows indicate continuous mass of tissue spanning from the frontonasal to lateral nasal prominence. **(D-I)** Section RNA *in situ* hybridizations of injected and uninjected embryos. **(D-E)** Viral probe (*RSCH*, yellow*)* is not detected in uninjected embryos, but is expressed throughout FNP (f) neural crest cells of RCAS-Wnt injected embryos. **(F-G)** Injected embryos have robust up-regulation of *WNT2B* (yellow) in FNP neural crest relative to uninjected embryos. **(H-I)** *BMP4* expression (red) is expanded throughout the FNP neural crest in RCAS-Wnt injected embryos, relative to uninjected controls. Black scale bar denotes 200 μm, white scale bar denotes 250 μm. f, frontonasal prominence; fe, facial ectoderm; ln, lateral nasal promienence; mn, mandibular prominence; mx, maxillary prominence; te, telencephalon.

Localization of Wnt activity in the face varies among avian species

Since our collaborators observed dramatic outgrowth of a chick FNP with excessive Wnt signaling, we hypothesized that different spatial patterning of Wnt signaling could account for shape differences in the chicken beak and duck bill. To test regions of Wnt responsiveness in the developing beak, we developed a Wnt reporter construct (Brugmann et al. 2007) in which enhanced green fluorescent protein (eGFP) is under the control of seven TCF binding sites (7xTCF-eGFP). We examined Wnt responsiveness in both chick and duck *in ovo* by infecting embryos at HH13 with the GFP reporter, and examining them after 48 hrs and 96hs, at HH25 and HH28, respectively (Figure 4-2). HH13 was chosen for injections because the neural crest cells that contribute to the upper beak have populated the FNP by that stage, but growth has yet to ensue; consequently, injections at this stage produce widespread infection by HH20 (Brugmann et al. 2007). HH25 and HH28 chicks displayed a robust region of reporter activity in a midline stripe down the frontonasal prominence, in keeping with the dramatically elongated V-shaped frontonasal prominence in chicks (Figure 4-2A,C). In contrast, duck embryos showed prominent GFP expression

in two lateral domains of the FNP (Figure 4-2B,D); this expression corresponds to outgrowth of the U-shaped bill of ducks. These experiments suggest that differential regulation and location of Wnt signaling may contribute to species-specific beak morphology through alteration of the growth trajectories of the FNP and regulation of Bmp signaling, and functionally validate the dramatic changes in Wnt signaling identified by the microarray analysis presented in **Chapter 2**.

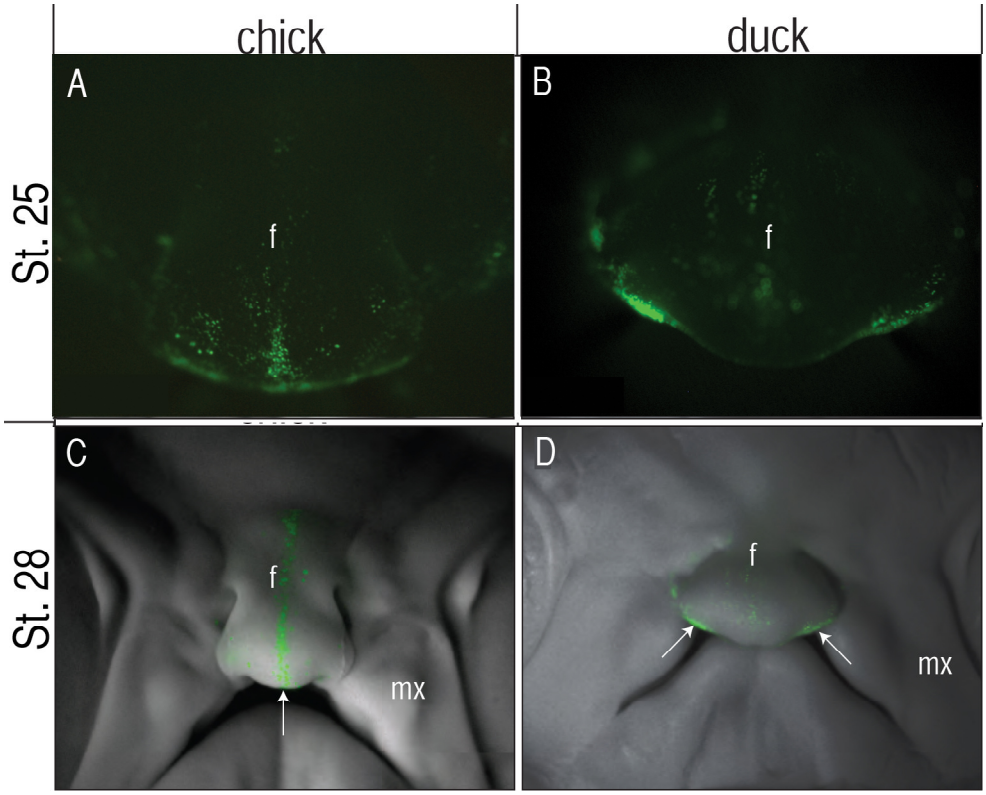

Figure 4-2. Regions of Wnt responsiveness spatially differ in chick and duck. Chicken and duck frontonasal prominences were injected with 7xTCF-eGFP at HH13 and examined after 48hrs **(A-B)** and 96hrs **(C-D)**, at HH St.25 and HH St.28, respectively. **(A,C)** Wnt responsiveness (visualized by GFP expression) is present at the midline (white arrow) in the chicken frontonasal prominence (f). **(B,D)** In the duck frontonasal prominence, Wnt responsiveness is absent at midline, but present in lateral domains (white arrows). f, frontonasal prominence; mx, maxillary prominence.

Correlation of miR-27a and miR-302b with protein levels of putative targets

While it is possible to over-express microRNAs using viral vectors similar to those used to examine the Wnt pathway described above (Hornstein et al. 2005), this approach is both labor and time-intensive. As an alternative strategy to correlate specific microRNAs with their *in vivo* mRNA targets, I measured protein levels of known or predicted targets for two differentially expressed microRNAs, miR-27a and miR-302b (Table 3-2).

MiR-27a has been demonstrated to directly target the fibroblast growth factor (Fgf) antagonist *SPRY2* and promote proliferation in human pancreatic cell lines (Ma et al. 2010). As described in **Chapter 3**, miR-27a is expressed at higher levels in the duck than the chicken at both HH20 and HH25 (Table 3-2 and Table 3-3). Consistent with this, I determined by western blotting that SPRY2 protein is at lower levels in duck FNPs compared to chicken at both stages (Figure 4-3) indicating that *SPRY2* is also a plausible target of miR27a in the FNP.

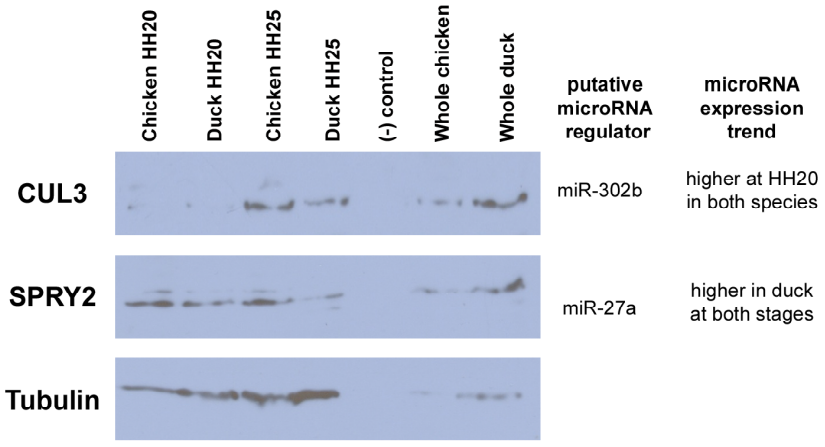

Figure 4-3: Western blot analysis of putative targets of miR-302b and miR-27a. Tubulin is used as control for variation in total protein loaded.

The miR-302 family is associated with an undifferentiated cell fate (Lin et al. 2010, Lin et al. 2008), but direct targets of miR-302b have yet to be identified. In order to identify putative targets for this miRNA, I used two online target prediction tools, Microcosm (http://www.ebi.ac.uk/enright-srv/microcosm/htdocs/targets/v5/, version 5) and TargetScan (http://www.targetscan.org/, version 5.1), both of which require perfect alignment between a microRNA seed (nt 2-8) and the target 3' UTR and imperfect alignment within the 3' region of the miRNA. While both algorithms predict a large number of potential targets (687 and 292 targets in Microcosm and TargetScan, respectively), only 32 targets were predicted by both programs (Table 4-1).

BAMBI	*HIF1AN*	*PRSS23*	*TRIM36*
C11orf30	*HLF*	*RAPGEF2*	*TRIP11*
CUL3	*INOC1*	*RORA*	*TRPS1*
EFEMP1	*LATS2*	*RPS6KA3*	*TSHZ3*
EIF2C1	*MAP3K2*	*RRAGD*	*UBE2B*
FGD4	*MLL3*	*RSBN1L*	*UHRF1*
FOXK2	*NTN4*	*SNRK*	*UPF3A*
GUCY1A3	*PAK7*	*TOR1B*	*ZC3H6*

Table 4-1: Putative targets of miR-302b predicted by both Microcosm and TargetScan algorithms.

I chose to further analyze *CULLIN3 (CUL3)* as a potential target of miR-302b (see Discussion for the rationale behind this choice). In both chicken and duck, miR-302b is more highly expressed at HH20 (Table 3-2 and Table 3-3).

CUL3 protein is at lower levels in chicken and duck FNPs at HH20 relative to HH25, consistent with *CUL3* being a target of miR-302b (Figure 4-3). However, steady-state mRNA levels have not been analyzed for either *SPRY2* or *CUL3* and it is yet to be determined if their differential expression is indeed due to microRNA regulation or other mechanisms.

Expression of miR-222 correlates with changes in the cell cycle regulator p27 protein but not with its steady state mRNA levels

Previous studies have identified the mRNA encoding the cell cycle regulator *p27(KIP1)* as one target of miR-222 (Galardi et al. 2007, Lambeth et al. 2009). This miRNA is expressed at similar levels in the chicken, duck, and quail at HH20 (**Chapter 3**). However, by HH25, miR-222 has been down-regulated 1.8-fold in both chicken and quail, though it remains at higher levels in HH25 duck neural crest cells (Table 3-2 and Table 3-3). I sought to determine whether this miRNA may be altering p27 levels in the developing face by measuring levels of p27 protein by western blotting in chicken and duck FNPs from HH17, when neural crest cell have completed migration into the facial prominences, to HH31, when the adult bill is taking shape (Hamburger and Hamilton 1951, Lumsden et al. 1991).

From HH17 to HH23, when the duck and chicken embryos are still morphologically similar (Brugmann et al. 2010b), p27 protein is present at similar levels in the FNP by western blotting (Figure 4-4A). However, once the chicken

and duck diverge morphologically at HH25, I observed changes in the levels of p27 protein. At HH25, the levels of p27 increase in the chicken but remain relatively constant in duck FNP (Figure 4-4A), correlating with the observed decrease in miR-222 in the chick (Table 3-2). The levels of p27 protein remain at higher levels in chicken FNP through to the end of the time course at HH31. These observations were substantiated by a less quantitative measure, whole-mount immunohistochemistry. Consistent with the above western blotting results (Figure 4-4A), immunohistochemistry showed that p27 protein levels are at similar levels in the chicken and the duck from HH17 to HH23 (Figure 4-5). At HH25 and HH26, p27 has been up-regulated in the FNP of the chicken compared to the duck (Figure 4-5). However, for these immunohistochemistry experiments, I could not use the verified monoclonal anti-p27 antibody I employed for western blotting. Instead, I used a polyclonal anti-p27 antibody that was not of the same quality as the monoclonal antibody and detected several bands by western blotting (data not shown).

These increased levels of p27 protein are not accounted for by a corresponding increase in *p27(KIP1)* mRNA levels. By RT-PCR, steady state levels of *p27(KIP1)* transcripts remain relatively constant from HH17 to HH27 in both chicken and duck FNPs (Figure 4-4B), indicating that post-transcriptional regulation most likely accounts for the observed decrease in p27 protein (Figure 4-4A) and adding another piece of correlative evidence that changes in miR-222 may account for changes in p27 protein.

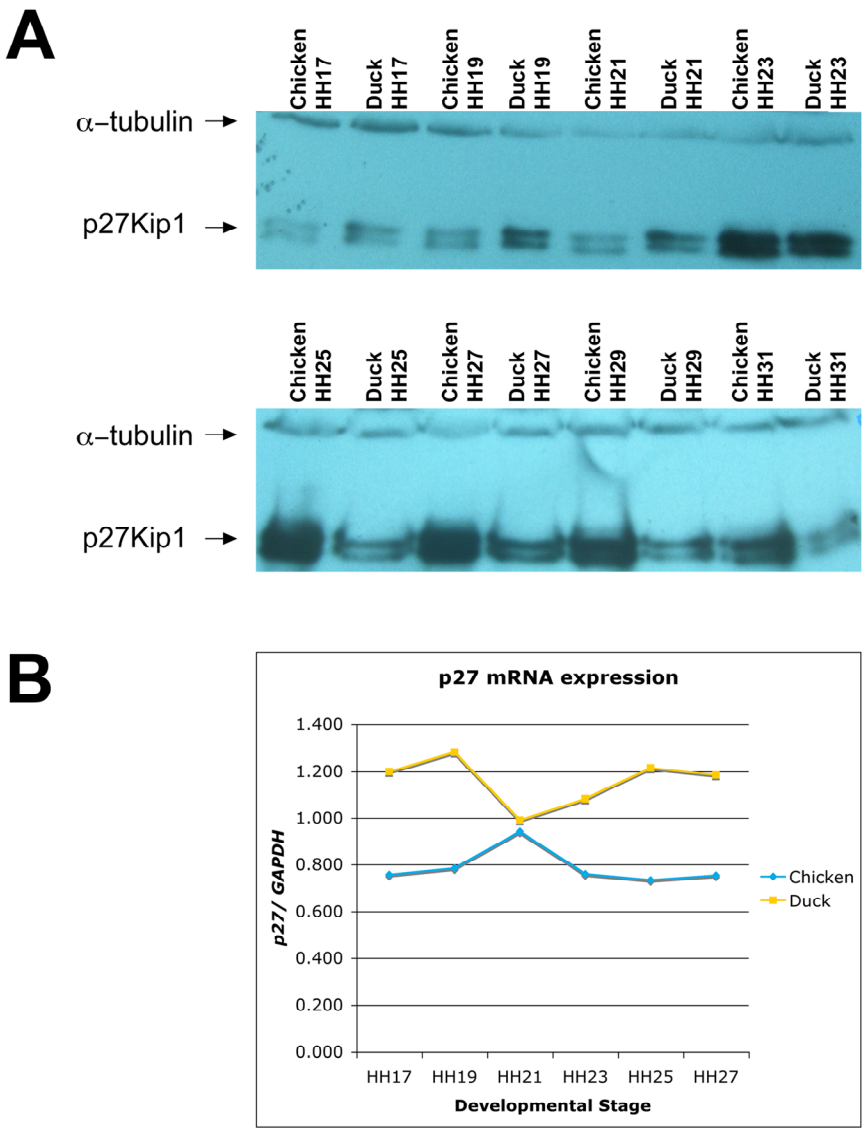

Figure 4-4: p27(Kip1) protein, but not mRNA, is differential between chicken and duck at the onset of morphological divergence. **(A)** Western blot analysis of p27 protein (lower doublet) relative to alpha-tubulin loading control (upper band) in HH17-HH31 chicken and duck frontonasal prominences. **(B)** Levels of *p27(KIP1)* mRNA transcripts relative to *GAPDH* control in chicken and duck frontonasal prominences, as measured by RT-PCR.

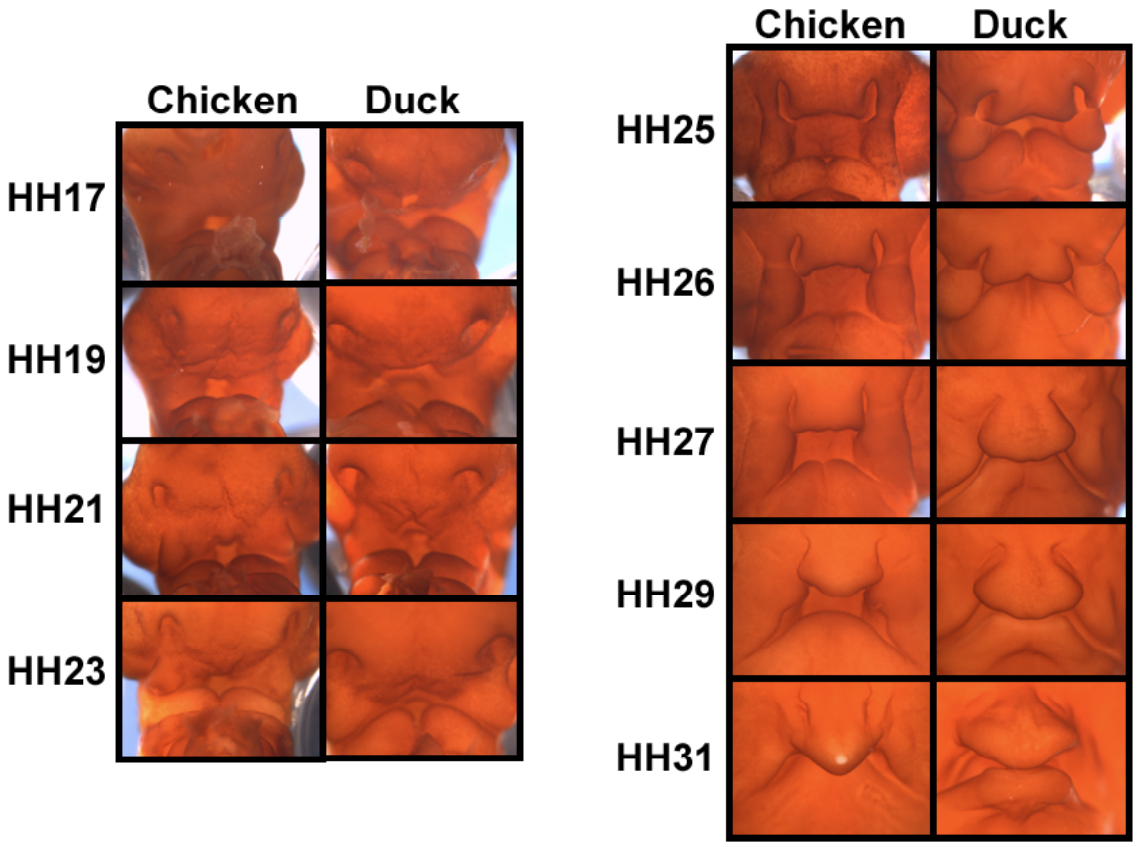

Figure 4-5: Whole-mount immunohistochemistry for p27(Kip1) in HH17 to HH31 chicken and duck heads.

miR-222 may be expressed in different tissue layers in chicken and duck

As mentioned above, my sequencing data shows that miR-222 is expressed at higher levels in duck neural crest at HH25 compared to HH20 (Table 3-2). I confirmed these higher levels of miR-222 in isolated frontonasal neural crest of duck versus chicken by qRT-PCR (7.06-fold higher levels in duck). However, comparisons of whole frontonasal prominences, including both epithelia and neural crest cells, showed roughly equal levels of miR-222 in duck and chicken FNPs at each stage from HH23 to HH27 (Table 4-2). This is consistent with miR-222 being expressed in different tissue layers in the chicken

and the duck. That is, miR-222 is expressed at higher levels in duck neural crest (Table 3-2 and qRT-PCR results above), but this miRNA is expressed at higher levels in chicken surface epithelia and/or neuroectoderm. Thus, measures of miR-222 levels in whole FNP samples show equivalent expression (Table 4-2) but the underlying tissues show differential expression.

Comparison	miR-222 fold change
Duck HH23/ Chicken HH23	**1.32**
Duck HH24/ Chicken HH24	**1.42**
Duck HH25/ Chicken HH25	**-1.01**
Duck HH26/ Chicken HH26	**1.04**
Duck HH27/ Chicken HH27	**-1.50**

Table 4-2: qRT-PCR results for miR-222 levels in stage-matched chicken and duck whole frontonasal prominences. Level of miR-222 is relative to *RNU6B* in all samples. Fold changes are expressed as duck relative to chicken, where a negative fold change is expressed at lower levels in the duck versus chicken.

Assessing whether measuring species-specific variations in gene expression is a useful source of candidate genes for human craniofacial disorders

Given the conservation of the molecular "toolkit" used to build the face across vertebrates (Abzhanov et al. 2004, Albertson et al. 2005, Liu et al. 2005, Suzuki et al. 2009), insights gained from work in evolutionary models may benefit human health. In **Chapter 2**, I employed a novel comparative genomic approach exploiting natural variation in bird beak shape as a potential tool to discover new candidate genes that regulate mammalian craniofacial development.

In order to assess whether this approach enriches for genes implicated in human facial disorders, I first compiled a list of genes and genomic intervals

previously correlated with a variety of mammalian craniofacial defects, as listed in the Online Mendelian Inheritance in Man database (OMIM, http://www.ncbi.nlm.nih.gov/omim/ and included in a recent review (Dixon et al. 2011) (see also **Materials and Methods**). Of the 334 genes differentially expressed among NC cells from the three bird species (Table 2-1 and Table 2-2), 17 genes (e.g. *FGFR2, JAGGED2, OSR2, SATB2,* and *TGFB3*) have previously been implicated in human facial defects. Remarkably, an additional 104 genes (nearly 1/3 of the data set) reside in genomic intervals associated with various human craniofacial abnormalities (Table 4-3), and may serve as a new source of candidate genes for these disorders (see discussion below).

Locus	OMIM#	Region size (Mb)	Title	Differentially expressed genes
1p34	%606713	12.2	Van Der Woude Syndrome 2	*GJB5, LOC51058, MYCBP, PTCH2*
1p36	#607872	28	Chromosome 1p36 Deletion Syndrome	*HES5, ID3*
1p36.3	%119530	7.2	Orofacial cleft 1	*HES5*
1p36.32	#202370	3.1	Adrenoleukodystrophy, Autosomal Neonatal Form	*HES5*
1p36.32	#214100	3.1	Zellweger Syndrome	*HES5*
1q22	#214100	1.5	Zellweger Syndrome	*MTX1, THBS3*
1q4	%119530	34.8	Orofacial cleft 1	*FLJ12517, FLJ22301, TGFB2, ZNF496*
1q42-q44	#612337	25.2	Chromosome 1q43-q44 Deletion Syndrome	*FLJ12517, FLJ22301, ZNF496*
2p13	%602966	6.4	Orofacial cleft 2	*BMP10, RAI15*
2q31	%183600	13.3	Split-Hand/Foot Malformation 1	*EVX2, HOXD1, NFE2L2*
2q31	%606708	13.3	Split-Hand/Foot Malformation 5	*EVX2, HOXD1, NFE2L2*
2q32-q33	#612313	26	Chromosome 2q32-q33 Deletion Syndrome	*FZD5, FZD7, NAB1, SATB2*
2q34-q36	%185900	22	Syndactyly, Type I	*WNT6*

2q37.1-q37.3	%236100	12.2	Holoprosencephaly 1	*SP100, TNRC15*
2q37.1-q37.3	%605934	12.2	Holoprosencephaly 6	*SP100, TNRC15*
3q29	%609425	5.7	Chromosome 3q29 Microdeletion Syndrome	*HES1*
4p16	%600593	11.3	Craniosynostosis, Adelaide Type	*WHSC1*
4p16.3	#194190	4.5	Wolf-Hirschhorn Syndrome	*WHSC1*
4q33-qter	%607258	21.1	Hypercalciuria, Absorptive, 1	*DUX4, MORF4*
6p24.3	%119530	3.5	Orofacial cleft 1	*RREB1*
6p25	%608545	7.1	Larsen-Like Syndrome	*FOXF2, FOXQ1*
6q21-q22	%218400	24.8	Craniometaphyseal Dysplasia, Autosomal Recessive	*FOXO3A, SCML4*
7p11.2	#180860	4	Silver-Russell Syndrome	*FLJ39963*
7q11	#214100	17.6	Zellweger Syndrome	*GTF2I*
7q11.23	#194050	5.3	Williams-Beuren Syndrome	*GTF2I*
7q11.2-q21.3	%129900	36.3	Ectrodactyly, Ectodermal Dysplasia, and Cleft Lip/Palate Syndrome 1; EEC1	*FZD1, GTF2I*
7q11-q21	%608027	38.1	Pontocerebellar Hypoplasia Type 3	*FZD1, GTF2I*
7q36	#120200	11.2	Coloboma, Ocular	*BC052625, CDK5, PAXIP1*
8q24.3	%612858	6.5	Orofacial cleft 12	*ARC*
10p14-p13	%601362	10.7	DiGeorge Syndrome/Velocardiofacial Syndrome Complex 2	*TAF3*
10q24	%600095	8.8	Split-Hand/Foot Malformation 3	*CNNM1, FLJ10895, HOX11*
11p11.2	#601224	5.3	Potocki-Shaffer Syndrome	*ZFPM1*
11q23-q24	%225000	20.4	Rosselli-Gulienetti Syndrome	*HSPC063, LZTS1, OCT11*
12p13.3	#214100	10.1	Zellweger Syndrome	*CCND2, WNT5B, ZNF384*
13q12.2-q13	%157900	12.3	Moebius Syndrome	*HMG1*
13q14	%601499	15.2	Axenfeld-Rieger Syndrome, Type 2	*KBTBD7, RGC32*
13q31.1-q34	%610361	36.2	Orofacial cleft 9	*ZIC5*
14q13	%609408	4.5	Holoprosencephaly 8	*PAX9*
14q21-q22	%608664	20.3	Seckel Syndrome	*CDKN3, TRIM9*
14q32	%164210	17.5	Hemifacial Microsomia	*CRIP1, JAG2, TRIP11*
17p11.2	#610883	6.2	Potocki-Lupski Syndrome	*ALDH3A2, SREBF1*
17p11.2	%604547	6.2	Van Der Woude Syndrome Modifier	*ALDH3A2, SREBF1*
17p12-p11.1	#119540	13.3	Cleft Palate, isolated	*ALDH3A2, SREBF1*

17p13.3	#247200	3.3	Miller-Dieker Lissencephaly Syndrome	*HIC1*
17q24.3 -q25.1	%261800	7.7	Pierre Robin Syndrome	*FLJ14297, GPRC5C*
18p11.3 1-q11.2	%606744	22.1	Seckel Syndrome 2	*GATA6, TAF2C2*
19q13	%600757	26.7	Orofacial cleft 3	*AB075831, AK128361, ATF5, DKFZp686B0797, FLJ12586, FLJ13265, FLJ14779, FLJ22059, FLJ23233, FLJ32191, HIF3A, KIAA0798, LISCH7, MGC4400, RELB, ZNF211, ZNF223, ZNF42*
21q22.3	%236100	5.5	Holoprosencephaly 1	*PFKL, PTTG1IP*
22q11	#115470	11.2	Cat Eye Syndrome	*LZTR1, PCQAP*
22q11.2	#145410	8	Opitz GBBB Syndrome, Autosomal Dominant	*LZTR1, PCQAP*
22q11.2	#608363	8	Chromosome 22q11.2 Microduplication Syndrome	*LZTR1, PCQAP*
22q11.2	#611867	8	Chromosome 22q11.2 Deletion Syndrome, Distal	*LZTR1, PCQAP*
22q11.2	#192430	8	Velocardiofacial Syndrome	*LZTR1, PCQAP*
22q12-q13	%603116	25.4	CDAGS Syndrome	*HRIHFB2122, LOC90322, MFNG, PPARA, SOX10, TCF20*
Xp11.23 -q13.3	%311900	29.6	Tarp Syndrome	*CITED1, MLLT7, PHF16, ZNF21*
Xp22	#300209	24.9	Simpson-Golabi-Behmel Syndrome, Type 2	*MID2*
Xq24-q27.3	#300243	30.6	Mental Retardation, X-Linked, Syndromic, Christianson Type	*FGF13*
Xq26-q27	%300238	18.4	Mental Retardation, X-Linked, Syndromic 11	*FGF13*
Xq26-q27	%300712	18.4	Craniofacioskeletal Syndrome	*FGF13*
Xq28	%300261	8.2	Armfield X-Linked Mental Retardation Syndrome	*FMR2*

Table 4-3: Genes differentially expressed in chicken, duck, and quail that reside within genomic intervals associated with human craniofacial disorders. See Tables 2-1 and 2-2 for additional gene annotation.

Identification of putative avian specific miRNAs

The miRNA arsenal is relatively dynamic across the metazoan lineage (Grimson et al. 2008, Heimberg et al. 2008, Hertel et al. 2006, Prochnik et al. 2007, Sempere et al. 2006, Wheeler et al. 2009) compared to transcription factors and signaling pathways, which are largely conserved from sponges to humans (Larroux et al. 2008, Nichols et al. 2006). The initiation rate for new microRNAs is estimated to be from 1-12 new miRNAs per million years (Berezikov et al. 2010, Lu et al. 2008), and there are numerous examples of microRNAs that appear to be restricted to specific vertebrate lineages, from primates to insects (Bentwich et al. 2005, Berezikov et al. 2006, Brameier 2010, Li et al. 2010, Yuan et al. 2010). In all of these cases, miRNA evolution is determined by sequence homology, and it is still to be determined if these microRNAs are an evolutionary dead-end or have functional roles in development or species divergences.

The studies in **Chapter 3** represent the first large-scale evaluation of miRNAs in multiple avian species. Therefore, I was interested in assessing whether any of the miRNAs that are detectably expressed in the frontonasal neural crest of chickens, ducks, and quails might be specific to the avian lineage. Birds and mammals shared a last common ancestor ~310 million years ago (Kumar and Hedges 1998), and the earliest divergences within birds occurred nearly 120 million years ago (Figure 4-6) (van Tuinen and Hedges 2001).

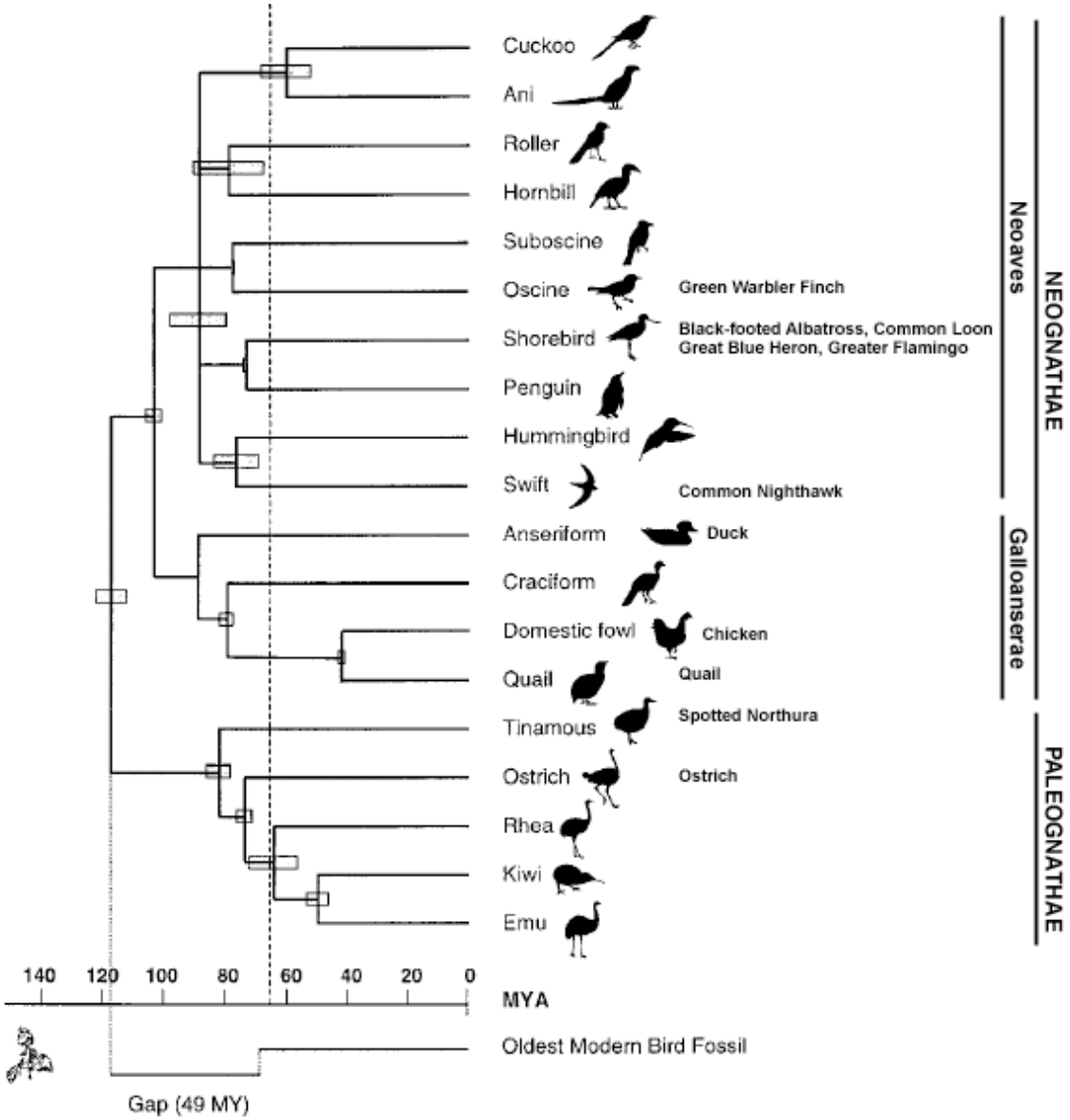

Figure 4-6: Phylogeny of avian species, adapted from (van Tuinen and Hedges 2001). Classification of birds used for miRNA sequencing and PCR of miR-2954 and miR-2954* are as indicated, excepting Gray-chested Dove (Neoave). See also Table 6-5.

As described in **Materials and Methods**, I compiled a list of seven mature miRNAs that are only annotated in chicken and zebrafinch in miRBase (http://mirbase.org/, release version 16) (Griffiths-Jones et al. 2008), as identified in other miRNA deep sequencing projects (Burnside et al. 2008, Glazov et al.

2008). These sequences are also detectable by sequence alignment searches only in chicken and/or zebrafinch and (as determined by my studies) are expressed in the frontonasal neural crest of the chicken, duck, and quail (Table 4-4).

mature miRNA	miRBase Accession	miRNA sequence
gga-miR-1451	MIMAT0007324	UCGCACAGGAGCAAGUUACCGC
gga-miR-1559	MIMAT0007416	UUCGAUGCUUGUAUGCUACUCC
gga-miR-2131	MIMAT0011207	AUGCAGAAGUGCACGGAAACAGC
gga-miR-2131*	N/A	CUGUUACUGUUCUUCUGAUG
gga-miR-2954	MIMAT0014448	CAUCCCCAUUCCACUCCUAGCA
gga-miR-2954*	MIMAT0014623	GCUGAGAGGGCUUGGGGAGAGGA
tgu-miR-2970	MIMAT0014479	GACAGUCAGCAGUUGGUCUGG

Table 4-4: Mature miRNAs that are putatively specific to the avian lineage.

I chose to further analyze two of these mature miRNAs, gga-miR-2954 and gga-miR-2954*. These miRNAs are also detectable (and differentially expressed) at a substantial level in a second miRNA sequencing dataset we have recently derived from the chicken inner ear (Ku, personal communication). PCR and subsequent sequence analysis using the zebrafinch locus as a reference (data not shown) indicates that the hairpin precursor of these miRNAs is indeed conserved across the entire avian lineage (~118.6 million years since last common ancestor) (van Tuinen and Hedges 2001), from tinamous and ratites to songbirds (Figure 4-6 and see **Materials and Methods** for listing of species analyzed).

As yet, there are no known functions for the seven microRNAs that may be restricted to the avian lineage. These microRNAs may just be an evolutionary novelty, but they may also influence species-specific differences. To evaluate potential functionality of these seven putative avian-specific microRNAs, I identified potential targets using TargetScan (http://www.targetscan.org/, version 5.1; note that the Microcosm prediction software does not include nor allow prediction of targets for any of these miRNAs) (Table 4-5). Many of these predicted targets are members of developmental pathways (e.g. Fgf, Tgfb, and Wnt signaling), regulate body patterning (e.g. *HOX* genes), or influence chromatin modifications (e.g. *HDAC4*) (Table 4-6). These possible miRNA:mRNA target relationships are attractive follow-up candidates for species-specific regulation of these important developmental regulators.

miRNA	total targets predicted	Predicted target	Gene description
gga-miR-1451	8	*HOXA10*	homeobox A10
		ONECUT2	one cut homeobox 2
gga-miR-1559	2	*HDAC4*	histone deacetylase 4
gga-miR-2131	142	*ACVR2A*	activin A receptor, type IIA
		ACVR2B	activin A receptor, type IIB
		CALM2	calmodulin 2
		EN2	engrailed homeobox 2
		FGF9	fibroblast growth factor 9
		FZD10	frizzled homolog 10
		HMGA2	high mobility group AT-hook 2
		ONECUT2	one cut homeobox 2
		SMAD2	SMAD family member 2
		TWIST1	twist homolog 1
		ZEB1	zinc finger E-box binding homeobox 2
		ZEB2	zinc finger E-box binding homeobox 2

gga-miR-2131*	44	*CALM2*	calmodulin 2
		LRP6	low density lipoprotein receptor-related protein 6
gga-miR-2954	20	*HMGB1*	high-mobility group box 1
gga-miR-2954*	54	*CTNNB1*	beta-catenin
		LRP6	low density lipoprotein receptor-related protein 6
		NUP153	nucleoporin 153kDa
		ONECUT2	one cut homeobox 2
tgu-miR-2970	132	*ACVR1B*	activin A receptor, type IB
		CUL3	cullin 3
		EYA4	eyes absent homolog 4
		HOXA9	homeobox A9

Table 4-5: Selected predicted targets of miRNAs that are potentially limited to the avian lineage.

Conclusions

Our collaborators demonstrated that a Wnt signal is capable of inducing *BMP4* expression in the FNP cranial neural crest (Figure 4-1). Given that my studies were completed at stages prior to identifiable species-specific facial morphologies (Figure 2-1), this suggests that the transcription factors and signaling pathways identified in **Chapter 2** may function upstream of, and likely in conjunction with, the Bmp and Calmodulin pathways to influence species-specific facial morphology. Additionally, activation of the Wnt signaling pathway promoted regional growth fields that collectively influence the growth trajectory of the facial prominences. Further, our collaborators showed that discrete domains of Wnt activity differ in birds with distinct beak shapes, and these domains correlate with morphological differences (Figure 4-2). Taken together, these experiments integrate my results from **Chapter 2** into the existing framework of craniofacial morphogenesis (Abzhanov et al. 2004, Abzhanov et al. 2006, Wu et

al. 2004, Wu et al. 2006) by showing that Wnt signals regulate Bmp pathway activity and regional growth in the embryonic face, and in doing so, control morphological variation within and among vertebrate species.

I then correlated expression levels of specific miRNAs and their known or computationally predicted targets. For instance, levels of miR-27a inversely correlate with protein levels of the Fgf signaling antagonist SPRY2 (Figure 4-3), which has been shown to be a direct target of this miRNA in other cell types (Ma et al. 2010). Fgfs are critical for a number of processes in facial development (Nie et al. 2006). Additionally, proper levels of SPRY2 appear to be critical for normal facial morphogenesis (Goodnough et al. 2007, Welsh et al. 2007), indicating the importance of transcriptional and translational control of this gene by mechanisms such as miRNA regulation.

I also demonstrated that levels of miR-302b inversely correlated with protein levels of a computationally predicted target, CUL3 (Figure 4-3). CUL3 is an E3 ubiquitin ligase, which specifically identifies targets to be marked for degradation by the proteasome. Thus, modulations in protein level may affect a wide range of genes and pathways. CUL3 has also been shown in other systems to target CyclinE to regulate mitosis (Sumara et al. 2008), and thus proliferation, as well GLI3 (Jiang 2006), an effector molecule of Hedgehog signaling, a pathway critical in facial development (Brugmann et al. 2006, Brugmann et al. 2010a).

However, much of the follow-up presented in this chapter relates to miR-222. I speculated that differences in miR-222 levels in the duck versus chicken at HH25 could regulate morphological differences in the beak via its target, the cell cycle regulator p27(Kip1) (Galardi et al. 2007, Lambeth et al. 2009). My hypothesis is that higher levels of miR-222 in HH25 duck, and the commensurate decrease of p27 protein, could result in an increased proliferation level. On the other hand, lower miR-222 levels in the beaked chicken and quail could lead to a release of p27 repression and a consequent decrease in proliferation. This model agrees with previous analysis that identified higher proliferation levels in HH26-HH31 duck bills compared to chicken beaks (Wu et al. 2004, Wu et al. 2006).

I first demonstrated p27 protein is expressed at similar levels in the FNP of the chicken and duck while they are morphologically similar (Figure 4-4). However, at HH25, when species-specific morphologies are evident, p27 levels are dramatically different in the chicken and duck, in patterns consistent with alterations in miR-222 expression levels (Figure 4-4). Further, these changes in p27 protein are not associated with changes in mRNA level, indicating that post-transcriptional mechanisms (such as miRNA inhibition) are important for proper regulation of this cell cycle regulator. Additionally, preliminary qRT-PCR data suggests that miR-222 may be expressed in different tissues (neural crest versus epithelia) in the chicken and the duck, though this observation needs further analysis.

In order to assess the application of my analysis in **Chapter 2** to human health, I evaluated the overlap of candidates from a number of genomic studies with genes and genomic loci implicated in a variety of human craniofacial disorders. First, many genes in my data set have been previously implicated in mammalian craniofacial disorders. Second, 1/3 of the genes I identified lie within genomic loci linked to facial disorders for which causative genes have not been unequivocally identified (Table 4-3). For example, deletions and duplications of a 3Mb region at 22q11.2 have been associated with DiGeorge, Opitz GBBB, and velocardiofacial syndromes, and result in craniofacial dysmorphisms such as broad nasal root, midface hypoplasia, and cleft palate (Lindsay 2001). While *TBX1* has been proposed as a candidate gene for these disorders, mutations in this gene do not explain all cases (Lindsay 2001), suggesting additional genes may have roles in disease pathogenesis. Within the 3Mb region, I observe differential expression of the transcription factors *LZTR1* and *PCQAP*, suggesting they may also serve as candidate genes for these disorders.

Finally, I assessed potential avian-specific miRNAs. I identified seven mature miRNAs that appear to be specific to the avian lineage by sequence alignments (Table 4-4) and further evaluate two of these using PCR. The hairpin precursor for miR-2954 and miR-2954* was detected across the entire avian lineage, which has been evolving for nearly 120 million years (van Tuinen and Hedges 2001). This is the first described example of a validated avian-specific miRNA and joins several other examples of miRNAs that have independently

evolved within defined vertebrate lineages (Bentwich et al. 2005, Berezikov et al. 2006, Brameier 2010, Li et al. 2010, Yuan et al. 2010). My computational analysis of the putative targets of these avian-specific miRNAs (Table 4-5) suggests that they may indeed regulate important developmental regulators of morphogenesis.

References

Abzhanov A, Protas M, Grant BR, Grant PR, Tabin CJ. 2004. Bmp4 and morphological variation of beaks in Darwin's finches. Science 305: 1462-1465.

Abzhanov A, Kuo WP, Hartmann C, Grant BR, Grant PR, Tabin CJ. 2006. The calmodulin pathway and evolution of elongated beak morphology in Darwin's finches. Nature 442: 563-567.

Albertson RC, Streelman JT, Kocher TD, Yelick PC. 2005. Integration and evolution of the cichlid mandible: the molecular basis of alternate feeding strategies. Proc Natl Acad Sci U S A 102: 16287-16292.

Bentwich I, et al. 2005. Identification of hundreds of conserved and nonconserved human microRNAs. Nat Genet 37: 766-770.

Berezikov E, Thuemmler F, van Laake LW, Kondova I, Bontrop R, Cuppen E, Plasterk RH. 2006. Diversity of microRNAs in human and chimpanzee brain. Nat Genet 38: 1375-1377.

Berezikov E, Liu N, Flynt AS, Hodges E, Rooks M, Hannon GJ, Lai EC. 2010. Evolutionary flux of canonical microRNAs and mirtrons in Drosophila. Nat Genet 42: 6-9; author reply 9-10.

Brameier M. 2010. Genome-wide comparative analysis of microRNAs in three non-human primates. BMC Res Notes 3: 64.

Brugmann SA, Tapadia MD, Helms JA. 2006. The molecular origins of species-specific facial pattern. Curr Top Dev Biol 73: 1-42.

Brugmann SA, Allen NC, James AW, Mekonnen Z, Madan E, Helms JA. 2010a. A primary cilia-dependent etiology for midline facial disorders. Hum Mol Genet 19: 1577-1592.

Brugmann SA, Powder KE, Young NM, Goodnough LH, Hahn SM, James AW, Helms JA, Lovett M. 2010b. Comparative gene expression analysis of avian embryonic facial structures reveals new candidates for human craniofacial disorders. Hum Mol Genet 19: 920-930.

Brugmann SA, Goodnough LH, Gregorieff A, Leucht P, ten Berge D, Fuerer C, Clevers H, Nusse R, Helms JA. 2007. Wnt signaling mediates regional specification in the vertebrate face. Development 134: 3283-3295.

Buchtova M, Kuo WP, Nimmagadda S, Benson SL, Geetha-Loganathan P, Logan C, Au-Yeung T, Chiang E, Fu K, Richman JM. 2010. Whole genome microarray analysis of chicken embryo facial prominences. Dev Dyn 239: 574-591.

Burnside J, et al. 2008. Deep sequencing of chicken microRNAs. BMC Genomics 9: 185.

Dixon MJ, Marazita ML, Beaty TH, Murray JC. 2011. Cleft lip and palate: understanding genetic and environmental influences. Nat Rev Genet 12: 167-178.

Fowles LF, Bennetts JS, Berkman JL, Williams E, Koopman P, Teasdale RD, Wicking C. 2003. Genomic screen for genes involved in mammalian craniofacial development. Genesis 35: 73-87.

Galardi S, Mercatelli N, Giorda E, Massalini S, Frajese GV, Ciafre SA, Farace MG. 2007. miR-221 and miR-222 expression affects the proliferation potential of human prostate carcinoma cell lines by targeting p27Kip1. J Biol Chem 282: 23716-23724.

Glazov EA, Cottee PA, Barris WC, Moore RJ, Dalrymple BP, Tizard ML. 2008. A microRNA catalog of the developing chicken embryo identified by a deep sequencing approach. Genome Res 18: 957-964.

Goodnough LH, Brugmann SA, Hu D, Helms JA. 2007. Stage-dependent craniofacial defects resulting from Sprouty2 overexpression. Dev Dyn 236: 1918-1928.

Griffiths-Jones S, Saini HK, van Dongen S, Enright AJ. 2008. miRBase: tools for microRNA genomics. Nucleic Acids Res 36: D154-158.

Grimson A, Srivastava M, Fahey B, Woodcroft BJ, Chiang HR, King N, Degnan BM, Rokhsar DS, Bartel DP. 2008. Early origins and evolution of microRNAs and Piwi-interacting RNAs in animals. Nature 455: 1193-1197.

Hamburger V, Hamilton HL. 1951. A Series of Normal Stages in the Development of the Chick Embryo. J Morphology 88: 49-92.

Heimberg AM, Sempere LF, Moy VN, Donoghue PC, Peterson KJ. 2008. MicroRNAs and the advent of vertebrate morphological complexity. Proc Natl Acad Sci U S A 105: 2946-2950.

Hertel J, Lindemeyer M, Missal K, Fried C, Tanzer A, Flamm C, Hofacker IL, Stadler PF. 2006. The expansion of the metazoan microRNA repertoire. BMC Genomics 7: 25.

Hornstein E, Mansfield JH, Yekta S, Hu JK, Harfe BD, McManus MT, Baskerville S, Bartel DP, Tabin CJ. 2005. The microRNA miR-196 acts upstream of Hoxb8 and Shh in limb development. Nature 438: 671-674.

Jiang J. 2006. Regulation of Hh/Gli signaling by dual ubiquitin pathways. Cell Cycle 5: 2457-2463.

Kumar S, Hedges SB. 1998. A molecular timescale for vertebrate evolution. Nature 392: 917-920.

Lambeth LS, Yao Y, Smith LP, Zhao Y, Nair V. 2009. MicroRNAs 221 and 222 target p27Kip1 in Marek's disease virus-transformed tumour cell line MSB-1. J Gen Virol 90: 1164-1171.

Larroux C, Luke GN, Koopman P, Rokhsar DS, Shimeld SM, Degnan BM. 2008. Genesis and expansion of metazoan transcription factor gene classes. Mol Biol Evol 25: 980-996.

Li J, Liu Y, Dong D, Zhang Z. 2010. Evolution of an X-linked primate-specific micro RNA cluster. Mol Biol Evol 27: 671-683.

Lin SL, Chang DC, Lin CH, Ying SY, Leu D, Wu DT. 2010. Regulation of somatic cell reprogramming through inducible mir-302 expression. Nucleic Acids Res.

Lin SL, Chang DC, Chang-Lin S, Lin CH, Wu DT, Chen DT, Ying SY. 2008. Mir-302 reprograms human skin cancer cells into a pluripotent ES-cell-like state. RNA 14: 2115-2124.

Lindsay EA. 2001. Chromosomal microdeletions: dissecting del22q11 syndrome. Nat Rev Genet 2: 858-868.

Liu W, Sun X, Braut A, Mishina Y, Behringer RR, Mina M, Martin JF. 2005. Distinct functions for Bmp signaling in lip and palate fusion in mice. Development 132: 1453-1461.

Lu J, Shen Y, Wu Q, Kumar S, He B, Shi S, Carthew RW, Wang SM, Wu CI. 2008. The birth and death of microRNA genes in Drosophila. Nat Genet 40: 351-355.

Lumsden A, Sprawson N, Graham A. 1991. Segmental origin and migration of neural crest cells in the hindbrain region of the chick embryo. Development 113: 1281-1291.

Ma Y, Yu S, Zhao W, Lu Z, Chen J. 2010. miR-27a regulates the growth, colony formation and migration of pancreatic cancer cells by targeting Sprouty2. Cancer Lett 298: 150-158.

Nichols SA, Dirks W, Pearse JS, King N. 2006. Early evolution of animal cell signaling and adhesion genes. Proc Natl Acad Sci U S A 103: 12451-12456.

Nie X, Luukko K, Kettunen P. 2006. FGF signalling in craniofacial development and developmental disorders. Oral Dis 12: 102-111.

Prochnik SE, Rokhsar DS, Aboobaker AA. 2007. Evidence for a microRNA expansion in the bilaterian ancestor. Dev Genes Evol 217: 73-77.

Sempere LF, Cole CN, McPeek MA, Peterson KJ. 2006. The phylogenetic distribution of metazoan microRNAs: insights into evolutionary complexity and constraint. J Exp Zool B Mol Dev Evol 306: 575-588.

Sumara I, Maerki S, Peter M. 2008. E3 ubiquitin ligases and mitosis: embracing the complexity. Trends Cell Biol 18: 84-94.

Suzuki S, et al. 2009. Mutations in BMP4 are associated with subepithelial, microform, and overt cleft lip. Am J Hum Genet 84: 406-411.

van Tuinen M, Hedges SB. 2001. Calibration of avian molecular clocks. Mol Biol Evol 18: 206-213.

Welsh IC, Hagge-Greenberg A, O'Brien TP. 2007. A dosage-dependent role for Spry2 in growth and patterning during palate development. Mech Dev 124: 746-761.

Wheeler BM, Heimberg AM, Moy VN, Sperling EA, Holstein TW, Heber S, Peterson KJ. 2009. The deep evolution of metazoan microRNAs. Evol Dev 11: 50-68.

Wu P, Jiang TX, Suksaweang S, Widelitz RB, Chuong CM. 2004. Molecular shaping of the beak. Science 305: 1465-1466.

Wu P, Jiang TX, Shen JY, Widelitz RB, Chuong CM. 2006. Morphoregulation of avian beaks: comparative mapping of growth zone activities and morphological evolution. Dev Dyn 235: 1400-1412.

Yuan Z, Sun X, Jiang D, Ding Y, Lu Z, Gong L, Liu H, Xie J. 2010. Origin and evolution of a placental-specific microRNA family in the human genome. BMC Evol Biol 10: 346.

CHAPTER 5

General Conclusions

The face is our external identity to the world. There are over six billion human faces, and each is unique. Moreover, other vertebrates, and particularly birds, have extraordinary variation in their facial structures. Avian beaks have evolved to scoop, tear, crush, pry, sip, and pluck, as suits their ecological niche best. Yet despite these drastic differences in adult structures, embryonic facial primordial are remarkably similar at stages when neural crest cells have populated the face and are beginning to grow to form the beak. These neural crest cells form all the bones and cartilage of the face and contain species-specific patterning information.

In the previous chapters, I described the use of cross-species microarrays and Next-Generation sequencing to identify the transcription factor genes, developmental signaling pathways, and microRNAs that encode species-specific patterning information in the neural crest cells of chickens, ducks, and quails. Changes in gene expression for the neural crest of the presumptive upper beak were analyzed in the three species prior to (HH20) and after (HH25) morphological variation was evident. Using custom microarrays I identified 334 transcription factors and members of developmental signaling pathways that are expressed in a species-specific pattern that predates morphological variation. Duck neural crest had particularly dramatic changes in Wnt signaling components compared to either the chicken or the quail. Further experiments demonstrated that regions of Wnt activation correlate with differing beak

morphology, and this pathway may contribute to species-specific facial structures by promoting growth in particular facial regions.

I also observed differential expression of the Calmodulin and Bmp/TGFβ signaling pathways among the developing beak primordial of chickens, ducks, and quails. These pathways were previously shown to influence the formation of narrower and broader beaks in Darwin's finches. While the beak of the chicken and quail are more conical in shape, roughly similar to the finches, the bill of the duck is broad and flat—a very different sort of facial adaptation. Despite this morphological distinction, it appears that similar genes and pathways may regulate the development of very different facial shapes within birds. It will be interesting to see whether cases of morphological convergence in the face (e.g. broad versus narrow jaws in both birds and fishes) are also influenced by the same molecular genetic regulators.

Previous QTL analyses of morphological variation in the faces of mice, baboons, and fish estimated that one to forty genes account for variability in various features of the face. This raises the question, why did I detect changes in so many genes? While the genes I identified as being differentially expressed in the developing beaks of chickens, ducks, and quails predate morphological variation, many (if not most) are likely to be downstream effectors. That is, a set of "master regulator" genes begins a cascade that ultimately results in differential expression of hundreds of genes to control species-specific facial morphologies.

BMP4 appears to be one such downstream gene. It is only differentially expressed in the mesenchyme of the developing upper beak after morphological variation is evident, and we show that its expression can be induced by Wnt signaling. Whether there is a linear relationship between Wnt signaling and *BMP4*, or whether multiple signals converge on *BMP4* to influence facial shape is yet to be determined. But it is clear that these downstream effectors can have a major influence on species-specific facial form; ectopic expression of *BMP4* alone is sufficient to alter beak shape.

In addition to the microarray analysis, I also comprehensively identified changes in microRNAs between chicken, duck, and quail neural crest samples using high-throughput Next-Generation sequencing. In contrast to the subtle changes in mRNA expression observed in my mRNA analysis, many microRNAs dramatically change in expression between the two developmental stages that I examined. Interestingly, the changes in microRNA expression revealed potential new insights into neural crest biology. Prior to my study, little was known about neural crest cells from the time they finish migrating to the facial prominences (HH14-HH15) to when they begin bone pre-condensation (HH25-HH26). MicroRNA profiling indicates that the HH20 to HH25 developmental window may be a transition state from a population of multipotent, proliferative neural crest cells, and those that have the molecular signatures of differentiation. Further, differences in microRNA expression between the species are consistent with this transition being delayed in the duck. This delay would allow a prolonged period

of neural crest proliferation in duck, which may ultimately influence differential facial form.

The genomic studies described here represent a number of “firsts:” the first large-scale insights into cross-species facial morphology, the first comprehensive analysis of microRNAs in the developing face, and the first evaluation of miRNAs in multiple avian species. Numerous studies can be initiated from this work, from hypothesis-driven testing of specific genes and pathways in facial development (e.g. the Wnt pathway) to evaluations of microRNA evolution within the avian lineage. I hope that, by revealing for the first time the broader spectrum of mRNA and miRNA expression differences in this important developmental process, my studies will provide a new set of candidate genes and pathways for studying the evolution of species-specific facial structures and overall facial development in both avians and mammals.

CHAPTER 6

Materials and Methods

Frontonasal mesenchyme tissue isolation

Chick, quail, and duck embryos were obtained through AA Farms (Westminster, CA). Eggs were set in a rocking incubator at 37°C and windowed at 48hrs to determine developmental stage. Staging was done according to Hamburger-Hamilton criteria (Hamburger and Hamilton 1951). Frontonasal prominences (FNPs) were isolated in cold PBS from Hamburger-Hamilton stage 20 (HH20) and HH25 embryos, by cutting off the head between pharyngeal arches 1 and 2, and collecting the tissue rostral to the eyes. To isolate frontonasal mesenchyme, FNPs were placed in 1.26U dispase in 1x PBS at room temperature for 15mins, then into Dulbecco's Modified Eagle Medium (DMEM) supplemented with 10% fetal bovine serum (FBS). Surface ectoderm and forebrain neuroectoderm were removed using sharpened tungsten needles. Unlike the other facial prominences, FNP mesenchyme consists of a pure population of neural crest cells, rather than a combination of neural crest and mesoderm (Tapadia et al. 2005).

Total RNA isolation

Isolated samples of frontonasal mesenchyme (neural crest) from 40 embryos were pooled and homogenized in 500μl of TRIZOL (Invitrogen), and total RNA extracted per manufacturer's instructions. After adding 120μl of chloroform to the TRIZOL, the tube was inverted 4-6 times to mix. Samples were incubated at room temperature for 2-3 mins, and then centrifuged at 13000 x g

for 3 mins in a bench-top centrifuge. The upper, aqueous layer was removed and placed in a new tube. To precipitate the total RNA, a volume of cold isopropanol equal to that of the aqueous layer is added (generally 300μl) with 1μl of 20mg/ml glycogen as a carrier to aid in precipitation. The tube was inverted 4-6 times to mix, and incubated at room temperature for 30 mins. Samples were spun at 13000 x g at 4°C for 20 mins, inverted 4-6 times, and spun at the same conditions for an additional 20 mins. Supernatant was removed, and the pellet was washed with 500μl 80% cold ethanol. Samples were inverted to mix and spun at 13000 x g at 4°C for 5 mins. After removing the supernatant, the pellet was air dried and resuspended in 5-20μl of RNase-free water.

cDNA amplification

Due to limited cell numbers, cDNA was linearly amplified as previously described (Hawkins et al. 2003, Hawkins et al. 2007). Briefly, polyadenylated RNA was isolated using 10μl paramagnetic oligo-dT_{25} beads (Dynal), then subjected to cDNA synthesis and PCR amplification. In all steps, supernatant can be removed from beads by placing the tube next to a magnet, keeping the beads in place as liquid is aspirated by pipette. Beads were washed twice with binding buffer (20mM Tris-HCl pH 7.5, 1M LiCl, 2mM EDTA). Total RNA was denatured at 65°C for 5 mins, combined with an equal volume of binding buffer, and allowed to cool in the presence of the washed oligo-dT beads at room temperature for 20 mins with periodic mixing. Beads (and bound polyadenylated

mRNAs) were washed twice in 50μl wash buffer (10mM Tris-HCl pH 7.5, 0.15M LiCl, 1mM EDTA), then once in 50μl 1x reverse transcriptase (International Chicken Genome Sequencing Consortium) buffer (50mM Tris-HCl pH 8.3, 75mM KCl, 3mM $MgCl_2$). A 10μl cDNA synthesis reaction was conducted on the beads using 200U Superscript II reverse transcriptase enzyme (Invitrogen) at 42°C for 1 hr in 1X RT buffer supplemented with 0.5mM each dNTP, 10mM dithiothreitol (DTT), and 1uM 3G-SP6-NotI primer (5'-GCGGCCGCTATTTAGGTGACACTATAGAAGAGGG-3'). During this RT reaction, the RT enzyme adds three cytosines (Burnside et al.) to the 3' end of the first-strand cDNA (which corresponds to the 5' end of the mRNA transcript). The 3G-SP6-NotI primer anneals to these 3 Cs, providing a template to extend the first-strand cDNA and adding an SP6 promoter sequence upstream of the mRNA coding region. Because the RT enzyme is likely to add another set of Cs at the end of the primer sequence, the 3G-SP6-NotI primer also contains a NotI restriction enzyme site to remove concatenated primers. The beads with attached cDNA were washed twice with 50μl sterile water and once with 50μl 1X digestion buffer (50mM Tris-HCl pH 7.5, 10mM $MgCl_2$, 100mM NaCl, 1mM DTT) prior to a 10μl digestion with 5U NotI enzyme (Invitrogen) at 37°C for 20 mins in 1X digestion buffer. Beads were washed three times with 50μl sterile water.

The resultant cDNA was linearly amplified with 16 total cycles of PCR. An initial 6 rounds of PCR were conducted on the beads in a 50μl reaction with 0.5mM each dNTP, 0.2uM CDSII primer (5'-

AAGCAGTGGTAACAACGCAGAGTACTTTTTTTTTTTTTTTVN-3'), 0.2uM SP6-5' primer (5'-ATTTAGGTGACACTATAGAA-3'), and 1x Advantage 2 Taq polymerase mix (Clontech) in 1x Advantage 2 PCR buffer (40mM tricine-KOH pH 8.7, 15mM potassium acetate, 3.5mM magnesium acetate, 3.75ug/ml bovine serum albumin [BSA], 0.005% Tween-20, 0.005% nonidet-P40). Cycle settings included an initial denaturation at 95°C for 2 mins, followed by 6 cycles of 95°C for 10 secs, 34°C for 10 secs, and 68°C for 6 mins, and finally a 4 min elongation at 68°C. During this reaction, the SP6 5' primer binds to the SP6 promoter sequence added to the 5' end of the mRNA transcript, while the CDSII primer binds to the polyadenine (polyA) tract of the mRNA and adds a known nucleotide sequence on the 3' end of the transcript (after the polyA) to use in the second set of PCR reactions detailed below. After these 6 cycles of PCR, the supernatant was transferred to a new PCR tube for an additional 10 PCR cycles and the beads were washed three times with 50μl sterile water prior to storage at 4°C. The supernatant from first set of PCRs serves as template for the second set of PCRs and was supplemented with a 50μl reaction with 0.5mM each dNTP, 0.5uM PCR3' primer (5' - AAGCAGTGGTAACAACGCAG - 3'), 0.5uM 3G-SP6-NotI primer used in the RT reaction, and 1x Advantage 2 Taq polymerase mix (Clontech) in 1x Advantage 2 PCR buffer. Cycle settings included an initial denaturation at 95°C for 2 mins, followed by 10 cycles of 95°C for 10 secs, 60°C for 10 secs, and 68°C for 6 mins, and finally a 4 min elongation at 68°C. During this reaction, the 3G-SP6-NotI primer binds to the SP6 promoter sequence

added to the 5' end of the mRNA transcript, while the PCR3' primer aligns to the sequence added 3' of the polyA sequence. Amplified cDNA was desalted on a Sephadex G50 minicolumn and concentrated in a vacuum centrifuge.

In vitro transcription (RNA run-offs)

The purified cDNA was used as template for an in vitro transcription using the SP6 promoter (Ambion Megascript kit) per manufacturers protocols. Approximately 300ng-1.0µg of cDNA was incubated at 37° overnight (approximately 12-16hr) in a 20µl reaction with 5mM each nucleotide (ATP, CTP, GTP, and UTP) and 2µl SP6 enzyme mix in 1x reaction buffer (Ambion). Following this, the reaction was supplemented with 2U TURBO DNase (Ambion) and incubated at 37°C for 15 minutes to degrade the cDNA template. Run-off RNAs were LiCl precipitated by adding 30 µl lithium chloride (LiCl) solution (7.5M LiCl, 50mM EDTA) and 30 µl nuclease-free water to the reaction, mixing, and incubating at -20°C for at least 1hr. RNA was pelleted by spinning samples at 13000 x g at 4°C for 15 mins. Supernatant was removed, and the pellet was washed with 500µl 80% cold ethanol. Samples were inverted to mix and spun at 13000 x g at 4°C for 5 mins. After removing the supernatant, the pellet was air dried and resuspended in 30-50µl of RNAse-free water at a concentration of 0.5-1.0 µg/µl. The quality of cDNA and run-off products was assessed by gel electrophoresis. This protocol generally produced over 25µg of purified, sense strand polyadenylated RNA for use in microarray hybridizations.

Microarray target labeling

Sense strand RNAs from each sample were used as templates in cDNA synthesis reaction using an oligo dT17-primer tagged with either Cy3- or Cy5-specific oligonucleotide sequence (3DNA Array 50 kit, Genisphere) per manufacturers instructions. 1 μg of run-off RNAs was incubated in a total volume of 24μl with 5pmole of either Cy3-RT primer (5'-TTCTCGTCTTCCGTTTGTACTCTAAGGTGGA-T_{17}-3') or Cy-5 RT primer (5'-ATTGCCTTGTAAGCGATGTGATTCTATTGGA-T_{17}-3') at 80°C for 10 mins, then snap-cooled on ice for 3 mins. The oligo dT tract of these primers bind to the polyA tail of the sense mRNAs, while the remaining sequence provide a specific "capture sequence" to which the Cy3 and Cy5 dye molecules hybridize in later steps. The RNA/primer sample was supplemented to a total reaction volume of 40μl with 200U Superscript II reverse transcriptase enzyme (Invitrogen), 0.5mM each dNTP, 10mM dithiothreitol (DTT), and 1μl Superase-In RNase inhibitor (Genisphere) in 1x RT buffer (50mM Tris-HCl pH 8.3, 75mM KCl, 3mM $MgCl_2$) and incubated at 42°C for 2 hrs. The RNA was degraded by adding 7μl of 0.5M NaOH/50mM EDTA and incubating at 65°C for 10 mins. After neutralizing the hydrolysis with 10μl of 1M Tris-HCl ph 7.5, Cy3- and Cy5-labeled RT reactions were pooled, then cleaned and concentrated using a Microcon YM-30 centrifugal filter (Millipore) to a final volume of 20μl.

Transcription factor microarray design

Oligonucleotide probes on the array are 50-70mers designed to coding regions of genes, thus allowing cross-species comparisons. The probes on the array interrogate ~2,000 known transcription factors genes, as well as many genes and ESTs predicted to contain transcription factor motifs (Messina et al.). An additional ~400 morphogens implicated in craniofacial development and growth factors, including nearly all components of the fibroblast growth factor (Fgf), Wnt, transforming growth factor beta/bone morphogenetic protein (TGFbeta/ BMP), Pax-Eya-Six-Dach, Notch, and Hedgehog signaling networks. As necessary, new 50-70mer Tm-matched probes were designed using OligoWiz 2.0 design software (Nielsen et al. 2003, Wernersson and Nielsen 2005) to conserved 3' coding regions of genes. When suitable probes could not be designed to conserved regions, species-specific probes were designed. Sequence comparisons between our human and mouse probes and their chicken orthologs indicate that ~98% of our probes have >70% sequence identity with the correct chicken orthologs (data not shown). We have previously shown that these probes accurately report in the chicken when used under appropriate hybridization conditions (Hawkins et al. 2003, Hawkins et al. 2007).

Microarray slide processing and production

Glass slides for printing were pre-treated by washing at room temperature for 2 hrs in a 10% (w/v) NaOH, 57% (v/v) ethanol solution. Slides were then rinsed four times in water. They were coated in a solution of 10% poly-L-lysine (v/v), 10% 1xPBS (v/v) at room temperature for 1 hr, rinsed in water, dried by spinning in floor centrifuge at 1000 rpm for 5 minutes, and baked at 45°C for 10 minutes. Oligonucleotides were resuspended at a concentration of 60μM in printing buffer (6% dimethyl sulfoxide [DMSO], 1.5M betaine for oligonucleotides) and spotted in duplicate on prepared glass slides using a Genetic Microsystems GMS 417 arrayer. After printing, slides were baked at 80°C for 2 hrs, then cross-linked at 65 milliJoules (mJ) before use.

Microarray hybridizations

Labeled cDNA was supplemented to a final volume of 40μl in 1x hybridization buffer (0.5M $NaPO_4$, 0.5% SDS, 1mM EDTA, 1x saline sodium citrate (SSC) buffer [0.3M NaCl, 30mM trisodium citrate, pH 7.4], 2x Denharts solution [0.04% w/v Ficoll 400, 0.04% w/v polyvinylpyrrolidone, 0.04% w/v BSA]). Samples were denatured at 80°C for 5 mins and hybridized at 42°C overnight (12-16 hrs) in humidified chambers. This temperature was calculated assuming approximately 70-75% sequence identity between chicken (target) and human or mouse (probe) sequences (International Chicken Genome Sequencing Consortium). Slides were washed in 2x SSC plus 0.2% SDS and 10mM DTT at

60°C for 15 mins, then 2x SSC at room temperature for 10 mins, and finally 0.2x SSC at room temperature for 10 mins, before being dried by spinning in a floor centrifuge at 1000 rpm for 5 minutes. Cy3 and Cy5 capture reagents (Genisphere) contain approximately 50 fluorescent dyes per molecule, connected to an oligonucleotide that binds to the "capture sequence" added to cDNAs in the labeling RT reaction. 2μl of capture reagent for each dye was combined with 1μl of Anti-Fade reagent (Genisphere) in 1x hybridization buffer with a final volume of 34μl. Dyes were denatured at 80°C for 5 minutes and hybridized at 42°C for 3 hrs in the dark in humidified chambers. Slides were washed and dried as above and scanned using a GMS 418 scanner at gains ranging from 18-40 scanner units.

Microarray comparisons

For each species, the early (HH20) was compared to the later (HH25) developmental stage. Stage-matched comparisons were also performed for each pair of bird species at both HH20 and HH25. A minimum of four separate microarray hybridizations (two replicates and two dye switches) was carried out for each comparison. Given that the neural crest samples were a mixed pool containing at least 40 embryos from various hatchings, replicate biological samples were not necessary. A total of 55 array comparisons were conducted for this study. All data, array designs, and analysis parameters are available through http://www.ncbi.nlm.nih.gov/geo/ under accession number GSE11099

and comply with the “minimum information about a microarray experiment” (MIAME) requirements.

Microarray data analysis

Microarray image intensity levels were quantitatively measured using confocal laser scanning (GMS 418 Scanner, Affymetrix) and the resulting data was analyzed with the BioDiscovery Imagene 6.0. Data from raw intensity values was normalized by locally weighted linear regression (LOWESS), which compensates for non-linear intensity variations (Quackenbush 2001). After normalization, fold changes from replicate oligonucleotide probes were averaged. Unsupervised hierarchical clustering was then performed using the dChip software package (http://biosun1.harvard.edu/complab/dchip/) to determine the quality of replicate microarray experiments. I implemented an arbitrary cut-off for background intensity values for each microarray chip based on the intensity of control oligonucleotides that are designed against *C. elegans* and moss transcripts. Low intensity filtering was performed to exclude genes with intensities lower than this specified threshold. I next selected genes that followed the same trend in at least 80% of the replicated hybridizations; genes that did not follow the same trend over replicate hybridizations were excluded from further analysis. P-values were calculated using a one-sample t-test on fold change data from replicate hybridizations.

The genes identified by the above methods did not necessarily meet all criteria for all comparisons. For instance, a gene may be significant in duck relative to the other species, but not between chicken and quail comparisons. Therefore, I manually extracted the data for "missing" comparisons, allowing an analysis of the patterns of expression across all comparisons.

Sequence homology analysis

For all genes with nucleotide sequences for chicken, duck, and quail in the NCBI GenBank database (http://www.ncbi.nlm.nih.gov/genbank/), nucleotide sequences were compiled and aligned using BLAST (http://blast.ncbi.nlm.nih.gov/Blast.cgi). Regions of cDNA to which microarray probes align were amplified by PCR for *OSR1, SATB2, TCEA2,* and *TGFB2* in quail and duck and for *CALM2* in quail only using the primers listed in Table 6-1. Fragments were gel purified and 350ng were used as template for a 12μl sequencing reaction with 2.5μl BigDye Terminator v3.1 (Ambion) and 2.5μl of 2μM either forward or reverse primer (Table 6-1). Cycle settings included an initial denaturation at 95°C for 5 mins, followed by 26 cycles of 95°C for 30 secs, 50°C for 10 secs, and 60°C for 4 mins, and finally a 7 min elongation at 60°C. Unincorporated dye was removed using the Qiagen DyeEx 2.0 Spin kit. Half to all of the sequencing reaction was analyzed on a polyacrylamide gel on an ABI Prism 377 DNA sequencing machine.

Gene	Forward primer	Reverse primer	Product size (bp)
CALM2	5'-GCTGCAGAACTTCGTCATGT-3'	5'-CAGTAAGGGAAAAACCTTTTACAGA-3'	240
OSR1	5'-CATCCAGCCCAAGCAAGAG-3'	5'-TGGCATATGTCGCATGTGTA-3'	327
SATB2	5'-CGGGATCGAATCTATCAGGA-3'	5'-TTGGCAAACAGAGCTTGAGA-3'	236
TCEA2	5'-ACCCGCATTGGTATGTCAGT-3'	5'-TGCAGAGCTGTTGTCAGCAT-3'	320
TGFB2	5'-AGAAGCGTGCTCTAGATGCTG-3'	5'-GCACGGAGAGGCAGAAGC-3'	239

Table 6-1: Primers used to amplify cDNA regions that bind to microarray probes.

In situ hybridization

PCR primers (Table 6-2) were used to amplify DNA products from highly conserved regions of chicken; all products were sequence verified. A T7 viral promoter (5'-CTCTAATACGACTCACTATAGGG-3') was added to the 5' end of either the sense (negative control) or antisense (experimental) strand using PCR. Digoxigenin (DIG)-labeled RNA probes were generated from the cDNA fragments using Ambion MEGAscript T7 transcription kits (Ambion) per manufacturers protocols. Approximately 1.0µg of cDNA was incubated at 37° for 6hrs in a 20µl reaction with 7.5mM ATP, CTP, and GTP, 3.75mM UTP, 0.5mM Digoxigenin-11-UTP (Roche) and 2µl T7 enzyme mix in 1x reaction buffer (Ambion). RNA probes were DNase treated, LiCl precipitated, analyzed by gel electrophoresis as described above, and resuspended in 1ml *in situ* hybridization buffer (Ambion).

Probe Name	Forward primer	Reverse primer	Probe size (bp)
CALM2 (coding)	5'-AGGAGTTGGGGACTGTGATG-3'	5'-CATGGAGGAATGGCCTTCTA-3'	501
CALM1 UTR	5'-GAACTCGAAAGTTCCATTTGCT-3'	5'-GTTGTGCTGAAGTCCACAGG-3'	535
CALM2 UTR	5'-TAGGGTCAGCATCTCGCTTT-3'	5'-CAGCGAAGTGAAGACGTTGT-3'	419
PHF16	5'-GAACTGGGCCTCCCTAAACT-3'	5'-AAATGGCTCCTTTGACATCG-3'	504
SATB2	5'-GGAAAGAGTGGAAAGAGAAAACC-3'	5'-TGTGCGGTTGAATGCTACTC-3'	469
TBX20	5'-TCAGCTTTTACAACATCTGATAACC-3'	5'-ATTACTGCGGAGGAGTGACG-3'	323
WNT1	5'-ACGTCCTCAAAGACCGCTTC-3'	5'-AGTTGAGGCAGCTGACGTG-3'	348

Table 6-2: Primers used to amplify *in situ* hybridization probes.

HH25 chicken (*Gallus domesticus*, Ideal Poultry, Cameron, TX) and duck (*Anas platyrhynchos*, Metzer Farms, Gonzales, CA) embryo heads were dissected in cold 1xPBS and fixed in 4% paraformaldehyde in 1xPBS at 4°C overnight. Embryos were serially dehydrated to 100% methanol for storage, and serially rehydrated to PBS before *in situ* hybridization. Whole-mount RNA *in situ* hybridizations were then performed on stage-matched embryos as previously described (http://genepath.med.harvard.edu/~cepko/protocol/ctlab/ish.ct.htm). Duck and chicken hybridizations were conducted in parallel to ensure appropriate comparisons. All steps below were conducted at room temperature on an orbital shaker unless otherwise noted, allowing embryos to equilibrate for each step (i.e. samples do not float in the solution). Embryos were first bleached with 6% hydrogen peroxide in PBT (1xPBS with 0.1% Tween-20) for 1 hr, and then washed 3 times for 5 mins each with PBT. Samples were permeated by treating with 25μg/ml Proteinase K (Ambion) in PBT for 30 mins, then the enzyme was deactivated with a 10 min wash in 2mg/ml glycine in PBT. Embryos were washed twice for 5 mins each with PBT, post-fixed with 4% paraformaldehyde

and 0.2% glutaraldehyde (v/v) in PBS for 20 mins, and washed twice for 5 mins each with PBT. Embryos were serially equilibrated with 10-20 min washes in 25% hybridization buffer (Ambion)/75% PBT, 50% hybridization buffer/50% PBT, 75% hybridization buffer/25% PBT, and 100% hybridization buffer. Samples were pre-hybridized in 100% hybridization buffer at hybridization temperature (50-55°C for all samples but *CALM1* and *CALM2*, which were conducted at 70°C). Embryos were incubated in hybridization buffer (Ambion) containing DIG-labeled riboprobe at 1μg/ml for mRNA transcripts and 40nM of 5' DIG-labeled miRCURY LNA probe (Exiqon) for microRNA samples at hybridization temperature for 12-16 hrs. Non-specifically bound probe was removed by washing three times per solution in solution I (50% formamide, 5x SSC, 1% SDS) and solution II (50% formamide, 2x SSC, 0.1% Tween-20) at hybridization temperature for 30 mins per wash.

Hybridized probe was visualized using an antibody against DIG, followed by a color reaction. Embryos were washed 3 times in TBST (1xTBS with 1% Tween-20) for 5 minutes each, then blocked for 1 hr in 1% BMB (Boerhinger Mannheim blocking reagent [Roche] dissolved in 1x maleic acid buffer [100mM maleic acid, 150mM NaCl, pH 7.5]) and 1% mixed heat-inactivated sera (generally 25% goat serum, 25% sheep serum, 50% bovine serum) in TBST. Samples were incubated for 4 hrs in antibody solution (1% BMB, 0.1% mixed heat-inactivated sera, 1:5000 anti-digoxigenin-AP, Fab fragments [Roche]) that was pre-absorbed by incubating with shaking at 4°C for 1 hr (during block step).

Embryos were washed in TBST overnight at 4°C, then 5 times at room temperature for 10 minutes each in TBST in the morning. Prior to the color reaction, pH was equilibrated by incubating samples 3 times for 10 minutes each in NTMT (100mM NaCl, 100mM Tris-HCl pH 9.5, 50mM $MgCl_2$, 1% Tween-20). Signal is developed by providing substrates that produce a purple product when cleaved by the alkaline phosphatase conjugated to the anti-DIG antibody. Embryos were incubated in the color reaction mix (175 μg/ml 5-bromo-4-chloro-3-indolyl phosphate [BCIP, Roche] and 450 μg/mL nitro blue tetrazolium choloride [NBT, Roche] in NTMT) in the dark until the reaction is judged complete. Samples were washed in PBS for 5 mins, fixed in 4% paraformaldehyde in 1xPBS for 20 mins, PBS for 5 mins, then serially dehydrated to 100% methanol for storage and visualization.

Reverse transcription PCR (RT-PCR)

FNPs and hearts were collected from 2-3 embryos per stage from HH17-27 chickens and ducks, staged according to Hamburger-Hamilton criteria (Hamburger and Hamilton 1951). Total RNA was isolated as above, and the entire RNA sample was DNase treated in a 10μl reaction (1U DNase [Invitrogen] in 20mM Tris-HCl pH 8.4, 2mM $MgCl_2$, 50mM KCl) at room temperature for 15 mins. The reaction was stopped by adding 1μl of 25mM EDTA pH 8.0. cDNA was produced with the High Capacity cDNA Reverse Transcription kit (Applied Biosystems). 1μg oligo$(dT)_{20}$ primer (Invitrogen), 0.5mM each dNTP, 50U

MultiScribe Reverse Transcriptase (Applied Biosystems), and 1x RT buffer (Applied Biosystems) were added to the unpurified DNase-treated sample to a final volume of 20μl and samples were incubated at 25°C for 10 mins, 37°C for 2 hrs, and then 85°C for 1 min. RNA was degraded by adding 3.5μl of 0.5M NaOH/50mM EDTA and incubating at 65°C for 10 mins. cDNA samples were neutralized by adding 5μl of 1M Tris-HCl pH 7.4 and introduced directly into a PCR reaction. RT primers (Table 6-3) were designed with Primer3 (http://frodo.wi.mit.edu/primer3/) to 3' end of coding region, preferably crossing an intron. PCR was conducted on 1-2μl of cDNA in a 20μl reaction with 0.2mM each dNTP, 0.5uM each forward and reverse primer (Table 6-3), 1.5mM $MgCl_2$, and 0.075 U Taq DNA polymerase (Invitrogen) in 1x PCR buffer (20mM Tris-Hcl pH 8.4, 50mM KCl). Cycle settings included an initial denaturation at 95°C for 2 mins, followed by the cycles indicated (Table 6-3) of 95°C for 30 secs, specified annealing temperature (Table 6-3) for 30 secs, and 72°C for 30 secs, and finally a 7 min elongation at 72°C. To amplify *TBX20* in FNP samples, two sets of PCR were necessary; after 30 initial cycles, 5μl of the completed reaction was used as template for a further 30 PCR cycles.

Gene	Forward primer	Reverse primer	Anneal temp (°C)	Cycles	Product size (bp)
GAPDH	5'- CGTCAAGCTTGTTTCCTGGT-3'	5'- CTGCAGGATGCAGAACTGAG-3'	50	18-20	179
TBX20	5'-ATTGACAGCAACCCTTTTGC-3'	5'-CCTGGCTGTCATCTCCAAGA-3'	50	30	157
FZD1	5'- CCTGCAGAGGAAAAGTCAGG-3'	5'- TCTGCAAACGGGTTAAAAATG-3'	50	25	237
p27KIP1	5'-AACGTCCGCATTTCTAATGG-3'	5'-GGCTTGTGGTTCTGGAAATC-3'	50	30	200

Table 6-3: Primer sequences and reaction conditions for RT-PCRs in frontonasal prominences and hearts.

Wing and heart microarray comparisons

Hearts and wing buds were collected from 2-3 HH23 chicken and duck embryos, staged according to Hamburger-Hamilton criteria (Hamburger and Hamilton 1951). Total RNA extraction, cDNA amplification, *in vitro* transcription, microarray target preparation, microarray hybridization, and microarray data processing were conducted as described above.

MicroRNA isolation and processing

Tissue and total RNA were isolated from the frontonasal mesenchyme of ducks, chickens and quails as described above for 40 or 5 embryos for the first and second biological samples, respectively. Note that the first biological samples are the same total RNA samples used for microarray analysis. microRNA sequencing samples were prepared by a fellow graduate student, Yuan-Chieh Ku, who ligated adapters to mature miRNAs using the Illumina Small RNA Sequencing kit per manufacturers instructions (v1.5 sRNA 3' Adapter). 1μg of total RNA was incubated with 1μl of 0.5μM v1.5 sRNA 3' adapter (5'-P-AUCUCGUAUGCCGUCUUCUGCUUGUidT-3') in a 5μl reaction at 70°C for 2 minutes, then on ice for 2 minutes. The 3' adapter was ligated to RNAs in a 10μl reaction volume containing the total RNA, 3' adapter, 1.5μl T4 RNA Ligase 2 truncated (200U/μl, New England BioLabs), 0.5μl RNaseOUT (Illumina), and 1.6μl of 50mM $MgCl_2$ in 1x T4 RNA ligase reaction buffer (50mM Tris-HCl pH 7.5, 10mM $MgCl_2$, 1mM DTT) by incubating at 22°C for 1 hr. This 3' adapter is

specifically modified to target microRNAs and other small RNAs that have a 3' hydroxyl group resulting from enzymatic cleavage by DICER. The reaction was then supplemented with 1μl of 5μM SRA 5' adapter (5' GUUCAGAGUUCUACAGUCCGACGAUC-3'; previously incubated at 70°C for 2 minutes, then on ice for 2 minutes), 1μl of 10mM ATP, and 1μl of T4 RNA ligase (Illumina) and incubated at 20°C for 1 hr. To the 12μl ligation reaction, 3μl of 20μM SRA RT primer (5'-CAAGCAGAAGACGGCATACGA-3') was added and incubated at 65°C for 10mins, before snap cooling on ice for 2 mins. The RNA/primer sample was supplemented to a total reaction volume of 27μl with 1.5μl RNase OUT (Illumina), 1.5μl of 12.5mM dNTP mix, and 10mM dithiothreitol (DTT) in 1x RT buffer (50mM Tris-HCl pH 8.3, 75mM KCl, 3mM $MgCl_2$) and incubated at 48°C for 3 mins. After adding 3μl (200U/μl) SuperScript II Reverse Transcriptase (Invitrogen), the reaction was incubated at 44°C for 1 hr to perform reverse transcription on the 5' and 3' adapter-ligated RNAs.

The cDNAs were then amplified by PCR. The 30μl RT reaction was supplemented with 0.25mM each dTNP, 0.5uM GX1 primer (5'-CAAGCAGAAGACGGCATACGA-3'), 0.5uM GX2 primer (5'-AATGATACGGCGACCACCGACAGGTTCAGAGTTCTACAGTCCGA-3'), and 0.02U Phusion DNA polymerase (Finnzymese) in 1x Phusion HF PCR buffer (Finnzymes) to a final volume of 50μl. DNA was amplified with an initial denaturation at 98°C for 30 secs, followed by 15 cycles of 98°C for 10 secs, 60°C for 30 secs, and 72°C for 15 secs, and finally a 10 min elongation at 72°C.

The entire PCR reaction was loaded on a 6% Novex Tris-borate-EDTA (TBE) polyacrylamide gel (Invitrogen). cDNAs corresponding to 20-40bp RNA species (90-110bp on the gel) were gel extracted. The gel slice was dissolved in 200μl of 1x gel elution buffer (Illumina) by incubating with gentle rotation at room temperature for 2 hrs. Any remaining gel debris was removed using a Spin-X cellulose acetate filter (Illumina) and spinning at 14000 rpm for 2 mins. DNA was precipitated by adding 1μl of 20mg/ml glycogen, 20 μl of 3M NaOAc, and 650 μl of cold 100% ethanol. The sample was spun at 14000 rpm for 20 mins and supernatant was discarded. The remaining pellet was washed in 500μl of room temperature 70% ethanol by spinning at 14000 rpm for 5 mins. After removing the supernatant, the pellet was air dried and resuspended in 10μl of resuspension buffer (Illumina).

MicroRNA sequencing and analysis

Size-selected RNA samples were sequenced on a GAIIX platform (Illumina) by the Genome Technology Access Center (GTAC) core at Washington University in St. Louis. Raw reads were first processed using a custom Perl script to remove any adapter sequences and count the abundance of each read. Reads were then mapped to known chicken and human mature miRNAs, allowing zero to two mismatches, using the miRanalyzer program (version 2, parameters: mismatch for libraries [mRNA transcripts]=1, mismatches to genome=2, threshold of the posterior probability=0.9, minimum number of

models which predict the microRNA=3) (Hackenberg et al. 2009), which includes all microRNAs submitted to miRBase (http://mirbase.org/, release version 16) (Griffiths-Jones et al. 2008). For one sample, the second biological sample of HH25 chicken neural crest (Chick_HH25_BS2), data from two replicate sequencing runs was combined after verifying that runs correlated >95% (data not shown).

Quantitative real-time PCR (qRT-PCR)

In order to confirm differential expression of individual microRNAs between chicken and duck, I performed quantitative real-time polymerase chain (qRT-PCR) with TaqMan MicroRNA assays (Applied Biosystems), designed to the mature human microRNA sequence. First, a reverse transcription (International Chicken Genome Sequencing Consortium) reaction was performed on total RNA using a primer to a specific microRNA. 25ng of total RNA, 1mM each dNTP, 1μl MultiScribe reverse transcriptase (Applied Biosystems), 0.2μl of 20U/μl RNase inhibitor, 3μl TaqMan RT primer (Applied Biosystems), and 1x Reverse Transcription buffer (Applied Biosystems) were combined in a 15μl RT synthesis reaction and incubated on ice for 5 mins, 16°C for 30 mins, 42°C for 30 mins, and then 85°C for 5 mins. For the real time step, a total reaction of 20μl with 2μl of the RT reaction and 1μl TaqMan real-time primer (Applied Biosystems) in 1x TaqMan Universal PCR master mix, no AmpErase UNG (Applied Biosystems) was prepared. Real-time reactions and detection were

carried out using the Applied Biosystems Prism 7500 machine, with cycle settings of an initial denaturation at 95°C for 10 mins, followed by 40 cycles of 95°C for 15 secs and 60°C for 1 min. The levels of microRNA gene expression were determined by normalizing to the spliceosomal RNA *RNU6B*. All reactions were performed in triplicate.

RCAS production and infection

Our collaborators Samantha Brugmann and Jill Helms (Stanford University) prepared and injected replication competent retrovirus (RCAS) (Hughes 2004). Virus was produced, concentrated, and titered in DF-1 cells (American Type Culture Collection) as previously described (Logan and Tabin 1998). DF-1 cells were grown in Dulbecco's Modified Eagle Medium (DMEM) supplemented with 10% fetal bovine serum (FBS) and 1x L-glutamine to approximately 70-80% confluency in a 10-cm dish, and transfected with a plasmid encoding RCAS virus with a *WNT2B* transgene. 10μg of plasmid was diluted with water to 450μl, mixed with 50μl of 2.5M $CaCl_2$ and 500μl of 2x BES (50mM *N,N*-bis(2-hydroxyethyl)-2-aminoethanesulfonic acid, 280mM NaCl, 1.5mM Na_2HPO_4, pH 6.95), incubated at room temperature for 20-30 mins, and added to the medium in the plate. Cells were repeatedly grown until confluent and split until cells reached confluency on each of six 15-cm plates. Cells were grown for an additional 36-48 hrs until they became superconfluent. For each plate, medium was replaced with 10ml of DMEM with 1% FBS. Supernatant was

harvested every 24hrs for 3 days, stored at -80°C, and replaced with a fresh 10ml of DMEM with 1% FBS.

Viral supernatants were thawed, passed through a 0.45-μm filter, and spun in a Beckman Coulter ultracentrifuge at 21000 rpm at 4°C for 3hrs. Supernatant was carefully decanted, and the viral pellet was resuspended in the remaining media by shaking tubes on ice for 15 mins. In order to determine the titer of the concentrated virus, DF-1 cells were infected for 48hrs with viral stocks at a series of dilutions from 10^{-3} to 10^{-7}. Infected cells were detected with immunohistochemistry. Cells were washed twice in PBS, and fixed in 4% paraformaldehyde in 1xPBS for 15 mins. After three PBS washes, cells were blocked for 30 mins in MST (DMEM with 10% chicken serum and 0.2% Triton X-100), and incubated for 30 min with AMV-3C2 monoclonal antibody (Developmental Studies Hybridoma Bank, University of Iowa) against the gag protein of the virus, diluted 1:5 in MST. Cells were washed three times for 5-10 mins each in MST, and incubated in 1:400 goat α-mouse peroxidase conjugated secondary antibody (Sigma) in MST for 30 mins. Cells were washed three times for 5-10 mins each in PBT (PBS + 0.1% Tween-20). During these washes, one 10mg tablet of 3,3'-Diaminobenzidine (DAB, Sigma) was dissolved in 33ml PBT. Cells were incubated with DAB solution for 20 mins, and supplemented with 0.03% hydrogen peroxide. Cells positive for the 3C2 epitope (and therefore infected with the RCAS virus) develop a brown stain within 5-10 mins of hydrogen peroxide addition. Cells were washed with PBT and infected clones

were counted to determine viral titer.

For virus delivery, 2µl of viral supernatant (10^9 pfu/ml) was injected to the facial tissue of HH20 chickens. Transgene expression was assayed after injection by *in situ* hybridization with probes against *WNT2B* or the RCAS virus (Suzuki et al.). Phenotypic effects of transgene expression were analyzed by gross inspection and tissue sectioning.

Wnt reporter activity in the face

Our collaborators Samantha Brugmann and Jill Helms (Stanford University) constructed a Wnt reporter virus where enhanced green fluorescent protein (eGFP) expression was driven by seven Tcf binding sites (Veeman et al. 2003). This DNA construct (7xTcf-eGFP) was cloned into the RCAN vector and virions were produced by combining the construct with the VSV-G envelope plasmid and the packaging plasmid (Dull et al. 1998) then transiently transfecting 293T cells. The DNA was introduced into cells via calcium phosphate precipitation. Media was collected, pooled, filtered, and concentrated by ultra-centrifugation. The resulting viral pellet was resuspended in PBS then titered on chick embryonic fibroblasts. A control retrovirus expressing eGFP under a strong constitutive reporter was employed for all assays (Brugmann et al. 2007). HH13 embryos were infected with 1.0µl of a 10^6 virions/µl solution and incubated until they reached HH25 or HH28. The pattern of eGFP activity was determined by examination of whole embryos under fluorescent light, and by immunostaining of

tissue sections.

Western blotting

For Western blotting, FNPs were isolated in cold PBS. To lyse, tissues were incubated in 1x Radio Immuno Precipitation Assay (RIPA) buffer (150mM NaCl, 1.0% Triton X-100, 0.5% sodium deoxycholate, 0.1% SDS, 50mM Tris-HCl pH 8.0) supplemented with Complete Mini Protease Inhibitor Cocktail (Roche, 1 tablet per 1mL RIPA) and maintained with constant agitation at 4°C for 30 mins. Samples were then centrifuged at 13000 x g at 4°C for 20 mins to pellet cell debris. Supernatant (lysate) was transferred to a fresh tube and the pellet was discarded. Samples were harvested at a concentration of 2-3 FNPs per 10μl RIPA plus Protease Inhibitor Cocktail, yielding approximately 1-2μg/μl. Lysates were combined with equal volumes of 2x Laemmli buffer (4% SDS, 10% 2-mercaptoethanol, 20% glycerol, 0.004% bromophenol blue, 0.125M Tris-Hcl, pH 6.8), denatured by incubating at 95°C for 5 mins, snap-cooled on ice for 3 mins, and loaded at 10-20μg per lane.

Samples were resolved by 10% SDS/PAGE (5% stacking gel) and transferred to nitrocellulose membrane. Membranes were blocked for 1hr with agitation in 5% non-fat milk w/v in TBST (5% milk), and probed with primary antibodies diluted in 5% milk as indicated in Table 6-4. Membranes were washed 3 times for 5 mins each in TBST to remove residual primary antibody, then probed with secondary antibodies in 5% milk (Table 6-4). After secondary

antibody incubation, membranes were washed twice each for 10 mins and 5 mins in TBST, and proteins were visualized by enhanced chemiluminescence (ECL) substrate kits (Pierce). The α-alpha-tubulin antibody was used as a loading control.

Antibody	Supplier	Dilution	Incubation conditions	Protein size
Primary Antibodies				
mouse α-alpha-tubulin monoclonal	Santa Cruz Biotechnology	1:25000	room temperature, 35-45 mins	55kDa
mouse α-p27KIP1 monoclonal	BD Transduction Laboratories	1:1000-1:2000	4°C overnight	27kDa
rabbit α-CULLIN3 polyclonal	Abcam	1:666	4°C overnight	85kDa
rabbit α-SPRY2 polyclonal	Millipore/Upstate Cell Signaling	1:2000	4°C overnight	35-40kDa
Secondary Antibodies				
goat α-mouse peroxidase conjugate	Sigma	1:10000	room temperature, 90 mins	N/A
goat α-rabbit peroxidase conjugate	KPL	1:10000-1:20000	room temperature, 90 mins	N/A

Table 6-4: Details for antibodies used for Western blotting.

Whole-mount immunohistochemistry

HH25 chicken (*Gallus domesticus*, Ideal Poultry, Cameron, TX) and duck (*Anas platyrhynchos*, Metzer Farms, Gonzales, CA) embryos were staged according to Hamburger-Hamilton criteria (Hamburger and Hamilton 1951). Heads were dissected in cold 1xPBS, fixed in 4% paraformaldehyde in 1xPBS at 4°C overnight, and serially dehydrated to 100% methanol for storage. Whole-mount immunohistochemistry was then performed on stage-matched embryos as previously described (http://graeflab.stanford.edu/pdf/Whole-mount_immunohistochemistry.pdf). Duck and chicken processing were

conducted in parallel to ensure appropriate comparisons. All steps below were conducted at room temperature on an orbital shaker unless otherwise noted, allowing embryos to equilibrate for each step (i.e. samples do not float in the solution).

Embryos were first bleached with 5% hydrogen peroxide in methanol for 4 hrs, washed twice for 5 mins each with methanol, and then serially rehydrated to PBS. Embryos were blocked in 5% non-fat milk w/v and 0.1% TritonX-100 v/v in 1x PBS (PBSMT) with two washed of 1 hr each, then incubated in 1:25 rabbit α-p27 polyclonal antibody (Santa Cruz Biotechnology) in PBSMT at 4°C overnight. Samples were washed five times in PBSMT at 4°C for 1 hr each wash, then incubated in 1:500 goat α-rabbit peroxidase conjugate (Sigma) in PBSMT at 4°C overnight. Embryos were washed five times in PBSMT at 4°C for 1 hr each wash, then once in PBS for 20 mins. During the PBS wash, one 10mg tablet of 3,3'-Diaminobenzidine (DAB, Sigma) was dissolved in 33ml PBS. Embryos were incubated with DAB solution for 20 mins, and supplemented with 0.03% hydrogen peroxide for 5-10 mins. Once the reaction was judged complete, samples were washed in PBS for 5 mins and post-fixed in 2% paraformaldehyde, 0.1% glutaraldehyde in PBS at 4°C overnight. Embryo heads were washed in PBS twice for 5 mins each before being serially dehydrated to methanol for imaging and storage.

Compilation of genes and loci associated with human craniofacial disorders

The Online Mendelian Inheritance in Man (OMIM) database (http://www.ncbi.nlm.nih.gov/omim/) was interrogated to compile a list of genes and genomic loci previously associated with syndromic and non-syndromic human disorders with a variety of craniofacial defects. OMIM was searched with the terms “craniofacial,” “cleft,” “microcephaly,” and “craniostynostosis.” Results were individually verified to include craniofacial defects and manually compiled. OMIM entries fell into three classes: known genes, known loci, and unknown loci. For instance, Apert syndrome (MIM ID #101200) is caused by mutations in the fibroblast growth factor receptor-2 gene (*FGFR2*) and was classified as a “known gene” (Table 6-5). Seckel syndrome type 3 (MIM ID %606744) is linked to the chromosomal region 14q21-q22, but a causative gene or mutation has yet to be identified, and was therefore classified as a “known loci” (Table 6-6) A third group of disorders (“unknown loci”) have yet to linked a specific chromosomal interval. The list of known genes (Table 6-5) was supplemented with additional genes from a recent review on the genetic causes of cleft lip and/or palate (Dixon et al. 2011).

ACAN	*DLX1*	*FREM2*	*MID1*	*RAB23*	*SOX9*
ACTB	*DLX2*	*FRZB*	*MSX1*	*RAI1*	*STAT3*
ADAMTS2	*DLX5*	*FTO*	*MSX2*	*RECQL4*	*STRA6*
AHR	*DNMT3B*	*GABRB3*	*MYCN*	*RELN*	*SUMO1*
ALK5	*E2F4*	*GDF5*	*MYH3*	*ROR2*	*TBCE*
ANKH	*EBP*	*GJA1*	*NDN*	*RPL11*	*TBX1*
ARX	*EFNB1*	*GLI2*	*NEB*	*RPL5*	*TBX15*
ATP6V0A2	*EPHB3*	*GLI3*	*NIPBL*	*RPS17*	*TBX5*
ATPAF2	*ERBB3*	*GLIS1*	*NSD1*	*RPS19*	*TCF3*
ATR	*ERCC5*	*GNAS1*	*OSR2*	*RPS7*	*TCOF1*
ATRX	*ESCO2*	*GPC3*	*p57(KIP2)*	*RUNX2*	*TERT*
B3GALTL	*EVC1*	*H19*	*PAX3*	*SATB2*	*TFAP2A*
BARX2	*EVC2*	*HCCS*	*PAX6*	*SC5DL*	*TFAP2B*
BCOR	*EXT1*	*HOXA2*	*PAX9*	*SEC23A*	*TGFA*
BMP2	*EXT2*	*HSD17B4*	*PEX1*	*SEMA3E*	*TGFB3*
BMP4	*EYA1*	*HSPG2*	*PEX14*	*SHH*	*TGFBR1*
BMPR1A	*EYA4*	*HYLS1*	*PEX26*	*SHOX*	*TGFBR2*
BRAF	*FAM20C*	*ICK*	*PEX3*	*SIL1*	*TGIF*
CASK	*FBN1*	*IGF2*	*PEX5*	*SIX3*	*TMEM70*
CD96	*FGD1*	*IRF6*	*PHF8*	*SKI*	*TNNT2*
CDKN1C	*FGF10*	*JAG1*	*PITX2*	*SLC26A2*	*TNNT3*
CHD7	*FGF8*	*JAG2*	*PLOD3*	*SLC35D1*	*TP63*
CHX10	*FGF9*	*KCNJ2*	*PQBP1*	*SLC3A1*	*TPM2*
COH1	*FGFR1*	*KCNK9*	*PREPL*	*SLC9A6*	*TRIM37*
COL11A1	*FGFR2*	*KIAA1279*	*PROK2*	*SMAD2*	*TRPS1*
COL11A2	*FGFR3*	*KRAS*	*PROKR2*	*SMS*	*TWIST1*
COL1A1	*FKHL15*	*LHX8*	*PTCH1*	*SNAI1*	*TBX22*
COL1A2	*FLNA*	*LIT1*	*PTEN*	*SNRPN*	*UBR1*
COL2A1	*FLNB*	*MED12*	*PTHR1*	*SNX3*	*WNT3*
CXORF5	*FOXC1*	*MEK1*	*PTPN11*	*SOX2*	*WTX*
DHCR24	*FOXC2*	*MEK2*	*PVRL1*	*SOX3*	*ZEB2*
DHCR7	*FRAS1*	*MEOX2*	*PYCR1*	*SOX6*	*ZIC2*

Table 6-5: Genes previously correlated with a variety of mammalian craniofacial defects. See text for details.

Loci	MIM ID#	Region size (Mb)		Loci	MIM ID#	Region size (Mb)
10p14-p13	%601362	10.7		2p13	%602966	6.4
10q23.31	%176920	3.4		2p15	#202370	2.8
10q24	%600095	8.8		2p15	#214100	2.8
11p11.2	#601224	5.3		2p16.1-p15	#612513	9.1
11q23-q24	%225000	20.4		2q14.2-q14.3	%210710	11.1
12p13.3	#214100	10.1		2q31	%183600	13.3
13q12.2-q13	%157900	12.3		2q31	%606708	13.3
13q14	%601499	15.2		2q32-q33	#612313	26
13q31.1-q34	%610361	36.2		2q34-q36	%185900	22
14q13	%609408	4.5		2q37.1-q37.3	%236100	12.2
14q21-q22	%608664	20.3		2q37.1-q37.3	%605934	12.2
14q32	%164210	17.5		3q29	%609425	5.7
15q26.1	#612813			4p16	%600593	11.3
17p11.2	#610883	6.2		4p16.3	#194190	4.5
17p11.2	%604547	6.2		4q21-q31	%608371	79.3
17p12-p11.1	#119540	13.3		4q33-qter	%607258	21.1
17p13.3	#247200	3.3		5q23	#225410	
17q24.3-q25.1	%261800	7.7		6p24.3	%119530	3.5
18p	#146390	17.2		6p25	%608545	7.1
18p11.31-q11.2	%606744	22.1		6q21-q22	%218400	24.8
18q	#601808	60.9		7p11.2	#180860	4
19q13	%600757	26.7		7p13	241800	2.1
1p34	%606713	12.2		7p22-p21	#607371	
1p36	#607872	28		7q11	#214100	17.6
1p36.3	%119530	7.2		7q11.23	#194050	5.3
1p36.32	#202370	3.1		7q11.2-q21.3	%129900	36.3
1p36.32	#214100	3.1		7q11-q21	%608027	38.1
1q21.1	#274000	4.4		7q21.2-q21.3	%183600	6.9
1q21.1	#612474	4.4		7q21.2-q21.3	%220600	6.9
1q22	#214100	1.5		7q36	#120200	11.2
1q4	%119530	34.8		8p23.3	#105650	2.2
1q42.2-q43	%119100	13		8q24.3	%612858	6.5
1q42-q44	#612337	25.2		9q32	%154400	2.8
21q22.3	%236100	5.5		Xp11.23-q13.3	%311900	29.6
22q11	#115470	11.2		Xp22	#300209	24.9
22q11.2	#145410	8		Xq24-q27.3	#300243	30.6
22q11.2	#608363	8		Xq25-q26.1	%313850	9.5
22q11.2	#611867	8		Xq26-q27	%300238	18.4
22q11.2	#192430	8		Xq26-q27	%300712	18.4
22q12-q13	%603116	25.4		Xq28	%300261	8.2

Table 6-6: Genomic loci previously correlated with a variety of mammalian craniofacial defects. See text for details.

Avian-specific microRNAs

The annotated microRNAs in miRBase (http://mirbase.org/, release version 16) (Griffiths-Jones et al. 2008) were compared across species by name and sequence. A list was compiled of those mature miRNAs only annotated in chicken (*Gallus gallus*, WASHUC2 genome build) and/or zebrafinch (*Taeniopygia guttata*, taeGut3.2.4 genome build), the only two avians with their genomes sequenced. Sequence reads for these miRNAs was assessed in the chicken, duck, and quail FNP mesenchyme libraries. miRNAs annotated in the chicken and/or zebrafinch and expressed in all three species in my miRNA libraries were further analyzed. Potential specificity to the avian lineage was assessed by BLAST (http://blast.ncbi.nlm.nih.gov/Blast.cgi) analysis, the current standard for assessing linage-specific microRNAs (Bentwich et al. 2005, Berezikov et al. 2006, Brameier 2010, Li J. et al. 2010, Li S. et al. 2009, Yuan et al. 2010), against genomic sequences of zebrafish (*Danio rerio*, danRer 7 genome build), ilzard (*Anolis carolinensis*, anoCar1 genome build), frog (*Xenopus tropicalis*, xenTro2 genome build), *Caenorhabditis elegans* (ce6 genome build), *Drosophila melanogaster* (dm3 genome build), platypus, (*Ornithorhynchus anatinus*, ornAna1 genome build), cow (*Bos Taurus*, bosTau4 genome build), dog (*Canis lupus familiaris*, canFam2 genome build), mouse (*Mus musculus*, mm9 genome build), and human (*Homo sapiens*, hg19 genome build). PCR to amplify the miR-2954 hairpin precursor was conducted on DNA from birds that span the avian lineage (Table 6-7 and Figure 4-5) (Sibley and Ahlquist 1990) using primers

designed against the zebrafinch reference (5'- CCAAATCGGTGTTTCTTGGT-3' and 5'-GTTCCCTAGCTCAGCCACAC-3').

Common name	Scientific name	Sample ID	Source
Black-footed Albatross	*Phoebastria nigripes*	UAMX789	UAM
Common Loon	*Gavia immer*	UAMX2231	UAM
Common Nighthawk	*Chordeiles minor*	JMM075	UAM
Gray-chested Dove	*Leptotila cassini*	KSW4287	UAM
Great Blue Heron	*Ardea herodias*	UAMX1947	UAM
Greater Flamingo	*Phoenicopterus ruber*	KSW3611	UAM
Green Warbler Finch	*Certhidea olivacea*	1801	UC
Ostrich	*Struthio camelus*	B-29767	LSUMNS
Spotted Northura (tinamou)	*Nothura maculosa*	KGM252	UAM

Table 6-7: Bird species used to assess avian-specific microRNAs. LSUMNS, Louisiana State University Museum of Natural Sciences; UAM, University of Alaska Museum, UC, Kenneth Petren (University of Cincinnati).

References

Bentwich I, et al. 2005. Identification of hundreds of conserved and nonconserved human microRNAs. Nat Genet 37: 766-770.

Berezikov E, Thuemmler F, van Laake LW, Kondova I, Bontrop R, Cuppen E, Plasterk RH. 2006. Diversity of microRNAs in human and chimpanzee brain. Nat Genet 38: 1375-1377.

Brameier M. 2010. Genome-wide comparative analysis of microRNAs in three non-human primates. BMC Res Notes 3: 64.

Brugmann SA, Goodnough LH, Gregorieff A, Leucht P, ten Berge D, Fuerer C, Clevers H, Nusse R, Helms JA. 2007. Wnt signaling mediates regional specification in the vertebrate face. Development 134: 3283-3295.

Burnside J, et al. 2008. Deep sequencing of chicken microRNAs. BMC Genomics 9: 185.

Dixon MJ, Marazita ML, Beaty TH, Murray JC. 2011. Cleft lip and palate: understanding genetic and environmental influences. Nat Rev Genet 12: 167-178.

Dull T, Zufferey R, Kelly M, Mandel RJ, Nguyen M, Trono D, Naldini L. 1998. A Third-Generation Lentivirus Vector with a Conditional Packaging System. J. Virol. 72: 8463-8471.

Griffiths-Jones S, Saini HK, van Dongen S, Enright AJ. 2008. miRBase: tools for microRNA genomics. Nucleic Acids Res 36: D154-158.

Hackenberg M, Sturm M, Langenberger D, Falcon-Perez JM, Aransay AM. 2009. miRanalyzer: a microRNA detection and analysis tool for next-generation sequencing experiments. Nucleic Acids Res 37: W68-76.

Hamburger V, Hamilton HL. 1951. A series of normal stages in the development of the chick embryo. J. Morphol. 88: 49-92.

Hawkins RD, Bashiardes S, Helms CA, Hu L, Saccone NL, Warchol ME, Lovett M. 2003. Gene expression differences in quiescent versus regenerating hair cells of avian sensory epithelia: implications for human hearing and balance disorders. Hum. Mol. Genet. 12: 1261-1272.

Hawkins RD, Bashiardes S, Powder KE, Sajan SA, Bhonagiri V, Alvarado DM, Speck J, Warchol ME, Lovett M. 2007. Large Scale Gene Expression Profiles of Regenerating Inner Ear Sensory Epithelia. PLoS ONE 2: e525.

Hughes SH. 2004. The RCAS vector system. Folia Biol (Praha) 50: 107-119.

International Chicken Genome Sequencing Consortium. 2004. Sequence and comparative analysis of the chicken genome provide unique perspectives on vertebrate evolution. Nature 432: 695-716.

Li J, Liu Y, Dong D, Zhang Z. 2010. Evolution of an X-linked primate-specific micro RNA cluster. Mol Biol Evol 27: 671-683.

Li S, Mead EA, Liang S, Tu Z. 2009. Direct sequencing and expression analysis of a large number of miRNAs in Aedes aegypti and a multi-species survey of novel mosquito miRNAs. BMC Genomics 10: 581.

Logan M, Tabin C. 1998. Targeted gene misexpression in chick limb buds using avian replication-competent retroviruses. Methods 14: 407-420.

Messina DN, Glasscock J, Gish W, Lovett M. 2004. An ORFeome-based analysis of human transcription factor genes and the construction of a microarray to interrogate their expression. Genome Res. 14: 2041-2047.

Nielsen HB, Wernersson R, Knudsen S. 2003. Design of oligonucleotides for microarrays and perspectives for design of multi-transcriptome arrays. Nucleic Acids Res 31: 3491-3496.

Quackenbush J. 2001. Computational analysis of microarray data. Nat Rev Genet 2: 418-427.

Sibley CG, Ahlquist JE. 1990. Phylogeny and classification of birds. New Haven: Yale University Press.

Suzuki S, et al. 2009. Mutations in BMP4 are associated with subepithelial, microform, and overt cleft lip. Am J Hum Genet 84: 406-411.

Tapadia MD, Cordero DR, Helms JA. 2005. It's all in your head: new insights into craniofacial development and deformation. J Anat 207: 461-477.

Veeman MT, Slusarski DC, Kaykas A, Louie SH, Moon RT. 2003. Zebrafish Prickle, a Modulator of Noncanonical Wnt/Fz Signaling, Regulates Gastrulation Movements. Curr. Biol. 13: 680-685.

Wernersson R, Nielsen HB. 2005. OligoWiz 2.0--integrating sequence feature annotation into the design of microarray probes. Nucleic Acids Res 33: W611-615.

Yuan Z, Sun X, Jiang D, Ding Y, Lu Z, Gong L, Liu H, Xie J. 2010. Origin and evolution of a placental-specific microRNA family in the human genome. BMC Evol Biol 10: 346.